République Algérienne Démocratique et Populaire
Ministère de l'Enseignement Supérieur et de la Recherche Scientifique
Université AKLI MOHAND OULHADJ-BOUIRA

Faculté des sciences de la Nature et de la Vie et des sciences de la Terre
Département Biologie
Laboratoire de Gestion et Valorisation des Ressources Naturelles et Assurance Qualité

THÈSE

EN VUE DE L'OBTENTION DU DIPLOME DE DOCTORAT

Domaine : SNV **Filière : Science Biologique**

Spécialité : Physiologie cellulaire and physiopathologie

Présentée par
MOUSSA Hamza

Thème

Extraction assistée par microondes/ultrasons des métabolites secondaires de *Carthamus caeruleus* L. et *Salvia officinalis* L. : optimisation, phytochimie et activités antioxydantes

Soutenue le : 31/07/2023 **Devant le Jury composé de :**

Nom et Prénom	**Grade**		
M. KADRI Nabil	Professeur	Univ. de Bouira	Président
M. DAHMOUNE Farid	Professeur	Univ. de Bouira	Rapporteur
M. BOURNINE Lamine	MCA	Univ. de Bouira	Examinateur
Mme. YALAOUI-GUELLAL Drifa	MCA	Univ. de Bouira	Examinatrice
M. AOUN Omar	Professeur	Univ. de M'sila	Examinateur
M. BENSOUICI Chawki	Maitre de recherche A	CRBT de Constantine	Examinateur

Année Universitaire : 2022/2023

Democratic and Popular Republic of Algeria
Ministry of Higher Education and Scientific Research
University of AKLI MOHAND OULHADJ-BOUIRA

Faculty of natural and life sciences and earth sciences
Departement of Biology
Laboratory of Management and Valorization of Natural Resources and Quality Assurance

THESIS
SUBMITTED FOR OBTAINING A DOCTORAL DEGREE

Domain: Science of Nature and Life **Sector: Biological Sciences**
Option: Cell Physiology and physiopathology

Presented by
MOUSSA Hamza

Thesis title

Ultrasound/Microwave-assisted extraction of secondary metabolites from *Carthamus caeruleus* L. et *Salvia officinalis* L.: optimization, phytochemistry and antioxidant activities

Supported on: 31/07/2023 **TO THESIS COMMITTEE:**

First and Last Name	**Grade**		
Mr. KADRI Nabil	Professor	Univ. of Bouira	Chairman
Mr. DAHMOUNE Farid	Professor	Univ. of Bouira	Supervisor
Mr. BOURNINE Lamine	Lecturer	Univ. of Bouira	Examiner
Mrs. YALAOUI-GUELLAL Drifa	Lecturer	Univ. of Bouira	Examiner
Mr. AOUN Omar	Lecturer	Univ. of M'sila	Examiner
Mr. BENSOUICI Chawki	Research Master A	NCBR of Constantine	Examiner

Academic Year: 2022/2023

Publications and communications

Scientific publications

- Moussa, Hamza, et al. "Optimization of ultrasound-assisted extraction of phenolic-saponin content from *Carthamus caeruleus* L. rhizome and predictive model based on support vector regression optimized by dragonfly algorithm." *Chemometrics and Intelligent Laboratory Systems* 222 (2022): 104493.
- Moussa, Hamza, et al. "Definitive screening design and *I*-optimal design for optimization of ultrasound-assisted extraction of phenolic content and antioxidant capacity from *Salvia officinalis* L. leaves." *Sustainable Chemistry and Pharmacy* 29 (2022): 100820.

Communications

- **Moussa, Hamza**, Farid Dahmoune, Hocine Remini, and Lotfi Mouni.**"** Valorization of *Portulaca oleracea* and *Globularia alypum*'s extracts obtained by a green extraction technology.**"** 1^{ere} *Séminaire en Ligne sur les Produits Bioactifs et Valorisation de la Biomasse, SNPBVB-1*, ENS KOUBA (Algiers), November 16-17, 2021.
- **Moussa, Hamza**, Farid Dahmoune, Hocine Remini, and Lotfi Mouni.**"** Ultrasound assisted extraction of antioxydant compounds *Rhamnus alaternus* and *Ruta graveolens* **"**. 10^{th} national days of natural and life sciences, University of Abdelhamid Ibn Badis-Mostaganem, November 16-18, 2021.
- **Moussa, Hamza**, Farid Dahmoune, Djellal Samia, Bouchemal Samah, Hocine Remini, and Lotfi Mouni.**"** Scavenging free radical activity of ethanolic extracts of *Portulaca oleracea* and *Globularia alypum* obtained by ultrasound assisted extraction **"**. *1er Séminaire National des Plantes Aromatiques et Médicinales de l'Est Algérien (SNPAMEA-1)*, ENSET de Skikda,

September 14-15, 2021.

- **Moussa, Hamza**, Farid Dahmoune, Hocine Remini, and Lotfi Mouni.**"** Optimization of Ultrasound assisted extraction of phenolic compounds from *C. caeruleus*' rhizome through response surface methodology **"**. *At the first international Symposium 'Environment and sustainable Development'*, Relizane (Algeria), Februry 10, 11, 2020.

Acknowledgments

The completion of my Doctoral research would have been impossible without the invaluable support and assistance of many individuals who were involved in the project. I would like to sincerely express my gratitude to ***Pro. F. DAHMOUNE****, my supervisor, for his unwavering support, guidance, and expert advice that he generously offered throughout the entire research journey. I am truly grateful for his invaluable assistance, which has played a significant role in making this accomplishment possible.*

I would like to express my sincere gratitude to the ***members of my thesis committee****; their expertise, insights, and feedback have been invaluable in guiding me through this research journey. I am grateful for their commitment and dedication to this project, as well as their willingness to share their knowledge and expertise.*

This is a matter of pleasure for me to acknowledge my deep sense of gratitude to the ***Faculty of Nature and Life and earth sciences-University of BOUIRA*** *for giving me the opportunity to finish my thesis work via an internship program. In addition, I wish to acknowledge the dean of our faculty* ***Prof. F. Zouggagh****, and the Department Heads including* ***M. Mahjoub, A. Arab, R. Abdelwahab*** *(earlier), and* ***H. Remini (earlier)*** *for their generous support by giving me access to all the laboratories of the faculty.*

I would like to express my sincere gratitude and appreciation to ***Prof. M. Lotfi****, the head of our laboratory, for their invaluable support throughout my research journey.*

I would like to express my gratitude and appreciation to ***Gdansk University of Technology*** *(Poland) and especially the Department of Chemistry, Technology, and Biotechnology of Food, for allowing me to finish my thesis work via an internship program.*

I would like to express my sincere gratitude to my internship supervisor ***Prof. Barbara Kusznierewicz*** *for her valuable guidance and for working in the Lab for completing the work in a short time. I am indeed thankful for* ***Marika Mróz****, without her kind assistance, my work would not have been completed. The information provided by Prof. Barbara Kusznierewicz and her Ph.D. student has contributed to making this project as comprehensive as possible.*

I would like to express my gratitude and appreciation to ***Dr. S. Bensmail*** *for her support and advice throughout the development of this research project. I would like to express my gratitude to* ***S. Hamid*** *for your kindness and willingness to lend a helping hand, I hope to be able to return the favor in the future, and I look forward to continuing to work with you in the future.*

I would like to express my sincere gratitude to the laboratory technicians especially Mrs. ***K. Mesrane*** *for their invaluable assistance and support during the course of my thesis research. I am grateful for their professionalism, enthusiasm, and kindness. Without their help, my thesis research would not have been possible. I am grateful to the staff of the library of the faculty for their assistance in accessing the resources I needed for my research.*

Finally, I would like to acknowledge my beloved family and friends for their unwavering support and encouragement. Their love and belief in me have been a constant source of motivation. Without the help and support of these individuals and organizations, this dissertation would not have been possible. Thank you all from the bottom of my heart.

MOUSSA Hamza

Dedication

I dedicate this doctoral thesis to my beloved family who has been my constant source of love, support, and encouragement throughout my academic journey.

*To **my mother** Mebarka Rabhi, you have been my guiding light and my biggest supporter. You have always been there to lend an ear, offer advice, and provide comfort when I needed it the most. Your strength, courage, and resilience are a constant source of inspiration to me, and I am grateful for the sacrifices you have made to ensure my well-being.*

*To **my father** Slimane, you have taught me the value of hard work, determination, and perseverance. Your unwavering support and encouragement have helped me overcome countless challenges, and I am grateful for your guidance and wisdom. I admire your strength, your kindness, and your unwavering commitment to our family.*

*To **my grandparents**, you have been a constant source of love and support throughout my life. Your wisdom, experience, and knowledge have been invaluable to me, and I cherish the memories that we have shared together. You have shown me what it means to be strong, resilient, and compassionate, and I am grateful for the lessons that you have taught me.*

*To my **dear aunts** Nacira, Noura, Samira, and L'ward who have played a significant role in shaping who I am today. Your wisdom and advice have been invaluable, and I am thankful for the bond we share.*

*To my **brothers** Ayoub, Tahar, and **my sister** Imene who have been my pillars of strength and support. Your love and encouragement have helped me through every challenge, and I am blessed to have you in my life.*

*To my **colleagues and best friends**, who have been my companions on this academic journey. Your encouragement and support have been invaluable, and I am grateful for the memories we have created together.*

Thank you all for being a part of my life and for helping me reach this important milestone.

MOUSSA Hamza

Acronyms

AARD average absolute relative deviation.

AI artificial intelligence.

ANN artificial neural network.

ANOVA anlaysis of variance.

BA Bat algorithm.

BBD Box-Behnken design.

BRT boosted regression tree.

DA dragonfly algorithm.

DOE design of experiments.

DSD definitive screening design.

GA genetic algorithm.

GC-MS gas chromatography combined with mass spectrometry.

HPTLC high-performance thin layer chromatography.

HPU high power ultrasound.

LC-MS liquid chromatography combined with mass spectrometry.

LoF lack of fit.

LPU low power ultrasound.

MAE mean of absolute error.

MAE microwave-assisted extraction.

MRPE mean relative percentage error.

PSO particle swarm optimization.

RMSE root mean square error.

RSD relative standard deviation.

SVM support vector machine.

SVR support vector regression.

SVR-DA support vector regression optimized using dragonfly algorithm.

TAC total antioxidant capacity.

TEAC trolox equivalent antioxidant capacity.

TPC total phenolic content.

TSC total saponin content.

UAE ultrasound-assisted extraction.

UHPLC-HRMS ultra high performance liquid chromatography combined with high resolution mass spectrometry.

List of Tables

List of Figures

Contents

Chapter1

General introduction

Cellular damage or oxidative injury induced by reactive oxygen species (ROS) is a key mechanism implicated in various human neurodegenerative disorders, autoimmune pathologies, inflammation, diabetes, and digestive system disorders (Atawodi, 2005). Free radicals are chemical species with high reactivity characterized by the presence of an unpaired electron in their outer shell. Because of this unpaired electron, free radicals are highly reactive and can participate in a variety of chemical reactions. Free radicals can be produced by the human's normal metabolic processes as well as by being exposed to environmental chemicals (smoke, radiation, and pollution) and other xenobiotics as well as endogenous chemicals, especially stress hormones (Cheeseman and Slater, 1993). An increasing number of studies indicate that ROS can be scavenged by using natural antioxidant compounds found in foods and medicinal plants as chemo-prevention (Cuppett and Hall, 1998; Khalaf et al., 2008; Pietta et al., 1998).

Medicinal plants are "traditions of yesterday and drugs of tomorrow", have garnered increased interest in recent years due to their potential in treating chronic diseases such as cancer, and Alzheimer's disease, and diabetes (Gurib-Fakim, 2006). They are also known to have fewer side effects and are more sustainable compared to synthetic drugs. With their natural healing properties and affordability, medicinal plants have proven to be an essential component in traditional medicine and an exciting area of research for modern medicine (Gurib-Fakim, 2006). These health benefits have been attributed to plant-derived compounds known as bioactive compounds, which are secondary metabolites present ubiquitously in the plant kingdom and are considered non-nutritional but vital ingredients for the maintenance of human health (Patil et al., 2009). Many classes of secondary metabolites such as phenolic compounds (Flavonoids and Non- Flavonoids) have been identified in several plant families including Asteraceae, and Lamiaceae (Afonso et al., 2021; Dai et al., 2013; Skendi et al., 2017; Wang et al., 1998; Zi-

aková and Brandšteterová, 2003). The composition and amount of bioactive compounds in plants are influenced by various factors such as the specific chemo-type of the plant, the geographical region where it is harvested, the climate conditions. Consequently, there is a growing interest in employing more systematic and comprehensive approaches for characterizing these compounds. Techniques such as liquid chromatography combined with mass spectrometry (LC-MS), and high-performance thin layer chromatography (HPTLC), and gas chromatography combined with mass spectrometry (GC-MS) among others, have been widely utilized for this purpose (Nayak et al., 2015; Pachura et al., 2022; Reguigui et al., 2023).

The main challenge while extracting these bioactive compounds is to choose the appropriate extraction technique. Traditionally, methods such as soxhlet, maceration, decoction, etc., which uses simple and low-cost equipment, high amount of solvents, and long extraction time, working at atmospheric pressure and at higher extraction temperatures, and eventually had a negative impact on the environment (Rodriguez De Luna et al., 2020). Environmentally-friendly extraction methods, including ultrasound-assisted extraction (UAE), microwave-assisted extraction (MAE), pressurized liquid extraction, pulsed electric field, enzyme-assisted extraction, and high-voltage electrical discharges, have emerged as non-conventional approaches. These methods utilize advanced equipment, enabling efficient extraction within shorter timeframes and flexible operating conditions of pressure and temperature (Berkani et al., 2020; Dahmoune et al., 2015; Darvishzadeh and Orsat, 2022; Garcia-Vaquero et al., 2020; Rodriguez De Luna et al., 2020). Moreover, it has been reported that different extraction parameters such as the nature of the solvent, time, solid-to-solvent ratio, temperature, and pressure may affect significantly the efficiency of these environmentally-friendly methods to extract bioactive compounds (Dahmoune et al., 2015; Frontuto et al., 2019; Liu et al., 2013; Tabaraki and Nateghi, 2011).

The utilization ofdesign of experiments (DOE) and artificial intelligence (AI) can prove beneficial in optimizing and predicting the extraction process of secondary metabolites from medicinal plants. DOE, as a statistical technique, enables the rapid optimization of system efficiency by considering known input variables (Uy and Telford, 2009). Various DOE methodologies, including full and fractional factorial design, central composite design (CCD), and Box-Behnken design (BBD), have been widely employed to screen and optimize the MAE and UAE of secondary metabolites from medicinal plants (Kwon et al., 2003; Uy and Telford, 2009; Xu et al., 2020). Recently, new statistical designs have been developed such as definitive screening design (DSD) and I-optimal design (Goos and Jones, 2011; Jones

and Nachtsheim, 2011). DSD allows the simultaneous screening of multiple factors (qualitative and quantitative) and their interactions while minimizing the number of experiments required (Jones and Nachtsheim, 2011). On the other hand, *I*-optimal designs are particularly useful when resources are limited and the number of experiments that can be conducted is restricted (Goos and Jones, 2011). The *I*-optimal design minimizes the average variance of parameter estimates over the experimental region, which leads to a more precise and accurate model (Goos and Jones, 2011). Furthermore, AI can be used to model the extraction of bioactive compounds from medicinal plants. AI can help to optimize the input variables by predicting the optimal conditions for maximum yield and quality of output variables. Support vector machine (SVM), artificial neural network (ANN), and boosted regression tree (BRT) as supervised machine learning algorithms have gained more interest, especially in chemistry and biology by accelerating research, improving drug discovery, and providing new insights into complex biological processes (Asgari et al., 2017; Ciric et al., 2020; Elith and Leathwick, 2017; Hua and Sun, 2001; Suleiman et al., 2016).

The yield and potency of bioactive compounds of medicinal plants can be influenced by various factors, including the region in which the plants are grown. However, there are several limitations to the effect of regions on the yield of bioactive compounds. One of the primary limitations is variations in soil quality, and climate can significantly affect the chemical composition of the plants (Frontuto et al., 2019; Liu et al., 2013; Tabaraki and Nateghi, 2011). Additionally, the genetic variability of plants within a species can also affect the concentration and diversity of bioactive compounds. Another limitation is the variability in the extraction and analysis methods used to measure the bioactive compound content. Extraction methods can vary in terms of cost, time, and environmental impact, which can yield varying amounts and types of compounds, making it difficult to compare results across different studies. The stability and solubility of bioactive compounds can pose challenges during extraction, as they may be prone to degradation or require specific conditions to extract efficiently (Frontuto et al., 2019; Liu et al., 2013; Tabaraki and Nateghi, 2011).

As far as our knowledge extends, there is a limited amount of research available about the optimization and prediction of UAE and MAE of secondary metabolites from medicinal plants of the Bouira region using DOE, and supervised learning models. Therefore, the present study attempts to valorize the medicinal plants of the Bouira region including *Carthamus caeruleus* L. and *Salvia officinalis* L. by optimizing and modeling UAE and MAE of their secondary metabolites using new statistical designs and supervised learning model.

The study is divided into two main parts; **a)** the first part aimed to optimize and model the UAE of total phenolic content (TPC) and total saponin content (TSC) from the rhizome part of *Carthamus caeruleus* L. using Box-Behnken design and support vector regression optimized by the dragonfly algorithm (SVR-DA). The antioxidant activity of the optimal UAE of rhizome extract was evaluated and compared to the antioxidant activity of leaves extract using different methods *in vitro*. The second part **(b)** aimed to screen and optimize the UAE and MAE extraction conditions of TPC, Trolox equivalent antioxidant capacity (TEAC) and total antioxidant capacity (TAC) from *Salvia officinalis* L. leaves using new classes of experimental designs such as DSD and I-optimal design. Furthermore, a differential analysis using ultra-high performance liquid chromatography combined with high resolution mass spectroscopy (UHPLC-HRMS) between the phenolic profile of MAE optimal extract and UAE optimal extract of *S. officinalis* L. leaves were carried out to evaluate the effect of MAE and UAE on TPC, and antioxidant activity. This Doctoral Dissertation is structured in three main parts, as explained below:

- **Part I: Literature Review**, where
  - A comprehensive overview of the current state of knowledge on the studied plants and their health benefits (*Carthamus caeruleus* L. and *Salvia officinalis* L.) **(Chapter 1)**.
  - Review the different types of secondary metabolites found in medicinal plants. Review the existing research on the extraction of secondary metabolites from plants and the different techniques used for this purpose **(Chapter 2)**.
- **Part II: Materials and Methods**, where the materials and methods used in this study are described, as well as all the detailed information on the plant species studied are provided. The extraction techniques and analytical techniques used to extract and identify the secondary metabolites from the studied plants also are described **(Chapter 3)**.
- **Part III: Results and discussion**, where the results obtained during this Ph.D. thesis are presented and discussed in two main **Chapters:**
  - **Chapter 4** of this study focuses on two main aspects, namely the optimization of the UAE process to extract phenolic-saponin content from the rhizome of *C. caeruleus* L., and the development of a predictive model using support vector regression that was optimized using the dragonfly algorithm

  - **Chapter 5** of this study, two design methodologies, namely definitive screening design and I-optimal design, are employed to optimize the ultrasound and microwave-assisted extraction processes for phenolic content and antioxidant capacity from the leaves of *S. officinalis* L. Additionally, each chapter is preceded by an abstract that provides a concise summary of its contents.
  - General Conclusion, where the most relevant findings achieved during this Ph.D. are summarized. The broader implications of this research for the field of medicinal plants and the extraction of their secondary metabolites using unconventional extraction techniques combined with the design of experiments and artificial intelligence are discussed. Some future works and perspectives on the topic also are provided **(Chapter 6)**.

- More sections are included at the end of this Dissertation:
  - Annexes, and references, where the list of all research works cited relevant to the topic of this Ph.D. dissertation is presented.
  - The scientific articles published in Elsevier journals, related to the work, and Abstract.

Part I

Literature review

Chapter2

Medicinal plants and their Health benefits

2.1 *Carthamus caeruleus* L.

2.1.1 Cytotaxonomy and classification

The family of Asteraceae is the largest angiosperm with 23600 species, widespread in temperate regions (Ababsa et al., 2018), recent years have seen considerable attention on their biological activities, where the Asteraceae plants have been used widely as traditional herbals medicine (Albayrak et al., 2010; Brandão et al., 1997; Passero et al., 2011). The genus of *Carthamus* belongs to the family of Asteraceae that comprises of 25 species including *Carthamus tinctorius* L., *Carthamus lanatus*, *Carthamus Oxyacantha*, and *C. caeruleus* L (Toubane et al., 2017).

Figure 2.1: Picture of *C. caeruleus* L. (herbarium of Gérard de Belair , GdB)

Several attempts to make cytotaxonomy and classification of *C. caeruleus* L. clear, Pomel (1874) classified *C. caeruleus* into the genus of Lamottea under the scientific name of *Lamottea caerulea* (L.) Pomel. on the basis of carpological characters, after that Quezel et al. (1962) transferred it to *Carthamus* genus on the basis of pappus characteristics (Vilatersana et al., 2000). Based on internal transcribed spacer (ITS) sequences of nuclear ribosomal DNA, Vilatersana et al. (2000) were in agreement with the classification of Lopez Gonzalez (1989) to moved *C. caeruleus* L. back to Lamottea genus McPherson et al. (2004).

Ashri and Knowles (1960), have categorized the species of *Carthamus* for many sections based on chromosome numbers, morphology, and ability of hybridization: section I, II, III, and section IV having respectively 12, 10, 22, and 32 pairs of chromosomes. *C. caeruleus* L., with 2n = 24, was not assigned to sections because it is not able to hybridize with other species. Within this context, many Artificial crosses with *C. caeruleus* L. with other species of *Carthamus* confirm that it failed to produce seed except for a single cross with *C. leucocaulos*, which offspring produced is a single sterile with low pollen viability (McPherson et al., 2004).

The botanical classification was given by Quezel et al. (1962):

Kingdom:	Plantae
Phylum:	Tracheophyta
Subphylum:	Angiospermae
Class:	Dicotyledones
Order:	Asterales
Family:	Asteraceae
Sub-family:	Tubulifloreae
Tribe:	Cynareae
Genus:	*Carthamus*
Species:	*Carthamus caeruleus* L.

Vernacular names: Arabic: Mers'gousse, Kendjar, Gargaa; Kabyle: Amegres; French: Cardoncelle Bleue, Carthame bleue.

2.1.2 Botanical characteristics and geographical distribution

Two models of *C. caeruleus* L. leaves were recognized; radical leaf attenuate, oblong, dentate or lyrate-pinnatifid, is growing and situated at the base of the stem which has hairs long and rigid (hispid); and cauline leaf sessile, amplexicaul and ovate-lanceolate, dentate-spiny margin are borne and spread out on an aerial stem (Fig. 2.1) (Battandier, 1888). *C. caeruleus* L. is a blue-flowered perennial species

with dark anthers, its flowers head are ovoid or globose; Achenes are globular or subglobular, whitish and glabrous, which are shorter than pappus; involucre with external bracts ciliates-pectinated and internal bracts have a fimbriate appendix. Every single flower's head rises approximately 20-60 cm which is based on ascending stems (erect), monocephalic, and usually simple (Fig. 2.1), generally it is a biennial plant (Battandier, 1888; McDonald and Edwards, 1807; Quezel et al., 1962).

Bioclimatic zones and the geographical position of Algeria allowed the growing of many varieties of plants. *C. Caeruleus* L. is a Mediterranean plant, it is a native of Barbary is abundantly present in North Africa, southern European countries like Spain, Greece, and Italy, in Algeria *C. Caeruleus* L. is widespread in fields and uncultivated places (McDonald and Edwards, 1807; Quezel et al., 1962; Toubane et al., 2017).

2.1.3 Major components of *Carthamus caeruleus* L.

phytochemicals are abundant in various parts of medicinal plants, including *C. Caeruleus* L. rhizome, which has been found to be a rich source of primary metabolites such as lipids (8%) and starch (22%), along with secondary metabolites with a water content of 60% (Hamadi et al., 2014). Moreover, Ten compounds were characterized from methanol extract of *C. Caeruleus* L. root, such as sennosides, flavonoids, anthocyanins, free quinones, tannins, leucoanthocyanins, saponins, glycosides, mucilage, and coumarins (Baghiani et al., 2010; Dahmani et al., 2018), In addition to compounds mentioned previously, Toubane et al. (2017) were identified 13 compounds such as sesquiterpenes and fatty acids. Moreover, 4 polyunsaturated fatty acids such as linolenic acid and, linoleic acid, palmitic acid, and arachidonic acid, and a high quantity of sterols were revealed in the rhizome part, These compounds have demonstrated their effectiveness in safeguarding and renewing skin cells. Palmitic acid contributes to preserving the integrity of the skin's surface, specifically the stratum corneum, while linoleic acid functions as a protective agent against skin cancer (Hamadi et al., 2014). In addition, sterols are recognized for their ability to regenerate skin cells (Hamadi et al., 2014). Overall, the predominance of mucilage, fatty acids, and phenolic compounds in *C. Caeruleus* L. rhizome explains its healing properties for irritated tissues and its antimicrobial, anti-fungal, antioxidant, and anti-inflammatory activities (Baghiani et al., 2010; Dahmani et al., 2018; Hamadi et al., 2014; Toubane et al., 2017).

2.1.4 Biological activities of *Carthamus caeruleus* L.

2.1.4.1 Antimicrobial activity

The emergence of resistance to antimicrobial agents has evolved into a significant global issue, increasingly prevalent worldwide. In US hospitals, approximately 70% of cases involve the acquisition of bacterial strains that are resistant to treatment each year (Cushnie and Lamb, 2005a). Within this context, the antimicrobial activity of *C. Caeruleus* L. leaf and root extract were tested *in vitro* and the results showed that leaf and root extracts have a positive effect against several microorganisms including Gram-negative, and Gram-positive bacteria (*Staphylococcus aureus*, *Bacillus cereus*, and *Acinetobacter bowie*) and pathogenic fungus (*Ascochyta rabiei* and *Fusarium Var coerileum*) (Karima et al., 2013). Moreover, the root extracts are more effective and efficient than leaf extract against the tested microorganism (Karima et al., 2013).

2.1.4.2 Antioxidant capability

Under physiological conditions, reactive oxygen species (ROS) and antioxidant defense are in balance, an imbalance of one of them may induce oxidative stress which is considered an etiological agent for many diseases like cardiovascular and neurodegenerative diseases, such as cancer, Alzheimer, diabetes, and aging (Rojas and Buitrago, 2019). More importantly, the prevention of oxidative stress and those diseases by natural antioxidants has been suggested (Cushnie and Lamb, 2005b).

In their study, Baghiani et al. (2010) assessed the TPC, total flavonoids content, and antioxidant capacity of four sub-fractions obtained from the root extract of *C. Caeruleus* L. The findings revealed that the ethyl acetate extract exhibited the highest TPC, with a value of 75.710 ± 4.878 mg_{GAE}/g. The chloroform extract followed closely behind with a TPC of 36.899 ± 1.863 mg_{GAE}/g. However, the chloroform extract exhibited remarkable antioxidant activity, surpassing other extracts, with an IC_{50} value of 53.26 $\mu g\,mL^{-1}$. Notably, its effectiveness even surpassed that of the synthetic antioxidant butylated hydroxytoluene (BHT). Additionally, Toubane et al. (2017) highlighted that the ethanol extract of *C. Caeruleus* L. demonstrated the highest antioxidant capacity, with an IC_{50} value of 1.51 $mg\,mL^{-1}$, when compared to the hexane and methanol extracts obtained through accelerated solvent extraction.

2.1.4.3 Anti-inflammatory activity

In this case, the root's anti-inflammatory activity was induced by Carrageenan in the hind paw of the mice model; the results showed that ethanol extract was better to reduce the swelling induced in the mice paw than methanol extract, hexane extract, and even with standard treatment, the anti-inflammatory activity probably due to inhibition the stimulating the release of inflammatory mediators (Toubane et al., 2017). Also, Dahmani et al. (2018) confirmed that the methanol extract has an important diminution in hind paw volume induced similar to positive controls, caused by many bioactive compounds such as flavonoids are known to target prostaglandins mediator, which is involved in the late phase of acute inflammation, and palmitic acid as an anti-inflammatory agent has a significant inhibition of phospholipase A enzyme. According to Dahmani et al. (2018), caryophyllene oxide and 5-hydroxyméthylfurfural are additional phytochemicals that possess beneficial biological effects, including analgesic and anti-inflammatory properties, as well as bacteriostatic action.

2.1.4.4 Wound-healing capacity

In Algeria, a lot of the Asteraceae family including *C. Caeruleus* L. has been used for many years in the healing of wounds and burns as an antiseptic agent (Meddour and Meddour-Sahar, 2015). According to Dahmani et al. (2018), the root extract of *C. Caeruleus* L. has been identified as a beneficial source of palmitic acid. This compound has demonstrated the ability to induce a wound healing effect *in vivo* using an incision wound model, primarily by reducing oxidation and inflammation. Additionally, the extract has exhibited positive effects in a hair growth-promoting test by enhancing the distribution of sebaceous glands, capillaries around hair follicles, and promoting vasodilation (Dahmani et al., 2018). In their study, Benhamou and Fazouane (2013) formulated a healing cream utilizing the rhizome of *C. Caeruleus* L. and examined its efficacy on an animal model with second-degree burns and incisional wounds. The histopathological analysis revealed a notable regeneration of epithelial tissue, indicating the positive healing properties of the cream.

2.2 *Salvia officinalis* L.

2.2.1 Taxonomy and distribution

The Lamiaceae family is recognized as one of the most significant families of medicinal plants, encompassing a diverse range of plant species with extensive bi-

Figure 2.2: Aerial part of *Salvia officinalis* L (El-Feky and Aboulthana, 2016).

ological and therapeutic applications. Within this family, the *Salvia* genus stands out as the most prominent, comprising an impressive collection of approximately 900 species (Ghorbani and Esmaeilizadeh, 2017; Uritu et al., 2018). Garden sage or common sage, scientifically known as *Salvia officinalis* L., is an herbaceous plant. The name "Salvia" originates from the Latin term "salvare," which translates to "healer," reflecting the plant's renowned therapeutic properties (Afonso et al., 2021) (Fig. 2.2). According to (Grdiša et al., 2015; Quezel et al., 1962), the classification of *Salvia officinalis* L. was given as follows:

Kingdom:	Plantae
Phylum:	Tracheophyta
Subphylum:	Angiospermae
Class:	Dicotyledones
Family:	Lamiaceae
Sub-family:	Nepetoideae
Tribe:	Mentheae
Genus:	*Salvia*
Species:	*Salvia officinalis* L

Vernacular names : Arabic: Souaq en nebi, Miramiya, salma; Kabyle: Tazzourt, Agourim, Imeksaouen; French: sauge commune, English: Common sage, Garden sage.

Sage is native to the northern Mediterranean region and the Middle East, it has been distributed throughout Southern Europe, Southeast Asia, and America (Jakovljevic et al., 2019). Sage is cultivated in the world as a culinary herb in the USA, Spain, Italy, Yugoslavia, Greece, Albania, Argentina, Germany, France, Malta, Turkey, England, and Canada (Sharma et al., 2019).

2.2.2 Botanical aspects

The common sage, also known as *Salvia officinalis* L., is a fragrant shrub that can be an annual or perennial and reaches a height of up to 100 cm (Altindal and Altindal, 2016). The plant features opposite and simple leaves with a grayish-green color. These leaves are oblong-lanceolate, measuring approximately 8.5 × 2.5 cm, and have petioles. They possess an acute apex, finely crenate margins, and a dense covering of hairs that obscure the glandular punctate glands (Bagchi and Srivastava, 2003; Jakovljevic et al., 2019). According to Jakovljevic et al. (2019), the stems of *Salvia officinalis* L. can either be erect or procumbent and are characterized by plentiful hairy dark green branches. The flowers, resembling violets, measure 2 to 4 mm in length and are arranged in pseudoverticillasters. Each pseudoverticillaster consists of 5 to 10 violet-blue colored flowers, forming clusters that resemble spurious spikes. The flowering period spans from March to July (Altindal and Altindal, 2016; Jakovljevic et al., 2019). *S. officinalis* L. may contain both male and female organs or only female organs (Altindal and Altindal, 2016).

2.2.3 Major components of *Salvia officinalis* L.

Using UPLC/ESI-MS, the key bioactive compounds present in the leaves of *Salvia officinalis* L. were effectively identified. The analysis revealed a notable presence of various compounds, including flavan-3-ols, flavonols, hydroxybenzoic acids, flavones, hydroxycinnamic acids, lignans, and anthocyanins indicating their higher concentration in the plant (Čulina et al., 2021). In addition, Boufadi et al. (2020) found that kaempferol, cirsimaritin, quercetin, catechin, acacetin, rosmarinic acid, and salvianolic acid were the most abundant bioactive compounds in the ethanol-water extract of sage leaves of the west of Algeria.

Additionally, the sage extract from Croatia exhibits a diverse range of bioactive compound families, including monoterpenes, oxygenated monoterpenes, sesquiterpenes, oxygenated sesquiterpenes, diterpenes, triterpenes, esters, and waxes. These compound families were identified using advanced analytical techniques such as GC-FID and GC-MS (Glisic et al., 2011). The same bioactive compounds were also found in the sage extract of East of Serbia by Velickovic et al. (2006), which found that hydro-ethanolic extract exhibited a high concentration of camphene, cis-thujon, trans-thujone, 1,8-cineol, camphor, α-humulene and α-pinene.

On the other hand, the essential oil of sage leaves exhibited medicinal properties and is employed in many pharmaceutical and food industries. Radulescu et al. (2004) identified 35 compounds in the essentiel oil of sage leaves, in which thujone

(α and β), camphor, 1-octen-3-ol, and 1,8-cineole were found in high concentration compared to the others compounds. Furthermore, it has been documented that the composition of the essential oil derived from *Salvia* species can vary significantly due to factors such as genetic variations, seasonal fluctuations, climatic conditions, and environmental influences (Hamidpour et al., 2014).

2.2.4 Extraction of secondary metabolites from *Salvia officinalis* L. leaves

Sage leaves contain numerous bioactive compounds that showcase diverse biological activities, making them valuable in various industries. Extracting these compounds is a vital process for isolating and identifying their bioactive constituents. Table 2.1, highlights that maceration, UAE, and MAE have been utilized to extract total phenolic content, flavonoids, and phenolic acids from *Salvia officinalis* L. Su et al. (2020) optimized aqueous enzymatic extraction of rosmarinic acid from sage leaves, which found that the optimal parameters for the extraction of rosmarinic acid were; 4.49% of Cellulase A and Protamex mixture (1:1, w/w) in distilled water, 1/25.76 g mL^{-1} of solid to liquid ratio, and 54.3 °C, for two 2 h using maceration as extraction method (Table 2.1). Furthermore, different preliminary studies were carried out to study the effects of different extraction parameters of maceration on the extraction of TPC, which found that the extraction solvent, solid-to-solvent ratio, temperature, and extraction time highly showed significant effects on the extraction of these compounds (Dragovic-Uzelac et al., 2012; Durling et al., 2007).

Furthermore, the UAE and MAE of phenolic compounds from sage leaves were also performed as depicted in table 2.1, which showed high extraction efficiencies than maceration by maximizing the recovery of phenolic compounds, and minimizing the extraction time. Jakovljević et al. (2021) applied the deep eutectic solvent (DES) as a green solvent for the extraction of carnosic acid and carnosol from sage leaves, which found that 82.36 min of time, 69.84 °C of temperature, 50/1 mg mL^{-1} of solid to solvent ratio were the optimal UAE parameters. On the other hand, optimization of the antioxidant compounds extraction from sage by-products using ultrasound and microwave was also carried out, which found that the optimal UAE parameters were 80 min of time, and 75 °C of temperature, whereas the MAE parameters were 18.7 min of time, and 1/40 g mL^{-1} of solvent to solid ratio (Table 2.1).

Table 2.1: Extraction methods and design of experiments used for the extraction of secondary metabolites from *S. officinalis* L.

				Optimal extraction conditions				
Extraction methods	**DOE**	**Equipement's characteristic**	**Target compounds**	**Time**	**Temperature**	**solid/liquid ratio (g/mL)**	**Solvent concentration**	**References**
UAE	N/A	Ultrasonic probe output power 400 W frequency 30 kHz	TPC RA	11 min	N/A	1/20	Ethanol (30%)	(Dent, 2015)
	BBD	37 Hz 50 W	Carnosic acid carnosol	82.36 min	69.84 °C	50/1 (mg/mL)	DES-H2O 11.05% of water addition	(Jakovljević et al., 2021)
	N/A	400 W 24 kHz	TPC	10 min	40 °C	1/10	Ethanol (80%)	(Dogan et al., 2019)
	BBD	42.54 W/L 40 kHz	TPC and TFC	80 min	75 °C	1/20 (fixed)	Ethanol (60%) (fixed)	(Zeković et al., 2017a)
MAE	N/A	500 W 2450 MHz	TPC	9 min	80°C	1/45	Ethanol (30%) Acetone (30%)	(Dragovic-Uzelac et al., 2012)
	N/A	2450 MHz 100 - 500 W	TPC RA	10 min	80 °C	1/45	TPC (30% acetone) RA (30% ethanol)	(Putnik et al., 2016)
	BBD	600 W	TPC TFC	18.7 min	N/A	1/40	Etahanol (46.2%)	(Zeković et al., 2017a)
Maceration	N/A	N/A	RA CC EO	3 h	40 °C	1/6	Ethanol (55 to 75%)	(Durling et al., 2007)
	BBD	N/A	RA	2 h	54.3 °C	1/25.76	cellulase A and protmex mixture (1:1 w/w) (4.49%)	(Su et al., 2020)
	N/A	N/A	TPC	30 min	80 °C	1/45	30 % ethanol and 30% acetone	(Dragovic-Uzelac et al., 2012)

TPC: Total phenolic compounds, **RA**: Rosmarinic acid, **CC**: carnosic compounds, **EO**: Essentiel oil, **DES**: deep eutectic solvents, **BBD**: Box-Behnken design, **DOE**: design of experiments

2.2.5 Sage and health benefits

Sage has long been utilized in traditional medicine due to its abundant bioactive compounds. Its medicinal properties have been recognized for decades, with applications in alleviating labor pain, treating ulcers, relieving coughs and hoarseness, reducing perspiration, managing seizures, addressing gout and rheumatism, combating inflammation, mitigating dizziness and tremors, relieving paralysis, alleviating diarrhea, managing hyperglycemia, and aiding contractions (Altindal and Altindal, 2016; Ghorbani and Esmaeilizadeh, 2017).

Sage is renowned for its ability to enhance cognitive function, boost memory, heighten sensory perception, and slow down the decline of cognitive abilities associated with aging (Lopresti, 2017). Research suggests that rosmarinic acid present in sage leaves can mitigate various detrimental effects caused by amyloid-beta peptide, such as the generation of reactive oxygen species, lipid peroxidation, DNA fragmentation, activation of caspase-3, and hyperphosphorylation of tau protein. Consequently, sage holds potential as a treatment option for Alzheimer's disease (Iuvone et al., 2006). In support of this, a clinical trial demonstrated the efficacy of extracts derived from *Salvia officinalis* L. in managing mild to moderate Alzheimer's disease (Akhondzadeh et al., 2003). Furthermore, sage is rich in ursolic acid, a type of pentacyclic triterpenoid carboxylic acid. This compound has been shown to possess notable properties in reducing lipid peroxidation and effectively reversing learning and memory impairments induced by D-galactose (Wu et al., 2011). Additionally, various sage extracts from different sources have been found to possess numerous biological activities, as outlined in Table 2.2. These extracts exhibit robust antioxidant, antidiarrheal, antispasmodic, antidiabetic, gastroprotective, anticancer, antiangiogenic, and wound healing properties, while also enhancing ovarian function 2.2.

Furthermore, the sage extracts have demonstrated effectiveness against leishmanial infections and antimicrobial activity against bacteria associated with dental caries and periodontal diseases, as indicated in Table 2.3. Notably, the compound manool has been identified as the key contributor to the antimicrobial activity of *Salvia officinalis* L. (Mendes et al., 2020; Moreira et al., 2013). Moreover, sage exhibited higher inhibitory activity against gram-positive and gram-negative pathogenic strains including *Micrococcus luteus*, *Bacillus subtilis*, *Bacillus cereus*, *Staphylococcus aureus*, *Escherichia coli*, *Pseudomonas aeruginosa* and *Enterococcus faecalis* (Table 2.3). On the other hand, the antiparasitic, and antifungal activity of sage leaves were also reported (Table 2.3). Based on the available literature, no adverse side effects have been reported in relation to the use of *Salvia*

officinalis L. However, it is crucial to exercise caution when using *Salvia officinalis* L. due to its high concentration of thujone, which can have detrimental effects if consumed excessively (Hamidpour et al., 2014). To ensure safe usage of sage leaves, it is advised to restrict consumption to a range of 1 to 2 grams per day or 5 milligrams per day per person of thujone. It is important to refrain from surpassing this recommended amount for a duration exceeding two weeks (EMA, 2009).

Table 2.2: Biological activities displayed by *S. officinalis* L. leaves

Origin	Biological activity	Test used	References
Romania (Alba) Portugal (Viseu) Algeria	Antioxidant capacity	Phosphomolybdenum assay, $DPPH^{\bullet}$, $ABTS^{\bullet}$, CUPRAC, $NO^{\bullet}$ and O^{2-}, FRAP assays	(Mocan et al., 2020) (Pereira et al., 2018) (Bouteldja et al., 2021)
Romania (Alba)	Neuroprotective activity	Acetylcholinesterase (AChE) and butyrylcholinesterase (BChE) inhibitory	(Mocan et al., 2020)
Romania (Alba) Iran (karaj) Portugal (Viseu)	Antidiabetic activity	α-amylase and α-glucosidase inhibitory streptozotocin induced diabetic rats	(Mocan et al., 2020) (Pereira et al., 2018) (Eidi and Eidi, 2009)
Portugal (Viseu)	Metabolic Enzyme Activity	Pancreatic Lipase inhibitory	(Pereira et al., 2018)
Brazil	Gastroprotective activity	Induction of acute gastric lesion	(Mayer et al., 2009)
Saudi Arabia	Antidiarrheal and antispasmodic activities	*In Vivo*	(Khan et al., 2010)
Iran	Antiangiogenic activity	*In Vitro* and *Ex Vivo*	(Keshavarz et al., 2010)
Iran (Urmea)	Wound healing activity	*In Vivo*	(Karimzadeh and Farahpour, 2017)
Slovakia (Bratislava)	Protease inhibition assay	Inhibition activity against trypsin, hrombin, urokinase, and cathepsin B	(Jedinák et al., 2006)
Slovakia (Bratislava)	Anticancer activity	*In vitro*	(Jedinák et al., 2006)
Saudi Arabia	Enhancing ovarian function	*In Vivo*	(Alrezaki et al., 2021)

Table 2.3: Antimicrobial, antiparasitic, antifungal, anti-leishmanial acitivity of *S. officinalis* L. leaves

Origin	Biological activity	Pathogenic strains	References
Iran (Tehran) Moroco Algeria	Anti-leishmanial activity	*Leishmania major* promastigotes (strain MROH/IR/75/IR)	(Nikmehr et al., 2014) (Et-Touys et al., 2016) (Serakta et al., 2013)
Brazil	Antimicrobial activity against bacteria associated with dental caries	*Streptococcus mutans*	(Moreira et al., 2013)
Brazil	Antibacterial activity	Periodontopathogens	(Mendes et al., 2020)
Algeria	Antibacterial activity	*Micrococcus luteus*, *Bacillus subtilis*, *Bacillus cereus*, *Staphylococcus aureus*, *Escherichia coli*, *Pseudomonas aeruginosa* E*nterococcus faecalis*	(Bouteldja et al., 2021)
Iran	Antiparasitic effect	*Syphacia obvelata*, *Aspiculoris tetrapetra* *Hymenolepis nana parasites*	(Amirmohammadi et al., 2014)
Algeria (Annaba)	Antifungal activity	*Candida albicans*, *Candida glabrata*, *Candida parapsilosis*	(Kerkoub et al., 2018)

Chapter3

Bio-active compounds and extraction technologies

3.1 Secondary metabolites from plant matrices and their classification

Polyphenols, classified as secondary metabolites, are abundantly present in various plant species, particularly in fruits and vegetables. These compounds typically consist of at least two phenyl rings and one or more hydroxyl groups. The plant kingdom boasts an extensive array of approximately 10,000 distinct phenolic structures, which can also be found in a wide range of foods (Saparbekova et al., 2023). Polyphenols can be classified into two main groups, namely flavonoids and non-flavonoids, based on the number of phenol units, substituent groups, or the type of linkage between phenol units in their molecular structure. These polyphenols can be further divided into subclasses such as flavonoids, stilbenoids, phenolic acids and lignans as mentioned by Singla et al. (2019).

3.1.1 Flavonoids

Flavonoids have a common carbon skeleton of diphenyl propane, consisting of two aromatic rings (ring A and B) attached to 3C atoms, which form an oxygenated heterocycle as shown in figure 3.1 (D'Archivio et al., 2007). Based on the degree of oxidation of the central pyran ring, flavonoids are classified into six subclasses: flavones, flavonols, anthocyanidins, isoflavones, and flavanols (catechins and proanthocyanidins) (D'Archivio et al., 2007).

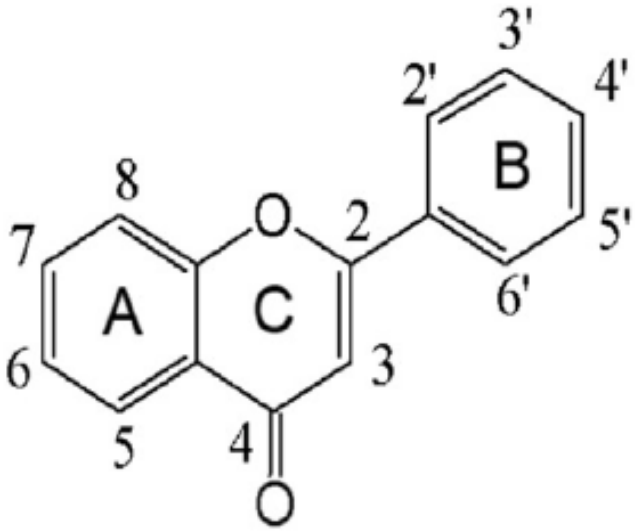

Figure 3.1: Flavonoids' structure (D'Archivio et al., 2007)

3.1.1.1 Flavonols

Flavonols, a specific subclass of flavonoids, are distinguished by the presence of a double bond between carbon atoms 2 and 3, as well as a hydroxyl group at the C3 position of the C ring. Prominent members of this subclass include myricetin, kaempferol, and quercetin, which are commonly found in various vegetables and fruits such as leeks, kale, onions, broccoli, apples, and cranberries (Alara et al., 2018).

3.1.1.2 Flavones

Flavones, a distinct subclass of flavonoids, are identified by the presence of a ketone at position 4 of the C ring and a double bond between positions 2 and 3 of the C ring. The arrangement of hydroxyl groups at other positions, particularly position 7 of the A ring or positions 3′ and 4′ of the B ring, may vary depending on the taxonomic classification of the specific vegetable or fruit. In most flavones found in vegetables and fruits, it is common to observe the presence of a hydroxyl group at position 5 of the A ring (Panche et al., 2016). Among the notable flavones are luteolin and apigenin (as illustrated in Figure 3.3), which are primarily sourced from sweet bell peppers, celery, and parsley (Alara et al., 2018).

3.1.1.3 Isoflavones

Isoflavonoids constitute a prominent and wide-ranging subclass of flavonoids, primarily sourced from soybeans and other leguminous plants. These compounds are characterized by their limited occurrence within the plant kingdom (Panche et al., 2016). Isoflavones, such as daidzein (depicted in Figure 3.4), bear a structural re-

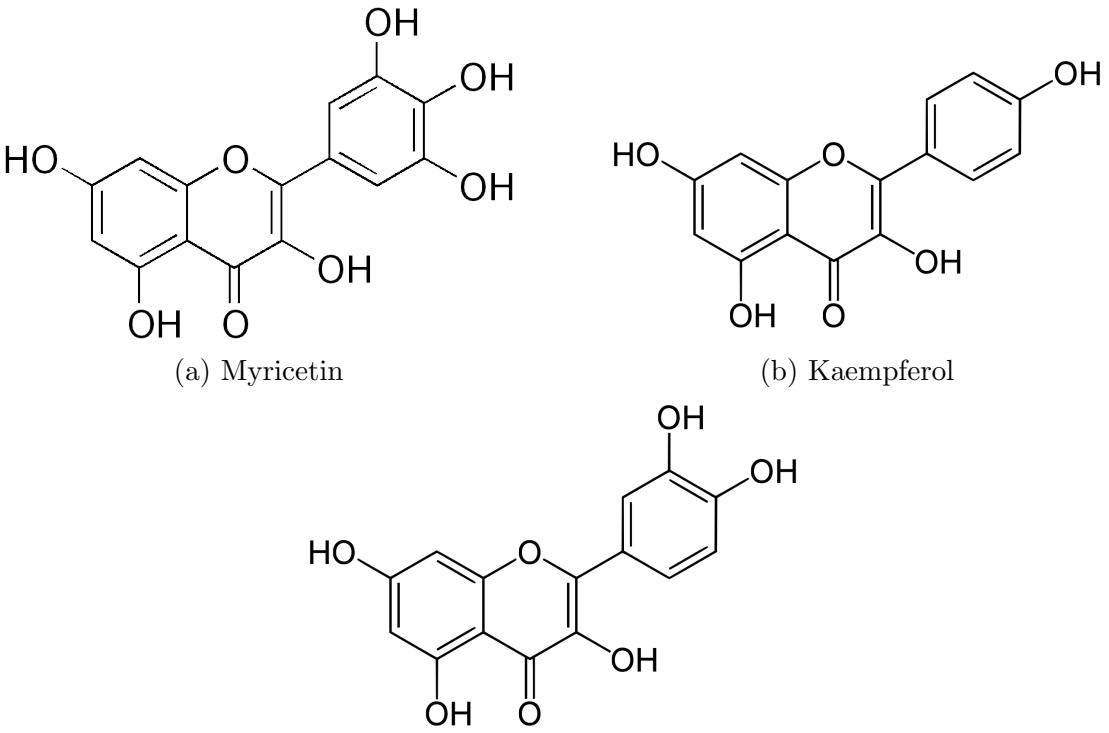

(a) Myricetin

(b) Kaempferol

(c) Quercetin

Figure 3.2: Structure of flavonols (Alara et al., 2018)

semblance to estrogens due to the presence of hydroxyl groups at positions C7 and C4, similar to the estradiol molecule (D'Archivio et al., 2007). They are classified as phytoestrogens, as they possess the capability to bind to estrogen receptors (D'Archivio et al., 2007).

3.1.1.4 Anthocyanidins

Anthocyanidins, which are soluble in water and serve as pigments, contribute to the blue, red, and purple observed in vegetables, fruits, flowers, and various other plant tissues (Pérez-Chabela and Hernández-Alcántara, 2018). These anthocyanidins naturally occur as glycosides, referred to as anthocyanins, and their number has surpassed 600 in identification (Tuladhar et al., 2021). The pigments are derived from six primary anthocyanidins, namely cyanidin (illustrated in Figure 3.5), pelargonidin, delphinidin, petunidin, peonidin, and malvidin, collectively responsible for more than 700 reported compounds (Celli et al., 2019).

3.1.1.5 Flavanols (catechins and proanthocyanidins)

Flavanols, also known as flavan-3-ols or catechins, are derivatives of flavanones with a hydroxyl group at position 3 of the C ring, distinguished by the absence of a double bond between positions 2 and 3 (Panche et al., 2016). Catechin, which has

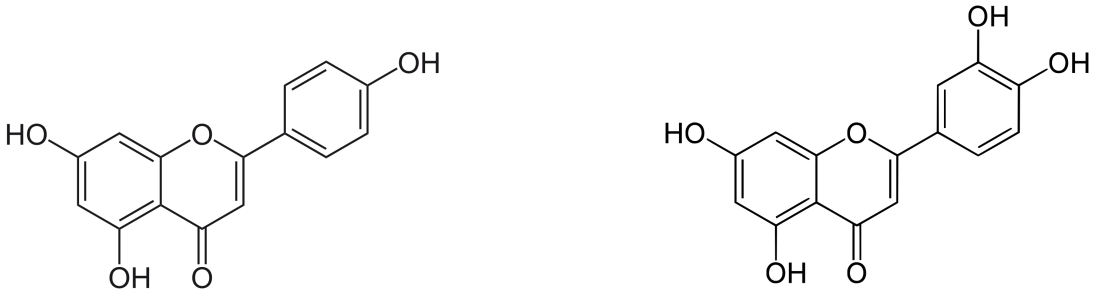

(a) (b)

Figure 3.3: Structure of apigenin (A) and luteolin (B) (Panche et al., 2016).

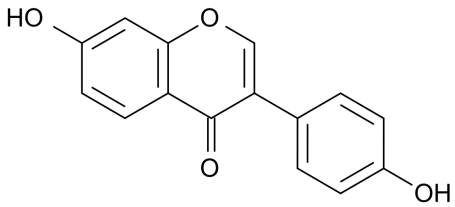

Figure 3.4: Daidzein's structure (Panche et al., 2016).

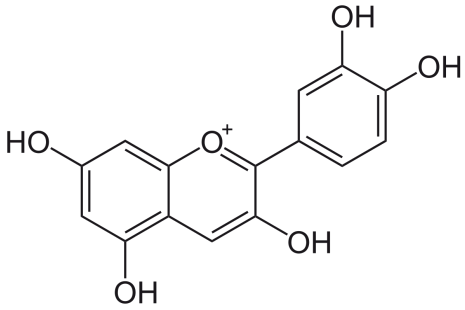

Figure 3.5: Structure of cyanidin (D'Archivio et al., 2007).

a trans-configuration, and epicatechin, which has a cis-configuration, are notable isomers found predominantly in the skins of grapes, apples, and blueberries (as depicted in Figure 3.6) (Pérez-Chabela and Hernández-Alcántara, 2018). Furthermore, proanthocyanidins, also classified as flavanols, are referred to as condensed tannins. These compounds, which include dimers, oligomers, and polymers of catechins, contribute to the astringent taste found in fruits, cider, tea, beer, and the bitterness of chocolate (Pérez-Chabela and Hernández-Alcántara, 2018).

3.1.2 Non-flavonoids

Non-flavonoid compounds, including phenolic acids, lignans, and stilbenes possess a distinct structural framework compared to flavonoids. Unlike flavonoids, which feature a carbon skeleton consisting of two aromatic rings, non-flavonoids are characterized by a single aromatic ring as their fundamental structure (Singla

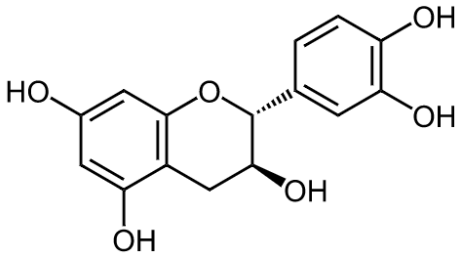

Figure 3.6: Structure of catechin (D'Archivio et al., 2007).

et al., 2019)

3.1.2.1 Phenolic acids (PAs)

Phenolic acids, which are widely distributed in the plant kingdom, are significant organic acids and serve as important secondary metabolites. There are two primary types of phenolic acids: hydroxybenzoic acids (HBA) and hydroxycinnamic acids (HCA) (Heleno et al., 2015). The key distinction between HBA and HCA lies in their chemical structure. HBAs feature a phenol ring with a carboxylic acid group (-COOH) attached to it (as illustrated in Figure 3.7a). On the other hand, HCAs possess a phenol ring with an unsaturated three-carbon chain (an acrylic acid side chain) attached to it (as depicted in Figure 3.7b) (Yusoff et al., 2022).

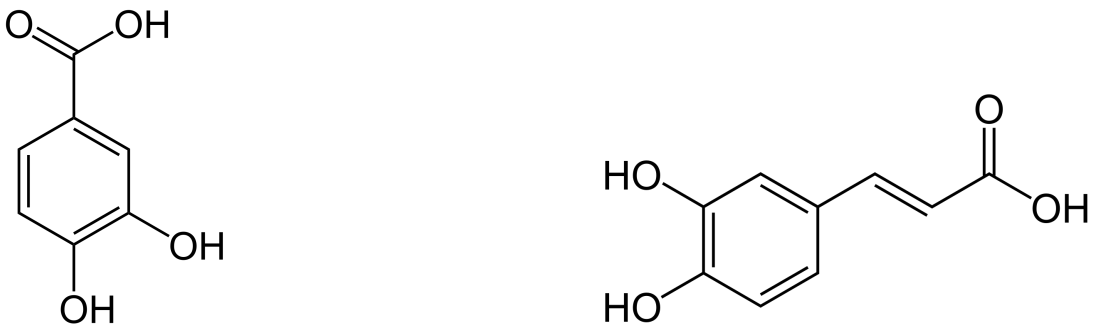

(a) (b)

Figure 3.7: Chemical structure of protocatechuic acid (a), and caffeic acid (b)(Heleno et al., 2015).

3.1.2.2 Stilbenes

Stilbenes possess a distinct C6-C2-C6 structure and exist in two isomeric forms. They are synthesized in plants as a response to various biotic and abiotic stresses, including microbial infections, high temperatures, and oxidative conditions. The primary role of stilbenes in many plants is to serve as phytoalexins, which are defensive substances produced in response to infections (Teka et al., 2022). Hydroxylated stilbenes, including (E)-resveratrol (Fig. 3.8), are present in a variety

of plant sources, such as grapes, berries, and peanuts. Resveratrol is recognized for its antioxidant and anti-inflammatory effects, and research has indicated that it may have a role in reducing inflammation and lowering blood pressure, potentially aiding in the prevention of heart disease (De Filippis et al., 2017).

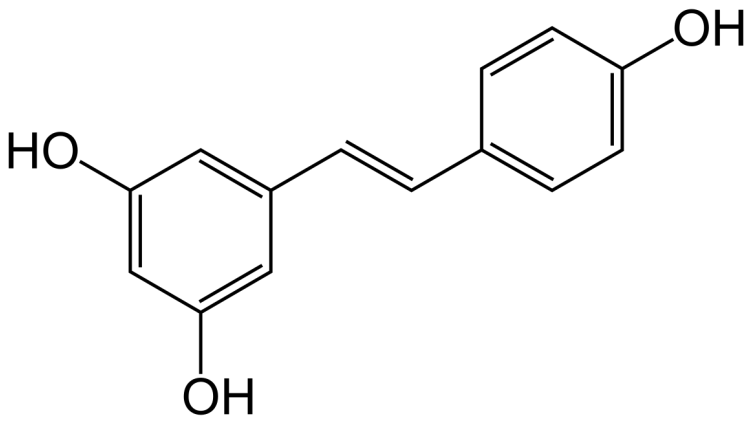

Figure 3.8: Chemical structure of resveratrol (De Filippis et al., 2017).

3.1.2.3 Lignans

Lignans, which are polyphenols derived from phenylalanine, are classified as phytoestrogens and are naturally present in plants. Plant lignans, including lariciresinol (as shown in Figure 3.9), can undergo metabolism by intestinal bacteria and exhibit antioxidant properties. Additionally, they have the ability to bind to estrogen receptors in breast tissue (Higuchi, 2014). Furthermore, lignans such as enterodiol and enterolactone have been demonstrated to act as cytostatic agents against colon cancer cell lines (Wcislo and Szarlej-Wcislo, 2014).

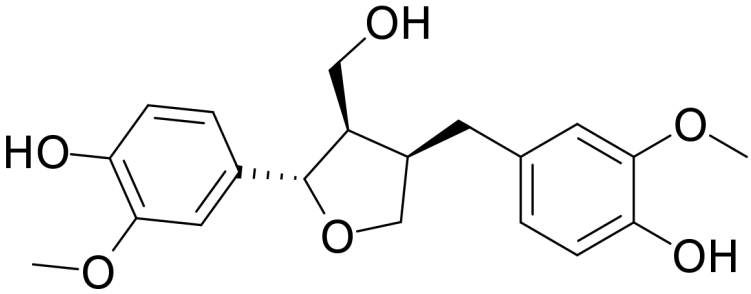

Figure 3.9: Chemical structure of lariciresinol (Higuchi, 2014).

3.2 Extraction aided by ultrasound technology (UAE)

3.2.1 Ultrasound's history

The origins of ultrasound can be traced back to Lazzaro Spallanzani (1794), an Italian physiologist who observed that bats used ultrasound to navigate in the dark. Spallanzani discovered this by studying bats' sensory abilities and noted that even when a bat was blind, it was still able to fly confidently. However, if a bat was deaf in one ear, it was unable to fly safely. Based on these observations, Spallanzani proposed that bats used sound rather than vision to navigate (Kane et al., 2004; Kaproth-Joslin et al., 2015).

For many years, the "Spallanzani's bat problem" remained a mystery in the scientific community until 1938 when two Harvard students, Donald Griffin, and Robert Galambos, proposed the concept of echolocation. They suggested that bats generate high-frequency clicks that bounce off objects in their surroundings, and then use the echoes to locate and navigate their environment with accuracy (Kane et al., 2004; Kaproth-Joslin et al., 2015).

In 1826: Jean-Daniel Colladon – A Swiss physicist and his assistant, Jacques Charles-Francois Sturm used a Church Bell (early ultrasound) under water to calculate the speed of sound through water and prove that sound traveled faster through water than air (Griffin and Galambos, 1941; Kaproth-Joslin et al., 2015).

Jacques (1856–1941) and Pierre (1859–1906) Curie were the first to discover piezoelectricity (1880), which is derived from the Greek term piezen, which means to press or squeeze. They proved that under pressure, crystals of tourmaline, quartz, topaz, cane sugar, or Rochelle salt can produce electricity (Manbachi and Cobbold, 2011; Mould, 2007). They also showed that under pressure, these crystals may produce pressure waves when a voltage is applied. These crystals' ability to transmit and receive pressure waves at megahertz frequencies permitted the development of current transducer technology (Kaproth-Joslin et al., 2015; Manbachi and Cobbold, 2011).

Following the sinking of the Titanic in 1912, physicist Paul Langevin invented the hydrophone, which served as the first transducer. This device was designed to detect icebergs and submarines during World War I. It consisted of quartz crystals affixed between two steel plates. Over time, this apparatus underwent improvements, particularly during World War II, leading to the emergence of the field now known as sonar (short for sound navigation and ranging) (Kaproth-Joslin

et al., 2015; Zimmerman, 2002).

3.2.2 Fundamental of ultrasonic assisted extraction (UAE)

3.2.2.1 Ultrasonic wave

UAE is crucial for the extraction of plants' bioactive substances. As shown in fig 3.10, there are two categories of ultrasound: low-power (high-frequency) ultrasound, also known as diagnostic ultrasound, and high-power (low-frequency) ultrasound, which has frequencies between 16 and 100 kHz (Lavilla and Bendicho, 2017; Mason and Peters, 2002). Diagnostic ultrasound or low power ultrasound (LPU) is frequently utilized in non-destructive analysis for quality assurance and process control purposes. In contrast, high power ultrasound (HPU)) finds widespread use in various industrial applications such as cleaning, homogenization, filtering, drying, defoaming, crystallization, sterilization, degassing, dispersion, oxidation, depolymerization, aerosol formation, chemical activation, soldering, erosion, and extraction (Lavilla and Bendicho, 2017; Rutkowska et al., 2017).

Ultrasound is a form of energy that travels through a medium in the form of pressure waves. These waves undergo cycles of compression and expansion, which are referred to as rarefaction cycles. When a liquid medium undergoes sonication, it experiences the presence of an acoustic pressure (P_a) in addition to the hydrostatic pressure (P_h) within the medium P_a responds to the following equation :

$$P_a = P_A \sin(2\pi f t) \tag{3.1}$$

P_A is maximum amplitude of wave; f is wave frequency (> 16 kHz); t is time (Lavilla and Bendicho, 2017; Mason and Peters, 2002).

During the compression phase of an ultrasound wave (positive pressure), the maximum pressure is achieved, while the rarefaction phase (negative pressure) corresponds to the minimum pressure. As a result, the pressure wave induces oscillation of molecules around their average position within a liquid medium (Lavilla and Bendicho, 2017; Mason and Peters, 2002).

Wave intensity (I) or energy transmitted per second and per cm^2 of fluid responds to the following equation:

$$I = P_A^2 (2\rho c) \tag{3.2}$$

ρ is the density of the medium; c is the sound velocity in the medium (Lavilla and Bendicho, 2017; Mason and Peters, 2002).

Ultrasonic waves experience attenuation as they penetrate a liquid medium, resulting in a reduction in intensity and some heat generation (which depends on the nature of the medium). This attenuation can be described by the following equation:

$$I = I_0\, e^{(-2\alpha d)} \tag{3.3}$$

I_0 is the initial intensity; α is the absorption; d is the distance coefficient (Lavilla and Bendicho, 2017; Mason and Peters, 2002).

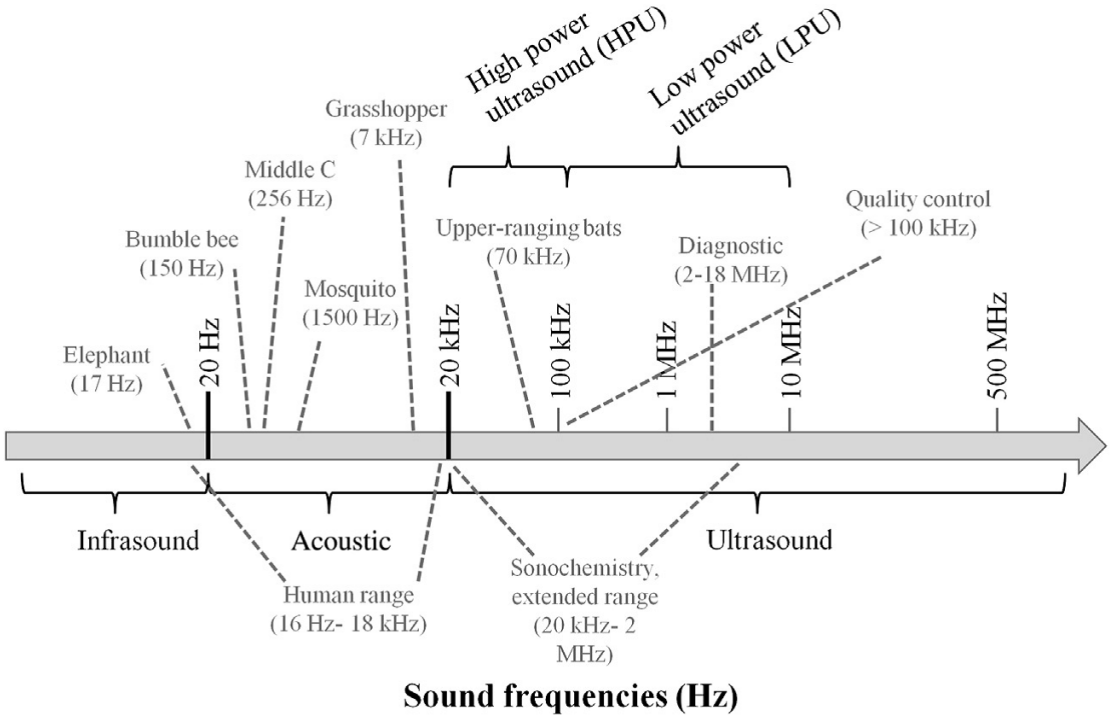

Figure 3.10: Sound frequency's ranges (Lavilla and Bendicho, 2017).

3.2.2.2 Cavitation phenomenon

The cavitation phenomenon, which depends on the formation of vapor bubbles, is primarily responsible for the effects of ultrasound (Lavilla and Bendicho, 2017; Rutkowska et al., 2017).

As stated earlier, during the compression phase, the molecules of the medium are brought closer together under positive pressure. Conversely, during the rarefaction phase, the molecules experience a negative pressure that causes them to separate. The negative pressure can be mathematically described using the following expressions:

$$P_c = P_a - P_h \tag{3.4}$$

$$p_c = 2\,\sigma / R \tag{3.5}$$

σ is the surface tension; R is the distance between molecules (Lavilla and Bendicho, 2017; Mason and Peters, 2002).

When ultrasound is applied with enough energy, the negative pressure (Pc) produced by the rarefaction cycles overcomes the attractive intermolecular forces, which induces cavities that form in the liquid medium (Lavilla and Bendicho, 2017; Mason and Peters, 2002; Suslick, 1989). It has been noted that producing enough negative pressure for pure liquids (those with high hydrostatic pressure) can be difficult depending on the type and purity of the liquid (Lavilla and Bendicho, 2017; Mason and Peters, 2002; Suslick, 1989). However, the cavitation threshold can be lowered by the contaminants, primarily gases and small particles (Lavilla and Bendicho, 2017; Mason and Peters, 2002; Suslick, 1989).

There are two main types of cavitation: transient and stable. Stable cavities are bubbles that undergo oscillations, often in a non-linear manner, around a certain equilibrium size. These bubbles are relatively long-lasting and can continue to oscillate for multiple cycles of the acoustic pressure (Neppiras, 1980). According to Lavilla and Bendicho (2017), stable cavitation generally arises at low intensities. In contrast, transient bubbles exist for a shorter duration, typically less than one cycle, during which they rapidly expand to more than double, and often many times their original size before violently collapsing and frequently breaking into a cluster of smaller bubbles (Neppiras, 1980). This transient cavitation can occur at high intensities ((Lavilla and Bendicho, 2017)).

3.2.2.3 UAE of secondary metabolites from plants matrices

During the compression and rarefaction, the cavitation phenomena were generated leading to the formation of the cavitation bubbles in the liquid medium (Fig. 3.12). These bubbles collapse during the compression phase, leading to the creation of hot spots and extreme local conditions. In these regions, temperatures can rise up to 5000 K, and there can be a significant increase in pressure, reaching up to 1000 atm (Kumar et al., 2021; Rutkowska et al., 2017) (Fig. 3.12). Asymmetrical micro-jets and shock waves are produced when cavitation bubbles burst close to solid surfaces due to the release of high pressure and temperature (Kumar et al., 2021; Rutkowska et al., 2017).

These latter accelerated inter-particle collisions cause the fragmentation in cellular structure (Fig. 3.12). Rapid fragmentation first allows solvent to enter the matrix, reducing particle size and improving solvent penetration. It then allows

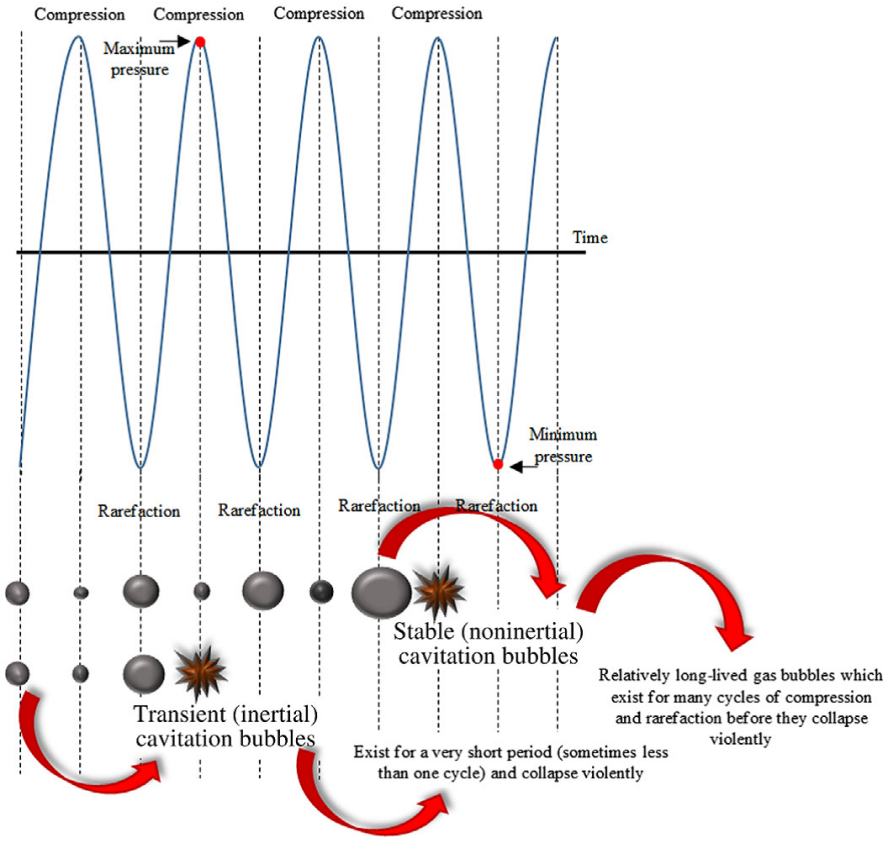

Figure 3.11: Generating cavitation phenomena throughout compression and rarefaction cycles (Rutkowska et al., 2017).

extracts to be released from the matrix (larger contact surface area between the solid/liquid phases) (Kumar et al., 2021; Rutkowska et al., 2017) (Fig. 3.12). The enhanced solubilization of bioactive compounds from plant matrices, resulting in higher product yields, can be primarily attributed to the benefits of UAE. These advantages include the reduction of particle size, increased surface area, and high rates of mass transfer in the boundary layer of the solid matrix (Kumar et al., 2021; Rutkowska et al., 2017).

3.2.3 Laboratory and industrial ultrasonic extraction

In the laboratory, two ultrasonic devices, namely a cleaning bath and a probe-type ultrasonic, were utilized to extract bioactive compounds from medicinal plants. The cleaning bath ultrasound allowed for both direct and indirect extraction methods, as demonstrated in Fig. 3.13, with multiple ultrasonic transducers positioned at the bottom and sides of the extraction vessel, as illustrated in Fig. 3.14 (Vinatoru, 2001). Piezoelectric and electromagnetic transducers were highly used in UAE, When the transducers are not in direct contact with the sample, there are large acoustic energy losses to the vessel and surroundings. However, when

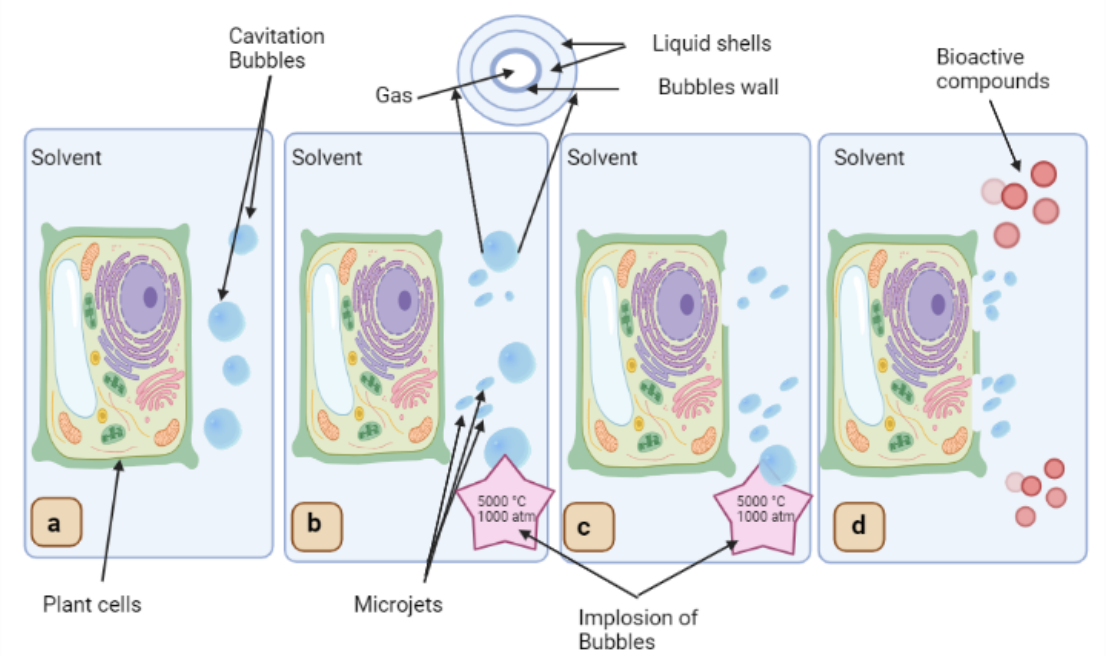

Figure 3.12: The process of ultrasound-assisted extraction for obtaining bioactive compounds from plant cells involves several stages. (a) Cavitation bubbles form near the surface of the plant cells. (b) These bubbles collapse, leading to the release of a micro-jet that applies pressure and temperature to the cell surface. (c) As a result, the plant cell walls rupture, enabling direct contact between the bioactive compounds inside the cells and the surrounding solvent. (d) Finally, the bioactive compounds are released from the plant cells and become accessible outside (Kumar et al., 2021; Rutkowska et al., 2017).

the transducers are in direct contact with the sample, the extraction efficiency is enhanced, and at the same time, acoustic energy losses are minimized (Frost, 1979; Tiwari, 2015). The use of sonication on the probes/horn is also widespread for the extraction of bioactive compounds from medicinal plants (Fig. 3.15), the ultrasonic probe operates as a direct sonication in which the energy is applied directly to the sample, and energy losses are minimal, in comparison with ultrasonic bath, this system provides higher power intensity, approximately 100 times higher (Nowacka and Dadan, 2022)

For industrial large-scale extraction, the Romanian team designed and built the first industrial ultrasonic reactor under a EUCOPERNICUS program (1995), where the reactor with $1m^3$ capacity (700 to 850 L working capacity) was used for solvent extraction of herbs as mentioned in fig. 3.16a (Vinatoru, 2001). Furthermore, Valachovic et al. (2001) used an industrial ultrasonic probe operating at 20 kHz (600 W) supplied by Ultragen Nitra (acoustic horn with 97 cm of height and 5 cm of diameter) was applied to produce the medicinal tincture from *Salvia officinalis* L. and *Valeriana officinalis* L (Fig. 3.16b). Moreover, many companies

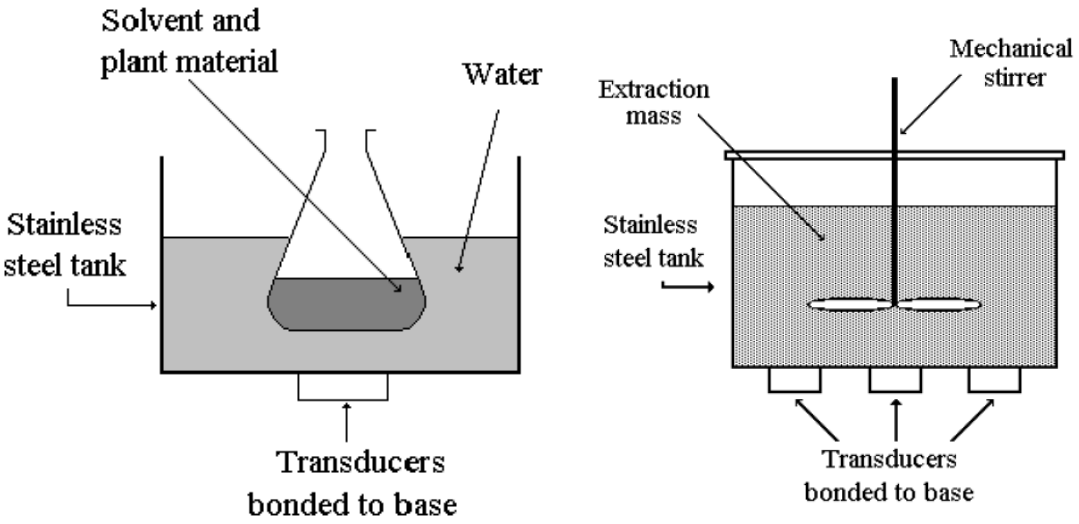

Figure 3.13: Ultrasound-assisted extraction types in cleaning bath ultrasound: (a) Indirect Extraction, (b) Direct extraction with mechanical stirring (Vinatoru, 2001).

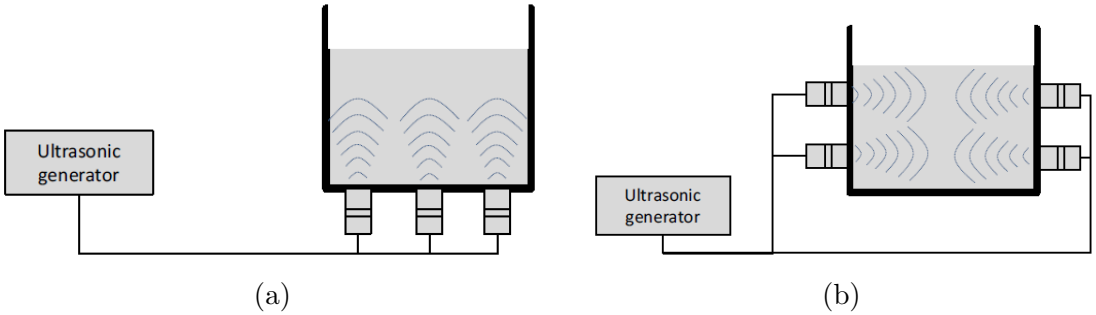

Figure 3.14: Placement schematic of an ultrasonic transducer in bath system: (a) Bottom placement of ultrasonic transducer, (b) Side placement of ultrasonic transducer (Tiwari, 2015).

developed large-scale ultrasound (bath and ultrasonic probe) such as Hielscher (Germany), REUS (France), Euphytos, Giotti, GMC (G. Mariani & C. Spa) company (Chemat et al., 2017). Paolo and Cravotto (2012) designed and patented a continuous sono-reactor operating at continuous mode at higher acoustic power density as depicted in Fig. 3.16c.

3.2.4 Factors contributing to UAE of secondary metabolites

The application of ultrasonic-assisted extraction (UAE) has demonstrated notable advantages over conventional techniques. However, the effectiveness of UAE relies on the optimization process, which is vital for reducing material and solvent waste and obtaining a substantial yield of phenolic compounds with superior quality. To

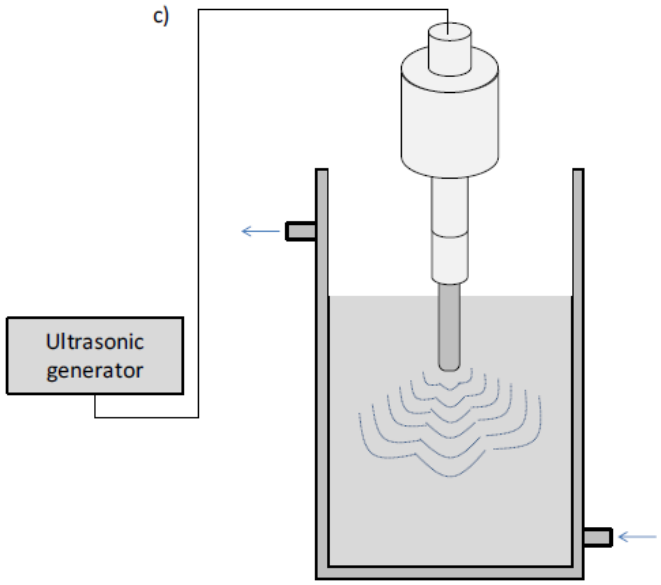

Figure 3.15: Illustrative scheme of an Ultrasonic Probe (Tiwari, 2015).

achieve successful extraction of TPC, it is crucial to optimize various parameters such as extraction time, frequency, power, temperature, and solvent-to-solid ratio, as they significantly impact the efficiency of the extraction process.

3.2.4.1 Ultrasonic power

The ultrasound power delivered during the extraction process is commonly represented as an amplitude percentage ranging from 0 to 100%, and as power density ($W\,mL^{-1}$), which is calculated by dividing the power dissipated by the volume of the extraction medium (Kumar et al., 2021). Studies have shown that the yield of UAE increases initially with an increase in ultrasonic power and then declines after reaching a maximum point. This behavior can be attributed to the intensified effect of the cavitation bubble collapse caused by higher ultrasonic power. There is a positive correlation between resonant bubble size and ultrasonic power, meaning that as the bubble size increases, the implosion effect also intensifies (Kumar et al., 2021). However, it has been noted that at high ultrasonic power levels, the production of hydroxyl radicals ($OH^{\bullet}$) may occur, which can react with secondary metabolite and lead to their degradation, particularly when there is a high-water content present (Dzah et al., 2020).

3.2.4.2 Frequency of ultrasonic

The most often used ultrasonic frequencies for ultrasound-assisted extraction are between 20 and 100 kHz (1 Hz = 1 cycle per second) (Rutkowska et al., 2017).The extraction process is notably influenced by the frequency of ultrasound, as it plays

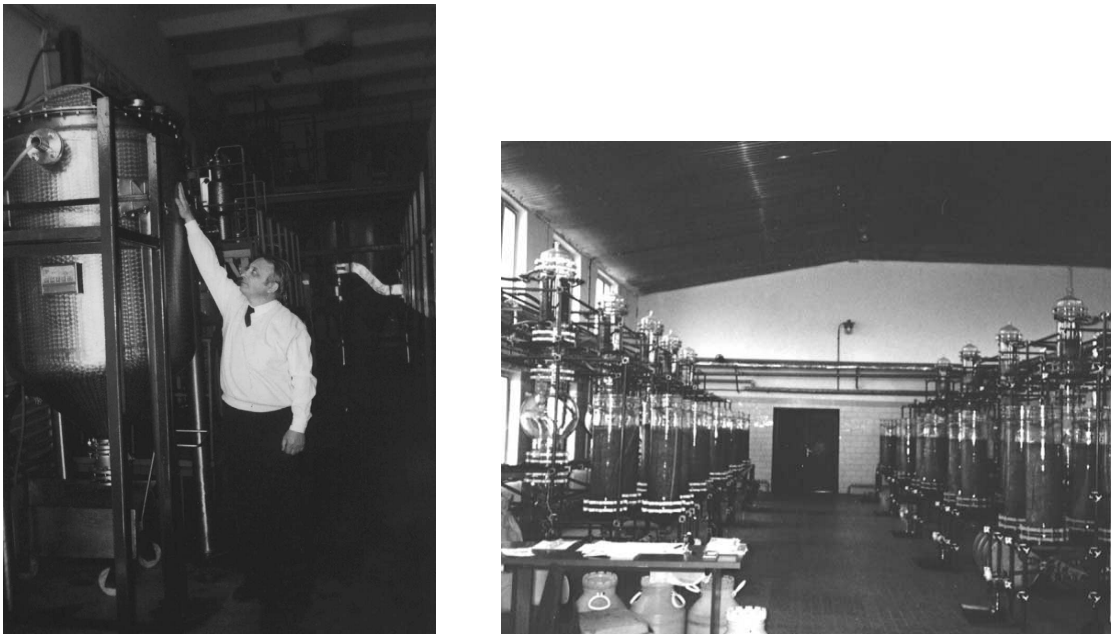

(a) (b)

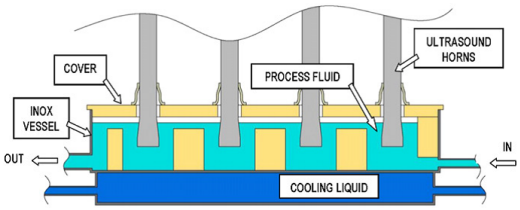

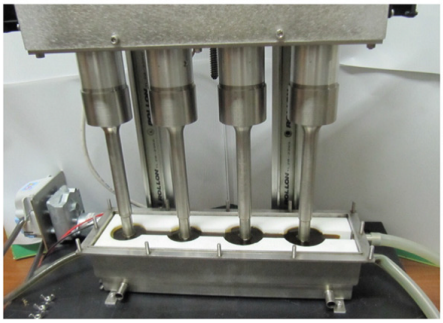

(c)

Figure 3.16: Pilot reactor used for industrial-scale extraction, (a): Ultrasonic bath, (b): Ultrasonic probe, (c): Multi-horn flow reactor (Paolo and Cravotto, 2012; Valachovic et al., 2001; Vinatoru, 2001).

a crucial role in determining the size of microbubbles and affecting mass transfer resistance. When the frequency of ultrasound is increased, there is a decrease in the production and intensity of cavitation within the liquid (Esclapez et al., 2011; Rutkowska et al., 2017). The occurrence of the cavitation phenomenon becomes challenging at high frequencies, as the compression-rarefaction cycles may become too short to achieve the necessary size of microbubbles. Consequently, the duration of the rarefaction phase is inversely proportional to the ultrasound frequency (Rutkowska et al., 2017). Furthermore, the selection of ultrasound

frequencies, in combination with the intensity of ultrasound, serves as a means to control the formation of cavitation bubbles to ensure the desired level of cavitation is achieved (Tiwari, 2015).

3.2.4.3 Solvent used in ultrasonic extraction

Cellular distribution of secondary metabolites is determined by their solubility, which is dictated by their polarity. Hydrophilic compounds are predominantly found in cell vacuoles, whereas hydrophobic substances like lignins, flavonoids, and water-insoluble polyphenols tend to accumulate in the cell wall through hydrophobic interactions with proteins and polysaccharides. Hence, the choice of extraction solvent is crucial and should be based on the solubility of the specific compounds targeted in the extraction process (Medina-Torres et al., 2017). Due to the diverse polarity of secondary metabolites and their compatibility with human consumption, hydro-alcoholic combinations, specifically ethanol, have been identified as the most suitable solvent systems for extraction (Berkani et al., 2020; Chen et al., 2015; Muniz-Marquez et al., 2013).

Furthermore, the cavitation process is notably affected by the physical characteristics of the solvent, including surface tension, viscosity, and vapor pressure Wen et al. (2018). In general, an increase in vapor pressure and surface tension of the solvent leads to a decrease in the intensity of cavitation Wen et al. (2018). Higher vapor pressures enable the volatilized solvent to readily penetrate cavitation bubbles, thereby cushioning their collapse. This phenomenon suggests that less expensive solvents, such as water mixtures, might exhibit improved performance compared to volatile pure solvents typically employed in conventional extraction methods (Esclapez et al., 2011).

3.2.4.4 Liquid to solid ratio

The ratio of solid-to-solvent is an essential parameter in UAE and deserves careful consideration. When a fixed amount of solid matrix is used, increasing the amount of solvent leads to a greater concentration gradient between the plant material and the solvent. Consequently, this concentration gradient facilitates a faster extraction rate (Esclapez et al., 2011). By employing a higher solvent-to-material ratio, the mixture density decreases, leading to an increase in the velocity (v) at which ultrasound waves propagate. Consequently, this reduces the attenuation of ultrasound power (p) and enhances the transfer of energy (E) over distance covered (d) per unit of time (t). This relationship can be quantified using the following equation.:

$$p = K_{(\imath/\rho)}[(E * v)/d] \tag{3.6}$$

where $\imath$ is material stiffness

Because of the lower mixture density, there is a more effective transfer of energy, which improves extraction efficiency. Additionally, the decreased mixture density enhanced the cavitation phenomenon (Dzah et al., 2020).

3.2.4.5 UAE Temperature

Temperature is one of the main extraction parameters involved in the UAE. In general, a high temperature of solvent during extraction increases the diffusion rate and helps to break the interaction between the phenolic compounds and matrix, increase the compound solubility, enhance mass transfer, reduction in viscosity and tension of the solvent (Medina-Torres et al., 2017). However, higher extraction temperatures decrease cavitation phenomena because voids are filled by solvent vapors, resulting in a less violent collapse; whereas, lower temperatures allow cavitation bubbles to collapse violently because the solvent's vapor pressure is low (Tiwari, 2015).

3.2.4.6 Sonication time

For any UAE process, there is an optimum UAE time. Beyond this time, the extractable phenolic compounds can be degraded (Tiwari, 2015). The extraction of TPC from plant matrices using ultrasound is followed by two main stages. In the first step, which is referred to as the "washing" step, the soluble components on the matrix's surfaces are dissolved during the period of 10 to 20 minutes of UAE, where up to 90% of TPC can then be recovered, demonstrating a significantly fast extraction rate. During the "slow extraction" stage, the solute undergoes mass transfer and osmotic processes as it diffuses from the matrix into the solvent. This stage typically lasts for a duration of 60 to 100 minutes (Sahin and Samli, 2013).

3.2.5 UAE Optimization of secondary metabolites

As previously discussed, the efficacy of UAE in secondary metabolites is significantly impacted by several extraction parameters, including power, frequency, solvent-to-solid ratio, temperature, and time. While these effects have been individually discussed, it is crucial to emphasize that they interact with each other throughout the extraction process. The outcome of this interaction is reflected in

both the quantity and quality of the extracted phenolic compounds.

The optimization of ultrasound-assisted extraction of bioactive compounds was performed using several designs of experiments, in which different optimal extraction conditions were obtained (Table 3.1). Based on the previous works, hydro-ethanol (30% to 80%) as green solvent was the most employed for the extraction of bioactive compounds including antioxidant activity from different plant matrices (Table 3.1). Furthermore, sonication time ranged from 15 min to 60 min, temperature from 30 to 60°C, and solid-to-solvent ratio ranged from 1/20 to 1/50 $g\,mL^{-1}$, these variations of extraction parameters depended on the nature of plants matrices, target compounds, type of ultrasound device (probe or bath), and the characteristic of ultrasound used in the extraction process (frequency, power) (Table 3.1).

Table 3.1: Optimization of UAE parameters for high yield of bioactive compounds: Experimental Design Approach

				Optimal conditions for UAE of secondary metabolites				
DOE used	Characteristic of material	Target compounds	Solvent used	Time	Temperature	Ratio solid-liquid	Concentration of solvent	References
CCD	35 KHz	TPC	Ethanol	45 min	60 °C	5 % of plant concentration	/	(Tekin et al., 2015)
BBD	100 W 40 kHz	TPC	Ethanol	29.9 min	60 °C	NS	76.8 %	(Arteaga-Crespo et al., 2020)
BBD	40 KHz, IP (500 W), HP (800 W)	puerarin	Ethanol	49.08 min	/	21.72 $mL\,g^{-1}$	71.35 %	(Wu et al., 2012)
BBD	40 KHz, IP (500 W), HP (800 W)	TI	Ethanol	55 min	/	12.81 $mL\,g^{-1}$	80 %	(Wu et al., 2012)
CCD	150 W, 25 KHz	TPC yield flavonones	Ethanol	30 min	40 °C	0.25 $g\,mL^{-1}$	80 %	(Khan et al., 2010)
BBD	25 KHz, 300 W	TPC	Ethanol	40 min	ambient	19.21 $mL\,g^{-1}$	75.3 %	(Wang et al., 2013)
CCD	40 KHz, 250 W	TPC	Ethanol	25 min	60 °C	1/20 $g\,mL^{-1}$	64 %	(Wang et al., 2008)
CCD	25 KHz, 150W	TPC, TFC	Ethanol	15 min	30 °C	1/50 $g\,mL^{-1}$	/	(Rodrigues et al., 2008)
BBD	100 W	TPC, AA	Ethanol	30 min	50 °C (Fixed)	1/40 $g\,mL^{-1}$	33 %	(Chen et al., 2018)
BBD	400 W	TPC TA	Ethanol	23.67 min	61.03 °C	21.07 $g\,mL^{-1}$	70 %	(He et al., 2016)
CCD	250 W, 40 KHz	TPC	Ethanol	29.03 min	56.03 °C	1/50 $g\,mL^{-1}$	53.15 %	(Ghafoor et al., 2009)
BBD	150 W, 50Hz	TPC AA	Ethanol	60 min	60 °C	1/50 $g\,mL^{-1}$	70 %	(Dang et al., 2017)

TPC: Total phenolic compounds, TFC: Total flavonoids content, AA: antioxidant activity, TA: Total anthocyanin, TI: Total isoflavone, NS: Not significant IP: Input power, HP: Heating power

3.3 Microwave assisted extraction (MAE)

3.3.1 Microwave's history

Microwave radiation has been employed as a heating method for many years. A serendipitous finding occurred in 1946 during the laboratory testing of a new vacuum tube called a magnetron. Dr. Percy Le Baron Spencer made an accidental discovery when he observed that a candy bar in his pocket melted upon exposure to microwave radiation. After initially discovering that microwaves could be used for heating, Dr. Spencer further developed the idea and eventually demonstrated its feasibility. Then, in 1947, he designed and produced the first-ever microwave oven intended for domestic use. In the last few years, the microwave has been extensively employed for several purposes in analytical laboratories including drying, moisture measurements, extraction of primary and secondary metabolites from plant matrices, chromogenic reactions, and nebulization of sample solutions (Chaturvedi, 2018).

3.3.2 Fundamentals of microwave heating

Microwaves (MW) are a segment of the electromagnetic spectrum that encompasses wavelengths ranging from 1 meter to 1 millimeter and frequencies between 300 MHz and 300 GHz. Microwave (MW) energy is within the range of $1.24 * 10^{-6}$ to $1.24 * 10^{-3}\, eV$, which is considerably lower than the ionization energies of biological compounds ($(13.6\, eV)$), bond energies ($2\, to\, 5\, eV$), and van der Waals intermolecular interactions ($< 2\, eV$). As a result, MW is categorized as non-ionizing radiation that does not cause any significant impact on the molecular structure (Alvi et al., 2022; Flórez et al., 2015).

The ability of a material to interact with electromagnetic energy can be measured by the relative permittivity, a dimensionless value expressed as

$$\epsilon = \epsilon^{'} - j\, \epsilon^{''}$$

Let j denote the imaginary unit. The dielectric constant $\epsilon^{'}$ is a parameter that quantifies the ability of a dielectric material to store electrical energy, specifically its ability to polarize in response to an electric field. Dielectric compounds with significant permanent dipole moments tend to exhibit higher dielectric constants. The dielectric loss or loss factor, denoted as $\epsilon^{''}$, represents the imaginary component that reflects the relaxation time or delay between the electric field and the polarization movement of molecules. This delay results in energy dissipation in the

Table 3.2: Physical parameters of common solvents used in microwave applications (Desai et al., 2010; Teo et al., 2013)

Solvents	Dipole moment at 20 °C (debye)	Dielectric constant at 20°C	Dissipation factor at 2.45 GHz
Acetonitrile (ACN)	3.44	37.5	/
Ethyl acetate	1.88	6.02	/
Water	1.84	80.4	0.123
Methanol	1.70	33.7	0.659
Ethanol	1.69	25.7	0.941
1-Butanol	1.66	/	0.571
Acetone	/	21.4	/
Diethyl ether	/	4.389*	/
Chloroform	/	4.8	/
Hexane	<0.1	1.88	/

*at 18°C.

form of heat (Flórez et al., 2015; Martin and Navarrete, 2018). The effectiveness of MW heating at a specific frequency and temperature relies on the material's capacity to absorb electromagnetic energy and release heat. This characteristic can be evaluated by:

$$\tan\delta = \epsilon'/\epsilon$$

Materials can be categorized based on their microwave absorbing capabilities, determined by the value of the loss tangent ($\tan\delta$). High absorbing materials are characterized by ($\tan\delta > 0.5$), medium absorbing materials fall within the range of ($0.5 \geq \tan\delta \geq 0.1$), while low absorbing materials exhibit ($\tan\delta < 0.1$). (Flórez et al., 2015; Martin and Navarrete, 2018).

Solvents that possess both a high dielectric constant and dissipation factor have the ability to effectively distribute heat throughout a given matrix, ultimately leading to an increase in the extraction yield of solutes. Water, in particular, stands out as a solvent with a high dielectric constant and low dielectric loss when compared to other alcoholic solvents (see Table 3.2). This characteristic results in a higher rate of microwave energy absorption by water, rather than the dispersion of this energy as heat. In contrast, non-polar solvents, with their low dielectric constant and dissipation factor, remain transparent to microwaves and do not experience significant heating during microwave irradiation(Flórez et al., 2015; Martin and Navarrete, 2018). Table 3.2 shows the common solvents used in MW application with their dipole moments, dielectric constants, and dissipation factors.

3.3.3 Configuration and instrumentation in MAE systems

Most microwave devices typically comprise four main components, namely a magnetron which serves as the source of radiation, a waveguide responsible for transmitting the microwave energy from the magnetron to the microwave cavity, an applicator that houses the sample, and circulators that help to reflect and homogenize the microwave radiation (Desai et al., 2010). The operational compartment of an MAE system is designed to receive the microwave radiation produced by the magnetron and delivered through the waveguide. The radiation is then uniformly distributed to prevent the occurrence of standing waves (Kubrakova and Toropchenova, 2008). The equipment can be classified into multimode and monmode systems (systems with focused radiation) depending on how MW radiation is distributed; in a multi-mode system, MW radiation propagates through a large MW chamber, reflects off the walls, and is homogenized by circulators (Akhtar et al., 2019).

In laboratory settings, there are generally two primary configurations of microwave systems utilized for extracting bioactive compounds from medicinal plants. These are typically either closed extraction vessels or open microwave ovens (Llompart et al., 2019). The modern MW system that is enclosed operates using a feedback mechanism that includes temperature and pressure sensors. This system functions by switching off the magnetron when the specified temperature or pressure level is attained and then turning it back on to maintain the desired temperature or pressure while in continuous operation mode (Kubrakova and Toropchenova, 2008). Hence, closed-vessel systems offer several advantages. Firstly, the vessel's increased pressure enables quick attainment of higher temperatures. Secondly, volatile compounds are not lost into the environment but instead are retained as part of the extract. Thirdly, closed systems have a lower risk of contamination. Fourthly, since the solvent is not evaporated during heating, a minimal amount of solvent is required for the procedure. Finally, procedures such as acid digestions are made safer since fumes do not escape, making them easier to handle (Akhtar et al., 2019).

Recently developed multimode MAE systems have the capability to extract as many as 40 samples simultaneously in just 10 to 15 minutes, as illustrated in Fig. 3.17. The modern MAE platforms are equipped with two magnetrons, enabling extraction at up to 2000 W. Additionally, an autosampler is integrated into these systems to allow for the extraction of sequences samples. This feature greatly speeds up the method optimization process since each extraction can be performed under different experimental conditions (Llompart et al., 2019).

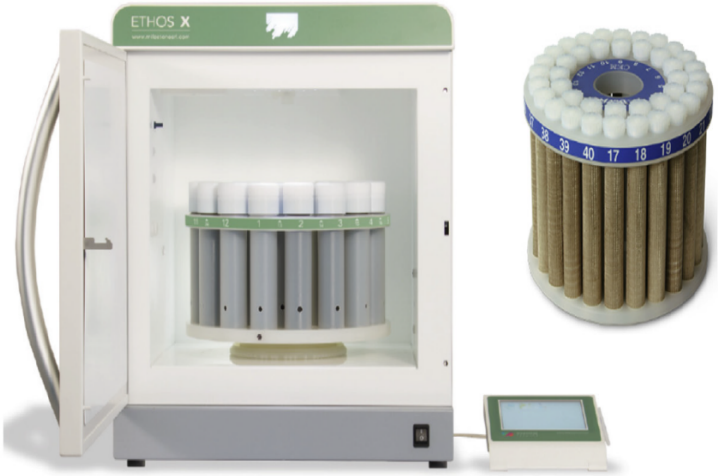

Figure 3.17: A milestone commercial MAE instrument with 40-position carousel for closed-vessel microwave-assisted extraction (MAE) (Llompart et al., 2019)

In addition, an open MW system comprises a focused microwave source where the microwave wave-guide acts as the applicator, and the extraction vessels are placed directly in the cavity and a water condenser. Due to the transparency of glass to microwaves, the upper portion of the vessel remains cool while only a small portion of the bottom is exposed to the microwaves (Delazar et al., 2012) (Fig. 3.18). The configuration of this open system offers more safety than the closed MW systems because they can be operated at atmospheric pressure. Nonetheless, open systems offer less temperature control than closed systems and cannot carry out multiple experiments concurrently (Delazar et al., 2012).

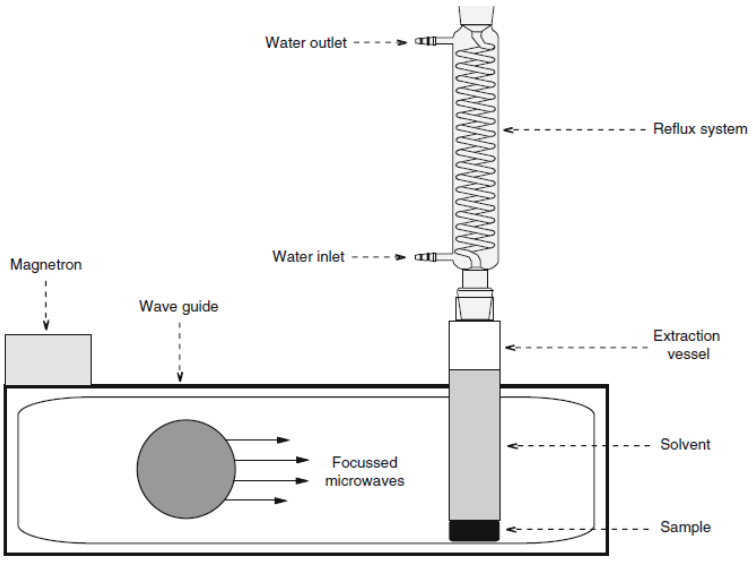

Figure 3.18: Illustration of an Open-Vessel Microwave-Assisted Extraction (MAE) System: Schematic Overview (Delazar et al., 2012)

3.3.4 Factors affecting MAE of plant matrix

3.3.4.1 Solvent nature and solvent-to-solid ratio

Choosing the most suitable solvent for MAE of secondary metabolites relies on several considerations. These include the dielectric constant of the solvent, its capacity to penetrate and interact with the plant matrix, as well as the solubility of the targeted secondary metabolites. The incorporation of water into the solvent system can enhance the efficacy of Microwave-Assisted Extraction (MAE) by improving the penetration of the solvent into the plant. This, in turn, enhances the efficiency of heating during the extraction process. Moreover, the quantity of solvent to plant matrix is also considered the most significant factor in MAE, where an optimum solvent-to-solid ratio provides homogeneous and effective heating (Chan et al., 2011). Many studies have shown that excessive amounts of solvent in the extraction medium can lead to inadequate microwave heating, as the solvent absorbs the microwave radiation and necessitates the use of additional power. Conversely, a low liquid-to-solid ratio creates a mass transfer barrier where the distribution of secondary metabolites becomes concentrated in specific regions of the cell plant. This concentration hinders the movement of these compounds out of the matrix, restricting their extraction (Mandal and Mandal, 2010).

3.3.4.2 Extraction time and cycle

For MAE, heating time is a highly sensitive parameter, where the extraction of plant's bioactive compounds can be enhanced with the optimization of extraction time. It has been reported that the MAE time could increase the yield of extracted bioactive compounds until the optimum point after that degradation of these compounds may occur with overheating of the solute/solvent system (Routray and Orsat, 2011). The dielectric properties of the solvent also impact the irradiation time, especially when exposed to solvents such as water, ethanol, and methanol over prolonged periods. Such extended exposure can lead to significant heating, potentially compromising the stability of thermolabile compounds (Mandal et al., 2007).

3.3.4.3 Temperature and microwave power

The relationship between microwave power and temperature is significant for MAE of bioactive compounds from plant matrices. Higher microwave power and temperature can promote the desorption of analyte from the plant matrix, leading to improved extraction efficiency in the MAE process (Bagade and Patil, 2021). Nevertheless, exceeding the optimal threshold of temperature and microwave power

can lead to a decrease in extraction yield due to the degradation of thermally sensitive compounds (Chan et al., 2011).

Part II

Materials and methods

Chapter4

Materials and Methods

In order to valorize the medicinal plants of the Bouira region, two species were selected including *C. caeruleus* L. (rhizome), and *S. officinalis* L. (leaves), these two plants have been frequently used for treating many diseases and pathological issues such as inflammation, gastric disorders, burns, and wounds. As illustrated in the flowchart (Fig.4.1), the two plants were cleaned and dried for the extraction of bioactive compounds and evaluation of their biological activities.

The optimization of TPC and TSC extraction from *C. caeruleus* L. (rhizome) was carried out using UAE with the aid of Box-Behnken design (BBD) and response surface methodology. The resulting data were then utilized to develop a predictive support vector regression optimized using dragonfly algorithm (SVR-DA) model, which serves as an interface for estimating the TPC and TSC levels in the rhizome extract. The antioxidant activity of the optimized UAE extract was evaluated using various methods, including $DPPH^{\bullet}$ and $ABTS^{\bullet+}$ free radical scavenging activity, TAC, and ferric reducing power (Fig. 4.1). Moreover, the antioxidant activity of the optimized rhizome extract was compared to that of the leaf extract of the same plant.

On the other hand, *S. officinalis* L. leaves also followed the same procedures, the optimization of UAE and MAE was carried out using new classes of designs of the experiment. Definitive screening design, and I-optimal design were employed for screening and optimization of TPC, TEAC, and TAC respectively of both MAE and UAE extracts. Moreover, Differential analysis using ultra high performance liquid chromatography combined with high resolution mass spectrometry (UHPLC-HRMS) was carried out to study the effect of MAE and UAE on the phenolic profiles of each extract (Fig. 4.1).

All the steps mentioned above in this work were carried out in the laboratories of the faculty of Biological sciences and faculty of agronomic sciences of Bouira

University.

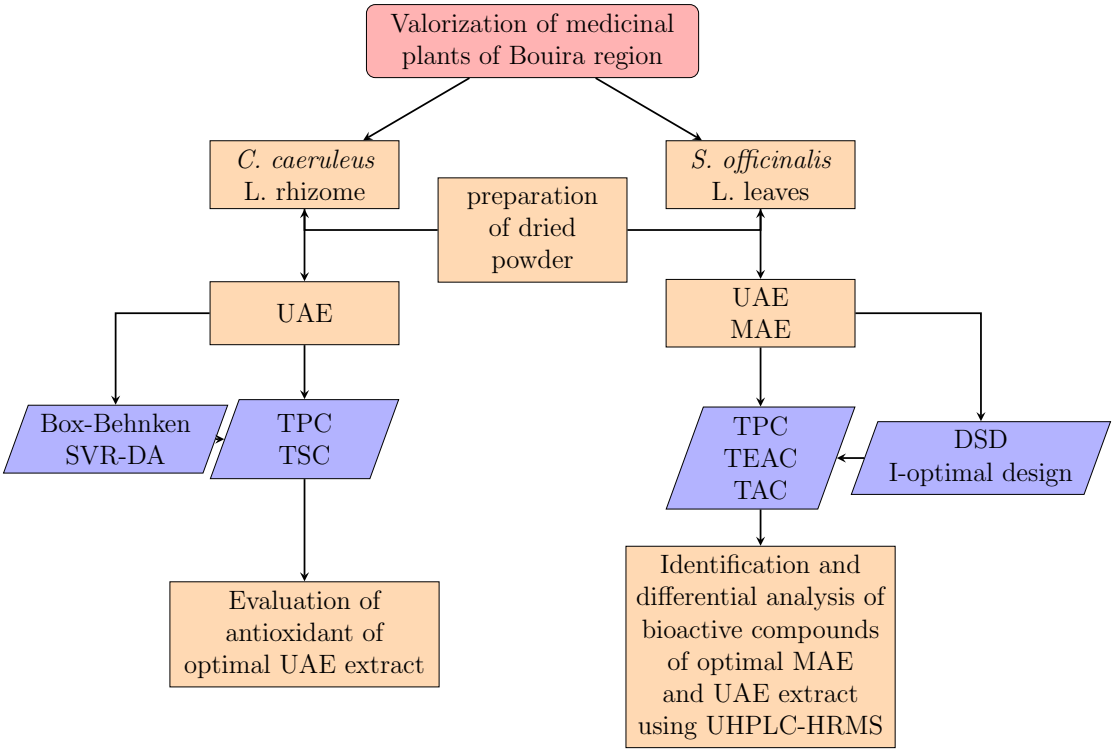

Figure 4.1: Optimization flowchart for UAE and MAE of bioactive compounds from medicinal plants of Bouira Region.

4.1 Reagents

All the analytical-grade reagents used for the optimization of UAE and MAE of bioactive compounds from *C. caeruleus* L. rhizome and *S. officinalis* L. leaves, as well as those used for the evaluation of biological activities are listed in table 6.12.

4.2 Preparation of sample

This study focused on two medicinal plants, namely *C. caeruleus* L. (both rhizome and leaves) and *S. officinalis* L. (leaves only). The rhizome and leaves parts of *C. caeruleus* L. were gathered from Ain Bessem province in the Bouira region (latitude 36.381707, longitude 3.711553, altitude 798 m) in February 2019. In contrast, the fresh leaves of *S. Officinalis* L. were collected from Ain Bessem province (latitude 36.325295; longitude 3.674675, altitude 690 m) in the Bouira region in April 2021.

The rhizome and leaves of the chosen plants were washed with distilled water to eliminate any impurities. Then, the rhizome was sliced into 1 mm thick pieces

and both the rhizome slices and leaves were dried using absorbent paper to remove excess water (Fig. 4.2a, 4.2b, and Fig. 4.3a). The moisture content of all parts of *C. caeruleus* L. and *S. Officinalis* L. were evaluated at 103 ± 2 °C in the ventilated oven (MEMMERT, B319.0656, Germany). Once the moisture content was determined, the rhizomes and leaves were oven-dried (MEMMERT, B319.0656, Germany) at a temperature of 40 °C until a constant moisture level was achieved. The resulting dried rhizome slices and leaves were then finely ground using an electric grinder (High star AR-1045) and sifted through a 0.2 mm diameter sieve (Fig. 4.2c, and Fig. 4.3b). The dried powders were stored in airtight bags until use.

(a) Fresh rhizome

(b) Slices of rhizome

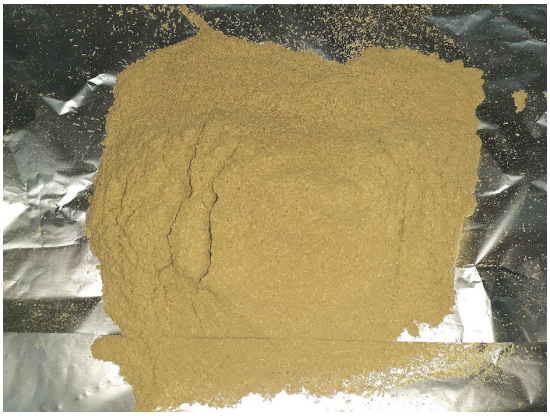

(c) Dried rhizome powder

Figure 4.2: Ventilated-oven drying procedure of rhizome part of *C. caeruleus* L.

4.3 Ultrasound-assisted extraction (UAE)

To extract bioactive compounds from the rhizome and leaves of *C. caeruleus* L. as well as the leaves of *S. Officinalis* L., an ultrasound-cleaning bath (J.P. SELECTA, s.a, Spain, SN. 3000865) equipped with two piezo-electric steel-aluminum transducers, a 120 W power generator, and a 75 W power heater. The cavity di-

(a) Fresh leaves

(b) Dried powder of leaves

Figure 4.3: Ventilated-oven drying procedure of *S. Officinalis* L. leaves.

mensions of the ultrasound-cleaning bath were 15 × 24 × 14 cm (H/W/D), and a frequency of 40 kHz was utilized for the extraction process (Fig. 4.4).

The experimental designs were used for the optimization of UAE of bioactive compounds, where both single factor at one time approach and BBD were employed for optimizing UAE of TPC and TSC from the rhizome of *C. caeruleus* L. Additionally, DSD and *I*-optimal design were utilized to optimize UAE of TPC and antioxidant activity from *S. Officinalis* L. The relevant details can be found in (Table 6.13, 4.2, 4.6, 4.8).

For the extraction process, 1 g of dried powders was submerged in varying volumes of extraction solvents (as outlined in Table 4.1 and 4.3). Methanol-water was utilized to extract TPC and TSC from the rhizome of *C. caeruleus* L., while ethanol-water was employed to extract TPC and other antioxidant compounds from *S. officinalis* L.

The samples were exposed to the sonication effect at determined time (Table 4.1, and 4.3). The ultrasonic temperature was controlled by a thermostat water bath and was adjusted using the ultrasound panel to the required temperatures (Table 4.1, and 4.3). During the sonication process, the samples were poured into a Beaker placed in front of a flask containing ice cubes to ensure that the temperature was always maintained at a constant temperature. The extracts from the rhizome and leaves were obtained by filtration through centrifugation (Sigma 3-16L, 172577, Germany) at 5000 rpm for 10 minutes to remove any insoluble particles, and then adjusted to the desired final volume. Subsequently, all the

extracts obtained through ultrasound-assisted extraction (UAE) were stored at a temperature of 4 °C for subsequent analysis

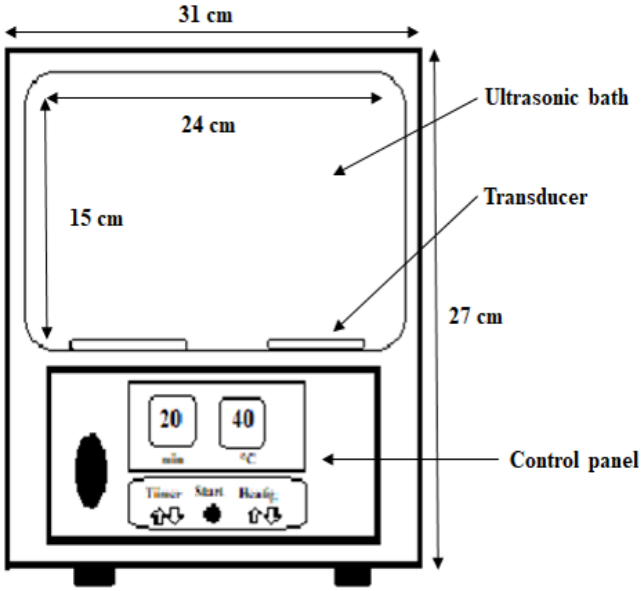

Figure 4.4: Ultrasound bath (J.P. SELECTA) dimensions employed in the extraction process.

4.4 Microwave assisted extraction (MAE)

The extraction of TPC and antioxidant compounds from the leaves of *S. officinalis* L. was conducted through microwave-assisted extraction (MAE) using a microwave that was equipped with a time controller and a circulating water-cooling system (NN-S674MF, Samsung, Malaysia). The microwave employed had a cavity size of 22.5 cm × 37.5 cm × 38.6 cm and operated at a frequency of 2450 kHz. 1 gram of dried powder obtained from *S. officinalis* L. leaves was added to a 250-mL vessel. The samples were then mixed with different concentrations of aqueous ethanol (ranging from 30 to 80%) at various solvent-to-solid ratios (20 to 50 mL g^{-1}), as listed in Table 4.4. The other MAE parameters studied were microwave power (ranging from 200 to 600 W) and extraction time (ranging from 60 to 300 s), as detailed in Tables 4.4, 4.6, and 4.9. After each MAE, the extract was filtered using centrifugation (Sigma 3-16L, 172577, Germany) at 5000 rpm for 10 min followed by filtration through a Whatman No. 4 filter paper, and the supernatant was stored at 4 °C for further analysis.

4.5 Optimization and prediction procedures

4.5.1 Optimization of UAE of TPC and TSC from rhizomes of *C. caeruleus* L.

4.5.1.1 Box-Behnken design (BBD)

Design of experiments, such as the BBD, is a statistical technique that is commonly utilized to optimize processes while conducting a minimal number of experiments (Yetilmezsoy et al., 2009). The Box-Behnken design (BBD) belongs to the category of rotatable or nearly rotatable second-order designs derived from incomplete factorial designs with three levels. One distinctive characteristic of the BBD is that all factors are simultaneously set to their maximum or minimum levels (Ferreira et al., 2007) (Fig. 4.5a). The number of design points can increase at the same rate as the number of polynomial coefficients due to a special arrangement of BBD levels (Aslan and Cebeci, 2007). For instance, a BBD with three factors, three blocks of four tests using a complete two-factor factorial design can be used, with the third factor's level set at zero (Fig. 4.5b) (Aslan and Cebeci, 2007). Box–Behnken design requires an experiment number according to $N = k^2 + k + c_p$, where (k) is the factor number and (c_p) is the replicate number of the central point (Aslan and Cebeci, 2007; Ferreira et al., 2007).

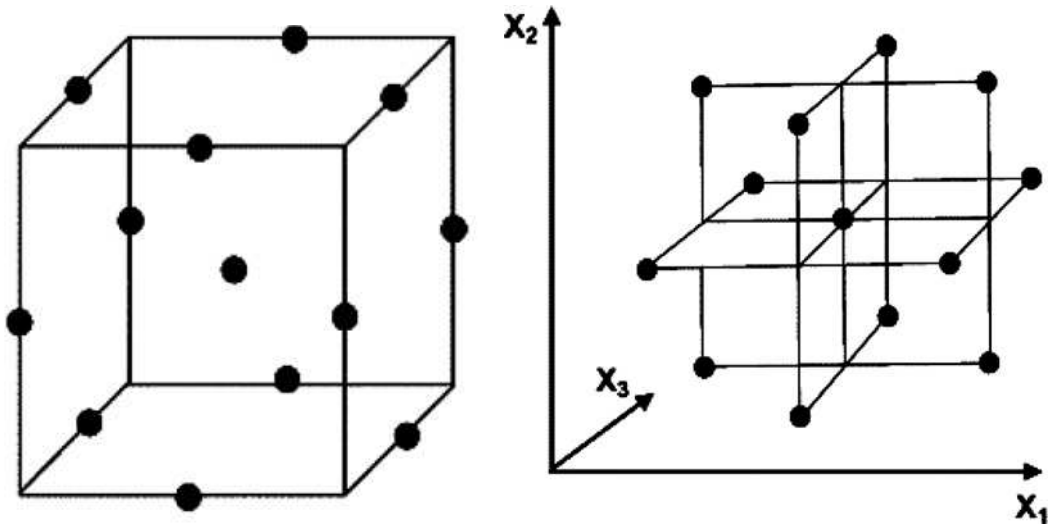

(a) (b)

Figure 4.5: Box-Behnken design: derivation from a cube (a) and representation as interlocking 2^2 factorial experiments (b).

In order to investigate the significant impact of UAE parameters on TPC and TSC of *C. caeruleus* L. rhizome, a preliminary single-factor experiment was conducted. The purpose of this study was to determine the approximate ranges of

UAE parameters, including the methanol-water mixture (x_1), temperature (x_2), time (x_3), and solvent to solid ratio (x_4) (refer to Table 6.13). Consequently, all the UAE parameters were chosen for further optimization (see Table 6.13). Building upon these findings, the Box-Behnken Design (BBD) was subsequently utilized to identify the optimal combinations of extraction variables for achieving the highest extraction yields of TPC and TSC (refer to Table 4.1 and 4.2). Three levels (-1, 0, and 1) of four UAE parameters including methanol-water mixture (60-90%), time (15-40 min), temperature (50-70 °C), and solvent to solid ratio (10 to 25 mL g^{-1}) were selected as mentioned in Table 4.1.

Table 4.1: Symbolized UAE Variables: Coded and real levels defined for Box-Behnken design.

	Coded Levels		
Independent variables	-1	0	+1
x_1: Methanol-water Mixture (%)	60	75	90
x_2: Temperature (°C)	50	60	70
x_3: Time (min)	15	27.5	40
x_4: Solvent to solid ratio (mL g^{-1})	10	17.5	25

The BBD matrix contain 27 experiments and three replicates at the central point as shown in Table 4.2. The TPC, and TSC were correlated with the four UAE parameters under the following second-order polynomial equation (Eq. 4.1):

$$Y = B_0 + \sum_{i=1}^{k} B_i x_i + \sum_{i=1}^{k} B_{ii} x_i^2 + \sum_{i=1}^{k-1} \sum_{i=1}^{k} B_{ij} x_i x_j + e \tag{4.1}$$

In the equation, Y represents the output variables (TPC, TSC), while B_0, B_i, B_{ii} (where i = 1,2,...,k), and B_{ij} (where i = 1,2,...,k; j = 1,2,...,k) are the regression coefficients for the mean, linear, quadratic, and interaction terms, respectively. The variables x_i and x_j are coded variables as indicated in Table 4.1 and Table 4.2. The error is represented by e. The independent variables were denoted as x_i based on the equation (Eq.,4.2):

$$x_i = \frac{X_i - X_0}{\Delta X_i} \tag{4.2}$$

In the given context, x_i represents the dimensionless coded value of the variable X_i, while X_i corresponds to the actual value of the variables. X_0 represents the actual value of x_j at the center point, and ΔX_i indicates the step change in the variable (Dahmoune et al., 2014).

Table 4.2: Box-Behnken design: 27-Run matrix for optimizing UAE of TPC and TSC from *C. caeruleus* L. Rhizome.

Runs	UAE extraction conditions			
	Methanol-water mixture (x_1)	Temperature (x_2)	Time (x3)	solvent to solid ratio (x_4)
1	-1	-1	0	0
2	-1	0	-1	0
3	-1	0	0	-1
4	-1	0	0	+1
5	-1	0	+1	0
6	-1	+1	0	0
7	0	-1	-1	0
8	0	-1	0	-1
9	0	-1	0	+1
10	0	-1	+1	0
11	0	0	-1	-1
12	0	0	-1	+1
13	0	0	+1	-1
14	0	0	+1	+1
15	0	+1	-1	0
16	0	+1	0	-1
17	0	+1	0	+1
18	0	+1	+1	0
19	+1	-1	0	0
20	+1	0	-1	0
21	+1	0	0	-1
22	+1	0	0	+1
23	+1	0	+1	0
24	+1	+1	0	0
25	0	0	0	0
26	0	0	0	0
27	0	0	0	0

4.5.1.2 Support vector regression optimized using dragonfly algorithm for predicting the TPC and TSC from *C. caeruleus* L. rhizome

As a supervised-learning approach, SVM is a robust technique that effectively performs nonlinear classification and regression tasks, based on the structural risk minimization principle from computational learning theory (Ghitescu et al., 2017; Jafarzadeh et al., 2016). In SVM classification, the initial aim is to establish decision boundaries in the feature space that can divide the data points into multiple classes (as shown in Fig. 4.6). This process leads to the creation of an optimal hyperplane that separates the two classes with maximum margin, thus minimizing generalization error and increasing classification accuracy (Fig. 4.6) (Deka et al.,

2014).

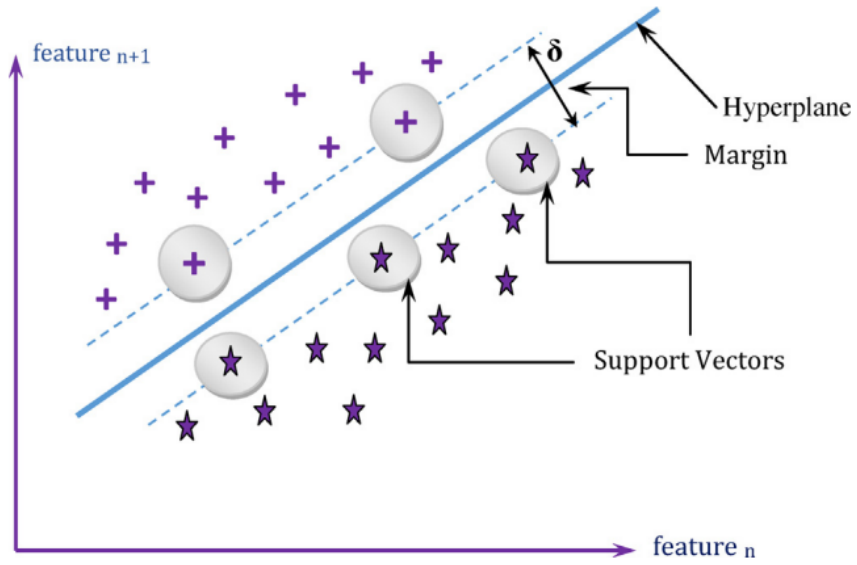

Figure 4.6: Maximum separation hyperplane using Support vector machine (SVM) (Deka et al., 2014)

SVM is a powerful technique for estimating real-value functions, known for its exceptional generalization capability and high prediction accuracy. This is achieved through the use of sparse solutions, kernels, control of the margin via Vapnik-Chervonenkis (VC) theory, and limiting the number of support vectors (Awad and Khanna, 2015). Moreover, SVM is designed to minimize the expected error of a learning machine, which reduces the risk of overfitting and improves its performance on unseen data (Yu et al., 2006). Furthermore, the kernel method in SVM not only can improve the computational efficiency of SVM training but also can be a convenient way to help prevent over-fitting classification problems (Pisner and Schnyer, 2020).

Various meta-heuristic algorithms, including particle swarm optimization (PSO), dragonfly algorithm (DA), genetic algorithm (GA), and Bat algorithm (BA) have been employed in optimizing the SVM's parameters (Xie et al., 2019). DA is a meta-heuristic algorithm introduced by Mirjalili (2015), which draws inspiration from the natural swarming behavior of dragonflies, both in static and dynamic scenarios. The algorithm utilizes these static and dynamic swarm behaviors to facilitate exploration and exploitation during the optimization process (Josephen et al., 2021). DA is a widely used meta-heuristic algorithm for solving diverse optimization problems. Combining the dragonfly algorithm with support vector machine has been found to strike an effective balance between exploration and exploitation by increasing the diversity of solutions (Meraihi et al., 2020). DA has been used to solve different optimization problems of SVM, the values of ker-

nel and penalty parameters were sent by the DA for training the SVM using the training data (Benimam et al., 2020; Laidi et al., 2021). Many previous studies reported that the performance of support vector regression (SVR) was achieved when the hyper-parameters are optimized using the Dragonfly algorithm (Laidi et al., 2021).

Due to the exceptional capabilities of SVM and DA in solving regression problems were chosen to predict TPC and TSC from *C. caeruleus* L. rhizome using UAE. The SVR-DA model was constructed using the input and output variables employed in the Box-Behnken design (BBD). The prediction of TPC and TSC is performed using the equation Eq. 4.3:

$$f(x) = \sum_{n=1}^{N} (a_n - a_n^*) G(x_n, x) + b \tag{4.3}$$

In Table 6.14, the kernel function $G(x_n, x)$ is described. Three kernel functions, namely Gaussian RBF, Linear, and Polynomial, were tested, and the Gaussian RBF kernel, which exhibited the most favorable outcomes, was selected for constructing the SVM. The dual problem coefficient, denoted as *Alpha*, is a vector comprising numeric values. The size of *Alpha* corresponds to the number of support vectors (m) present in the trained SVM regression model. For each support vector, the dual problem involves the introduction of two Lagrange multipliers. The values of *Alpha* correspond to the difference between the two estimated Lagrange multipliers for the support vectors ($a_n - a_n^*$). Additionally, $\boldsymbol{b}$ represents the bias term.

The methodology and optimization of hyperparameters for SVM can be elucidated by consulting the flowchart illustrated in Fig. 4.7. This visual representation serves as a helpful guide for implementing a systematic and effective approach, thereby enabling the attainment of optimal results (Abdelkader et al., 2021; Benimam et al., 2020; Hentabli et al., 2021; Mesllem et al., 2021). To enhance the optimization and facilitate convergence, the input data matrix (x_1, x_2, x_3, and x_4) was first subjected to normalization, whereby its numerical values were adjusted. This was achieved through the use of a normalization function, which is represented by the equation (Eq. 4.4):

$$x_n = x^{0.1} \tag{4.4}$$

Where x_n is normalized input data-set and x is input data

Next, To avoid overfitting, the entire data-sets of TPC and TSC from *C.*

caeruleus L. rhizomes were randomly split into two sets. The split was performed using the Holdout function, available in the statistical and machine learning toolbox of Matlab, allocating 80% of the data for training purposes and the remaining 20% for validation. Moreover, the validation dataset served as an independent set of data specifically employed to evaluate and test the performance of the SVR-DA model (Laidi et al., 2021; Mesellem et al., 2021). DA begins by randomly providing the SVR with a combination of hyper-parameters within their specified ranges, such as the size of insensitive zone (ϵ), the penalty parameter (C), and sigma (δ). This procedure is iteratively performed five times, where each iteration involves executing the steps from data partitioning to the creation of the SVR model. In each iteration, the obtained RMSE values are compared, and the best value is saved for further analysis, as depicted in Fig. 4.7. Additionally, a DA is employed to generate a fresh set of hyperparameters for SVR algorithm. The entire process is then repeated, leading to an improved RMSE outcome. This iterative step is performed for 100 trials, where the lowest and best RMSE values play a crucial role in determining the final optimal SVR model (Hentabli et al., 2021; Laidi et al., 2021). The RMSE and R^2 were calculated according to equations illustrated in Table 6.14 to assess the predictive power of the SVR-DA model.

In this study, a range of evaluation metrics were utilized to evaluate the goodness of fit and predictive accuracy of the optimized model. These metrics encompass the relative standard deviation (RSD), root mean square error (RMSE), the mean relative percentage error (MRPE), the average absolute relative deviation (AARD), the mean of absolute error (MAE), the determination coefficient (R^2) (refer to Table 6.14).

4.5.2 Optimization of UAE and MAE of phenolic compounds and antioxidant capacity from *Salvia officinalis* L.

4.5.2.1 Definitive screening design (DSD)

Traditionally, resolution III and IV fractional factorial designs have been popularly used for conducting screening experiments. However, a major drawback of the resolution III design is that the main effects are entirely confounded with one or more two-factor interactions, which creates significant ambiguity for the experimenter. To mitigate this ambiguity, additional experiments are required. While a resolution IV fractional factorial design confound two-factor interactions, if one is active, it requires more runs to resolve the active effects. Another limitation of these designs is that they have no capability for capturing curvature due to

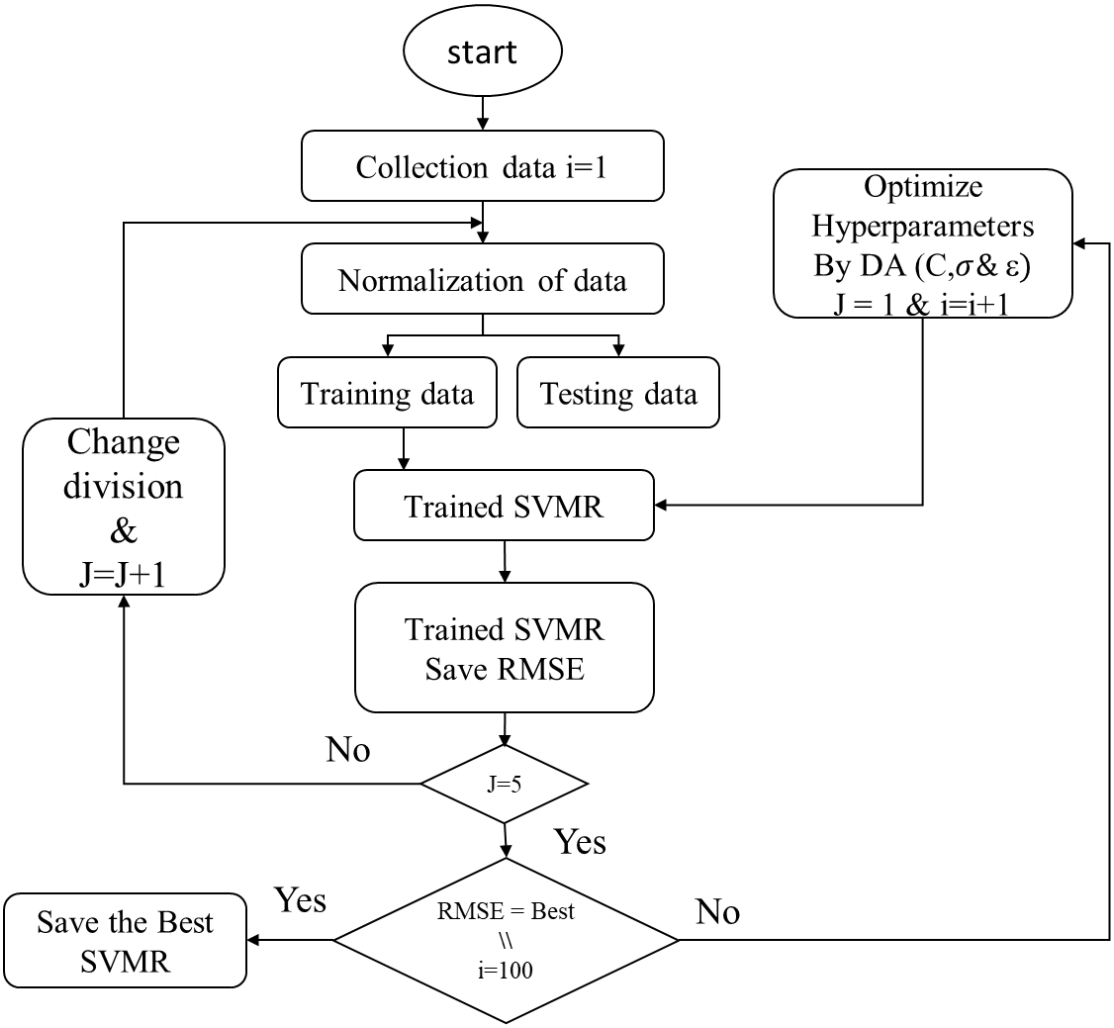

Figure 4.7: Utilization of SVR-DA technique for predicting TPC and TSC from *C. caeruleus* L. rhizome (Laidi et al., 2021).

pure-quadratic effects (Jones and Nachtsheim, 2011).

The DSD was created by Jones and Nachtsheim (2011) and has become a popular method in the field of Design of Experiments (DOE). This three-level design offers an alternative to fractional factorial designs when screening both continuous and categorical factors, and it can be used to generate a response surface design when only three or fewer factors are significant. This property is particularly useful when sequential experimentation is complex and expensive, making DSD an attractive and cost-effective solution. The construction of this design requires one more run than twice the number of factors $(2k + 1)$, where k is the number of factors, enabling the estimation of main effects and two-way interactions of all factors Jones and Nachtsheim (2011). The DSD method has been shown to be an effective tool for identifying the most important factors and their interactions in a systematic way while minimizing the number of experiments needed. This approach can significantly enhance efficiency by reducing the amount of time and

resources required for experimentation (Jones and Nachtsheim, 2011).

In JMP, DSD is created using conference matrice, as proposed by Xiao et al. (2012). Conference matrices are m x m matrices, where m is an even number. These matrices have zeros on the diagonal, and the off-diagonal elements can take the value of either 1 or -1, depending on the specific design requirements. Additionally, conference matrices need to satisfy the condition $C^TC = (m–1)I_{m*m}$, where C^T denotes the transpose of C, and I_{m*m} is the identity matrix of size mxm (Favre and Neto, 2021; Institute, 2013). The design matrix (D) for DSD can be constructed as:

$$D = \begin{pmatrix} C \\ -C \\ 0 \end{pmatrix}$$

The DSD has several desirable properties;

- Unlike resolution III designs, the main effects are completely independent of two-factor interactions, which ensures that estimates of main effects are not biased by the presence of active two-factor interactions. This is regardless of whether the interactions are included in the model.
- Two-factor interactions are not completely confounded with other two-factor interactions, although they may be correlated.
- Unlike resolution III, IV, and V designs with added center points, all quadratic effects can be estimated in models comprised of any number of linear and quadratic main-effects terms.
- Quadratic effects are orthogonal to main effects and not completely confounded (though correlated) with interaction effects.
- With 6 through (at least) 12 factors, these designs can estimate all possible full quadratic models involving three or fewer factors with high levels of statistical efficiency (Jones and Nachtsheim, 2011).

These properties make these designs useful and efficient for studying the effects of multiple factors in experimental settings, thus, the DSD was used to identify the UAE and MAE parameters that have the most substantial effects on the extraction of TPC, TEAC, and TAC from *S. Officinalis* L. leaves extracts. For UAE, 4 extraction parameters were selected including x_1: ethanol-water mixture, x_2: sonication time, x_3: extraction temperature, and x_4: solvent to solid ratio were studied at three levels, low, medium, and high levels as shown in table 4.3. On

the other hand, for the MAE, x_1: ethanol-water mixture, x_2: time, x_3: microwave power, x_4: solvent to solid ratio were studied as depicted in table 4.4.

Table 4.3: The extraction parameters and levels used for the screening and optimization of UAE.

	Coded levels		
UAE parameters	-1	0	+1
x_1: Ethanol-water mixture (%)	30	55	80
x_2: Time (min)	10	35	60
x_3: Temperature (°C)	30	45	60
x_4: Solvent to solid ratio ($mL\,g^{-1}$)	10	20	30

Table 4.4: The extraction parameters and levels employed for the screening and optimization of MAE

	Coded levels		
MAE parameters	-1	0	+1
x_1: Ethanol-water mixture (%)	30	55	80
x_2: Time (s)	60	180	300
x_3: Microwave power (W)	200	400	600
x_4: Solvent to solid ratio ($mL\,g^{-1}$)	20	35	50

In order to investigate the impact of UAE and MAE on TPC, TEAC, and TAC, a matrix of 17 experiments (including four additional runs) was designed for each extraction method (Table 4.6). The DSD matrix for UAE and MAE parameters were created using JMP software 13.0.0 Pro and had a D-efficiency of 85.61, a G-efficiency of 82.32, and an A-efficiency of 85.36. The average variance prediction for this design was 0.154 (Table 4.5). Conversely, the DSD matrix for MAE parameters had a higher G-efficiency compared to the DSD matrix for UAE parameters, while the other efficiency parameters remained the same as shown in the table 4.5

Table 4.5: DSD's Efficiency measures for UAE and MAE.

	UAE	MAE
D-Efficiency	85.61	85.61
G-Efficiency	82.32	92.39
A-Efficiency	85.36	85.36
Average variance of prediction	0.154	0.154

The color map (Fig. 4.8) displays four terms situated in the upper left corner, representing the main effects of UAE and MAE. The deep blue color observed in the map indicates a correlation value of 0, signifying that there are no correlations between the main effects and other main effects (Fig. 4.8). This implies that all

Table 4.6: Definitive screening design matrix employed for UAE and MAE of TPC and antioxidant capacity.

	Extraction parameters (UAE/MAE)			
Runs	x_1	x_2	x_3	x_4
1	-1	-1	-1	+1
2	-1	-1	+1	-1
3	-1	-1	+1	+1
4	-1	0	-1	-1
5	-1	+1	-1	+1
6	-1	+1	0	-1
7	-1	+1	+1	0
8	0	-1	-1	-1
9	0	0	0	0
10	0	+1	+1	+1
11	+1	-1	-1	0
12	+1	-1	0	+1
13	+1	-1	+1	-1
14	+1	0	+1	+1
15	+1	+1	-1	-1
16	+1	+1	-1	+1
17	+1	+1	+1	-1

main effects are orthogonal and can be independently estimated. The only red color present in the Fig. 4.8 is found on the main diagonal, confirming a perfect correlation of one for each term. This signifies that each term is entirely correlated with itself. Consequently, none of the main effects are completely confounded with any two-way interactions. However, it is important to note that the presence of active two-way interactions may introduce slight bias to the estimates of the main effects.

The mathematical equations of definitive screening design (Eq. 4.5) show the relation and the effect of each UAE or MAE parameters on TPC, TEAC, or TAC (Goos and Jones, 2011; Jones and Nachtsheim, 2011):

$$y_i = B_0 + \sum_{j=1}^{k} B_j x_{i,j} + \sum_{j=1}^{k-1} \sum_{k=j+1}^{k} B_{ijk} x_{i,j} x_{i,k} + \sum_{j=1}^{k} B_{jj} x_{i,j}^2 + \epsilon_i \tag{4.5}$$

In the given equation, k represents the number of continuous factors. The estimated coefficients for linear, interaction, and quadratic effects are denoted as B_0, B_{ijk}, and B_{jj} respectively. The coded factors, represented by $x_{i,j}$, $x_{i,k}$, and $x_{i,j}^2$, are associated with the factors of interest. The output variable, denoted as y_i, can take the values of TPC, TEAC, or TAC. Lastly, ϵ_i represents the error term in the equation.

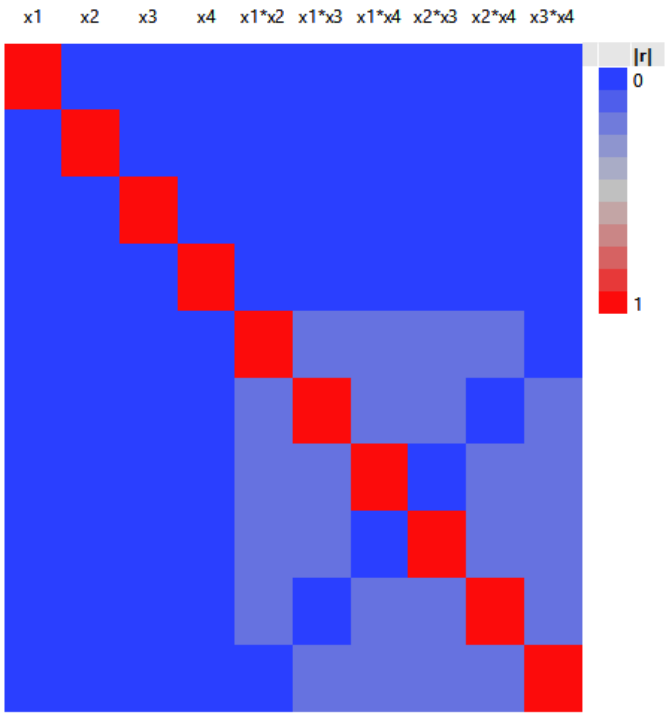

Figure 4.8: Color maps of DSD for absolute correlation between extraction parameters (UAE parameters or MAE parameters).

4.5.2.2 *I*-optimal design

The optimization of TPC, TEAC, and TAC from *S. Officinalis* L. powder using UAE and MAE was performed based on the *I*-Optimality criterion. The objective of *I*-Optimality is to minimize the average variance of prediction across the design space, making it a more suitable criterion than *D*-Optimality for predicting responses, determining optimal operating conditions, and identifying regions in the design space where the response falls within an acceptable range (Rodrigues et al., 2008). The prediction variance relative to the unknown error variance at a point $\mathbf{x}$ in the design space can be calculated using the following Eq.4.6 (Goos, 2012):

$$var(\hat{Y}/x) = f(\mathbf{x})^{'}(\mathbf{X}^{'}\mathbf{X})^{(-1)}f(\mathbf{x}) \tag{4.6}$$

Where $\mathbf{X}$ is the model matrix.

I-optimal designs minimize the integral I of the prediction variance over the entire design space, where $\mathbf{I}$ is given as follows (Eq.4.7) (Goos, 2012):

$$I = \int_R f(\mathbf{x})^{'}(\mathbf{X}^{'}\mathbf{X})^{(-1)}f(\mathbf{x})(dx) = trace\left[(\mathbf{X}^{'}\mathbf{X})^{(-1)}\mathbf{M}\right] \tag{4.7}$$

Where **M** is the moments' matrix (Eq.4.8),

$$\mathbf{M} = \int_R f(\mathbf{x}) f(\mathbf{x}^{'}) dx \tag{4.8}$$

In order to optimize the I-optimality criterion, the coordinate-exchange algorithm proposed by Meyer and Nachtsheim (1995) was employed. The coordinate-exchange algorithm was iteratively repeated numerous times until the maximum value of the optimality criteria was achieved, as illustrated in Fig. 4.9. For the I-optimal design matrix used for the optimization of three UAE parameters (Table 4.8), The D, G, and A- efficiency obtained in this study were 42, 77, and 29, respectively (Table 4.7). The average variance of prediction for this design was 0.351 (Table 4.7). On the other hand, the optimality criterion obtained for the I-optimal matrix used for the optimization of four MAE parameters (Table 4.9) were 42.41, 65.61, 30.63, 0.381 for The D, G, and A- efficiency, and the average variance of prediction respectively, which were similar to the optimality criterion of used for the optimization of three UAE parameters (Table 4.7).

Table 4.7: I-optimal design's Efficiency measures for the optimization of UAE and MAE.

	UAE	MAE
D-Efficiency	42.01	42.41
G-Efficiency	77.05	65.61
A-Efficiency	29.20	30.63
Average variance of prediction	0.351	0.381

For the optimization of UAE of TPC, TEAC, and TAC from *S. officinalis* L. leaves, three extraction parameters including x_1: ethanol-water mixture, x_3: temperature, x_4: solvent to solid ratio were selected as a significant factor based on the results of DSD, where the I-optimal matrix designed has 16 runs, including the center points as depicted in table 4.8. Whereas the I-optimal matrix used for the optimization of four MAE parameters (x_1: ethanol-water mixture, x_2: time, x_3: microwave power, x_4: solvent to solid ratio) consist of 21 runs including center points, which the matrix was used to maximize the TPC, TEAC, and TAC from *S. officinalis* L. leaves (Table 4.9).

According to the color map of correlations Fig. 4.10 shows the correlation between the effects of the UAE parameters (Fig. 4.10a) and the correlation between the effects of the MAE parameters (Fig. 4.10b). For the UAE, the main effects are represented by the three terms in the upper left corner of the map. The deep blue color corresponds to the uncorrelated effects between the main effects and other main effects. This means that all main effects are orthogonal and can

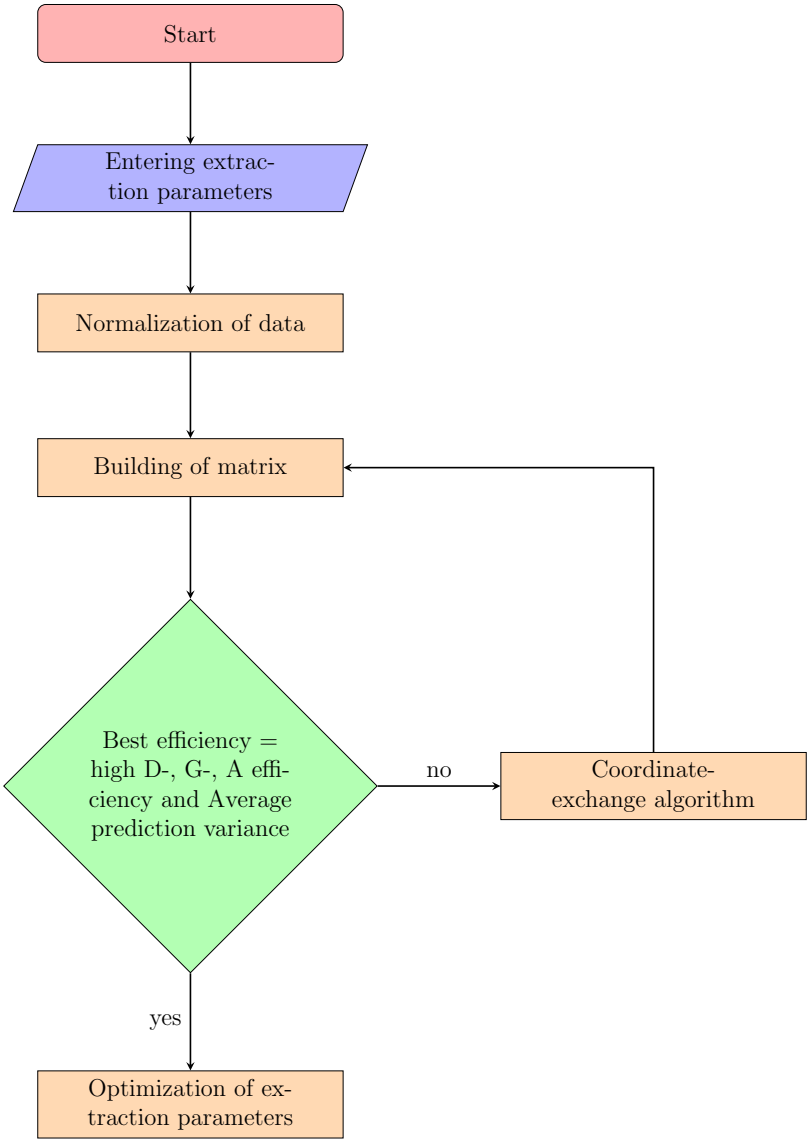

Figure 4.9: Optimization of optimality criteria for I-Optimal design through the coordinate exchange algorithm.

be estimated independently. The red line in Fig. 4.10a is on the main diagonal, reflecting that each UAE parameter is perfectly correlated with itself. It follows that no main effect is completely confounded by any two-way interaction. For the MAE, the four main effects in the upper left corner of the map are perfectly correlated with itself and each main effect is weakly correlated with other main effects or two-way interaction as depicted in Fig. 4.10b.

The mathematical equations of I-optimal design (Eq.4.9) show the relation and the effect of each UAE or MAE parameters on TPC, TEAC, or TAC (Goos and Jones, 2011; Jones and Nachtsheim, 2011):

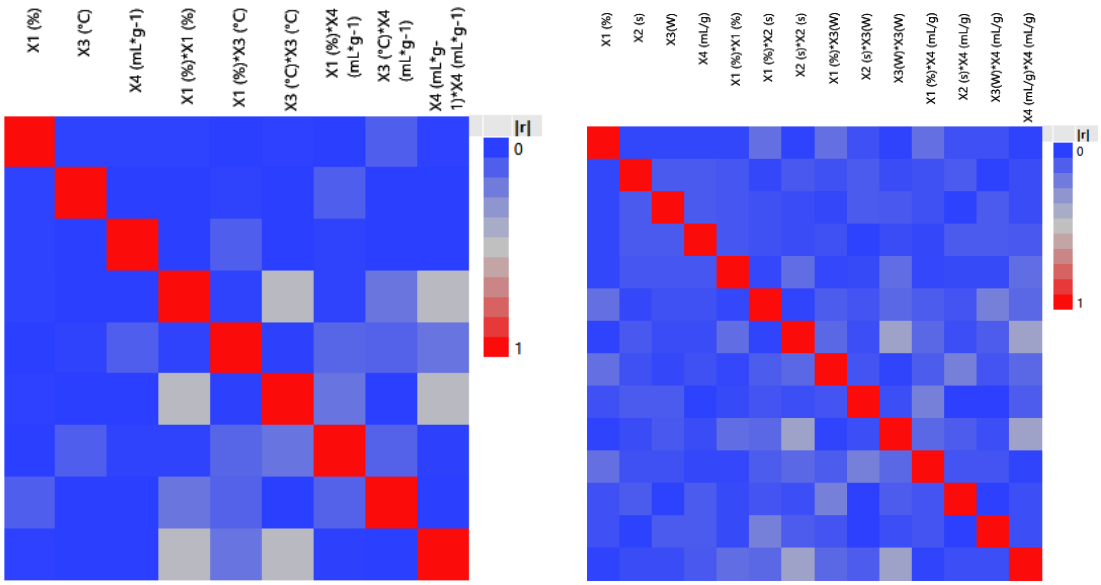

(a) (b)

Figure 4.10: Color maps of I-optimal design for correlation between (a) UAE parameters, (b) MAE parameters.

Table 4.8: I-optimal design matrix employed for the optimization of UAE of TPC and antioxidant capacity from *S. officinalis* L.

	UAE parameters		
Runs	x_1	x_3	x_4
1	-1	+1	+1
2	-1	0	-1
3	0	0	0
4	0	0	+1
5	+1	-1	+1
6	+1	+1	+1
7	0	0	0
8	0	0	0
9	0	+1	0
10	+1	+1	-1
11	-1	-1	+1
12	+1	-1	-1
13	+1	0	0
14	-0.11	-1	-1
15	-1	+1	-1
16	-1	-1	0

$$y_i = B_0 + \sum_{j=1}^{k} B_j x_{i,j} + \sum_{j=1}^{k-1} \sum_{k=j+1}^{k} B_{ijk} x_{i,j} x_{i,k} + \sum_{j=1}^{k} B_{jj} x_{i,j}^2 + \epsilon_i \qquad (4.9)$$

Where k is the number of continuous factors, and B_0,B_{ijk},B_{jj} are the esti-

mated coefficients for linear, interaction, and quadratic effects respectively, $x_{i,j}$, $x_{i,k}$, $x_{i,j}^2$ are the coded factors, y_i is the output variable (TPC, TEAC, or TAC), and ϵ_i is the error.

Table 4.9: *I*-Optimal design matrix employed for the optimization of MAE of TPC, TEAC, and TAC

	MAE parameters			
Runs	x_1	x_2	x_3	x_4
1	-1	-1	-1	0
2	-1	-1	0	-1
3	-1	0	-1	+1
4	-1	0	+1	-1
5	-1	+1	-1	-1
6	-1	+1	0	+1
7	-1	+1	+1	0
8	-0.3	-1	+1	+1
9	0	-1	-1	-1
10	0	+1	-1	+1
11	0	+1	+1	-1
12	+1	-1	-1	+1
13	+1	-1	+1	-1
14	+1	0	-1	-1
15	+1	0	0	0
16	+1	+1	-1	0
17	+1	+1	0	-1
18	+1	+1	+1	+1
19	0	0	0	0
20	0	0	0	0
21	0	0	0	0

4.6 Determination of TPC and TSC and evaluation of antioxidant activity of *C. caeruleus* L. rhizome

4.6.1 Determination of total phenolic compounds (TPC)

To determine the TPC of UAE extracts obtained from dried rhizomes of *C. caeruleus* L., the spectrophotometric method described by Georgé et al. (2005) was employed. In this method, 125 µL of the various methanol extracts were combined with 625 µL of a diluted Folin-Ciolcateu reagent (at a volume ratio of 1/10) and allowed to stand at room temperature for 2 minutes. Following this, 500 µL of a 7.5% Na_2CO_3 solution was added to the mixture, which was then incubated

for 15 minutes at 50°C in an unstirred water bath (NÜVE Bath, NB20). Subsequently, the reaction mixture was cooled in a water-ice bath, and the specific absorbance was measured at 760 nm using a UV–vis Spectrophotometer (Optizen pop, Korea).

The concentrations of TPC were determined using a Gallic acid standard curve. Various concentrations of Gallic acid ranging from 0.02 to 0.08 mg/mL were utilized to generate the standard curve using GraphPad software (Fig. 6.9). The linear equation obtained was $y = 12.089X + 0.0034$ with an R^2 value of 0.999. The TPC from the rhizome extracts were expressed as mg Gallic acid equivalent per 100 g of the dry weight of the fine powder of *C. caeruleus* L. ($mg_{GAE}/100\,g_{dw}$) according to Eq. 4.10. The analyses were conducted in triplicate, and the mean ± standard deviation (SD) was calculated.

$$TPC\,(mg_{GAE}/100\,g_{dw}) = \frac{c\,(mg_{GAE}/mL) * V\,(mL) * DF}{g_{dw\,rhizome\,powder}} * 100 \tag{4.10}$$

Where $c\,(mg_{GAE}/mL)$ represents the concentration of TPC obtained from the standard curve. $V(mL)$ denotes the volume of solvent used during the extraction process. DF represents the dilution factor. g_{dw} signifies the dry weight of the rhizome powder.

4.6.2 Quantitative determination of total saponin content (TSC)

For optimization purposes, the Vanillin-acid sulfuric method introduced by Hiai et al. (1976) was employed. This colorimetric assay was utilized to quantify steroidal sapogenins, triterpenoid sapogenins, sterols, and bile acids, which possess a hydroxyl (OH) group at their C-3 position and react with the reagents to form chromogens. The procedure involved combining 125 µL of diluted UAE extracts (at a volume ratio of 1/5) obtained from the dry weight of *C. caeruleus* L. rhizome powder with 125 µL of an 8% (w/V) vanillin solution dissolved in ethanol. Subsequently, 1.25 mL of 72% (V/V) sulfuric acid was added to the mixture. After thorough shaking, the mixture was incubated at 60 °C for 10 minutes in a water bath (NÜVE Bath, NB20). Following incubation, the absorbance of the cooled mixture was measured against a methanol blank, in which the other reagents were present (resulting in a distinct yellow color). The UV/Vis spectrophotometer (Optizen pop, Korea) was employed to scan the wavelength, and the maximum absorbance was determined to be at 515 nm. The analysis was repeated three

times, and the mean ± standard deviation (SD) was calculated.

4.6.3 Evaluation of antioxidant activity of *C. caeruleus* L. rhizome

The optimal rhizome extract and leaves extract from *C. caeruleus* L. were assessed for their antioxidant capabilities by means of four different assays, including $DPPH^{\bullet}$, $ABTS^{\bullet+}$, reducing power, and phosphomolybdenum assays.

4.6.3.1 Scavenging $DPPH^{\bullet}$ free radical activity

The $DPPH^{\bullet}$ scavenging capacity of *C. caeruleus* L. rhizome and leaves extracts was evaluated using a modified version of the method outlined by Dahmoune et al. (2015). To begin, 1 mL of a methanol solution containing $DPPH^{\bullet}$ (60 µM) was mixed with 100 µL of lyophilized extract at various concentrations. The mixture was then incubated in the dark at room temperature for 30 minutes. Following incubation, the absorbance of the solution was measured at 517 nm using a UV–vis Spectrophotometer (Optizen pop, Korea), with a methanol blank used as a reference. The antioxidant capacity was calculated as the percentage of $DPPH^{\bullet}$ scavenging using Eq.4.11:

$$\text{Free radical inhibition}\,(\%) = \frac{A_{control} - A_{Sample}}{A_{Control}} * 100 \tag{4.11}$$

Where, A_{Sample} represents the absorbance of the solution containing the free radical ($DPPH^{\bullet}$) and the sample extract at the designated time, A_{Blank} corresponds to the absorbance of the solution containing the free radical ($DPPH^{\bullet}$) and the extraction solvent, and A_{Control} denotes the absorbance of the working solution of the free radical. Additionally, the concentration necessary to inhibit 50% of the free radical ($DPPH^{\bullet}$) was determined through analysis of the inhibition curve.

4.6.3.2 Scavenging $ABTS^{\bullet+}$ free radical activity

The ABTS assay, following the procedure described by Dahmoune et al. (2014), was conducted to evaluate the reduction of $ABTS^{\bullet+}$ free radicals in the presence of antioxidants. Initially, a stock solution of $ABTS^{\bullet+}$ was prepared by combining 7 mM ABTS and 2.45 mM potassium persulfate. This stock solution was incubated in darkness for 16 hours, and then diluted with ethanol to achieve an absorbance of 0.700 ± 0.02 at 734 nm. Subsequently, 75 µL of lyophilized extracts of leaves and rhizome at various concentrations were added to 1425 µL of the diluted $ABTS^{\bullet+}$

solution. The antioxidant capacity was determined as a percentage after 6 minutes of incubation in the dark at 734 nm.

The antioxidant capacity was quantified as the percentage of scavenging of $ABTS^{\bullet+}$ and was calculated using Equation 4.12.

$$\text{Free radical inhibition}\,(\%) = \frac{A_{control} - A_{Sample}}{A_{Control}} * 100 \tag{4.12}$$

In the equation, $A_{,Sample}$ represents the absorbance of the solution containing the $ABTS^{\bullet+}$ free radical and the sample extract at the specified time. A_{Blank} denotes the absorbance of the solution containing the free radical $ABTS^{\bullet+}$ and the extraction solvent. $A_{,Control}$ represents the absorbance of the working solution of the free radical. Additionally, the concentration required to inhibit 50% of the free radical $ABTS^{\bullet+}$ was determined by analyzing the inhibition curve.

4.6.3.3 Total antioxidant capacity (TAC)

For the determination of total antioxidant capacity (TAC), a phosphomolybdenum reagent was used. Following the method described by Prieto et al. (1999), 200 µL of lyophilized extract from rhizome and leaves were combined with 2 mL of a test solution containing 0.6 M sulfuric acid, 4 mM ammonium molybdate tetrahydrate, and 28 mM sodium phosphate. The mixture was then incubated at 95 °C for 90 minutes. After cooling to room temperature, the absorbance was measured at 695 nm. To construct the standard curve, various concentrations of ascorbic acid (ranging from 0.02 to 0.4 mg/mL) were used to evaluate their total antioxidant activity under the same aforementioned conditions. The standard curve was plotted as $Y = 3.4169x - 0.0498$, with an R^2 value of 0.994 (Figure 6.10). The TAC results were expressed as (mg_{AAE}/g) of lyophilized extract, calculated using Equation 4.13:

$$TAC\,(mg_{AAE}/g_{dry\,extract}) = \frac{c\,(mg_{AAE}/mL)}{c\,(g/mL)} \tag{4.13}$$

Where $c\,(mg_{AAE}/mL)$ is the TAC of rhizome and leaves parts calculated from the standard curve, $c\,(g/mL)$ is the concentration of lyophilized extract.

4.6.3.4 Ferric reducing antioxidant power

The evaluation of the reducing power of *C. caeruleus* L. rhizome was performed following the methods described by Oyaizu (1986). To initiate the assay, 0.2 mL of various concentrations of the lyophilized extracts from *C. caeruleus* L. rhizome

were individually added to a mixture containing 0.5 mL of phosphate buffer (0.2 M, pH 6.6) and 0.5 mL of 1% potassium ferricyanide. The reaction mixture was then incubated in a water bath at 50°C for 20 minutes. Following the incubation period, the reaction mixture was cooled to room temperature, and 0.5 mL of 10% trichloroacetic acid (TCA) was added. The resulting mixture was subsequently centrifuged at 3000 rpm for 10 minutes. The supernatant (0.5 mL) was collected and combined with 0.5 mL of distilled water and 0.1 mL of ferric chloride (0.1%). The absorbance of the resulting solution was directly measured at 700 nm.

4.7 Determination of TPC and evaluation of antioxidant activity of *S. officinalis* L. leaves

4.7.1 Determination of total phenolic compounds

The total phenolic content (TPC) of the ethanol-water UAE and MAE extracts obtained from *S. officinalis* L. leaves was determined using Folin's assay, as described in the previous section (Section 4.6.1). A calibration curve was constructed using a Gallic acid standard (Figure 6.9), which was used to calculate the TPC of the UAE and MAE extracts of *S. officinalis* L., expressed as mg_{GAE}/g_{dw} using Equation 4.10. All results were reported as means ($N = 3$) ± standard deviations (SD).

4.7.2 Total antioxidant capacity (TAC)

TAC of the UAE and MAE extracts of *S. officinalis* L. leaves was carried out using a phosphomolybdenum reagent, following the protocol described in the aforementioned section (Subsubsection 4.6.3.3). A standard curve was constructed using ascorbic acid (Figure 6.10), which was used to calculate the total antioxidant capacity. The TAC results were expressed as mg_{AAE}/g_{dw}, based on Equation 4.14:

$$TAC\,(mg_{AAE}/g_{dw}) = \frac{c\,(mg_{AAE}/mL) * V\,(mL) * DF}{g_{dw\,leaves\,powder}} \tag{4.14}$$

In the equation, c represents the concentration of TAC in the extracts, measured in mg_{AAE}/mL. The value of V corresponds to the volume of solvent utilized during the extraction process, while DF represents the dilution factor. Finally, g_{dw} denotes the dry weight of the leaves powder.

4.7.3 Trolox equivalent antioxidant capacity (TEAC)

The methodology is based on the ability of antioxidant molecules present in *S. officinalis* L. to reduce the $ABTS^{\bullet+}$ radical, in comparison to Trolox, which serves as a water-soluble analog of vitamin E. This approach is described by Babbar et al. (2011). A stock solution of the blue-green chromophore $ABTS^{\bullet+}$ was prepared following the procedure outlined in the previous section (Section 4.6.3.2). Subsequently, 2 mL of diluted $ABTS^{\bullet+}$ solution was mixed with 20 µL of diluted ethanol-water extracts obtained through UAE and MAE. The mixture was thoroughly mixed, and the absorbance was measured using a UV-visible spectrophotometer (Optima, SP-3000nano, 5T5701-143132-00, Japan) after 6 minutes. The antioxidant capacity was calculated by comparing it to the Trolox standard curve depicted in Figure 6.15, utilizing Equation 4.15. The results were expressed as µmol of Trolox equivalent $(TE)/g_{dw}$ of *S. officinalis* powder. All assays were performed in triplicate, and the results were reported as mean ± standard deviation (SD).

$$TEAC\,(\mu mol_{\,TE}/g_{\,dw}) = \frac{c\,(\mu mol_{\,TE}/mL) * V\,(mL) * DF}{g_{dw\,leaves\,powder}} \tag{4.15}$$

In the equation, c represents the concentration of TEAC in the extracts, measured in $\mu mol_{\,TE}/mL$. The value of V corresponds to the volume of solvent utilized during the extraction process, while DF represents the dilution factor. Finally, g_{dw} denotes the dry weight of the leaves powder.

4.7.4 UHPLC-HRMS Characterization of bioactive compounds from *S. officinalis* leaves extracts

In order to evaluate the composition of bioactive compounds derived from extracts of *Salvia officinalis* L. obtained through UAE and MAE, a previously described method by Kusznierewicz et al. (2021) was employed. This method utilized ultra-high-performance liquid chromatography and high-resolution mass spectrometry (Dionex Ultimate 3000, RS Autosampler) to analyze the samples.

Chromatographic separation was performed using a C_{18} column (LUNA-OMEGA 1.6 µm Polar C_{18}, 100 A°, 150×2.1 mm). The mobile phase consisted of 0.1% (v/v) formic acid in water (A) and 0.1% (v/v) formic acid in acetonitrile (B). The mobile phase was pumped at a flow rate of 0.3 $mL\,min^{-1}$ using gradient elution. The gradient started with 15% B and gradually increased to 40% B within 15 minutes. Then, it was further increased to 100% B at 16 minutes and maintained for 7 minutes as a re-equilibration step. For both the UAE and MAE

extracts, the injection volume was 1 µL.

The UHPLC system was connected to a Dionex Ultimate 3000 RS-DAD and a Q-Exactive Focus quadrupole-Orbitrap mass spectrometer (Thermo Fisher Scientific, Bremen, Germany) equipped with a heated electrospray ionization source (HESI II). In negative polarity mode, the HESI parameters were set as follows: sheath gas flow rate at 35 arb, auxiliary gas flow rate at 15 arb, sweep gas flow rate at 3 arb, spray voltage at 2.5 kV, capillary temperature at 350°C, S-lens RF level at 50, and heater temperature at 300 °C. Data acquisition in the negative mode was performed using full scan at a resolving power of 70,000 FWHM. The AGC target was set to 1e6 and the maximum IT was set to auto. The scan range for the compounds of interest was selected as 100 - 1200 m/z. For data-dependent MS^2, the parameters were as follows: resolution of 17500, isolation window of 3.0 m/z, normalized collision energy of 30, AGC target of 1e6, and maximum IT set to auto. Mass calibration was conducted using a combination of n-butylamine, caffeine, Met-Arg-Phe-Ala (MRFA), and Ultramark 1621 in both positive and negative modes.

The bioactive compounds were identified by comparing the accurate mass and mass fragmentation pattern spectra with MS-MS spectra of known compounds. To facilitate this process, a customized database comprising various phytochemicals was constructed using published information on the Salvia species and integrated into the CD software. The data obtained from six experimental replicates of Salvia extracts obtained through MAE, UAE, and the extraction solvent (blank) were analyzed using a workflow described in the report by Kusznierewicz et al. (2021).

4.8 Statistical analysis

The software JMP Pro 13.0.0 (SAS Institute Inc.) was utilized on a Microsoft Windows 10 Professional (10.0.15063.0) operating system to construct the BBD, DSD, and I-optimal design, as well as to analyze the optimization results. The software was used to plot three-dimensional response surfaces based on the fitted model, while holding one independent variable constant at level-coded zero. The accuracy and adequacy of the BBD, DSD, and I-optimal models were evaluated using statistical methods such as anlaysis of variance (ANOVA), lack of fit (LoF), and determination coefficient R^2. The significance of these models and the estimated coefficients of UAE parameters were established at a threshold of $p < 0.05$. Furthermore, the desirability function and optimal extraction conditions for multiple responses, including TPC, TSC, TEAC, and TAC, were investigated using

JMP Pro 13.0.0 software.

The construction and analysis of SVR-DA involved various procedures and metrics, as described in Table 6.14. These tasks were performed using MATLAB R2019 (b) software (Mathworks, Natick, MA, USA) on a Microsoft Windows 10 operating system, utilizing a high-performance system with 6 GB of Random Access Memory and a 500 GB Hard Drive. The statistical and machine-learning toolbox within MATLAB was employed to build the SVR model, while the optimization method was implemented using the DA toolbox provided by Mirjalili (2015). GraphPad Prism 8.0.2 (263) software was utilized to generate standard curves and graphs for the antioxidant activity. All experimental results were reported as mean values (n = 3), along with their corresponding standard deviations.

Part III

Results and Discussion

Chapter5

Optimization of UAE of phenolic-saponin content from *C. caeruleus* L. rhizome and predictive model based on SVR-DA

Abstract

Chemometric techniques, namely BBD and SVR-DA, were utilized to optimize and predict the levels of TPC and TSC in *C. caeruleus* L. rhizome through the application of UAE. Additionally, a comparative analysis was conducted to evaluate the antioxidant activity of rhizomes and leaves. Various assays such as $ABTS^{\bullet+}$ and $DPPH^{\bullet}$ scavenging activity, FRAP, and phosphomolybdenum assays were employed. The findings confirmed the successful implementation of BBD, determining the ideal conditions for achieving maximum recovery of TPC and TSC. These optimal conditions included a methanol concentration of 78.66%, a temperature of 50 °C, and a sonication time of 26 minutes.The SVR-DA model, successfully established, demonstrated exceptional predictive capabilities for extracting TPC and TSC from *C. caeruleus* L. rhizome, yielding a high coefficient of determination ($R^2 = 0.99$) and minimal error. To facilitate its practical application in the pharmaceutical field, a user-friendly Matlab graphical interface was developed for the optimized SVR-DA model, enabling the prediction of TPC and TSC. Moreover, the optimized extracts obtained from the rhizome and leaves exhibited substantial antioxidant capacity, highlighting the potential of *C. caeruleus* L. as a promising candidate for utilization in the cosmetic and pharmaceutical industries.

5.1 Box-Behnken model Fitting

The adequacy of the Box-Behnken model for TPC and TSC extraction was evaluated using ANOVA and LOF, along with measures such as R-squared (R^2), adjusted R-squared (R^2_{Adj}), and coefficient of variation (C.V). Table 5.1 presents the BBD and its corresponding output variables. The RSM analysis yielded favorable results, as evidenced by the high R-squared values of 0.96 and 0.97 for TPC and TSC, respectively. These values indicate that 96% and 97% of the data points align with the regression model, demonstrating a robust fit. Additionally, the coefficient of variance (CV) for all responses remained below 10%, ensuring a reliable and consistent outcome (see Table 5.2). Furthermore, the adjusted R-square (R^2_{Adj}) values, reaching 92% and 93% for TPC and TSC, respectively (see Table 5.2), demonstrate that a significant portion of the observed variation in TPC and TSC extraction can be attributed to the independent variables considered in the study. Regarding the ANOVA analysis (see table 5.2), it was observed that the model exhibited significance, as indicated by a higher F-value and a $p-value < 0.0001$. Additionally, the lack of fit for each response (TPC and TSC) was found to be non-significant, reflected by a smaller F-value and a $p-value > 0.05$. These findings suggest a meaningful relationship between the predictors and the observed values of the responses. Therefore, the implemented BBD model proved to be suitable and capable of explaining a portion of the variations observed in the responses.

It is important to note that the obtained second-order polynomial equations were employed to predict the responses at different levels of each factor. These equations hold value in determining the impact of the independent variables by examining the estimated coefficients. The regression model for TPC and TSC can be seen in equations 5.1, and 5.2 respectively.

$$TPC\,(mg_{GAE}/100\,g_{dw}) = 349.652 - 24.730\,x_1 + 8.904\,x_2 + 14.993\,x_3 + 73.155\,x_4 - 72.940\,x_1^2 - 12.063\,x_2^2 - 33.260\,x_3^2 - 53.380\,x_4^2 - 36.879\,x_1x_2 - 32.743\,x_1x_3 + 9.047\,x_1x_4 + 28.349\,x_2x_3 + 28.349\,x_2x_4 + 0.948x_3x_4 \quad (5.1)$$

$$TSC\,(Abs) = 0.279 - 0.004\,x_1 - 0.0014\,x_2 + 0.003\,x_3 + 0.051\,x_4 - 0.035\,x_1^2 + 0.014\,x_2^2 - 0.019\,x_3^2 - 0.038\,x_4^2 - 0.023\,x_1x_2 - 0.027\,x_1x_3 + 0.005\,x_1x_4 - 0.010\,x_2x_3 - 0.015\,x_2x_4 - 0.011\,x_3x_4 \quad (5.2)$$

Table 5.1: Measured values of TPC, and TSC obtained using Box-Behnken design.

	Extraction conditions				Experimental results	
Runs	x_1	x_2	x_3	x_4	TPC ($mg_{GAE}/100g_{dw}$)	TSC (Abs)
1	-1	-1	0	0	267.737 ± 2.602	0.263 ± 0.006
2	-1	0	-1	0	223.274 ± 2.152	0.200 ± 0.004
3	-1	0	0	-1	187.085 ± 5.204	0.155 ± 0.004
4	-1	0	0	+1	301.169 ± 4.179	0.255 ± 0.003
5	-1	0	+1	0	310.130 ± 4.775	0.250 ± 0.003
6	-1	+1	0	0	321.849 ± 4.662	0.286 ± 0.004
7	0	-1	-1	0	302.892 ± 4.775	0.284 ± 0.005
8	0	-1	0	-1	192.255 ± 2.984	0.203 ± 0.006
9	0	-1	0	+1	323.572 ± 2.152	0.328 ± 0.002
10	0	-1	+1	0	294.276 ± 7.237	0.309 ± 0.004
11	0	0	-1	-1	170.196 ± 1.034	0.145 ± 0.0006
12	0	0	-1	+1	326.330 ± 1.790	0.275 ± 0.004
13	0	0	+1	-1	188.808 ± 2.067	0.19 ± 0.005
14	0	0	+1	+1	348.733 ± 0.600	0.273 ± 0.002
15	0	+1	-1	0	266.703 ± 6.728	0.272 ± 0.003
16	0	+1	0	-1	227.411 ± 2.602	0.208 ± 0.009
17	0	+1	0	+1	393.540 ± 5.757	0.271± 0.003
18	0	+1	+1	0	371.481 ± 1.580	0.255 ± 0.009
19	+1	-1	0	0	272.217 ± 0.598	0.275 ± 0.002
20	+1	0	-1	0	242.231 ± 4.304	0.248 ± 0.002
21	+1	0	0	-1	136.419 ± 6.059	0.159 ± 0.004
22	+1	0	0	+1	286.693 ± 1.579	0.279 ± 0.003
23	+1	0	+1	0	198.114 ± 4.738	0.190 ± 0.002
24	+1	+1	0	0	178.813 ± 1.579	0.207 ± 0.001
25	0	0	0	0	342.874 ± 5.167	0.280 ± 0.005
26	0	0	0	0	348.388 ± 9.827	0.288 ± 0.01
27	0	0	0	0	357.694 ± 9.325	0.271 ± 0.003

The values are expressed as means ± SD (n=3),$mg_{GAE}/100g_{dw}$: mg Gallic acid equivalent per 100 g dry weight of rhizome powder, Abs; Absorbance.

5.2 Temperature influence on TPC and TSC

The results presented in Table 5.2 and Eq. 5.1 indicate that the linear effect of temperature (x_2) within the range of 50 to 70 °C did not demonstrate statistical

significance ($p > 0.05$) on the extraction of TPC when ultrasound was employed. However, there was a significant negative impact ($p < 0.05$) on TPC extraction observed from the interaction between methanol concentration and temperature (x_1x_2), as evidenced by the significant estimated coefficient. Moreover, the interaction between temperature and sonication time (x_2x_3) exhibited a positive and statistically significant impact ($p < 0.05$) on the UAE (Ultrasound-Assisted Extraction) of TPC. This finding indicates that the influence of temperature is dependent on the combined effects of methanol concentration (x_1) and sonication time (x_3).

Regarding the impact of UAE temperature on TSC extraction, the findings presented in Table 5.2 and Eq. 5.2 reveal that the effect of temperature on TSC is significantly negative ($p < 0.05$) in both linear and interaction terms (x_1x_2, x_2x_4). Figure 5.1a, and Figure 5.1d illustrate the response plots of TPC and TSC, respectively, for *C. caeruleus* L. rhizome. These plots demonstrate the influence of temperature on TPC and TSC while considering the interaction with methanol concentration, with the remaining variables held constant at zero levels. The impact of temperature was examined in two distinct aspects, revealing a negative correlation when the methanol concentration was below 75%. Notably, the extraction yields of TPC and TSC exhibited a significant increase when the temperature was elevated from 50 °C to 70 °C. This parallel behavior between TPC and TSC can be attributed to the fact that higher extraction temperatures enhance the solubility of and the diffusion coefficient of both TPC and TSC (Jang et al., 2017; Pham et al., 2017). Furthermore, according to Teh and Birch (2014), increasing the heating temperature enhances the cavitation phenomenon of ultrasound, aiding in the breakdown of the cell wall during the extraction of TPC and TSC. In the second aspect, when the methanol concentration exceeded 75%, both TPC and TSC exhibited a significant decrease at higher temperature levels. This phenomenon can be attributed to the higher quantity of methanol in the extraction solvent, which lowers the boiling point of the solvent mixture. Consequently, at elevated extraction temperatures, methanol readily vaporizes during the extraction process, leading to a reduction in the yields of both TPC and TSC. In summary, the optimal yield of TPC was achieved at higher temperatures with a lower methanol concentration. On the other hand, for TSC, the highest yield was obtained with a higher methanol concentration and a lower temperature.

To further investigate the relationship between extraction temperature and other parameters, Figure 5.1c demonstrates that when the sonication time exceeded 25 min, there was a noticeable increase in the yield of TPC with higher extraction temperatures. Conversely, when the sonication time was below 25 min,

the TPC yield decreased as the temperature increased. These findings indicate that a higher TPC yield can be obtained with both high temperatures and long sonication times. Furthermore, for TSC, it was observed that the yield was highest at lower temperatures (around 50 °C) when the solvent-to-solid ratio exceeded 17.5 mL g^{-1}. However, the TSC yield significantly decreased when the temperature was increased to 70 °C (Figure 5.1f). According to Ali et al. (2018), the decrease in TPC at high temperatures exceeding 52 °C can be attributed to the thermal degradation of TPC. Although higher extraction temperatures facilitate solvent solubility within the plant cell by reducing medium viscosity, it can also lead to the degradation of TPC compounds. In conclusion, the recovery of TPC and TSC from *C. caeruleus* L. rhizome was notably affected by the extraction temperature, where the extraction temperature in UAE demonstrated a strong correlation with the other independent parameters, highlighting its significance in the overall extraction process.

5.3 Methanol concentration effect on TPC and TSC

The linear effect of methanol concentration on TPC was found to be significantly negative ($p < 0.05$), whereas its effect on TSC was not significant ($p > 0.05$). However, in the case of interaction terms ($x_1x_2, , x_1x_3$), methanol concentration's influence was significantly negative for both responses (TPC and TSC). These findings are presented in Table 5.2 and Eqs. 5.1 and 5.2.

Fig. 5.1a and 5.1b depict the influence of the interaction between methanol concentration and temperature (x_1x_2) and between methanol concentration and time (x_1x_3) on TPC from *C. caeruleus* L. rhizome, respectively. The temperature and time were fixed at zero levels. The figures show that the yield of TPC increased to its maximum value at approximately 65% methanol concentration and decreased significantly with an increase in methanol concentration above 65%. The study conducted by Cheok et al. (2012) also reported similar results where an increase in methanol concentration from 70% to 80% led to a decrease in TPC yield, and the highest TPC yield was obtained at 69.77% of methanol concentration. These findings align with the "like dissolves like" concept (Anslyn and Dougherty, 2006) which states that adding water to methanol increases the polarity of the solvent, thereby improving the yield of TPC. The results presented above suggest that the phenolic compounds present in the rhizome of *C. caeruleus* are hydrophilic in nature, as determined by the polarity of the optimal extraction solvent.

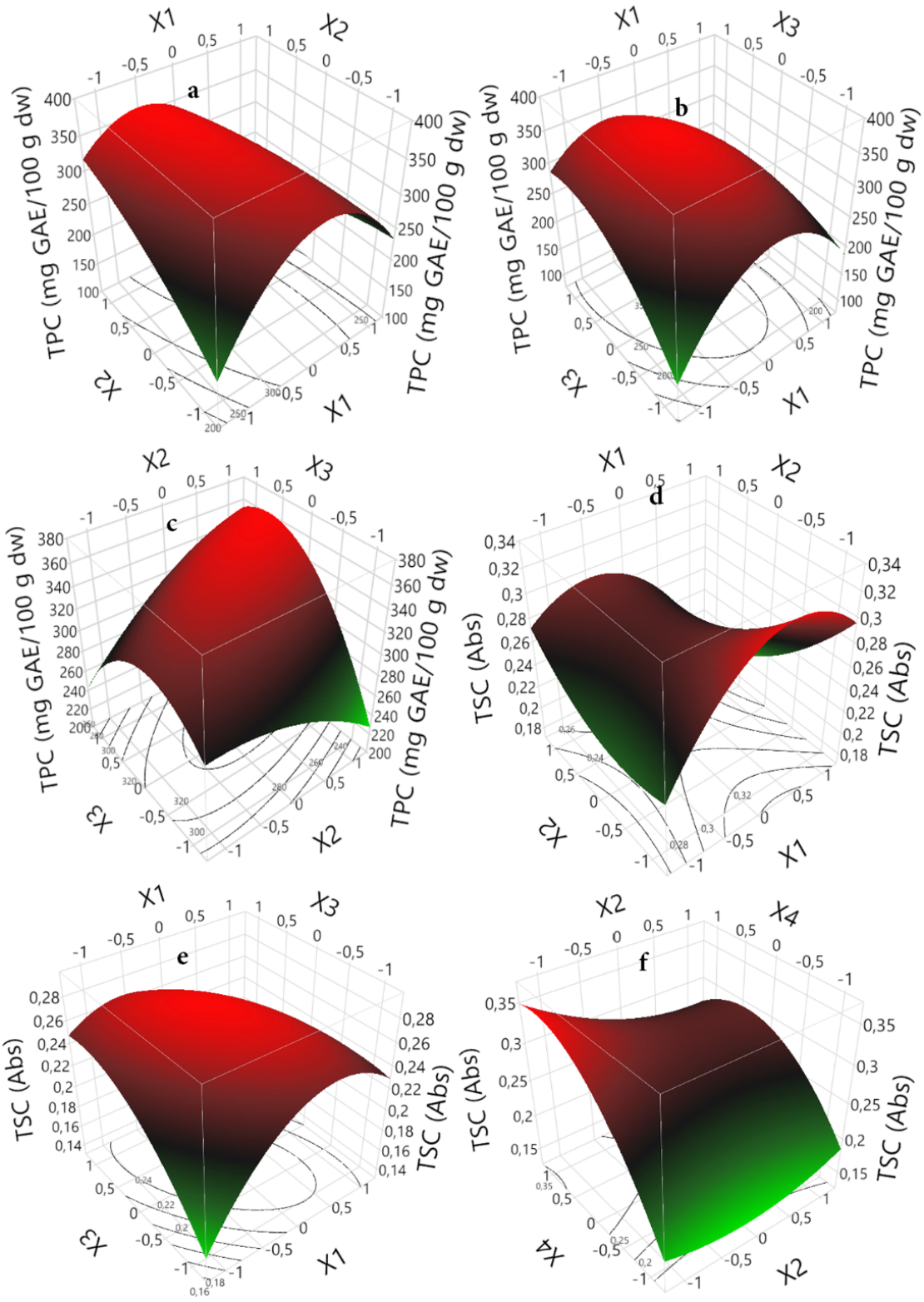

Figure 5.1: Three-Dimensional Plots Illustrating the Influence of UAE Factors on the Recovery of TPC in *C. caeruleus* L. Rhizome (a, b, and c) and TSC (d, e, and f).

As the methanol concentration in the aqueous solution increased from 60-90%, there was a significant increase in TSC. The response plots in Fig. 5.1d

and 5.1e demonstrate that the highest yield of TSC was achieved at a methanol concentration between 75-90%. The finding is consistent with the study conducted by Pham et al. (2017), which demonstrated that the maximum TSC was observed in extracts prepared using either absolute methanol or 75% methanol. In addition, the work of Sarvin et al. (2018) supported this finding by confirming that steroidal saponin compounds from *T. terrestris* L. can be easily dissolved by low-polarity organic solvents such as ethanol and methanol, with varying degrees of water. It was noted that methanol-water mixtures showed extended structures in solution, which may have an effect on the solubility and diffusivity of large hydrocarbon molecules of saponin (Shrestha and Baik, 2012). Based on the theory of similarity and intermiscibility, when the polarity of the solvent and solute is similar, the solute dissolves easily from the cells (Hadidi et al., 2020).

5.4 Time effect on TPC and TSC

Based on Table 5.2, Eq. 5.1, and Eq. 5.2, it was observed that the sonication time range from 15 to 40 min had a significant effect only on the linear terms of TPC. However, in interaction terms, sonication time was found to be a significant factor for TPC (x_1x_3, x_2x_3) and TSC (x_1x_3). These findings were consistent with the results of Zhang et al. (2019), who reported that a higher concentration of phenolic compounds was obtained at extended sonication time and a higher solvent-to-solid ratio. The interaction between sonication time and methanol concentration (x_1x_3) had a significantly negative impact, as revealed in the results. Specifically, when the concentration of methanol was lower (between 60-75%), longer sonication time led to higher TPC and TSC. Conversely, at higher methanol concentrations and longer sonication times, a lower yield of all responses was obtained (Fig. 5.1b, and 5.1e).

Based on the above results, it can be concluded that sonication time is a crucial parameter for the UAE of phenolic and saponin compounds from *C. caeruleus* L. rhizome and is directly related to other independent parameters. Numerous studies have suggested that a sonication time ranging from 20 to 35 min is the optimal range for achieving effective extraction of TPC and TSC (Pham et al., 2017; Shao et al., 2013; Shrestha and Baik, 2012; Teh and Birch, 2014). By prolonging the sonication time, the plant's cell wall becomes more susceptible to ultrasound acoustic cavitation, thereby enhancing the extraction yields of bioactive compounds. However, it is worth noting that Dong et al. (2010) reported that extending the sonication time beyond the point of maximum extraction yields can result in decreased permeability of the solvent into the plant cells. This decrease

in permeability can lead to a decline in the yield of bioactive compounds due to the suspension of impurities such as insoluble molecules, cytosol, and lipids in the extraction liquid. Additionally, there is a possibility of re-absorption of released molecules onto the larger fragmented plant particles.

Table 5.2: Standards regression and significance analysis of input variables on TPC and TSC of *C. caeruleus* L. Rhizome.

		TPC ($mg_{GAE}/100g_{dw}$)		TSC (Abs)	
	Parameters	EC	p-value	EC	p-value
Estimated parameters	Intercept	349.652	$<0.0001^{\mathbf{a}}$	0.279	$<0.0001^{\mathbf{a}}$
	Linear effects				
	x_1	-24.730	$0.0009^{\mathbf{a}}$	-0.004	0.3101^{b}
	x_2	8.904	$0.1402^{\mathbf{b}}$	-0.014	$0.0041^{\mathbf{a}}$
	x_3	14.993	$0.0208^{\mathbf{a}}$	0.003	$0.3858^{\mathbf{b}}$
	x_4	73.155	$<0.0001^{\mathbf{a}}$	0.051	$<0.0001^{\mathbf{a}}$
	Quadratic effects				
	x_1^2	-72.940	$<0.0001^{\mathbf{a}}$	-0.035	$<0.0001^{\mathbf{a}}$
	x_2^2	-12.063	$0.1792^{\mathbf{a}}$	0.014	$0.0257^{\mathbf{a}}$
	x_3^2	-33.260	$0.0020^{\mathbf{a}}$	-0.019	$0.0061^{\mathbf{a}}$
	x_4^2	-53.380	$<0.0001^{\mathbf{a}}$	-0.038	$<0.0001^{\mathbf{a}}$
	Interaction effects				
	x_1x_2	-36.879	$0.0026^{\mathbf{a}}$	-0.023	$0.0051^{\mathbf{a}}$
	x_1x_3	-32.743	$0.0057^{\mathbf{a}}$	-0.027	$0.0016^{\mathbf{a}}$
	x_1x_4	9.047	$0.3723^{\mathbf{b}}$	0.005	$0.4580^{\mathbf{b}}$
	x_2x_3	28.349	$0.0132^{\mathbf{a}}$	-0.010	$0.1420^{\mathbf{b}}$
	x_2x_4	8.703	$0.3902^{\mathbf{b}}$	-0.015	$0.0384^{\mathbf{a}}$
	x_3x_4	0.948	$0.9243^{\mathbf{b}}$	-0.011	$0.0995^{\mathbf{b}}$
Regression results	R^2	0.96		0.97	
	R^2_{Adj}	0.92		0.93	
	RMSE	$19.53^{\mathbf{a}}$		$0.013^{\mathbf{b}}$	
	C.V (%)	7.14		5.3	
	ANOVA (Model)	$<0.0001^{\mathbf{a}}$		$<0.0001^{\mathbf{a}}$	
	Lack of fit	$0.116^{\mathbf{b}}$		$0.288^{\mathbf{b}}$	

TPC; Total phenolic compounds, TSC; Total saponin content, EC; Estimated coefficient, RMSE; Root Mean Square Error, C.V; Coefficient of variance, $p-value^{a}$; statistically significant, $p-value^{b}$: statistically not significant; $RMSE^{a}$ of TPC is expressed in $GAE/100g_{dw}$; $RMSE^{b}$ of TSC is expressed in (Abs)

5.5 Solvent to solid ratio effect on TPC and TSC

Based on the results presented in Table 5.2, Eq.5.1, and Eq.5.2, the solvent-to-solid ratio was identified as the most significant factor affecting the extraction of TPC and TSC from *C. caeruleus* L. rhizome. The impact of solvent-to-solid ratio on both responses was highly significant in linear terms and interaction terms, including x_2x_4 for TSC.

Firstly, the solvent-to-solid ratio was found to be a highly significant factor in the extraction of total phenolic compounds, as shown in Table 5.2. An increase in the solvent-to-solid ratio led to a corresponding increase in the content of TPC. The high TPC values observed can be attributed to the improved solubility of phenolic compounds with an increase in the solvent-to-solid ratio until the point of solvent saturation. On the other hand, several studies have reported that increasing the sample-to-solvent ratios can increase the suspension density of the solution, which may negatively impact the solvation of bioactive compounds that are released during extraction (Pham et al., 2017).

The impact of the interaction solvent-to-solid ratio andtemperature on the variation of TSC from the rhizome of *C. caeruleus* L. is demonstrated in Fig. 5.1f. The figure indicates that an increase in the solvent-to-solid ratio from 10 to 25 $\mathrm{mL\,g^{-1}}$ led to an increase in TSC, and the maximum yield was obtained at a higher solvent-to-solid ratio and a lower temperature. The methanol-water mixture creates a concentration gradient in the medium, which in turn enhances the mass transfer phenomena of the system and improves the recovery of TSC. In a study conducted by Tian et al. (2020) on the optimization of microwave-assisted extraction (MAE) of saponin from *Aralia elata* (Miq.) Seem fruits and rachises, it was found that a solvent-to-solid ratio of 20 and 30 $\mathrm{mL\,g^{-1}}$ was optimal for the extraction of saponin. According to Ali et al. (2018), increasing the solvent-to-solid ratio may lead to the dissolution of more protein and polysaccharides in the solution, which may interfere with the dissolution of saponin. Additionally, excessive solvent ratios are not cost-effective and may not necessarily result in higher bioactive compound yields (Sarvin et al., 2018; Tian et al., 2020).

5.6 UAE optimization and model validation

A maximum desirability function was utilized to determine the optimal combination of factors that would result in the highest extraction of TPC and TSC from the rhizome of *C. caeruleus* L. The optimal condition for the maximum extraction of TPC and TSC from *C. caeruleus* L. rhizome was determined using BBD, with a methanol concentration of 78.66%, a solvent to solid ratio of 23 $\mathrm{mL\,g^{-1}}$, a temperature of 50°C, and an extraction time of 26 min. The predicted values of TPC and TSC were 349.209 $\mathrm{mg_{GAE}/100g_{dw}}$ and 0.339 (Abs), respectively, with confidence intervals of [321.826 - 377.494] and [0.320 - 0.358]. The experimental outcomes yielded a precise extraction yield of TPC, measuring 363.209 ± 11.284 $\mathrm{mg_{GAE}/100g_{dw}}$, and a value of 0.325 ± 0.005 (Abs).

These results illustrate the high accuracy and reliability of the BBD method.

Furthermore, the obtained results fell within the 95% prediction intervals determined by the second-order models, confirming their consistency with the predicted values. Additionally, the overall desirability, which represents the geometric mean of the desirability functions for individual responses, was evaluated according to the approach proposed by Derringer and Suich (1980) and Obermiller (2000). The desirability function utilized in this study yielded an overall score of 0.88, indicating the successful attainment of all targeted responses. The strong correlation observed between the predicted and observed responses signifies the high reliability of the developed models in accurately predicting the extraction of TPC and TSC from *C. caeruleus* L. rhizome using UAE.

5.7 Predicted SVR-DA model for TPC and TSC extraction from *C. caeruleus* L. rhizome

In this study, SVR-DA was employed to predict the extraction yield of TPC and TSC from *C. caeruleus* L. rhizome using UAE. Following the optimization of SVR-DA, the values of the penalty parameter (C), size of the insensitive zone (δ), sigma (σ), and 40 support vectors were determined and are listed in Table 5.3. Various kernel functions were tested, and the results in Table 6.14 demonstrate that the Gaussian RBF kernel yielded highly satisfactory outcomes, as confirmed by the results presented in Table 5.3.The dataset was divided into two groups, namely a training set consisting of 80% of the data and a validation set comprising the remaining 20%. This division was accomplished using the HOLDOUT method, as described Laidi et al. (2021); Mesellem et al. (2021); Soekarno et al. (2014). With the optimized hyper-parameters ($C = 900$, $\sigma = 2.47$, $\delta = 2.46 * 10^{-4}$), Fig. 5.2 illustrates the correlation between the measured and predicted TPC values. The training and validation sets achieved R^2 values of 0.99, and the RMSE for TPC was calculated to be 6.190 $mg_{GAE}/100\,g_{dw}$, as indicated in Table 5.3. Similarly, for TSC, the training and validation sets yielded R^2 values of 0.99 and 0.96, respectively, as depicted in Fig. 5.3. The RMSE for TSC was determined to be 0.0027 (Abs), as presented in Table 5.3.

Table 5.4 presents various metrics, including RMSE, R^2, AARD, MRPE, MAE, and RSD, to evaluate the prediction accuracy of the SVR-DA model. The values indicate that the optimized SVR-DA model has a high predictive R^2 of 0.9951 and a low RMSE of 4.2702. The AARD, MRPE, RSD, and MAE were also calculated and found to be 0.6460%, 5.9748%, 1.6881%, and 1.6165, respectively, indicating the good performance of SVR-DA in predicting the values of TPC and TSC. The results indicated that the optimized SVR-DA model is more suitable

Table 5.3: Optimal parameter values of support vector regression model optimized by the dragonfly algorithm.

Optimal parameters				
Penalty parameters (C)	Sigma (σ)	Size of the insensitive zone (ϵ)	Kernel Function	Amount of support vectors
900	2.47	$2.46 * 10^{-4}$	Gaussian	40
Output				
	TPC		TSC	
RMSE Training (80%)	0.2039[a]		0.000162[b]	
RMSE Validation (20%)	11.0150[a]		0.0068[b]	
RMSE All	6.1900[a]		0.0027[b]	

$RMSE^a$ of TPC is expressed in $mg_GAE/100g_dw$; $RMSE^b$

for modeling with limited experimental data and exhibits higher prediction accuracy. Furthermore, the marginal loss between the R^2 values for the training and validation of the optimized SVR-DA model is insignificant, indicating its high generalization performance in terms of R^2. These findings are consistent with the results of the previous results of Benimam et al. (2020) and Mesellem et al. (2021).

Table 5.4: SVR-DA performance for prediction of TPC and TSC from rhizome of *C. caeruleus* L.

	Training data	Validation data	All
RMSE	0.1829	9.5415	4.2702
R^2	1.0000	0.9722	0.9951
R	1.0000	0.9933	0.9978
b	0.2245	-12.9697	-1.6218
slop	0.9991	1.0716	1.0101
AARD (%)	0.0593	2.9927	0.6460
MRPE (%)	0.1087	5.9748	5.9748
MAE	0.1570	7.4548	1.6165
RSD (%)	0.0720	4.0517	1.6881

Additionally, a Matlab graphical user interface was developed based on the optimized SVR-DA model to facilitate the prediction of TPC and TSC from *C. caeruleus* L. rhizome (Fig. 5.4). This interface provides an efficient tool to calculate the output variables (TPC, TSC) by selecting the desired values of the extraction conditions, such as solvent concentration (%), temperature (°C), time (min), and solvent to solid ratio ($mL\,g^{-1}$). The user can obtain the predicted results quickly and easily, making this tool a practical and valuable resource for

researchers and industry professionals.

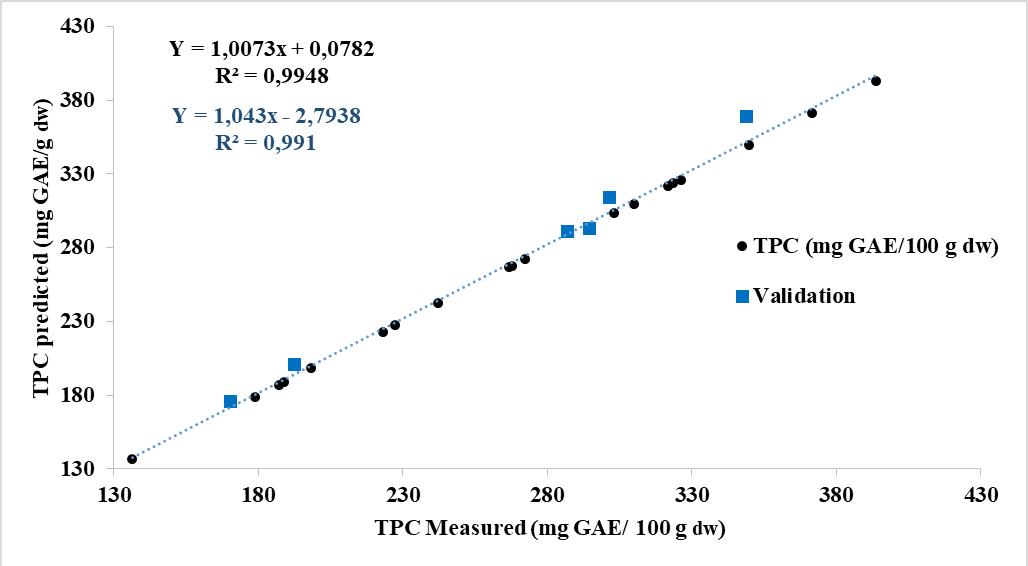

Figure 5.2: Scatter plot of experimental and predicted TPC obtained by SVR-DA.

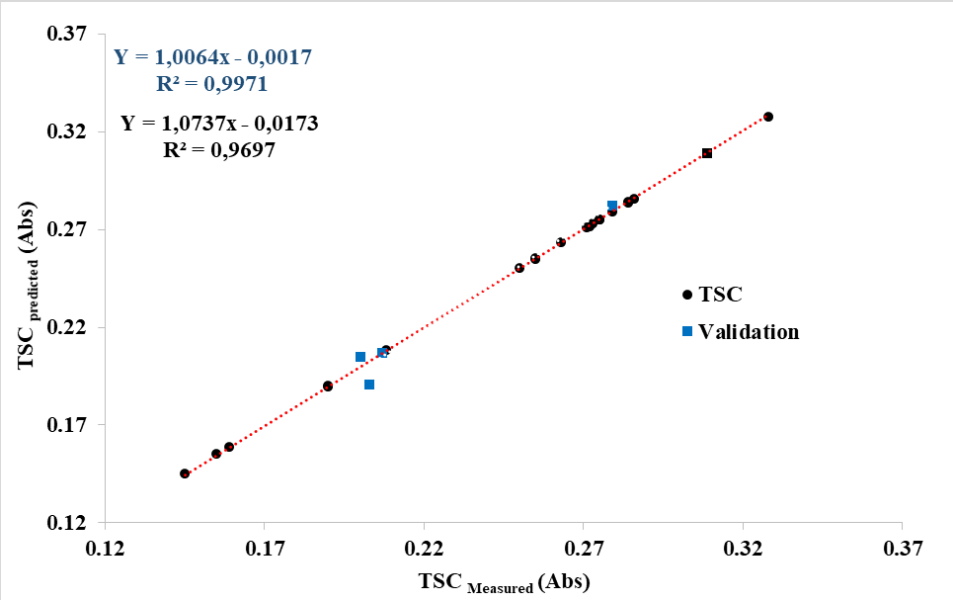

Figure 5.3: Scatter plot of measured and predicted total saponin content by SVR-DA model

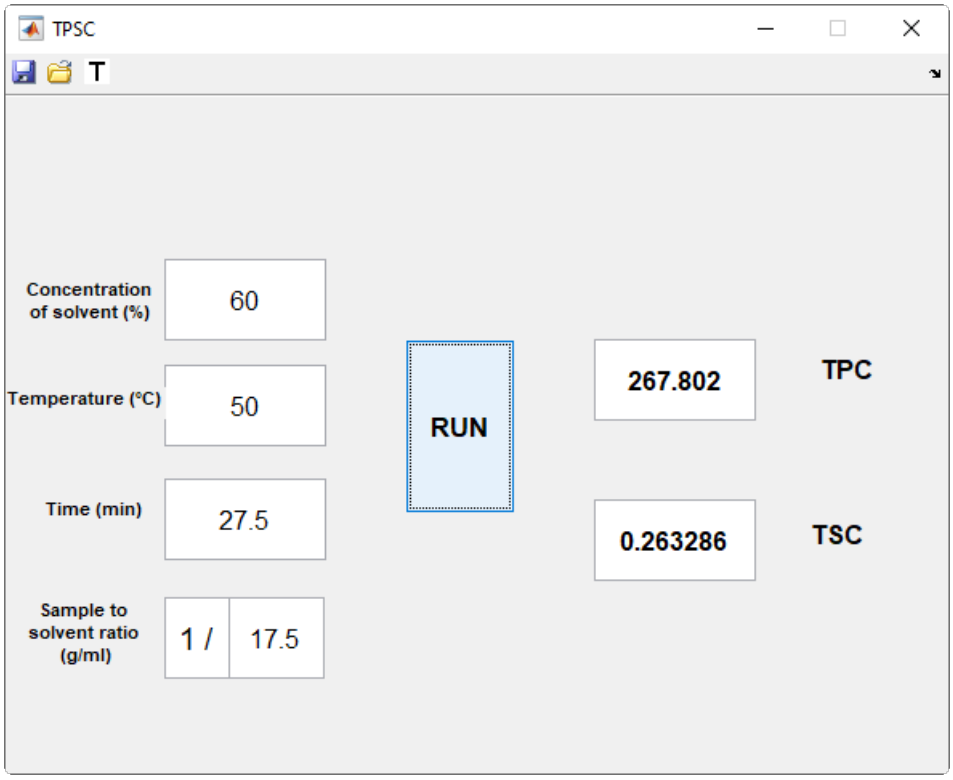

Figure 5.4: Matlab interface to predict TPC and TSC from *C. caeruleus* L. rhizome

5.8 Antioxidant capacity of *C. caeruleus* L.

For many years, *C. caeruleus* L. has been utilized for its therapeutic benefits. In this study, the extract from the rhizome of the plant was optimized under specific extraction parameters determined by BBD design: a methanol concentration of 78.66%, 23 mL g^{-1}, a temperature of 50 °C, and 26 min of sonication time. This optimized extract was then evaluated for its antioxidant activity using various antioxidant assays that utilize different mechanisms, including the $DPPH^{\bullet}$, $ABTS^{\bullet+}$, reducing power, and phosphomolybdenum assays. Furthermore, the antioxidant activity of *C. caeruleus* L. leaves extract under the same optimal conditions was also evaluated. The results obtained are illustrated in Fig. 6.11, 6.12, 6.13, and 6.14. The results of the $DPPH^{\bullet}$ scavenging activity showed that the leaves had a higher free radical scavenging activity than the rhizome, with an IC_{50} value of 157 ± 3 µg mL^{-1} of lyophilized powder for the leaves, and an IC_{50} value of 1606 ± 50 µg mL^{-1} of lyophilized powder for the rhizome (Fig. 6.11). A similar trend was observed in the decolorization of the $ABTS^{\bullet+}$ radical with the use of different parts of the plant. The IC_{50} of leaves was found to be 191 ± 3 µg mL^{-1}, while the IC_{50} of rhizome was 950 ± 22 µg mL^{-1}, as shown in Figure 6.12. These results confirmed that the leaves part of *C. caeruleus* L. showed the highest antioxidant

capacity than the rhizome part, although, the rhizome and leaves the part of *C. caeruleus* L. exhibited a higher capacity for scavenging free radicals than the rhizome extract of the same medicinal plant extracted using accelerated solvent extraction (Toubane et al., 2017). On the other hand, *C. caeruleus* L. also showed higher capacity than *Carthamus tinctorius* L. seed (Yu et al., 2013).

The TAC of rhizome and leaves of *C. caeruleus* L. was also measured using phosphomolybdenum assay, the leaves extract showed higher TAC than rhizome, at 1 mg mL^{-1} of lyophilized extract, the TAC was 90.917 ± 1.628 mg_{AAE}/g, and 33.551 ± 0.735 mg_{AAE}/g for leaves and rhizome respectively (Fig. 6.13). Furthermore, both parts of the plant demonstrated a significant capacity for reducing ferric (Fe^{3+}) ions to ferrous (Fe^{2+}) ions in the reducing power test. The leaves part displayed the highest absorbance value of 1.698 ± 0.007 at a concentration of 1 mg mL^{-1} of lyophilized extract, whereas the rhizome part exhibited an absorbance of 0.206 ± 0.013 in the same concentration. However, ascorbic acid was found to be more effective in reducing power compared to *C. caeruleus* L., as shown in Fig. 6.14. The higher and lower antioxidant activity of leaves and rhizome of *C. caeruleus* L. may be explained by the fact that the leaves produce bioactive molecules that display a higher donating capacity of hydrogen ions than the molecules produced by the rhizome part. According to Silva et al. (2005), the antioxidant activity of bioactive molecules depends on their structure, whether they are planar or spatial. The molecules that are derived from the shikimate pathway were found to have more antioxidant potential than those derived from the acetate pathway. This is significant as it can help prevent oxidative damage to cell membranes.

5.9 Conclusion

The study successfully optimized the UAE of phenolic-saponin fraction from *C. caeruleus* L. rhizome using response surface methodology based on BBD. The concentration of solvent, sonication time, temperature, and solvent-to-solid ratio were found to be the most significant UAE parameters. The optimal extraction conditions were achieved using 78.66% methanol concentration, 23 23 mL g^{-1} ratio of solvent-to-solid, 50°C temperature, and 26 min of extraction time. The study also demonstrated the high accuracy of SVR-DA in predicting TPC and TSC of *C. caeruleus* L., with a good correlation (R^2 = 0.99) and low RMSE. Furthermore, the researchers designed a graphical user interface using Matlab for predicting TPC and TSC from *C. caeruleus* L. rhizome.

The rhizome and leaves extracts demonstrated a high potential for scaveng-

ing free radicals, with an IC_{50} of 0.951 ± 0.022 mg mL^{-1} and 0.196 ± 0.0029 mg mL^{-1} for $ABTS^{\bullet+}$ assay, and an IC_{50} of 0.157 ± 0.003 mg mL^{-1} and 1.606 ± 0.05 mg mL^{-1} of lyophilized powder for $DPPH^{\bullet}$ assay, respectively. Furthermore, both the leaves and rhizomes exhibited a higher antioxidant capacity for reducing power and phosphomolybdenum assay. The rhizome of *C. caeruleus* L. has been traditionally used in folk medicine for treating burns and wounds. Saponin and phenolic compounds are believed to be the major bioactive compounds involved in the healing process. Thus, our study presents a useful tool in the form of a Matlab interface that can accurately predict the levels of TPC and TSC. This tool can be applied in the pharmaceutical industry for the development of products that utilize the healing properties of *C. caeruleus* L.

Chapter6

DSD and *I*-optimal design for optimization of UAE and MAE of TPC and antioxidant capacity from *S. officinalis* L. leaves

Abstract

To screen and optimize the extraction of total phenolic content (TPC) and antioxidant capacities (TEAC and TAC) from *Salvia officinalis* L. leaves, DSD and *I*-optimal design were employed for both ultrasound-assisted extraction (UAE) and microwave-assisted extraction (MAE). The optimal UAE conditions for achieving maximum TPC, TEAC, and TAC were determined as follows: a 52% ethanol-water mixture, and a UAE time of 10 min, a temperature of 60 °C, and ethanol-water mixture to solid ratio of 30 mL g^{-1}. Furthermore, the optimal conditions for microwave-assisted extraction (MAE) were determined as follows: a concentration of 60% ethanol-water mixture, an extraction time of 4.75 min, a power level of 600 W, and a liquid-to-solid ratio of 50 mL g^{-1}. At these optimal conditions obtained by MAE and UAE, the optimal MAE extract of common sage exhibited high TPC (46.12 ± 0.08 mg_{GAE}/g_{dw} and TEAC (268.39 ± 1.28 $\mu mol_{TE}/g_{dw}$) than optimal extract obtained by UAE, where TPC and TEAC were 31.84 ± 0.248 mg_{GAE}/g_{dw}, 237.95 ± 0.771 $\mu mol_{TE}/g_{dw}$, respectively. However, the UAE extract showed high TAC (38.928 ± 0.548 mg_{AAE}/g_{dw}) than the MAE extract with a TAC of 38.928 ± 0.548 mg_{AAE}/g_{dw}. Furthermore, Based on the UHPLC-MS analysis result, the quantitatively dominating compounds were rosmarinic acid, carnosol, carnosic acid, and methyl carnosate. Moreover, the MAE yielded a higher concentration of 181 bioactive compounds, while the UAE yielded a higher concentration of 87 compounds. In conclusion, this study provides valuable information for selecting the appropriate extraction technique for specific phenolic compounds.

6.1 Optimization of UAE and MAE using DSD and I-optimal

6.1.1 Optimization of Ultrasound assisted extraction of TPC, TEAC, and TAC

6.1.1.1 DSD fitting

In order to assess the impact of the ethanol-water mixture, extraction temperature, sonication time, and solvent-to-solid ratio on the extraction of TPC, TEAC, and TAC, the DSD approach was employed for screening purposes. Table 6.1 displays the data obtained from DSD along with the corresponding responses. The analysis of variance (ANOVA) and lack of fit results for the model are presented in Table 6.2.

The model exhibited high significance (p-value <0.0001) with no significant lack of fit. These findings indicate that the model performed well in predicting the relevant responses. Moreover, the high correlation coefficients ($R^2 \geq 0.97$) and adjusted R-squared values ($R^2_{Adj} \geq 0.94$) for all responses (TPC, TEAC, and TAC) demonstrate the strong fit of the DSD model. Moreover, the coefficient of variation (CV) provides insights into the dispersion of the data, with a value below 10% typically considered desirable (Koocheki et al., 2009). In our study, the calculated CVs for TPC, TEAC, and TAC were 9.7%, 4.3%, and 7.6%, respectively. These results indicate that the suggested model exhibited high precision and reproducibility. The mathematical equations (Eqs.6.1, Eq.6.2, and Eq.6.3) of DSD describe the relationships between TPC, TEAC, TAC, and the UAE factors as follows:

$$TPC\,(mg_{GAE}/g_{dw}) = 28.698 + 2.959\,x_1 + 1.997\,x_3 + 7.676\,x_4 - 6.662\,x_1^2 \quad (6.1)$$

$$TEAC\,(\mu mol_{TE}/g_{dw}) = 234.609 + 10.309\,x_1 + 15.107\,x_3 + 47.685\,x_4 - 31.866\,x_1^2 - 45.571\,x_4^2 - 7.397\,x_1x_4 \quad (6.2)$$

$$TAC\,(mg_{AAE}/g_{dw}) = 35.308 + 4.123\,x_1 + 2.335\,x_3 + 7.176\,x_4 - 7.649\,x_1^2 \quad (6.3)$$

Table 6.1: DSD's Matrix containing four UAE parameters and three responses.

Runs	x_1	x_2	x_3	x_4	TPC^a experimental	TPC^a predict	$TEAC^b$ experimental	$TEAC^b$ predict	TAC^c experimental	TAC^c predict
1	-1	-1	-1	+1	21.15 ± 0.46	20.99	186.32 ± 2.72	185.98	25.40 ± 0.26	26.12
2	-1	-1	+1	-1	8.99 ± 0.20	10.58	109.32 ± 1.48	111.79	13.67 ± 0.53	16.63
3	-1	-1	+1	+1	27.82 ± 0.19	25.99	223.31 ± 1.84	221.95	34.90 ± 0.22	33.21
4	-1	0	-1	-1	7.64 ± 0.33	5.788	71.27 ± 1.45	73.79	11.46 ± 0.13	9.04
5	-1	+1	-1	+1	19.48 ± 0.17	21.40	181.16 ± 2.55	181.93	23.47 ± 0.24	25.10
6	-1	+1	0	-1	7.20 ± 0.02	8.49	85.73 ± 0.29	89.75	11.20 ± 0.16	12.07
7	-1	+1	+1	0	22.72 ± 0.55	21.78	216.47 ± 2.63	208.39	28.63 ± 0.26	26.56
8	0	-1	-1	-1	16.77 ± 0.20	15.73	138.37 ± 1.48	128.27	24.55 ± 0.21	23.64
9	0	0	0	0	28.81 ± 0.45	28.69	234.25 ± 0.29	234.60	34.95 ± 0.11	35.30
10	0	+1	+1	+1	34.34 ± 0.24	35.49	240.06 ± 2.96	249.80	41.09 ± 0.15	41.64
11	+1	-1	-1	0	22.23 ± 0.42	23.29	195.12 ± 4.39	202.84	29.45 ± 0.12	31.16
12	+1	-1	0	+1	27.22 ± 0.13	29.35	207.72 ± 3.06	209.79	37.48 ± 0.22	35.69
13	+1	-1	+1	-1	16.02 ± 0.15	15.55	141.79 ± 2.66	141.45	25.01 ± 0.24	24.69
14	+1	0	+1	+1	31.64 ± 1.24	31.05	223.14 ± 3.63	220.00	35.60 ± 0.11	36.31
15	+1	+1	-1	-1	11.94 ± 0.44	12.97	108.98 ± 0.88	112.93	21.73 ± 0.05	21.41
16	+1	+1	-1	+1	30.88 ± 0.29	28.26	201.26 ± 1.84	193.51	33.67 ± 0.11	33.54
17	+1	+1	+1	-1	16.50 ± 0.24	15.96	139.91 ± 0.59	137.39	23.53 ± 0.13	23.67

TPC^a: mg_{GAE}/g_{dw} (mg Gallic acid equivalent per g of dry weight), $TEAC^b$: µmol$_{\mathrm{TE}}$/g$_{\mathrm{dw}}$ (µmol Trolox equivalent per g of dry weight), TAC^C:mg_{AAE}/g_{dw} (mg Ascorbic acid equivalent per g of dry weight), TPC: Total phenolic compounds, TEAC: Trolox equivalent antioxidant capacity, TAC: Total antioxidant capacity

Table 6.2: Regression results and estimated coefficient of DSD for screening UAE parameters.

		TPC (mg_{GAE}/g_{dw})		TEAC (µmol$_{\mathrm{TE}}$/g$_{\mathrm{dw}}$)		TAC (mg_{AAE}/g_{dw})	
		EC	p-value	EC	p-value	EC	p-value
Estimated parameters	Intercept	28.698	<0.0001^a	234.609	<0.0001^a	35.308	<0.0001^a
	Linear effects						
	x_1	2.959	0.0006^a	10.309	0.0009^a	4.123	<0.0001^a
	x_3	1.997	0.0059^a	15.107	<0.0001^a	2.335	0.0028^a
	x_4	7.676	<0.0001^a	47.685	<0.0001^a	7.176	<0.0001^a
	x_2	0.204	0.7317^b	-2.0267	0.3414^b	-0.509	0.3811^b
	Quadratic effects						
	x_1^2	-6.662	0.0001^a	-31.866	0.0002^a	-7.649	0.0004^a
	x_4^2	-3.082	0.0602^b	-45.571	<0.0001^a	-2.662	0.1019^b
	Interaction effects						
	x_1x_4	-0.028	0.9625^b	-7.397	0.0099^a	-1.112	0.1026^b
	x_1x_3	-0.502	0.4524^b	-2.877	0.2599^b	-1.207	0.1007^b
Regression results	R^2	0.97		0.99		0.97	
	R^2_{Adj}	0.94		0.98		0.94	
	RMSE	2.0120		7.497		2.057	
	C.V (%)	9.7		4.3		7.6	
	ANOVA (Model)	<0.0001^a		<0.0001^a		<0.0001^a	
	Lack of fit	/		/		/	

EC; Estimated coefficient, RMSE; Root Mean Square Error, C.V; Coefficient of variance, $p-value^a$; statistically significant, $p-value^b$; statistically not significant

The findings from the DSD analysis revealed a significant impact of various UAE parameters, such as the ethanol-water mixture, temperature, and solvent-to-solid solvent ratio, on the levels of TPC, TEAC, and TAC ($p < 0.05$). However,

it was observed that the extraction time had no significant effect on TPC and antioxidant activity, as indicated by a p-value obtained in Table 6.2.

In addition to examining UAE linear effects, the quadratic effects of the UAE factors on TPC, TEAC, and TAC were also taken into consideration. Among these factors, only the ethanol-water mixture exhibited high significance on TPC and TCA ($p < 0.01$). Regarding the quadratic effects of both ethanol-water mixture and solvent-to-solid ratio demonstrated a strong influence on TEAC (Table 6.2). Additionally, a noteworthy interaction effect between the ethanol-water mixture and solvent-to-solid ratio was observed, significantly impacting TEAC with a low p-value ($p < 0.01$), as illustrated in Table 6.2.

6.1.1.2 *I*-optimal design fitting

The DSD findings revealed that the extraction of TPC, TEAC, and TAC from *S. officinalis* L. leaves is influenced by three key factors: the ethanol-water mixture, temperature, and solvent-to-solid ratio. These factors were identified as significant based on the results presented in Tables 6.1 and 6.2. Consequently, for the optimization process outlined in Table 6.3, these factors were chosen. The analysis of variance and estimated parameters for the I-optimal design are presented in Table 6.4. In this study, the factors x_1, x_3, and x_4 were taken into consideration. The I-optimal models for TPC, TEAC, and TAC were derived and are represented by Eq. 6.4, Eq. 6.5, and Eq. 6.6, respectively.

$$TPC\,(mg_{GAE}/g_{dw}) = 24.998 + 1.054\,x_3 + 8.013\,x_4 - 4.697\,x_1^2 - 1.952\,x_4^2 - 1.340\,x_3x_4 \tag{6.4}$$

$$TEAC\,(\mu mol_{TE}/g_{dw}) = 214.925 + 12.820\,x_1 + 49.113\,x_4 - 32.106\,x_1^2 - 16.127\,x_1x_4 \tag{6.5}$$

$$TAC\,(mg_{AAE}/g_{dw}) = 34.174 + 3.355\,x_1 + 1.182\,x_3 + 7.766\,x_4 - 5.495\,x_1^2 \tag{6.6}$$

The ANOVA results revealed that the model exhibited a significantly low $P-value$ (< 0.01) for TPC, TAC, and TEAC. These findings indicate that the models developed for all the tested responses were statistically significant. Additionally, the lack of fit was found to be insignificant for all the responses, which further

Table 6.3: I-Optimal design matrix with the three UAE parameters and three output variables (TPC, TEAC, and TAC)

Runs	x_1	x_3	x_4	TPC^a experimental	TPC^a predict	$TEAC^b$ experimental	$TEAC^b$ predict	TAC^c experimental	TAC c predict
1	-1	+1	+1	29.42 ± 0.25	29.31	228.35 ± 1.27	221.22	35.34 ± 0.15	34.26
2	-1	0	-1	9.79 ± 0.15	11.17	89.69 ± 2.78	84.50	14.70 ± 0.48	14.17
3	0	0	0	24.61 ± 0.40	24.99	216.88 ± 3.49	214.92	34.95 ± 0.11	34.17
4	0	0	+1	31.94 ± 0.13	31.05	240.35 ± 10.98	243.78	39.63 ± 0.62	39.80
5	+1	-1	+1	30.17 ± 0.11	30.48	218.93 ± 6.87	209.27	36.70 ± 0.64	35.50
6	+1	+1	+1	28.88 ± 0.22	28.84	191.60 ± 6.72	192.88	36.79 ± 0.07	37.30
7	0	0	0	25.39 ± 0.24	24.99	216.55 ± 3.22	214.92	34.54 ± 0.11	34.17
8	0	0	0	25.20 ± 0.07	24.99	227.05 ± 7.45	214.92	33.95 ± 0.13	34.17
9	0	+1	0	27.60 ± 0.07	29.05	210.48 ± 1.50	217.87	34.57 ± 0.06	35.34
10	+1	+1	-1	14.62 ± 0.60	14.35	152.70 ± 5.42	142.05	25.01 ± 0.69	23.65
11	-1	-1	+1	28.08 ± 0.10	28.81	182.08 ± 4.04	194.16	28.51 ± 0.59	30.11
12	+1	-1	-1	10.38 ± 0.25	10.64	126.38 ± 5.10	128.16	22.31 ± 0.38	23.08
13	+1	0	0	20.31 ± 0.46	20.03	178.14 ± 9.22	195.63	30.75 ± 0.43	32.03
14	-0.11	-1	-1	15.96 ± 0.30	15.61	110.73 ± 1.16	115.69	22.77 ± 0.63	22.74
15	-1	+1	-1	18.12 ± 15.96	17.10	96.76 ± 4.04	105.87	14.48 ± 0.46	15.62
16	-1	-1	0	22.92 ± 0.24	21.98	150.78 ± 6.58	141.61	24.67 ± 0.26	23.54

confirms the good performance of the models in predicting the relevant responses (see Table 6.4). In addition, the adjusted coefficients (R^2_{Adj}) for TPC, TEAC, and TAC were found to be in close proximity to the determination coefficients (R^2), as shown in Table 6.4.

Significance was observed in both the linear interaction and quadratic effects ($P < 0.05$). It is noteworthy that all the linear effects (x_1, x_3, and x_4), quadratic effects (x_1^2, x_3^2, and x_4^2), and interaction effects (x_1x_4 and x_3x_4) exhibited a significant influence on the extraction of TPC, TEAC, and TAC, as indicated in Table 6.4.

6.1.1.3 UAE factors effects on TPC and antioxidant activity

To optimize the extraction process of TPC and the antioxidant activity of *S. officinalis* L. leaves, the I-optimal design was employed. The experimental design and the outcomes of TPC, TEAC, and TAC assays are presented in Table 6.3. The analysis of variance for the model and the estimated coefficient of each extraction parameter on TPC, TEAC, and TAC can be found in Table 6.4.

Figure 6.1a illustrates the interaction effect of ethanol-water concentration and temperature while keeping the third variable at a constant level. The combined influence of these two variables had a positive impact on the yield of TPC, resulting in a range of 16 to 31 mg_{GAE}/g_{dw}. The maximum TPC value of 31 mg_{GAE}/g_{dw} was achieved at an ethanol-water concentration of 50% and a UAE temperature of 60 °C (see fig. 6.1a).

Table 6.4: Regression results of I-optimal design and the estimated coefficients of UAE parameters for the TPC, TEAC, and TAC.

		TPC (mg_{GAE}/g_{dw})		TEAC ($\mu mol_{TE}/g_{dw}$)		TAC (mg_{AAE}/g_{dw})	
		EC	p-value	EC	p-value	EC	p-value
Estimated parameters	Intercept	24.998	<0.0001[a]	214.925	<0.0001[a]	34.174	<0.0001[a]
	Linear effects						
	x_1	-0.268	0.4933[b]	12.820	0.0270[a]	3.355	0.0004[a]
	x_3	1.054	0.0059[a]	10.236	0.0593[b]	1.182	0.0493[a]
	x_4	8.013	<0.0001[a]	49.113	<0.0001[a]	7.766	<0.0001[a]
	Quadratic effects						
	x_1x_1	-4.697	0.0007[a]	−32.106	0.0107[a]	-5.495	0.0012[a]
	x_4x_4	-1.952	0.0371[a]	-20.258	0.0602[b]	0.956	0.0669[b]
	x_3x_3	3.001	0.0064[a]	-7.287	0.4376[b]	-0.011	0.9912[b]
	Interaction effects						
	x_1x_3	-0.537	0.2540[b]	-10.859	0.0773[b]	-0.587	0.3320[b]
	x_1x_4	0.569	0.2294[b]	-16.127	0.0195[a]	-1.247	0.0663[b]
	x_3x_4	-1.340	0.0201[a]	-7.569	0.1893[b]	0.308	0.6005[b]
Regression results	R^2	0.99		0.97		0.99	
	R^2_{Adj}	0.97		0.92		0.96	
	RMSE	1.15		13.86		1.51	
	C.V (%)	5.09		7.82		5.15	
	ANOVA (Model)	<0.0001[a]		0.0007[a]		<0.0001[a]	
	Lack of fit	0.0806[b]		0.1199[b]		0.0713[b]	

The obtained TPC value of the *S. officinalis* leaf extract in this study was found to be close to the TPC value (27.05 mg_{GAE}/g_{dw}) reported by Maleš et al. (2022), and higher than the TPC value (25.58 mg_{GAE}/g_{dw}) of the hydro-methanolic extract reported by Doymaz and Karasu (2018). Furthermore, the TPC of the optimized *S. officinalis* extract exceeded the TPC value of 9.15 mg_{GAE}/g_{dw} in the supercritical fluid sage leaf extract, as well as the TPC value of 17.1 mg_{GAE}/g_{dw} in the sage methanol-acetone extract reported by Pavic et al. (2019) and Francik et al. (2020) respectively.

Similar effects of ethanol-water concentration and temperature on TEAC and TAC were observed, as shown in Fig.6.2a and Fig.6.2d. Both antioxidant activity assays exhibited an increase with higher ethanol concentration and temperature. The highest TEAC value of 220 $\mu mol_{TE}/g_{dw}$) and TAC value of 36 mg_{AAE}/g_{dw} were observed at a temperature of 60 °C and an ethanol-water mixture of 50%. In contrast, a decline in both TPC and antioxidant activity was observed when the ethanol concentration was increased from 50% to 90% (Figs. 6.2a and Fig. 6.2d). A study by Savic and Savic Gajic (2020) reported the optimal conditions for UAE of TPC in *Triticum aestivum* L. to be 56% (v/v) ethanol and a temperature of 59 °C, resulting in a TPC range of 105 to 155 mg_{GAE}/g_{dw}. Moreover, the optimal UAE parameters determined in this study align with the findings of Berkani et al. (2020), who reported that an ethanol concentration of 50.16% resulted in a high TPC value of 23.83 ± 0.87 mg_{GAE}/g_{dw} from *Zizyphus lotus* fruits. In terms of antioxidant

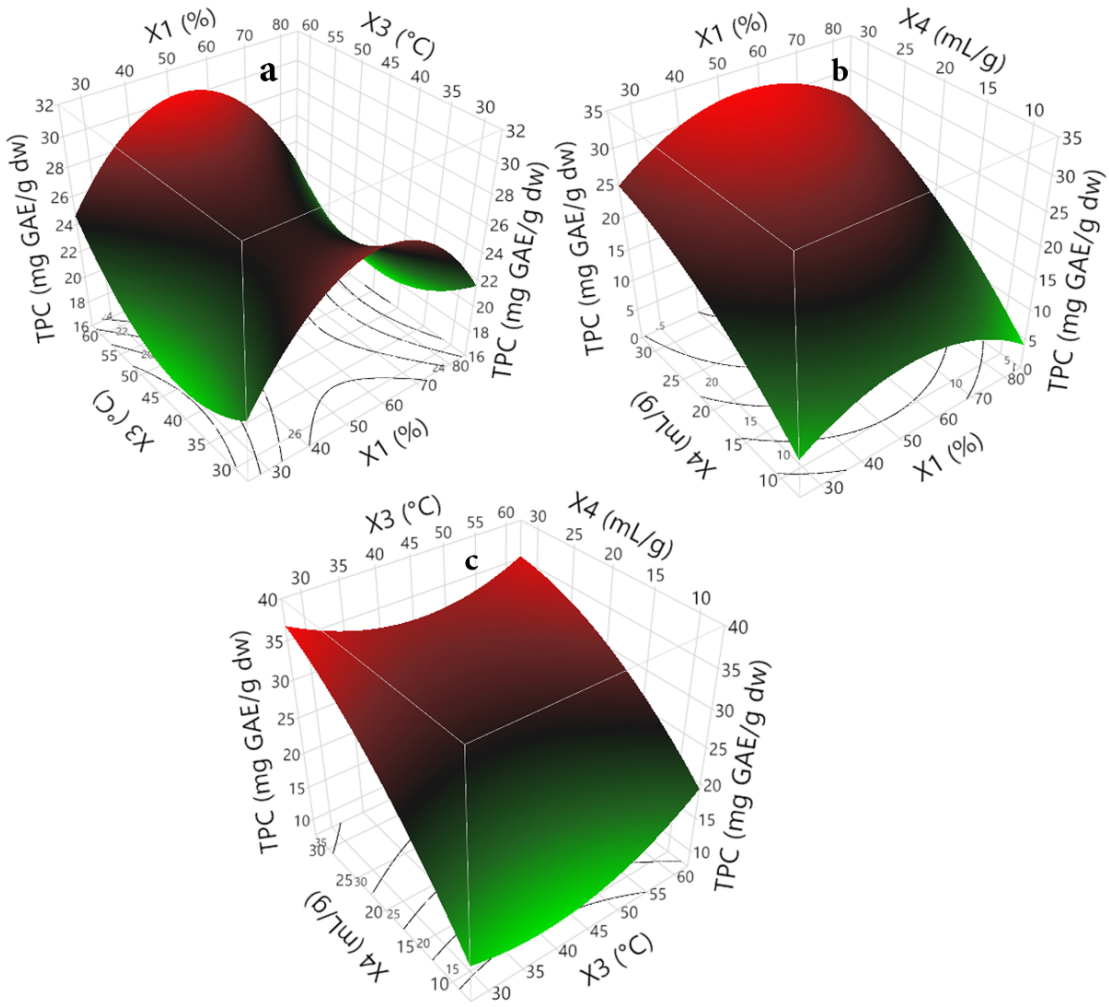

Figure 6.1: Three-dimensional plots of *S. officinalis* L. leaves showing the influence of UAE factors on the recovery of TPC

capacity, Chew et al. (2011) demonstrated that an extraction temperature of 60 °C resulted in a higher antioxidant capacity (7.65 $\mu mol_{TE}/g$) in the extract obtained from *Orthosiphon stamineus*.

The influence of ethanol concentration can be attributed to the principle of similarity and intermiscibility. When the ethanol-water mixture reached a concentration of 50%, its polarity became more comparable to that of the antioxidant compounds present in *S. officinalis* L. leaves, resulting in a significant enhancement of the antioxidant activity. Numerous studies have indicated that TPC and TFC exhibit high solubility in hydroalcoholic solutions, while compounds with antioxidant capacity tend to be more hydrophilic (Arteaga-Crespo et al., 2020; Palma et al., 2021). Furthermore, an increase in ethanol concentration has been found to enhance the solubility of antioxidant compounds by expanding the interface area between the extraction solvent and solutes (Ali et al., 2018).

In order to gain further insight into the impact of temperature, figures 6.1c,

6.2c, and 6.2e depicted the interaction effect of temperature with the solvent-to-solid ratio on TPC, TEAC, and TAC, respectively. The temperature effect was examined at two distinct levels, namely high and low amounts of solvent-to-solid ratios. The levels of TPC, TEAC, and TAC exhibited a gradual increase as the extraction temperature increased, particularly when the solvent-to-solid ratio was at low values. Conversely, the extraction of TPC displayed a slight decrease as the temperature rose from 30 °C to 45 °C. However, the TPC levels resumed a gradual increase with further temperature elevation from 45 °C to 60 °C, particularly when the solvent-to-solid ratio was at high values (Fig. 6.1c).

Moreover, when the solvent-to-solid ratio was high, the effect of temperature on TEAC was found to be insignificant. However, TAC exhibited a gradual increase with rising temperatures from 30 °C to 60 °C. Consequently, the highest levels of TPC (35 mg_{GAE}/g_{dw}), TEAC (250 $\mu mol_{TE}/g_{dw}$), and TAC (42 mg_{AAE}/g_{dw}) were achieved near the upper limits of both temperature (60 °C) and solvent-to-solid ratio ($30\,mL\,g^{-1}$).

Similar findings were reported by Ismail et al. (2019) and Pandey et al. (2018), who identified a solvent-to-solid ratio of $30\,mL\,g^{-1}$ as an optimal UAE parameter for maximizing phenolic and antioxidant compounds extraction from plant extracts. Higher temperatures have been shown to enhance the extraction of TPC and antioxidant activity in medicinal plants by increasing vapor pressure and reducing surface tension within the medium. This leads to an increased presence of solvent vapors within the bubble cavity and the generation of numerous cavitation bubbles (Chemat et al., 2017). Furthermore, elevated temperatures promote mass transfer phenomena by providing additional energy to analyte molecules, enabling them to overcome energy barriers associated with their interaction within the matrix (Capelo-Martínez, 2009).

Moreover, the impact of the solvent-to-solid ratio on TPC, TEAC, and TAC was observed to be positive. As illustrated in Figs. 6.1b, 6.1c, 6.2b, 6.2c, 6.2e, and 6.2f, all the tested responses exhibited exponential growth when the solvent-to-solid ratio was increased, reaching its peak at $30\,mL\,g^{-1}$.

According to the findings reported by Vural et al. (2018), an extraction process using a solvent-to-solid ratio of $30\,mL\,g^{-1}$ was identified as the optimal parameter. This specific extraction condition resulted in a notable increase in both TPC and antioxidant activity of grape seed extract, with values recorded as 25.87 $\pm$ 0.92 mg_{GAE}/g and 92.33% $\pm$ 0.47, respectively.

As indicated in prior research conducted by Ngamkhae et al. (2022), it has been established that augmenting the solvent quantity results in a larger sur-

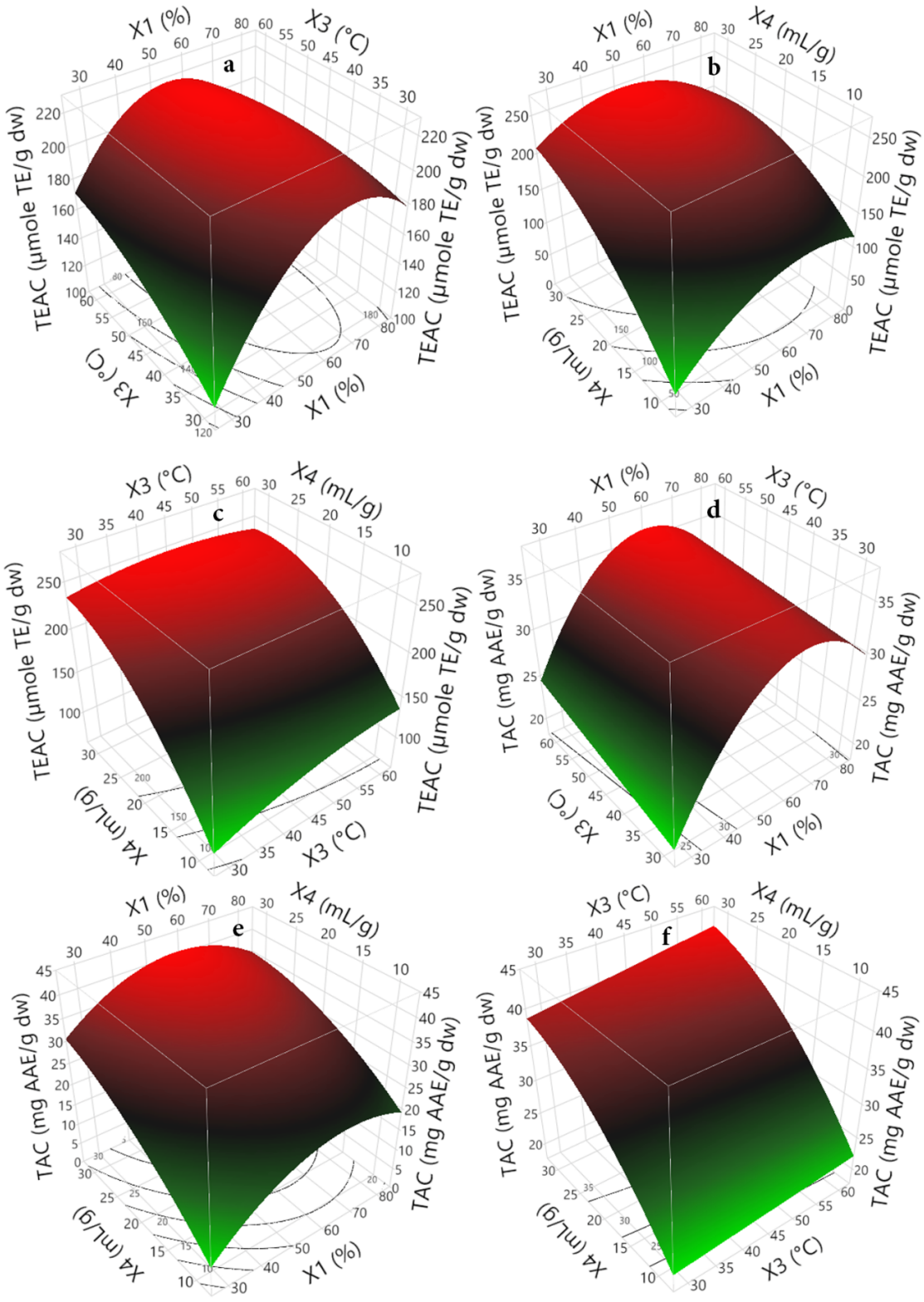

Figure 6.2: Three-dimensional plots of *S. officinalis* L. leaves showing the influence of UAE factors on TEAC (a, b, c) and TAC (d, e, f) respectively

face area for the formation of cavitation bubbles by the acoustic wave. This phenomenon subsequently enhances the mass transfer between the solvent and the sample. Furthermore, an elevated solvent-to-solid ratio leads to an increased suspension density within the solution, negatively affecting the solvation of liberated cellular compounds, as mentioned by Pham et al. (2017). Conversely, a low solvent-to-solid ratio results in a higher viscosity of the solution, posing challenges to the cavitation effect. In such cases, the negative pressure generated during the rarefaction cycle must overcome a stronger cohesive force due to the high viscosity, as highlighted by (Kumar et al., 2021).

6.1.1.4 Optimal UAE conditions for high TPC and antioxidant activity

The main objective of optimizing the parameters for UAE was to simultaneously enhance the three responses of interest - TPC, TEAC, and TAC, due to the interrelationship between the phenolic compounds and their antioxidant properties. Upon obtaining the optimized conditions, the verification of the obtained results was carried out using the DSD and the I-optimal design. These validation tests were conducted under the optimal conditions.

The optimum conditions determined by both models corresponded to a temperature of 60 °C and a solvent-to-solid ratio of 30 mL g^{-1}. The DSD model predicted that the ethanol-water mixture would constitute approximately 57% of the solvent, while the I-optimal model predicted a slightly lower value of 52%. The predicted values of TPC, TEAC, and TAC aligned well with the expected values, falling within the 95% prediction intervals generated by the DSD model. These results are summarized in Table 6.5. The obtained outcomes provided conclusive evidence regarding the precision and suitability of both the DSD and I-optimal models in effectively screening and optimizing the ultrasound-assisted extraction process for extracting TPC and antioxidant activity from the leaves of *S. officinalis* L. These findings validate the reliability and usefulness of these models for UAE procedure.

6.1.2 Optimization of microwave-assisted extraction of TPC, TEAC, and TAC

6.1.2.1 DSD fitting

For the evaluation of the impacts and interactions of four MAE parameters on the levels of TPC, TEAC, and TAC in *S. officinalis* L. leaves, a 17-run DSD was employed. The DSD experimental design consisted of three levels for each of the

Table 6.5: Predicted, obtained values and confidence intervals of optimal extract from *S. officinalis* L. leaves, generated by definitive screening design and I-optimal design

	Response	Predicted response	95% PI low	Observed response a	95% PI high
DSD	TPC (mg_{GAE}/g_{dw})	35.27	31.70	32.77 ± 0.35	38.83
	TEAC ($\mu mol_{TE}/g_{dw}$)	253.48	240.20	241.33 ± 1.26	266.76
	TAC (mg_{AAE}/g_{dw})	42.77	32.12	38.76 ± 0.23	46.41
I-optimal design	TPC (mg_{GAE}/g_{dw})	33.64	31.38	31.84 ± 0.24	35.90
	TEAC ($\mu mol_{TE}/g_{dw}$)	240.60	213.51	237.94 ± 0.77	267.70
	TAC (mg_{AAE}/g_{dw})	40.96	38.01	38.92 ± 0.54	43.92

PI: Predicted interval, *superscript*[a]: Values are expressed as mean ± standard deviation (n = 3).

four MAE parameters. The obtained results from the DSD experiments, showcasing the outcomes of these assessments, are presented in Table 6.6. Table 6.7 presents the outcomes of the second-order polynomial regression analysis and the statistical analysis of variance (ANOVA). The relationships between TPC, TEAC, and TAC with the MAE parameters are described by Equation 6.7, Equation 6.8, and Equation 6.9, respectively. These equations establish the mathematical expressions that capture the associations between the response variables and the MAE parameters.

$$TPC\,(mg_{GAE}/g_{dw}) = 32.50 + 0.20\,x_1 - 0.21\,x_2 + 7.14E^{-10}\,x_3 + 6.29\,x_4 - 0.97\,x_1^2 - 0.28\,x_2^2 + 1.39\,x_4^2 - 0.19\,x_1x_3 - 0.19\,x_2x_4 \quad (6.7)$$

$$TEAC\,(\mu mol_{TE}/g_{dw}) = 245.06 + 3.01\,x_1 - 12.33\,x_2 - 0.01\,x_3 + 25.60\,x_4 - 20.50\,x_1^2 - 14.63\,x_2^2 - 15.15\,x_4^2 - 5.21\,x_1x_3 - 11.24\,x_2x_4 \quad (6.8)$$

$$TAC\,(mg_{AAE}/g_{dw}) = 33.14 + 2.01\,x_1 - 2.60\,x_2 - 1.43\,x_3 + 2.62\,x_4 - 6.27\,x_1^2 - 0.30\,x_2^2 - 2.16\,x_4^2 + 1.10\,x_1x_3 - 0.18\,x_2x_4 \quad (6.9)$$

Table 6.6: DSD matrix to screen four MAE parameters that could have an impact on TPC, TEAC and TAC

Runs	x_1	x_2	x_3	x_4	TPC^a experimental	TPC^a predict	$TEAC^b$ experimental	$TEAC^b$ predict	TAC^C experimental	TAC^C predict
1	-1	-1	-1	+1	37.79 ± 0.20	39.16	203.03 ± 0.24	195.81	26.54 ± 0.5	25.76
2	-1	-1	+1	-1	25.58 ± 0.55	25.86	170.05 ± 1.12	175.40	15.43 ± 0.04	15.05
3	-1	-1	+1	+1	39.70 ± 0.19	39.31	183.85 ± 0.42	195.81	20.11 ± 0.05	20.67
4	-1	0	-1	-1	26.98 ± 0.29	26.31	184.00 ± 0.25	195.19	23.01 ± 0.02	22.61
5	-1	+1	-1	+1	40.01 ± 0.08	38.97	250.98 ± 1.85	249.93	29.95 ± 0.34	30.59
6	-1	+1	0	-1	24.75 ± 0.82	26.22	155.52 ± 0.48	169.29	21.47 ± 0.29	23.17
7	-1	+1	+1	0	31.34 ± 0.81	30.30	213.39 ± 0.23	222.55	26.60 ± 0.50	25.23
8	0	-1	-1	-1	27.98 ± 0.23	26.98	185.70 ± 0.49	175.40	28.13 ± 0.29	27.30
9	0	0	0	0	32.72 ± 0.64	33.12	246.93 ± 0.41	233.39	32.80 ± 0.47	33.14
10	0	+1	+1	+1	38.54 ± 0.76	39.13	265.48 ± 0.78	249.93	34.41 ± 0.39	34.89
11	+1	-1	-1	0	30.51 ± 0.92	31.15	194.16 ± 1.15	198.54	25.90 ± 0.28	26.92
12	+1	-1	0	+1	41.18 ± 1.60	39.65	200.55 ± 1.75	195.81	27.64 ± 0.56	27.23
13	+1	-1	+1	-1	26.60 ± 0.49	27.23	170.15 ± 1.03	175.40	20.47 ± 0.49	21.28
14	+1	0	+1	+1	39.03 ± 0.81	39.31	243.36 ± 1.90	245.72	28.97 ± 0.39	29.01
15	+1	+1	-1	-1	26.90 ± 0.12	26.71	176.01 ± 1.03	169.29	27.45 ± 0.23	27.51
16	+1	+1	-1	+1	37.71 ± 0.41	38.43	235.70 ± 1.23	249.93	32.94 ± 0.35	32.39
17	+1	+1	+1	-1	27.09 ± 0.28	26.56	183.13 ± 1.12	169.29	27.83 ± 0.20	26.85

TPC^a: mg_{GAE}/g_{dw} (mg Gallic acid equivalent per g of dry weight), $TEAC^b$: $\mu mol_{TE}/g_{dw}$ (µmol Trolox equivalent per g of dry weight), TAC^C:mg_{AAE}/g_{dw} (mg Ascorbic acid equivalent per g of dry weight), TPC: Total phenolic compounds, TEAC: Trolox equivalent antioxidant capacity, TAC: Total antioxidant capacity

The analysis of variance and goodness-of-fit of the DSD are summarized in Table 6.7. The statistical significance of the models for TPC, TEAC, and TAC is demonstrated by their considerably low p-value (< 0.0001). To assess the quality of the DSD models, various metrics such as the determination coefficient (R^2), adjusted determination coefficient (R^2_{adj}), and coefficient of variance (C.V) are considered. These metrics play a crucial role in evaluating the goodness-of-fit of the DSD models.

The determination coefficient (R^2) values for TPC, TEAC, and TAC exceeded 0.97, while the adjusted determination coefficient (R^2_{adj}) values were greater than 0.93. Additionally, the coefficient of variance (C.V) for all the response variables was below 5% (Table 6.7). These results indicate that the DSD model effectively captures a significant portion of the variation in the data with high precision and reliability. The high R^2 and R^2_{adj} values, along with the low C.V, validate the robustness and accuracy of the DSD model in explaining the observed variations in the responses.

Based on the significance level of the p-value, it can be concluded that only the linear coefficient (x_4) had a significant effect on TPC. On the other hand, for TEAC, the linear coefficient (x_4), quadratic coefficients (x_1^2 and x_4^2), and interaction term coefficients (x_2x_4) were all found to be significant (p-value < 0.05).

Moreover, TAC was influenced by all the linear coefficients (x_1, x_2, x_3, and x_4), quadratic coefficients (x_1^2 and x_4^2), as well as the interaction term coefficient (x_1x_4). These findings indicate which specific coefficients had statistically significant impacts on each of the response variables.

Table 6.7: DSD's regression results and the estimated MAE parameters for TPC, TEAC, and TAC

		TPC (mg_{AAE}/g_{dw})		TEAC ($\mu mol_{TE}/g_{dw}$)		TAC (mg_{AAE}/g_{dw})	
	MAE parameters	EC	p-value	EC	p-value	EC	p-value
Estimated parameters	Intercept	32.503	$<0.0001^a$	245.065	$<0.0001^a$	33.147	$<0.0001^a$
	Linear effects						
	x_1	0.206	0.604^b	3.016	0.215^b	2.007	0.0005^a
	x_3	$7.143 * E^{-10}$	1.000^b	-0.011	0.995^b	-1.436	0.0032^a
	x_4	6.290	$<0.0001^a$	25.601	$<0.0001^a$	2.626	$<0.0001^a$
	x_2	-0.214	0.7317^b	12.337	0.0008^b	2.601	$<0.0001^a$
	Quadratic effects						
	x_1^2	-0.978	0.365^b	-20.508	0.0102^a	-6.270	0.0002^a
	x_2^2	-0.282	0.798^b	-14.630	0.0503^b	0.309	0.745^b
	x_4^2	1.399	0.230^b	-15.150	0.0445^a	-2.169	0.0499^a
	Interaction effects						
	x_1x_3	-0.199	0.365^b	5.212	0.188^b	1.107	0.0380^a
	x_2x_4	-0.240	0.594^b	11.247	0.0034^a	-0.186	0.6420^b
Regression results	R^2	0.97		0.99		0.97	
	R^2_{adj}	0.94		0.93		0.94	
	RMSE	1.42		8.29		1.22	
	C.V	4.35		4.07		4.60	
	ANOVA (Model)	$<0.0001^a$		0.0001^a		$<0.0001^a$	
	Lack of fit	/		/		/	

EC; Estimated coefficient, **RMSE**; Root Mean Square Error, **C.V**; Coefficient of variance, $p - value^a$; statistically significant, $p - value^b$; statistically not significant

6.1.2.2 *I*-optimal design fitting

Based on the analysis of the DSD results (Tables 6.6 and 6.7), it was observed that the MAE parameters, namely the ethanol-water mixture (x_1), time (x_2), microwave power (x_3), and solvent-to-solid ratio (x_4), had a substantial influence on the levels of TPC, TEAC, and TAC. Due to their significant impact, all of these MAE parameters were considered for the subsequent optimization process using the I-optimal design. The selection of these parameters for optimization was based on their demonstrated influence on the responses of interest.

To thoroughly investigate the interactive influence of the MAE parameters on TPC, TEAC, and TAC, an I-optimal design was employed. This design allowed for the exploration of various combinations of the MAE parameters, and the corresponding experimental and predicted values are presented in Table 6.8.

The accuracy of the I-optimal design was assessed by conducting several tests, including analysis of variance, lack of fit, and model summary statistics, as outlined in Table 6.9. These tests were based on the experimental data, providing valuable insights into the precision and reliability of the I-optimal design.

The model exhibited the highest values of R^2 and (R^2_{adj}) and demonstrated a low coefficient of variation (C.V.) of less than 6% for all the response variables. The I-optimal design, characterized by significantly lower p-values (< 0.0001), and a lack of significant lack-of-fit, was identified as the most appropriate model for the extraction of TPC, TEAC, and TAC from *S. officinalis* L. This indicates that the quadratic model, implemented through the I-optimal design, effectively captures the relationship between the MAE parameters and the response variables, providing a reliable and accurate framework for the extraction process.

The empirical relationship between the response variables (TPC, TEAC, and TAC) and the MAE parameters in terms of coded values was established through the generation of second-order polynomial equations. These equations, denoted as Eq. 6.10, Eq. 6.11, and Eq. 6.12, provide predictive models that describe the interaction between the response variables and the MAE parameters. These equations offer a mathematical representation of the relationships for predicting the responses based on the coded values of the MAE parameters.

Table 6.8: I-Optimal design matrix with MAE conditions for maximizing TPC, TEAC, and TAC

Runs	x_1	x_2	x_3	x_4	TPC^a **experimental**	TPC^a **predict**	$TEAC^b$ **experimental**	$TEAC^b$ **predict**	TAC^C **experimental**	TAC^C **predict**
1	-1	-1	-1	0	33.96 ± 0.87	34.19	214.47 ± 4.18	214.51	26.52 ± 0.21	26.43
2	-1	-1	0	-1	26.85 ± 0.21	26.73	183.21 ± 0.71	183.24	22.25 ± 0.22	22.39
3	-1	0	-1	+1	38.59 ± 0.08	38.37	224.36 ± 1.24	224.30	29.05 ± 0.13	29.13
4	-1	0	+1	-1	29.27 ± 0.26	29.40	179.13 ± 1.24	179.08	22.31 ± 0.04	22.16
5	-1	+1	-1	-1	27.42 ± 0.43	27.43	197.19 ± 0.71	197.17	22.90 ± 0.29	22.88
6	-1	+1	0	+1	37.46 ± 0.26	37.51	234.89 ± 3.80	230.93	28.16 ± 0.36	29.08
7	-1	+1	+1	0	36.06 ± 0.33	36.01	213.06 ± 1.24	216.99	27.08 ± 0.11	26.15
8	-0.3	-1	+1	+1	39.92 ± 0.16	39.74	269.91 ± 5.19	270.40	33.82 ± 0.14	34.11
9	0	-1	-1	-1	37.85 ± 0.08	37.50	220.91 ± 3.56	221.50	28.72 ± 0.11	29.06
10	0	+1	-1	+1	44.24 ± 0.59	44.18	252.5 ± 4.49	257.20	35.66 ± 0.41	35.06
11	0	+1	+1	-1	36.47 ± 0.70	36.15	226.55 ± 1.88	223.33	26.63 ± 0.32	28.10
12	+1	-1	-1	+1	38.76 ± 0.36	38.96	241.17 ± 3.74	240.59	28.88 ±0.06	28.54
13	+1	-1	+1	-1	32.47 ± 0.21	32.68	218.78 ± 2.56	218.21	25.98 ±0.11	25.64
14	+1	0	-1	-1	36.88 ± 0.25	37.12	207.90 ± 0.97	207.62	26.47 ±0.42	26.31
15	+1	0	0	0	38.54 ± 0.33	37.50	235.73 ± 1.86	238.62	28.29 ±0.24	30.01
16	+1	+1	-1	0	39.67 ± 0.92	39.62	237.90 ± 7.83	233.53	28.82 ±0.11	29.61
17	+1	+1	0	-1	32.88 ± 0.70	33.09	210.0 ± 3.98	213.61	26.88 ±0.20	25.58
18	+1	+1	+1	+1	45.65 ± 1.02	45.86	273.65 ± 10.28	273.08	30.06 ±0.09	29.72
19	0	0	0	0	39.64 ± 0.2	38.85	253.84 ± 3.39	247.74	35.81 ±0.28	34.27
20	0	0	0	0	37.82 ± 0.33	38.85	254.22 ± 1.94	247.74	35.78 ±0.38	34.27
21	0	0	0	0	38.21 ± 1.29	38.85	237.67 ± 4.06	247.74	32.71 ±0.20	34.27

$$TPC\,(mg_{GAE}/g_{dw}) = 38.58 + 2.42\,x_1 - 1.24\,x_2 - 0.01\,x_3 + 3.86\,x_4 - 3.78\,x_1^2 - 1.17\,x_2^2 + 2.49\,x_3^2 - 0.62\,x_4^2 + 0.50\,x_1x_2 - 0.18\,x_1x_3 - 0.79\,x_1x_4 + 1.14\,x_2x_3 + 1.27\,x_2x_4 + 0.62\,x_3x_4 \quad (6.10)$$

$$TEAC\,(\mu\mathrm{mol}_{\mathrm{TE}}/\mathrm{g}_{\mathrm{dw}}) = 247.74 + 13.09\,x_1 + 1.15\,x_2 + 4.97\,x_3 + 21.88\,x_4 - 22.21\,x_1^2 + 2.10\,x_2^2 + 1.92\,x_3^2 - 6.755\,x_4^2 - 0.57\,x_1x_2 + 5.46\,x_1x_3 - 0.23\,x_1x_4 - 0.72\,x_2x_3 - 0.70\,x_2x_4 + 5.91\,x_3x_4 \quad (6.11)$$

$$TAC\,(mg_{AAE}/g_{dw}) = 34.27 + 1.12\,x_1 + 0.10\,x_2 - 0.11\,x_3 + 2.69\,x_4 - 5.39\,x_1^2 - 0.68\,x_2^2 - 0.30\,x_3^2 - 0.14\,x_4^2 - 0.01\,x_1x_2 + 0.12\,x_1x_3 - 0.56\,x_1x_4 - 0.48\,x_2x_3 + 0.19\,x_2x_4 + 0.27\,x_3x_4 \quad (6.12)$$

Table 6.9: Regression results of I-optimal design and the estimated parameters for the TPC, TEAC, and TAC

		TPC (mg_{GAE}/g_{dw})		**TEAC** (mg_{AAE}/g_{dw})		**TAC** ($\mu mol_{TE}/g_{dw}$)	
	MAE parameters	**EC**	***p*-value**	**EC**	***p*-value**	**EC**	***p*-value**
Esitmated parameters	**Intercept**	38.858	$<0.0001^a$	247.748	$<0.0001^a$	34.278	$<0.0001^a$
	Linear effects						
	x_1	2.428	$<0.0001^a$	13.093	0.0005^a	1.121	0.0564^b
	x_2	1.240	0.0014^a	1.158	0.569^b	0.103	0.833^b
	x_3	-0.013	0.953^b	4.974	0.0415^a	-0.113	0.817^b
	x_4	3.867	$<0.0001^a$	21.885	$<0.0001^a$	2.690	$<0.0013^a$
	Quadratic effects						
	x_1^2	-3.784	$<0.0001^a$	-22.214	0.0006^a	-5.391	0.0006^a
	x_2^2	-1.175	0.033^a	2.109	0.588^b	-0.682	$0.479b$
	x_3^2	2.491	0.0011^a	1.929	0.619^b	-0.304	0.747^b
	x_4^2	-0.623	0.193^b	-6.755	0.117^b	-1.532	0.141^b
	Interaction effects						
	x_1x_2	0.506	0.109^b	-0.571	0.814^b	-0.012	0.983^b
	x_1x_3	-0.189	0.508^b	5.466	0.0578^b	0.120	0.839^b
	x_1x_4	-0.792	0.026^a	-0.231	0.924^b	-0.560	0.364^b
	x_2x_3	1.143	0.0039^a	-0.722	0.751^b	-0.482	0.405^b
	x_2x_4	1.278	0.0023^a	-0.701	0.758^b	0.192	0.731^b
	x_3x_4	0.623	0.0478^a	5.918	0.0349^a	0.277	0.622^b
Regression results	R^2	0.99		0.97		0.94	
	R^2_{adj}	0.97		0.92		0.83	
	RMSE	0.79		6.90		1.69	
	C.V	2.15		3.02		5.88	
	ANOVA (Model)	$<0.0001^a$		0.0008^a		$<0.0088^a$	
	Lack of fit	0.732^b		0.859^b		0.602^b	

6.1.2.3 MAE parameters effect on TPC

The impact of the MAE parameters, including the ethanol-water mixture (x_1), time (x_2), microwave power (x_3), and solvent-to-solid ratio (x_4), on the MAE of TPC from *S. officinalis* L. was investigated using a three-level I-optimal design. By implementing this design, the interactive effects of the MAE parameters on TPC were explored through the construction of a three-dimensional response surface. This surface allowed for the visualization of how varying two extraction parameters while keeping the other parameter constant influenced the TPC levels. The response surface analysis enabled a comprehensive understanding of the relationships and interactions among the MAE parameters and their impact on TPC.

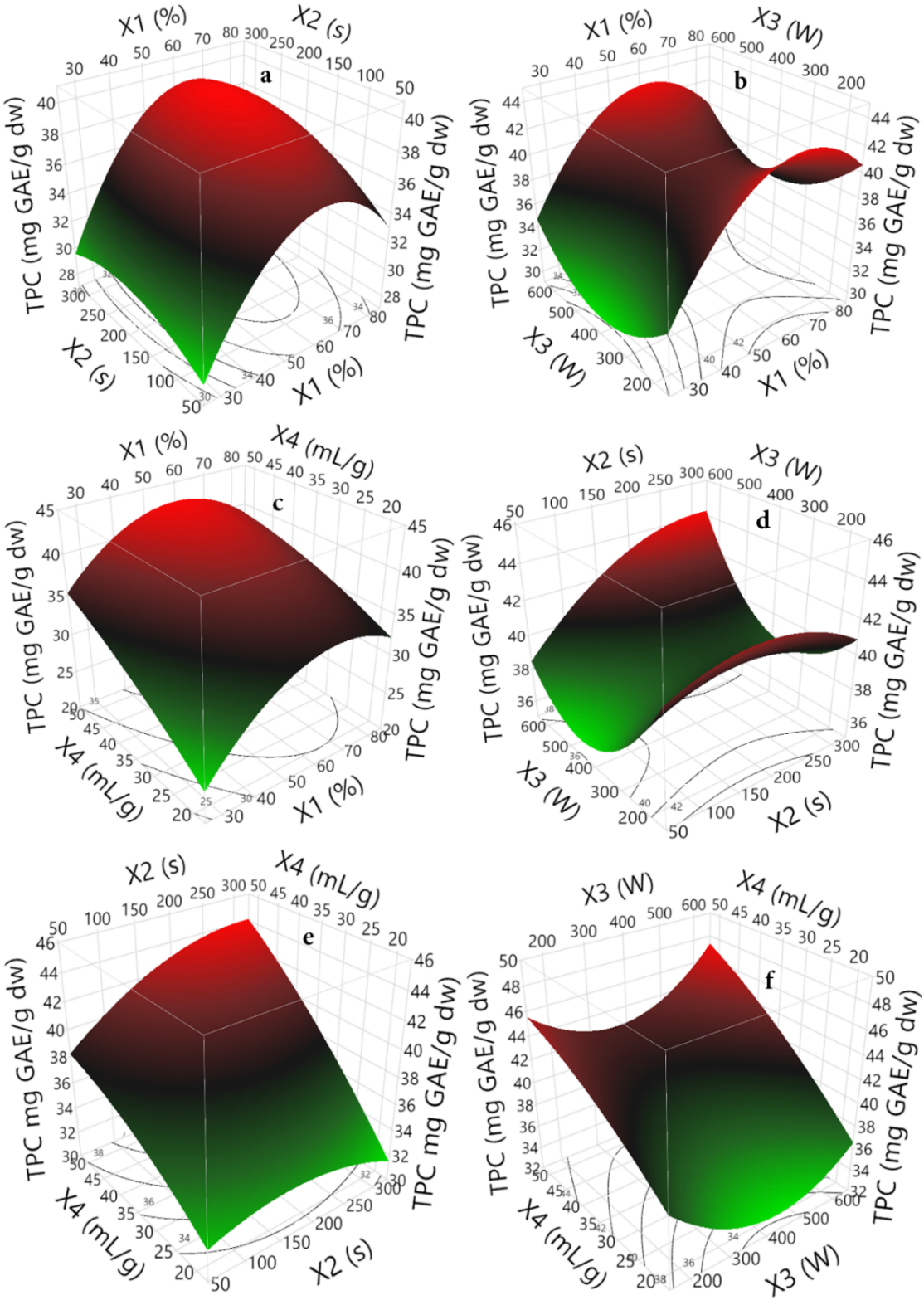

Figure 6.3: Three-dimensional response surface plot showing the effects of MAE parameters on TPC from *S. officinalis* L. **a**: effect of ethanol-water mixture and time, **b**: effect of ethanol-water mixture and power, **c**: effect of ethanol-water mixture and solvent to solid ratio, **d**: effect of time and power, **e**: effect of time and solvent to solid ratio, **f**: effect of power and solvent to solid ratio

The conducted experiments resulted in high levels of TPC extraction, ranging from 20 to 48 mg_{GAE}/g_{dw}. Analysis of the estimated coefficients (Table 6.9) revealed that the ethanol-water mixture had both positive and negative effects on TPC for the linear and quadratic terms, respectively. The influence of the ethanol-water mixture on TPC was particularly prominent, as depicted in Fig. 6.3a-b. When the ethanol-water mixture increased from 30 to 58%, there was a significant increase in TPC. However, beyond 58%, there was a substantial decline in TPC. This trend was consistently observed when considering the interaction between the ethanol-water mixture and other MAE parameters (Fig. 6.3a-b). In a study conducted by Darvishzadeh and Orsat (2022), it was observed that the use of ethanol-water mixtures at concentrations of 59% and 66% resulted in higher extraction of TPC from Russian olive leaves and flowers. Ethanol is known to be a favorable solvent for microwave-assisted extraction due to its ability to absorb microwaves effectively. Additionally, the presence of water in the solvent system enhances the penetration of the solvent into the sample matrix, thereby improving the efficiency of heating during extraction (Chan et al., 2011).

The MAE time was found to have a significant impact on TPC, as indicated by both the linear and quadratic terms in Table 6.9. The linear term had a positive effect, while the quadratic term had a negative effect on TPC. Fig. 6.3a demonstrates the interaction between the MAE time and the ethanol-water mixture, showing a slight positive effect on TPC. When the MAE time increased from 50 to 267 seconds, the TPC also increased from 20 to 30 mg_{GAE}/g_{dw}. However, when the time was extended beyond 267 s, a negative effect on TPC was observed. This trend was evident when the MAE time interacted with microwave power (Fig. 6.3d) and solvent to solid ratio (Fig. 6.3e). Similar findings have been reported in previous studies, where microwave durations of 5 to 6 min were found to yield higher TPC (Karami et al., 2015; Teng and Choi, 2013).

The solvent-to-solid ratio was another important parameter investigated in the MAE of TPC. The estimated coefficient confirmed that the solvent-to-solid ratio had a positive and highly significant effect on TPC, as indicated in Table 6.9. Increasing the solvent-to-solid ratio resulted in higher TPC values in the extract. The 3D surface plots (Fig. 6.3c, 6.3e, and Fig. 6.3f) showed that high TPC was achieved at a solvent-to-solid ratio of $50\,mL\,g^{-1}$, which aligns with the principles of mass transfer. These findings are consistent with the results reported by Sánchez-Camargo et al. (2021).

Moreover, the linear effect of microwave power did not show a significant impact on TPC, whereas the quadratic effect demonstrated a highly significant influence on TPC, as indicated by the estimated coefficient results presented in

Table 6.9.

Based on the three-dimensional response surface plots (Fig. 6.3b, 6.3d, and Fig. 6.3f), a slight decrease in TPC was observed in the range of 200 to 300 W for microwave power. However, a significant increase in TPC was observed at high microwave power (600 W), and this effect was particularly noticeable in interaction with other MAE parameters. In a study by Nana et al. (2021), it was found that 600 W of microwave power was identified as the optimal MAE condition for the extraction of total limonoid and antioxidant capacity from *Trichilia roka*. Similarly, Berkani et al. (2020) reported that high microwave power (600 W) and an extended MAE time were determined as the optimal operational parameters for the extraction of polysaccharides from Algerian Jujube. The optimal level of microwave power (600 W) can be explained by the high solvent-to-solid ratio ($50\,\mathrm{mL\,g^{-1}}$), as a larger amount of solvent requires more absorption of microwave energy to effectively heat the medium (Mandal and Mandal, 2010).

6.1.2.4 MAE parameters effect on TEAC and TAC

The range of TEAC and TAC in extracts of *S. officinalis* L. varied from 160 to 279 $\mu\mathrm{mol_{TE}/g_{dw}}$ and 20 to 35 $\mathrm{mg_{AAE}/g_{dw}}$, respectively. These variations are illustrated in Figure 6.4 and Figure 6.5. Based on the analysis of regression coefficients' p-values (see Table 6.9), it was found that the linear effects of x_1, x_3, and x_4 had significant impacts on TEAC. However, only the linear effect of x_4 showed a significant effect on TAC. Moreover, it was observed that only the quadratic effect (x_1^2) had a negative impact on both TEAC and TAC. When considering the interaction effect terms, the interaction between x_3 and x_4 exhibited a positive effect on TEAC. However, the remaining interactions did not show a significant impact on either TEAC or TAC.

Based on the response surface methodology analysis presented in Figure 6.4 and Figure 6.5, it was determined that the lowest values for TEAC and TAC were achieved when using a lower ethanol concentration (30%), shorter extraction time (60 s), lower microwave power (200 W), and a lower solvent-to-solid ratio ($20\,\mathrm{mL\,g^{-1}}$). On the other hand, the highest TEAC values were obtained when employing a moderate ethanol concentration (58%), longer extraction time (300 s), higher microwave power (600 W), and a higher solvent-to-solid ratio ($50\,\mathrm{mL\,g^{-1}}$).

The TAC exhibited higher values when using an ethanol concentration of 58%, an extraction time of 267 s, a microwave power of 600 W, and a solvent-to-solid ratio of $50\,\mathrm{mL\,g^{-1}}$. Similar observations were made for TEAC and TAC,

where increasing the ethanol-water mixture from 30% to 58% resulted in an increase in both TEAC and TAC. However, the two responses showed a significant decline when the ethanol-water mixture was further increased from 58% to 80%. These trends can be visualized in Figure 6.4 and Figure 6.5. Consistent findings have been reported in the literature, indicating that a high antioxidant activity in medicinal plants is achieved when using an ethanol-water mixture ranging from 49% to 58% (Luo et al., 2021; Shang et al., 2020; Song et al., 2011; Wen et al., 2015). The variations in antioxidant activity observed in the leaves of *S. officinalis* L. can be attributed to the distinct dielectric properties of the solvents used. For instance, at a frequency of 2.450 MHz and room temperature, the loss tangent ($\tan \delta$) of methanol and water is 0.94 and 9.88, respectively. A higher value of the loss tangent indicates better heating of the material under microwave irradiation (Chemat and Cravotto, 2012).

Another important parameter investigated for the extraction of antioxidants from *S. officinalis* L. using MAE is the extraction time. The impact of time on TEAC and TAC, when considered in interaction with the ethanol-water mixture and the solvent-to-solid ratio, was determined to be relatively less significant (as depicted in Figure 6.4a, 6.4e, 6.5a, and Figure 6.5e). With increasing extraction time, there was a slight improvement in the extraction efficiency of antioxidants. Moreover, the interaction between extraction time and microwave power had a more pronounced effect on TEAC and TAC (as shown in Figure 6.4d and Figure 6.5d). At lower levels of microwave power, there was a significant increase in TEAC and TAC with longer extraction times. However, at higher levels of microwave power, a significant decrease in TEAC was observed when the extraction time was extended from 60 to 150 s. Subsequently, TEAC increased again when the extraction time exceeded 150 s (Fig. 6.4d). Furthermore, when considering high levels of microwave power, there was a slight increase in TAC when the extraction time was extended from 60 to 150 s. However, a significant decrease in TEAC was observed when the extraction time was further extended from 150 to 300 s (Figure 6.5d). In previous studies by Wen et al. (2015) and Lovrić et al. (2017), it was found that an extraction time of 4 minutes for blackberry flowers and 5 minutes for blackthorn flowers was adequate for the extraction and recovery of phenolic and antioxidant compounds.

Furthermore, the microwave power was identified as a significant factor affecting the antioxidant capacity of *S. officinalis* L. leaves. It exhibited a positive impact on TEAC, specifically through the factors x_3 and x_3x_4, while showing a non-significant effect on TAC as indicated in Table 6.9. Increasing the microwave power from 200 to 600 W significantly enhanced the antioxidant capacity,

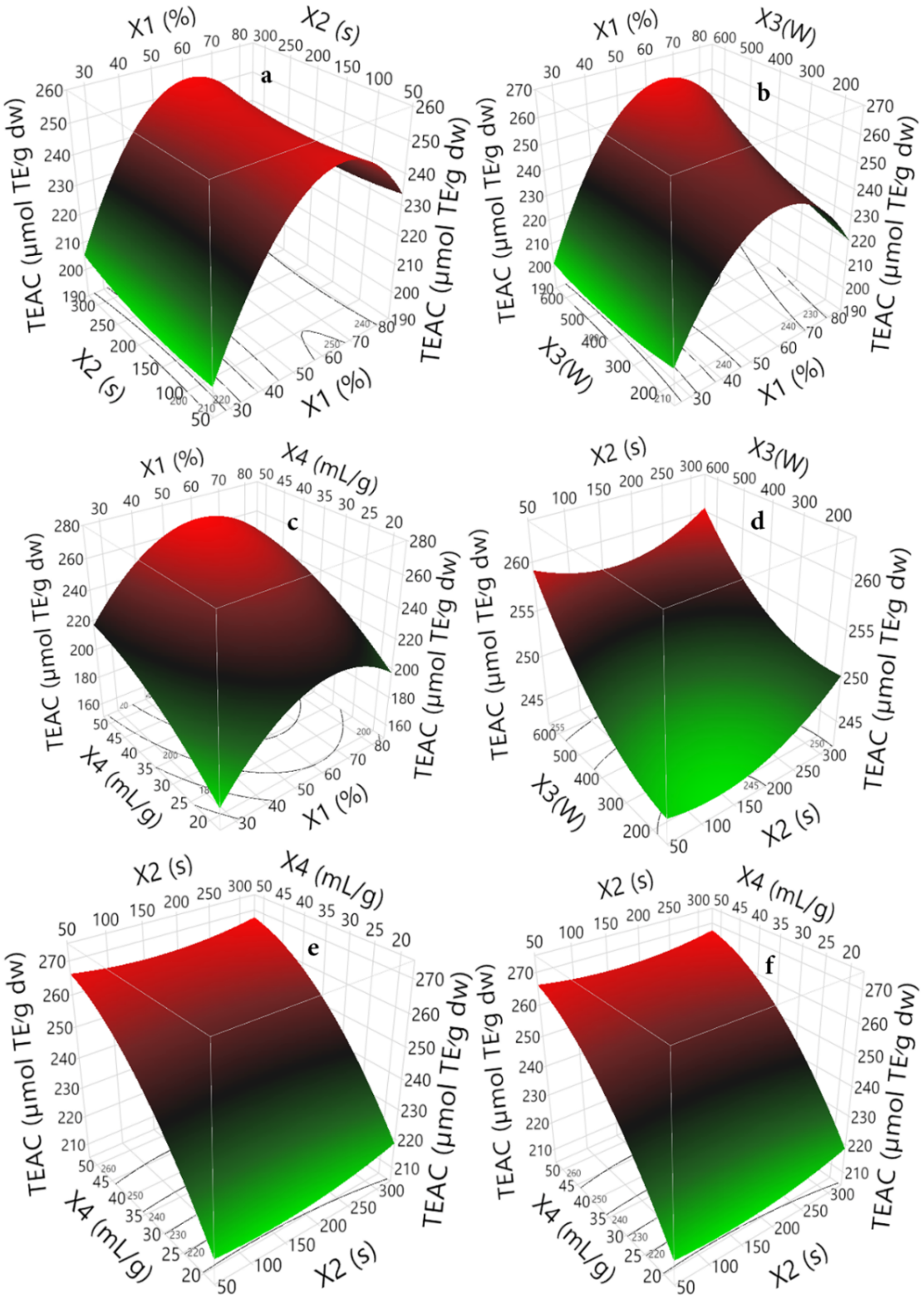

Figure 6.4: Three dimensional response surface plot showing the effects of MAE parameters on TEAC from *S. officinalis* L. **a**: effect of ethanol-water mixture and time, **b**: effect of ethanol-water mixture and power, **c**: effect of ethanol-water mixture and solvent to solid ratio, **d**: effect of time and power, **e**: effect of time and solvent to solid ratio, **f**: effect of power and solvent to solid ratio

as demonstrated in Figure 6.4b, 6.4d, and 6.5d. These findings regarding the influence of microwave power on the antioxidant activity of *S. officinalis* L. leaf extracts are consistent with previous studies by Liu et al. (2010) and Xueling et al. (2011).

Based on the results presented in Table 6.9, Figure 6.4, and Figure 6.5, the solvent-to-solid ratio emerged as the most influential parameter in MAE, positively enhancing both TEAC and TAC of *S. officinalis* L. leaves. The solvent-to-solid ratio exhibited a highly significant positive effect (with a p-value > 0.001).

The response surface plots depicted in Figure 6.4c, 6.4e, 6.4f, 6.5c, 6.5e, and 6.5f exhibit consistent patterns concerning antioxidant capacity. The increasing solvent-to-solid ratio is correlated with an increase in both TEAC and TAC, thereby enhancing the extraction efficiency of antioxidant compounds from *S. officinalis* L. leaves. Consequently, the optimal solvent-to-solid ratio for achieving a high antioxidant capacity was determined to be $50\,\mathrm{mL\,g^{-1}}$. These findings align with the results reported by Zeković et al. (2017b), Bhuyan et al. (2015), and Kaderides et al. (2019). These studies demonstrated that employing a higher solvent-to-solid ratio ranging from 40 to 60 $\mathrm{mL\,g^{-1}}$ resulted in a greater recovery of polyphenols from by-products of *Salvia officinalis* L.

6.1.2.5 Optimization of MAE conditions

The DSD and I-optimal designs were used for screening and optimization of the MAE parameters respectively. Based on the desirability function, the optimal MAE conditions for the maximum of TPC, and TEAC, and TAC given by DSD were: ethanol concentration of 55%, microwave power of 200 W, MAE time of 4.35 min, solid–to-liquid ratio of $50\,\mathrm{mL\,g^{-1}}$. Under these optimal MAE conditions, the desirability value was 0.90. While the optimal MAE conditions for the maximum of TPC, and TEAC, and TAC given by I-optimal design were: ethanol concentration of 60%, microwave power of 600 W, MAE time of 4.79 min, solid–to-liquid ratio of $50\,\mathrm{mL\,g^{-1}}$. Under these optimal MAE conditions, the desirability value was 0.92, where the maximum of TPC, TEAC, and TAC obtained in this study were illustrated in table 6.10.

For the validation of the optimum MAE conditions for both DSD and I-optimal design, triplicate confirmatory experiments were established under the optimized conditions, and the average of TPC, TEAC, and TAC were compared to the predicted values given by the employed models as mentioned in table 6.10. The results are closely related to the data obtained from the optimization process, indicating that DSD and I-optimal design could be effectively used to screen and

optimize the MAE for a maximum phenolic and antioxidant capacity from *Salvia officinalis* L.

Table 6.10: Predicted, obtained values and confidence intervals of optimal extract from *S. officinalis* L. leaves, generated by DSD and *I*-optimal design

	Response	Predicted response	95% PI low	Observed response a	95% PI high
DSD	**TPC** (mg_{GAE}/g_{dw})	39.68	37.03	39.37 ± 1.58	42.28
	TEAC ($\mu mol_{TE}/g_{dw}$)	264.99	249.84	266.05 ± 1.54	280.15
	TAC (mg_{AAE}/g_{dw})	37.03	34.79	35.85 ± 0.72	39.27
***I*-optimal design**	**TPC** (mg_{GAE}/g_{dw})	47.60	45.96	46.12 ± 0.08	49.24
	TEAC ($\mu mol_{TE}/g_{dw}$)	278.79	264.59	268.39 ± 1.28	292.99
	TAC (mg_{AAE}/g_{dw})	34.67	31.19	36.79 ± 0.20	38.15

PI: Predicted interval, *superscript*[a]: Values are expressed as mean ± standard deviation (n = 3).

6.2 Differential UHPLC-HRMS analysis of MAE and UAE extracts

To evaluate the efficiency of extraction techniques, the optimal MAE extract obtained in this study was compared to the optimal UAE extract. The optimal MAE extract of common sage exhibited high TPC (46.12 ± 0.08 mg_{GAE}/g_{dw}) and TEAC (268.39 ± 1.28 $\mu mol_{TE}/g_{dw}$) than optimal extract obtained by UAE, where TPC and TEAC were 31.84 ± 0.248 mg_{GAE}/g_{dw} , 237.95 ± 0.771 $\mu mol_{TE}/g_{dw}$, respectively. However, the UAE extract showed high TAC (38.928 ± 0.548 mg_{AAE}/g_{dw}) than the MAE extract with a TAC of 36.79 ± 0.20 mg_{AAE}/g_{dw}. These results could be explained by the ability of microwave energy to enter the cell matrix, interact with polar molecules, and heat the biomaterial in volume, which in turn raises the pressure inside the plant cell. As the pressure increases, cell walls break down and phenolic compounds are released (Nayak et al., 2015).

To study deeply the quality and quantity of phenolic compounds of common sage leaves present in MAE and UAE optimal extracts, UHPLC-HRMS was applied to identify the major phenolic compounds present in both extracts. As most phenolic compounds present one or more hydroxyl, carboxylic acid groups, or both, MS data were obtained in the negative ionization mode (Irakli et al., 2018). Total ion chromatograms of MAE and UAE extracts of common sage are shown in fig. 6.6 and fig. 6.7, while the major peaks identified by UHPLC-HRMS analysis

are presented in Table 6.11. Each identification was confirmed by comparing the observed compounds' MS spectra to those described in the literature. UHPLC-MS analysis of common sage leaves extracts allowed us to identify more than 80 different phenolic compounds presented in both MAE and UAE extracts. As mentioned in Table 6.11, different types of bioactive compounds were assigned including hydroxycoumarins, diterpene phenols, flavonol derivatives, flavones derivatives, flavanones derivatives, isoflavones, polymethoxy flavones, methoxycinnamic acid, 6-hydroxyflavones, 2-arylbenzofuran flavones, hydroxybenzoic acid, phenolic aldehyde, rosmarinic acid derivatives, carnosic acid derivatives, triterpenoids, lignin, organic acid, organic sugar, and sugar acid. Furthermore, the identified compounds have been already identified in the Lamiaceae family, especially in *Salvia* species (Castañeta et al., 2022; Irakli et al., 2018; Rahmani Samani et al., 2021; Shah et al., 2012; Sharma et al., 2020; Sulniute et al., 2017; Taamalli et al., 2015; Velamuri et al., 2020; Wojciechowska et al., 2020; Zhang et al., 2016, 2012; Ziani et al., 2019).

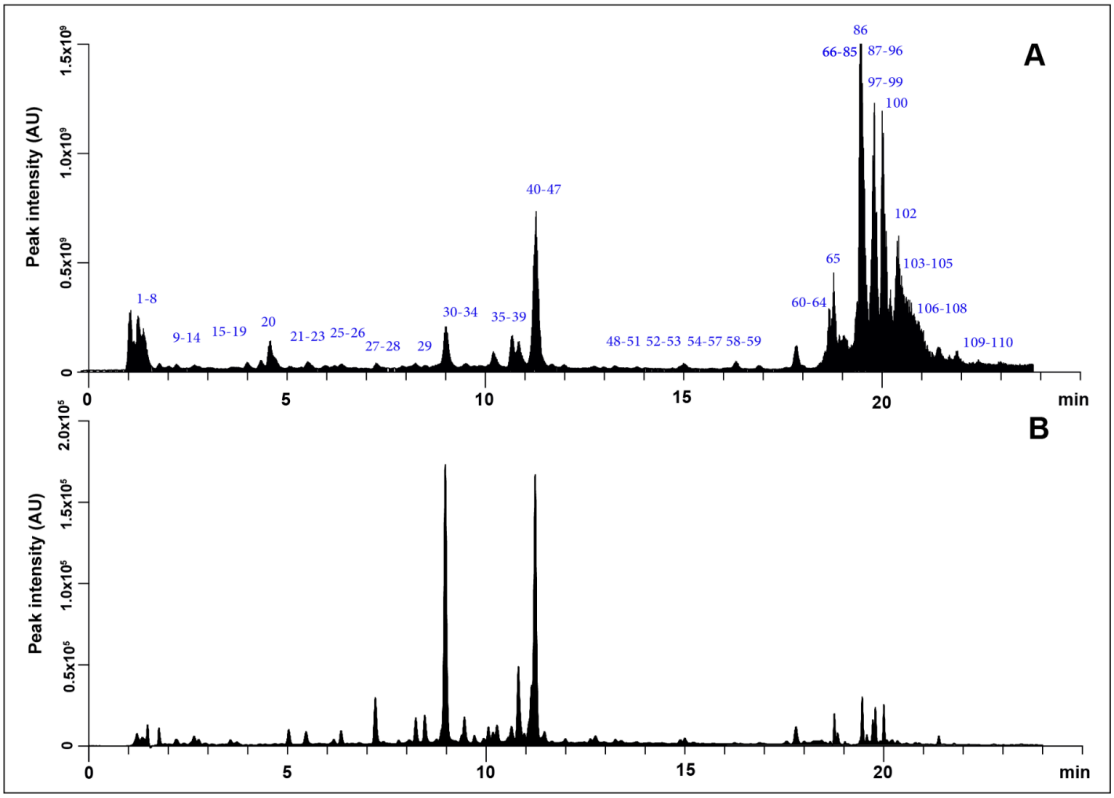

Figure 6.6: Total ion chromatogram of *S. officinalis* L. MAE extract detected by LC-Q-Orbitrap in negative mode (A) set with chromatogram registered by UV-Vis detector at 270 nm (B)

The volcano plot of UHPLC-HRMS analysis generated by Compound Discoverer software (Fig. 6.8) provides an effective tool for visualizing the direction,

magnitude, and significance of changes in the concentration of bioactive compounds present in both MAE and UAE extracts. Each point on the Volcano plot represents a bioactive compound. The log 2-fold differences between MAE/UAE are plotted on the x-axis and the -log10 p-value differences are plotted on the y-axis. The horizontal dashed line represents the significance threshold (p-value < 0.05). A total of 268 compounds were statistically significant lying above a horizontal threshold (Fig. 6.8). A closer log 2-fold change to one indicates less change while moving away from one in either direction indicates more change in concentration of bioactive compounds, of which 181 compounds were found in higher concentration in MAE extract (right of zero on the x-axis) including caffeic acid galactoside, caffeic acid glucoside, caffeoyl-hexosyl-hexose, 6-hydroxyluteolin-7-O-glucoside, 6-hydroxyluteolin 7-O-rhamnoside, Luteolin, Hydroxyursolic acid, quercetin-3-O-malonylglucoside,

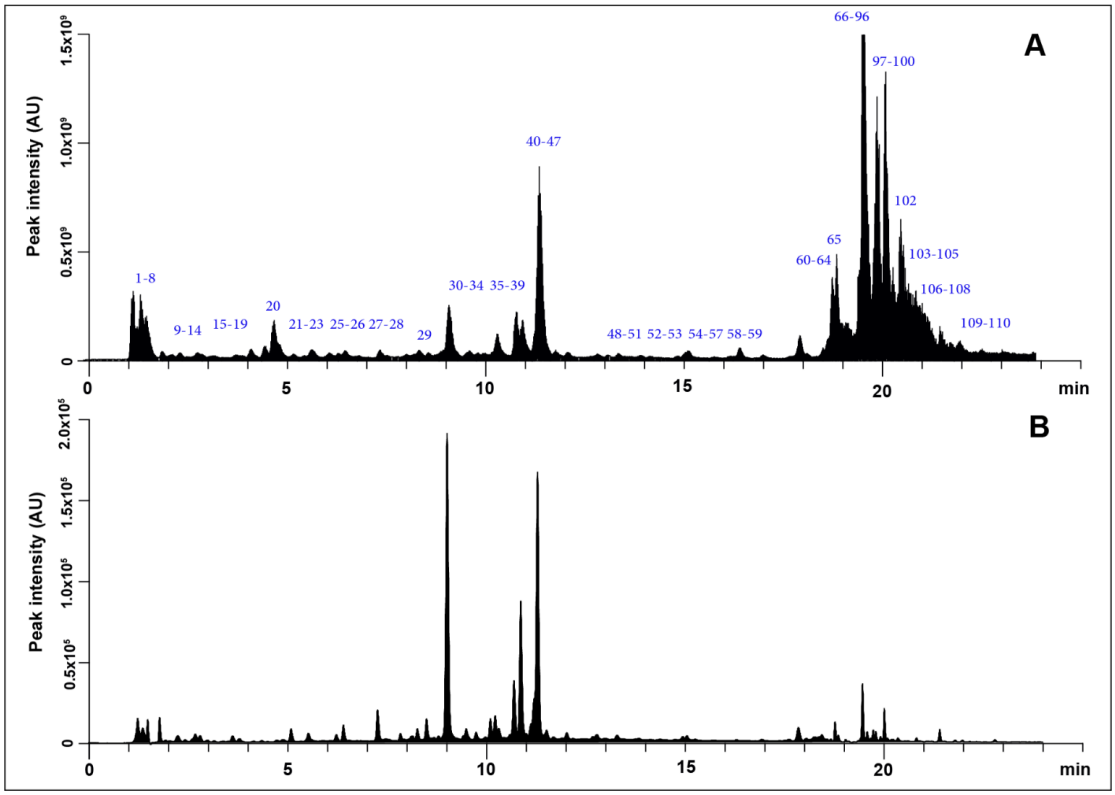

Figure 6.7: Total ion chromatogram of *S. officinalis* L. UAE extract detected by LC-Q-Orbitrap in negative mode (A) set with chromatogram registered by UV-Vis detector at 270 nm (B)

luteolin-7-O-glucoside, micromeric acid, ursolic acid, genistin, luteolin O-malonyl hexoside, isorhamnetin-O-hexose, nepitrin, homoplantaginin, trihexoside, dihexoside (Fig. 6.8, Table A.1). On the other hand, 87 compounds were found to be higher in UAE (left of zero on the x-axis) including 3,5-Dimethoxycinnamic acid, p-coumaric acid/m-coumaric acid, rosmadial, epirosmanol, salvianolic acid

B, epiisorosmanol, apigenin (Fig. 6.8, Table A.1). To conclude, the results confirm that hydrocinnamic acids, triterpenoids, and organic sugars were more abundant in MAE extract, which could be explained by the microwave heating provided by microwave power that acts as a driving force for MAE to destroy the cell wall of plant matrix (Chan et al., 2011). Similar results were obtained by (Dahmoune et al., 2014; Nayak et al., 2015; ŞÜMnÜ et al., 2013). However, MAE causes poor extraction of diterpenes phenols due to their sensitivity to microwave heating which confirm that ultrasound is more suitable for delicate or fragile bioactive compounds that require gentle extraction, while the microwave is more suitable for robust or resistant compounds that require rapid extraction.

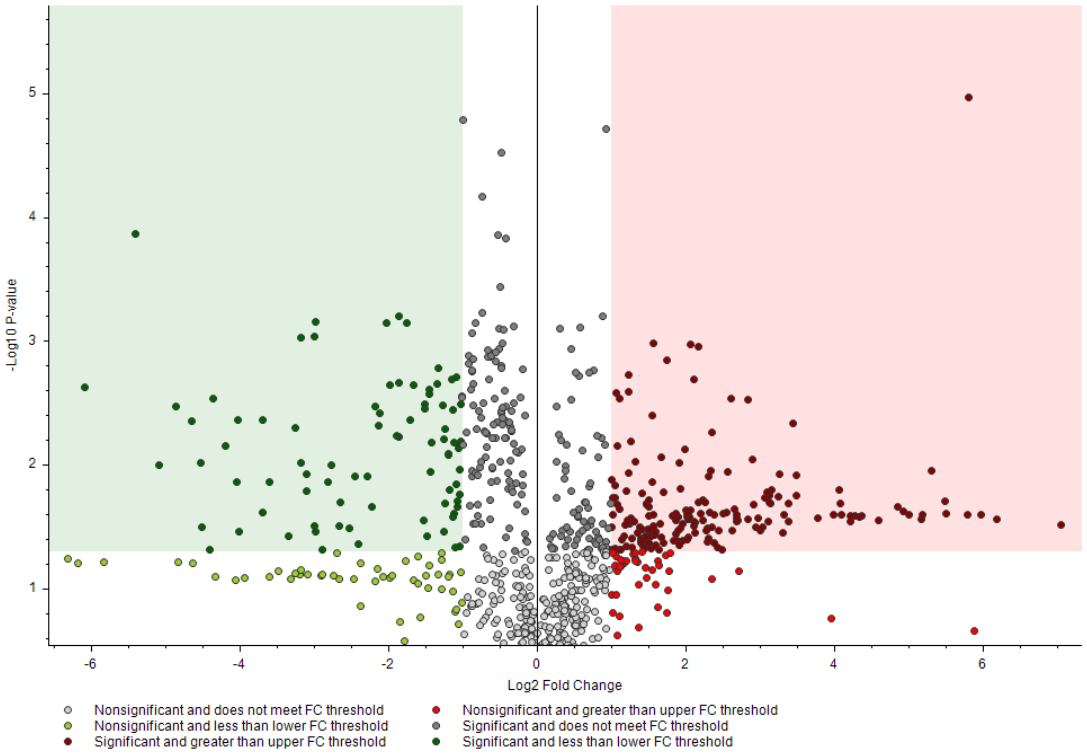

Figure 6.8: Differential content visualization of identified and unidentified MAE and UAE bioactive compounds with Volcano plot (Log2 Fold change =1)

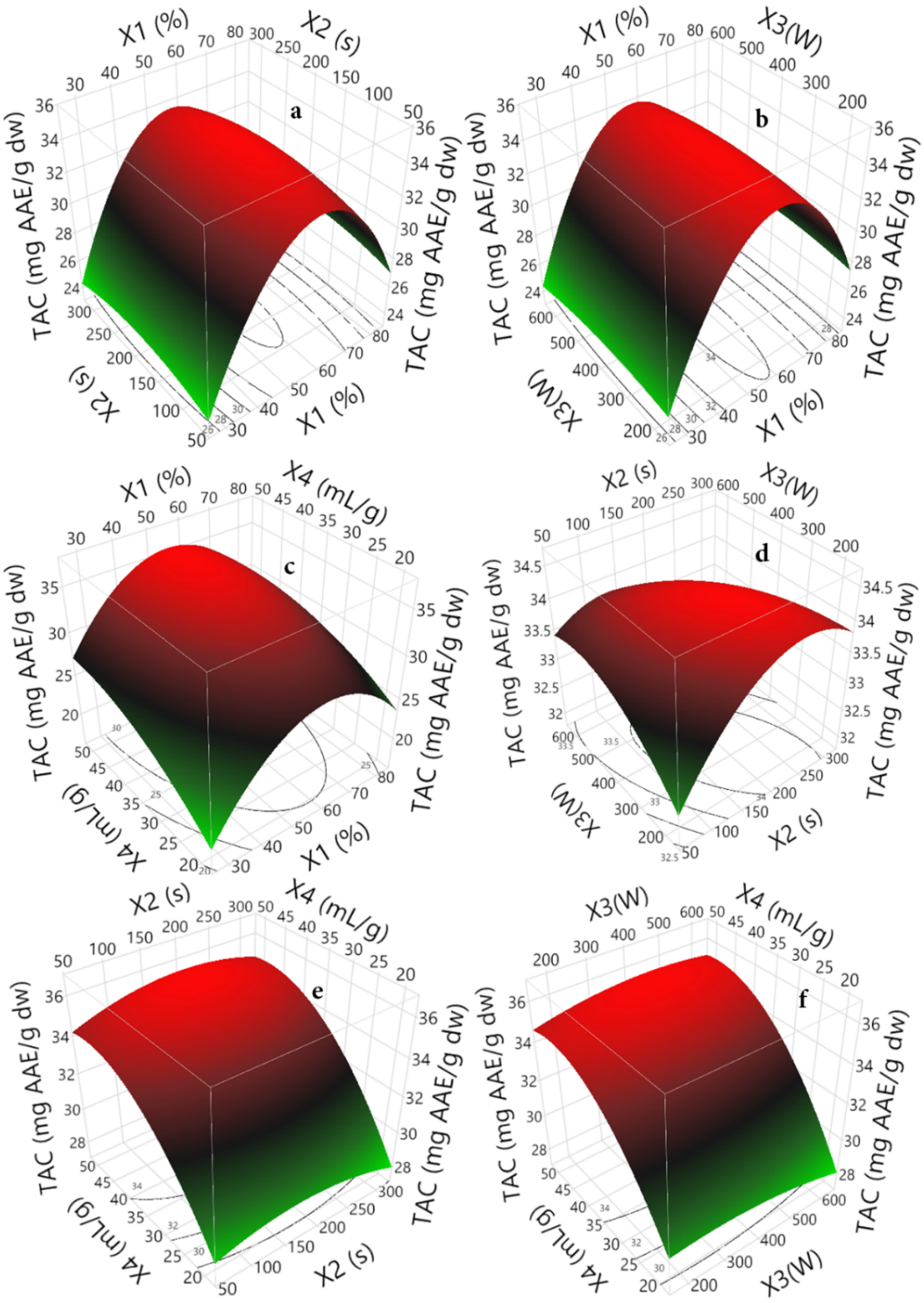

Figure 6.5: Three dimensional response surface plot showing the effects of MAE parameters on TAC from *S. officinalis* L. **a**: effect of ethanol-water mixture and time, **b**: effect of ethanol-water mixture and microwave power, **c**: effect of ethanol-water mixture and solvent to solid ratio, **d**: effect of time and microwave power, **e**: effect of time and solvent to solid ratio, **f**: effect of microwave power and solvent to solid ratio

Table 6.11: Compounds from *Salvia officinalis* L. extracts tentatively identified by using LC-Q-Orbitrap-HRMS in negative mode

N°	Tentative Identification	Formulas	Calculated MW	Experimental MW	Δ mass [ppm]	RT [min]	Adduct mass [M-H]-	MS/MS	Class	References
1	Trihexoside	$C_{19}H_{34}O_{18}$	550.1745	550.1747	-0.33	1.42	549.1674	/	OS	(Ibrahim et al., 2022)
2	Dihexose	$C_{12}H_{22}O_{11}$	342.1162	342.1163	-0.45	1.48	341.1089	59.012 ; 89.022; 71.012 ; 101.023	OS	(Ibrahim et al., 2022; Rahmani Samani et al., 2021)
3	Gluconic acid	$C_6H_{12}O_7$	196.0583	196.0576	3.31	1.53	195.0503	75.007; 59.012 ; 87.007 ; 72.991	SA	(Ibrahim et al., 2022; Zhu et al., 2022)
4	L-Threonic acid	$C_4H_8O_5$	136.0371	136.0364	5.40	1.51	135.0286	75.007 ; 72.991 ; 71.012 ; 59.012	SA	(Zhu et al., 2022)
5	Quinic acid	$C_7H_{12}O_6$	192.0633	192.0627	3.22	1.53	191.0553	85.028 ; 93.033 ; 59.012 ; 87.007	OA	(Borras Linares et al., 2011)
6	Hexose	$C_6H_{12}O_6$	180.0633	180.0625	4.55	1.56	179.0552	59.012 ; 87.007 ; 71.012 ; 75.007	OS	(Ibrahim et al., 2022)
7	α,α-Trehalose	$C_{12}H_{22}O_{11}$	342.1162	342.1162	-0.10	1.56	341.1089	59.012 ; 89.022 ; 71.012 ; 101.023	OS	(Zhu et al., 2022)
8	Caffeoylquinic acid	$C_{16}H_{18}O_9$	354.0950	354.0970	-5.52	1.57	353.0897	75.007 ; 191.036 ; 353.089 ; 165.039	HCA	(Celano et al., 2017)
9	Citric acid	$C_6H_8O_7$	192.0270	192.0263	3.51	2.00	191.0190	87.007 ; 111.007 ; 85.028 ; 57.033	OA	(Rahmani Samani et al., 2021; Zhu et al., 2022)
10	Protocatechuic acid 4-O-glucoside	$C_{13}H_{16}O_9$	316.07943	316.0799	-1.56	2.28	315.0726	123.043 ; 153.054 ; 108.020 ; 152.010	HBA	(Ali et al., 2021)
11	Danshensu	$C_9H_{10}O_5$	198.05282	198.0522	3.10	2.50	197.0448	72.991 ; 123.043 ; 135.044 ; 61.986	HCA	(Celano et al., 2017; Sulniute et al., 2017)
12	Unknown	$C_{20}H_{26}O_{13}$	474.1373	474.1376	-0.66	2.89	473.1302	161.023 ; 179.034 ; 89.023 ; 162.026	/	/

Continued on next page

Table 6.11 – Continued from previous page

N°	Tentative Identification	Formulas	Calculated MW	Experimental MW	Δ mass [ppm]	RT [min]	Adduct mass [M-H]-	MS/MS	Class	References
13	Unknown	$C_{15}H_{20}O_{10}$	360.1056	360.1059	-0.86	2.89	359.0986	59.012 ; 89.023 ; 71.012 ; 197.044	/	/
14	Unknown	$C_{20}H_{28}O_{13}$	476.1529	476.1532	-0.45	2.97	475.1459	135.043 ; 89.022 ; 161.023 ; 136.047	/	/
15	Caffeoyl-hexosyl-hexose	$C_{21}H_{28}O_{14}$	504.1479	504.1484	-1.07	3.22	503.1411	161.023 ; 179.034 ; 281.066 ; 323.077	HCA	(Celano et al., 2017; Rahmani Samani et al., 2021)
16	Caffeic acid galactoside	$C_{15}H_{18}O_9$	342.0950	342.0953	-0.68	3.27	341.0880	161.023 ; 135.043 ; 179.034 ; 177.054	HCA	(Kiselova-Kaneva et al., 2022)
17	Salicylic acid glucoside	$C_{13}H_{16}O_8$	300.0845	300.0847	-0.63	3.32	299.0774	93.033 ; 137.023 ; 94.036 ; 138.026	PG	
18	Caffeic acid glucoside	$C_{15}H_{18}O_9$	342.0950	342.0953	-0.68	3.71	341.0880	135.043 ; 179.034 ; 161.023 ; 177.054	HCA	(Ali et al., 2021; Kiselova-Kaneva et al., 2022)
19	*p*-Coumaric acid-4-O-glucoside	$C_{15}H_{18}O_8$	326.1001	326.1003	-0.64	3.90	325.0931	119.048 ; 163.039 ; 120.052 ; 164.042	HCA	(Ali et al., 2021)
20	Protocatechuic aldehyde	$C_7H_6O_3$	138.0316	138.0305	8.36	4.64	137.0232	108.020 ; 136.015 ; 91.017 ; 137.023	PAL	(MSBNK-BS-BS003265)
21	Apigenin 8-C-rhamnosyl-6-C-glucoside	$C_{27}H_{30}O_{15}$	594.1584	594.1588	-0.68	5.35	593.1515	593.151 ; 473.109 ; 594.155 ; 353.066	Fon	(Rahmani Samani et al., 2021; Taamalli et al., 2015)
22	Esculetin	$C_9H_6O_4$	178.026	178.0257	4.71	5.65	177.0185	89.038 ; 105.033 ; 133.028 ; 93.033	HC	(Ali et al., 2021)
23	Caffeic acid	$C_9H_8O_4$	180.0422	180.0414	4.72	5.79	179.0341	135.044 ; 134.0361 ; 89.038 ; 136.047	HCA	(Hossain et al., 2010; Velamuri et al., 2020)
24	p-Coumaric acid/m-Coumaric acid	$C_9H_8O_3$	164.0473	164.0468	3.32	5.90	163.0391	119.048 ; 93.033 ; 120.052 ; 117.033	HCA	(Ali et al., 2021; Hossain et al., 2010)

Continued on next page

Table 6.11 – Continued from previous page

N°	Tentative Identification	Formulas	Calculated MW	Experimental MW	Δ mass [ppm]	RT [min]	Adduct mass [M-H]-	MS/MS	Class	References
25	Unknown	$C_{16}H_{20}O_9$	356.1107	356.1110	-0.99	6.11	355.1038	175.039 ; 134.036 ; 193.050 ; 191.070	/	/
26	Unknown	$C_9H_{10}O_5$	198.0528	198.0522	3.10	6.50	197.0449	123.007 ; 89.001 ; 61.986 ; 95.012	/	/
27	6-Hydroxyluteolin -7-O-glucuronide	$C_{21}H_{18}O_{13}$	478.0747	478.0750	-0.57	7.53	477.0676	301.035 ; 302.038 ; 113.023 ; 85.028	Fan	(Ali et al., 2021; Sharma et al., 2020)
28	6-Hydroxyluteolin-7-O-glucoside	$C_{21}H_{20}O_{12}$	464.0954	464.0960	-1.18	7.58	463.0887	301.035 ; 300.027 ; 302.038 ; 463.088	Fan	(Sharma et al., 2020)
29	Lithospermic acid A isomer	$C_{27}H_{22}O_{12}$	538.1111	538.1115	-0.79	8.98	537.1043	295.061 ; 109.028 ; 296.064 ; 203.034	Aryl-flav	(Ziani et al., 2019)
30	Luteolin-7-O-glucoside	$C_{21}H_{20}O_{11}$	448.1005	448.1008	-0.59	9.19	447.0935	285.040 ; 284.032 ; 447.093 ; 286.043	Fon	(Rahmani Samani et al., 2021; Velamuri et al., 2020)
31	Quercetin 3-O-malonylglucoside	$C_{24}H_{22}O_{15}$	550.0958	550.0961	-0.48	9.30	549.0888	301.035 ; 505.099 ; 300.027 ; 302.038	Fol	
32	Scutellarin	$C_{21}H_{18}O_{12}$	462.0798	462.08005	-0.47	9.31	461.0729	285.040 ; 286.043 ; 113.023 ; 85.028	Fon	(Velamuri et al., 2020)
33	Nepitrin	$C_{22}H_{22}O_{12}$	478.1111	478.1114	-0.71	9.71	477.1042	315.049 ; 299.019 ; 300.026 ; 477.104	Fon	(Celano et al., 2017)
34	Isorhamnetin-O-hexose	$C_{22}H_{20}O_{13}$	492.0903	492.0907	-0.72	9.79	491.0834	315.051 ; 300.027 ; 316.054 ; 301.0309	Fol	(Mena et al., 2016)
35	Apigenin-7-O-rutinoside	$C_{27}H_{30}O_{14}$	578.1635	578.1640	-0.83	10.03	577.1567	269.045 ; 270.048 ; 311.056 ; 577.155	Fon	(Li et al., 2017)
36	Diosmin	$C_{28}H_{32}O_{15}$	608.1741	608.1743	-0.32	10.61	607.1668	299.056 ; 300.059 ; 284.032 ; 307.066	Fon	(Celano et al., 2017; Taamalli et al., 2015)
37	Genistin	$C_{21}H_{20}O_{10}$	432.1056	432.1059	-0.67	10.90	431.0985	268.037 ; 269.044 ; 431.098 ; 432.101	Iso-Fon	

Continued on next page

Table 6.11 – Continued from previous page

N°	Tentative Identification	Formulas	Calculated MW	Experimental MW	Δ mass [ppm]	RT [min]	Adduct mass [M-H]-	MS/MS	Class	References
38	Salvianolic acid B	$C_{36}H_{30}O_{16}$	718.1533	718.1539	-0.71	10.98	717.1465	295.061 ; 493.114 ; 519.093 ; 339.050	HCA	(Avula et al., 2022; Taamalli et al., 2015; Velamuri et al., 2020)
39	Unknown	$C_{15}H_{10}O_7$	302.0426	302.0428	-0.58	10.99	301.0355	133.028 ; 301.035 ; 137.023 ; 135.043	/	/
40	Apigenin-glucuronide	$C_{21}H_{18}O_{11}$	446.0849	446.0851	-0.58	11.14	445.0779	269.045 ; 270.048 ; 113.023 ; 85.028	Fon	(Rahmani Samani et al., 2021; Velamuri et al., 2020)
41	Luteolin O-malonyl hexoside	$C_{24}H_{22}O_{14}$	534.1009	534.1011	-0.41	11.20	533.0938	285.040 ; 489.104 ; 490.107 ; 286.043	Fon	(Celano et al., 2017)
42	Homoplantaginin	$C_{22}H_{22}O_{11}$	462.1162	462.1165	-0.81	11.29	461.1093	283.024 ; 461.109 ; 298.047 ; 446.085	Fon	(Rahmani Samani et al., 2021)
43	Hispidulin-glucuronide	$C_{22}H_{20}O_{12}$	476.0954	476.0956	-0.44	11.40	475.0884	299.056 ; 284.032 ; 113.023 ; 85.028	Fon	(Velamuri et al., 2020)
44	Salvianolic acid A	$C_{26}H_{22}O_{10}$	494.1213	494.1215	-0.40	11.46	493.1144	161.023 ; 135.043 ; 197.044 ; 179.034	HCA	(Sulniute et al., 2017)
45	Salvianolic acid K	$C_{27}H_{24}O_{13}$	556.1216	556.1218	-0.31	11.47	555.1146	161.023 ; 135.043 ; 197.044 ; 179.034	HCA	(Celano et al., 2017; Velamuri et al., 2020)
46	Rosmarinic acid	$C_{18}H_{16}O_8$	360.0845	360.0846	-0.38	11.57	359.0774	161.023 ; 72.991 ; 179.034 ; 135.043	HCA	(Avula et al., 2022)
47	6-Hydroxyluteolin 7-O-rhamnoside	$C_{21}H_{20}O_{11}$	448.1005	448.1009	-0.74	11.75	447.0936	285.040 ; 286.044 ; 284.032 ; 135.043	Fon	(Chen et al., 2021)
48	Hispidulin	$C_{16}H_{12}O_6$	300.0633	300.0636	-0.73	13.10	299.0563	284.032 ; 136.986 ; 285.036 ; 165.989	Fon	(Sharma et al., 2020)
49	Unknown	$C_{28}H_{36}O_{12}$	564.2206	564.2210	-0.62	13.57	563.2136	387.166 ; 175.039 ; 388.169 ; 563.213	/	/
50	Abscisic acid	$C_{15}H_{20}O_4$	264.1361	264.1362	-0.30	13.61	263.1289	203.107 ; 204.114 ; 136.051 ; 122.036	OA	(MSBNK Washington State Univ BML00514)

Continued on next page

Table 6.11 – Continued from previous page

N°	Tentative Identification	Formulas	Calculated MW	Experimental MW	Δ mass [ppm]	RT [min]	Adduct mass [M-H]-	MS/MS	Class	References
51	Isorinic acid (caffeoyl-4-hydroxyphenyl-lactic acid)	$C_{18}H_{16}O_7$	344.0896	344.0898	-0.68	13.76	343.0826	161.023 ; 181.049 ; 135.043 ; 163.039	PA	(Wojciechowska et al., 2020)
52	Rosmarinic acid - methyl ester	$C_{19}H_{18}O_8$	374.1001	374.1004	-0.74	14.13	373.0931	135.043 ; 175.039 ; 72.991 ; 160.015	RAD	(Zhang et al., 2016)
53	Unknown	$C_{20}H_{28}O_5$	348.1936	348.1940	-1.04	14.36	347.1867	283.170 ; 284.173 ; 301.180 ; 329.175	/	/
54	3,5-Dimethoxycinnamic acid	$C_{11}H_{12}O_4$	208.0735	208.0730	2.25	15.07	207.0657	133.028 ; 135.043 ; 134.036 ; 161.023	Meth-CA	(Ali et al., 2021; Prothmann et al., 2017)
55	Luteolin	$C_{15}H_{10}O_6$	286.0477	286.0479	-0.55	15.22	285.0406	133.028 ; 285.040 ; 151.002 ; 149.023	Fon	(Velamuri et al., 2020)
56	Isorhamnetin	$C_{16}H_{12}O_7$	316.0583	316.0585	-0.83	15.35	315.0513	300.027 ; 136.986 ; 301.030 ; 228.042	Fol	(Hossain et al., 2012; Velamuri et al., 2020)
57	Unknown	$C_{19}H_{32}O_9$	404.2046	404.2047	-0.38	15.97	403.1975	112.984 ; 59.012 ; 77.448 ; 204.289	/	/
58	Unknown	$C_{17}H_{32}O_9$	380.2046	380.2049	-0.85	16.09	379.1976	174.955 ; 146.960 ; 358.361 ; 206.236	/	/
59	9, 12,13-Trihode (10,15)	$C_{18}H_{32}O_5$	328.2249	328.2251	-0.54	16.65	327.2177	211.133 ; 171.101 ; 229.144 ; 183.138	FA	(Ibrahim et al., 2022; Rahmani Samani et al., 2021)
60	Apigenin	$C_{15}H_{10}O_5$	270.0528	270.0529	-0.62	18.02	269.0457	117.033 ; 151.002 ; 149.023 ; 107.012	Fon	(Ibrahim et al., 2022; Rahmani Samani et al., 2021)
61	9, 12,13-Trihome (10)	$C_{18}H_{34}O_5$	330.2406	330.2407	-0.42	18.05	329.2333	211.133 ; 229.144 ; 183.138 ; 171.101	FA	(Rahmani Samani et al., 2021)

Continued on next page

Table 6.11 – Continued from previous page

N°	Tentative Identification	Formulas	Calculated MW	Experimental MW	Δ mass [ppm]	RT [min]	Adduct mass [M-H]-	MS/MS	Class	References
62	Diosmetin	$C_{16}H_{12}O_6$	300.0633	300.0634	-0.23	18.13	299.0562	284.032 ; 136.986 ; 65.001 ; 285.036	Fon	(Sharma et al., 2020)
63	Jaceosidin	$C_{17}H_{14}O_7$	330.0739	330.0741	-0.56	18.34	329.0668	299.019 ; 313.035 ; 300.023 ; 314.041	Fon	
64	Jaceosidin	$C_{17}H_{14}O_7$	330.0739	330.0741	-0.49	18.42	329.0668	299.019 ; 313.035 ; 300.023 ; 314.041	Fon	
65	Rosmanol	$C_{20}H_{26}O_5$	346.1780	346.1780	-0.20	18.97	345.1705	301.180 ; 283.170 ; 258.126 ; 227.107	DT	(Sharma et al., 2020)
66	Pectolinarigenin	$C_{17}H_{14}O_6$	314.0790	314.0792	-0.60	19.07	313.0719	283.024 ; 284.028 ; 297.040 ; 255.029	Fon	(Sharma et al., 2020)
67	Unknown	$C_{21}H_{30}O_5$	362.2093	362.2093	-0.04	19.06	361.2019	302.188 ; 303.192 ; 317.211 ; 284.177	/	/
68	Epirosmanol	$C_{20}H_{26}O_5$	346.1780	346.1780	0.04	19.09	345.1705	283.170 ; 345.170 ; 301.180 ; 268.146	DT	(Sharma et al., 2020)
69	Eupatorin	$C_{18}H_{16}O_7$	344.0896	344.0897	-0.55	19.16	343.0825	313.035 ; 299.165 ; 298.011 ; 328.058	Fon	(Avula et al., 2022)
70	Cirsimaritin	$C_{17}H_{14}O_6$	314.0790	314.0791	-0.35	19.18	313.0718	283.024 ; 284.028 ; 297.040 ; 255.029	Fon	(Velamuri et al., 2020)
71	Epiisorosmanol	$C_{20}H_{26}O_5$	346.1780	346.1780	-0.11	19.22	345.1707	283.170 ; 345.170 ; 284.173 ; 346.174	DT	(Sharma et al., 2020)
72	Unknown	$C_{19}H_{24}O_6$	348.1572	348.1573	-0.17	19.30	347.1501	259.170 ; 260.173 ; 284.173 ; 190.099	/	/
73	Unknown	$C_{19}H_{20}O_4$	312.1361	312.136	-0.76	19.31	311.1292	311.129 ; 283.133 ; 223.169 ; 296.105	/	/
74	Octadecenedioic acid	$C_{18}H_{32}O_4$	312.2300	312.2302	-0.64	19.33	311.2229	223.169 ; 87.043 ; 311.129 ; 57.033	FA	(Ibrahim et al., 2022)
75	Genkwanin (Flavone)	$C_{16}H_{12}O_5$	284.0684	284.0685	-0.38	19.33	283.0613	268.037 ; 269.041 ; 240.042 ; 117.033	Fon	(Avula et al., 2022; Velamuri et al., 2020)

Continued on next page

Table 6.11 – Continued from previous page

N°	Tentative Identification	Formulas	Calculated MW	Experimental MW	Δ mass [ppm]	RT [min]	Adduct mass [M-H]-	MS/MS	Class	References
76	Asiatic acid	$C_{30}H_{48}O_5$	488.3501	488.3503	-0.34	19.36	487.3430	487.343 ; 488.346 ; 116.927 ; 112.984	TT	(Velamuri et al., 2020)
77	16-Hydroxy-20-deoxocarnosol	$C_{20}H_{28}O_4$	332.1987	332.1989	-0.42	19.37	331.1916	313.181 ; 285.185 ; 303.196 ; 331.191	DT	(Castañeta et al., 2022)
78	Royleanone	$C_{20}H_{28}O_3$	316.2038	316.2038	0	19.51	315.1965	285.185 ; 286.189 ; 315.196 ; 283.170	DT	(Rahmani Samani et al., 2021)
79	Unknown	$C_{22}H_{30}O_5$	374.2093	374.2095	-0.52	19.56	373.2021	283.170 ; 327.160 ; 299.165 ; 301.180	/	/
80	Rosmadial	$C_{20}H_{24}O_5$	344.1623	344.1623	0.11	19.63	343.1550	299.165 ; 343.154 ; 300.168 ; 344.158	DT	(Sharma et al., 2020)
81	Unknown	$C_{19}H_{22}O_4$	314.1518	314.1519	-0.35	19.66	313.1445	285.149 ; 313.144 ; 242.094 ; 286.152	/	/
82	Unknown	$C_{19}H_{24}O_3$	300.1725	300.1724	0.24	19.66	299.1651	299.165 ; 284.141 ; 297.149 ; 298.156	/	/
83	Unknown	$C_{19}H_{22}O_3$	298.1568	298.1569	-0.31	19.66	297.1497	299.165 ; 284.141 ; 297.149 ; 298.156	/	/
84	Unknown	$C_{19}H_{26}O_4$	318.1831	318.1831	-0.21	19.44	317.1760	317.175 ; 179.070 ; 318.179 ; 271.170	/	/
85	Epirosmanol-methyl ether	$C_{21}H_{28}O_5$	360.1936	360.1936	0.12	19.72	359.1864	300.173 ; 301.176 ; 315.195 ; 229.086	CAD	(Borras Linares et al., 2011)
86	Carnosol	$C_{20}H_{26}O_4$	330.1831	330.1831	-0.15	19.76	329.1758	285.185 ; 201.091 ; 214.099 ; 269.153	DT	(Velamuri et al., 2020)
87	Hydroxyepirosmanol	$C_{20}H_{26}O_6$	362.1729	362.1731	-0.44	19.85	361.1658	317.175 ; 318.179 ; 301.176 ; 316.200	DT	(Avula et al., 2022)
88	Unknown	$C_{19}H_{26}O_4$	318.1831	318.1832	-0.34	19.85	317.1760	317.175 ; 273.186 ; 318.179 ; 179.070	/	/
89	Unknown	$C_{42}H_{56}O_9$	704.3924	704.3926	-0.27	19.87	703.3853	285.185 ; 329.175 ; 373.202 ; 286.189	/	/
90	Rosmadial isomer	$C_{20}H_{24}O_5$	344.1623	344.1623	0.11	19.87	343.1549	299.165 ; 343.155 ; 315.160 ; 300.168	DT	(Sharma et al., 2020)

Continued on next page

Table 6.11 – Continued from previous page

N°	Tentative Identification	Formulas	Calculated MW	Experimental MW	Δ mass [ppm]	RT [min]	Adduct mass [M-H]-	MS/MS	Class	References
91	Unknown	$C_{19}H_{26}O_2$	286.1932	286.1932	0	19.87	285.1860	285.185 ; 286.189 ; 201.091 ; 229.123	/	/
92	Unknown	$C_{22}H_{30}O_5$	374.2093	374.2092	0.10	19.88	373.2020	283.170 ; 329.175 ; 227.107 ; 268.146	/	/
93	Lariciresinol	$C_{20}H_{24}O_6$	360.1572	360.1574	-0.33	19.90	359.1500	315.160 ; 232.073 ; 316.163 ; 359.150	Ln	
94	Carnosic acid quinone	$C_{20}H_{26}O_4$	330.1831	330.1831	-0.03	19.92	329.1758	285.186 ; 286.189 ; 201.091 ; 270.161	DT	(Zhang et al., 2012)
95	Unknown	$C_{19}H_{24}O_4$	316.1674	316.1678	-1.26	19.98	315.1612	285.186 ; 315.196 ; 286.189 ; 316.199	/	/
96	Unknown	$C_{19}H_{22}O_3$	298.1568	298.157	-0.35	19.98	297.1497	297.149 ; 282.125 ; 298.153 ; 281.118	/	/
97	Rosmaridiphenol	$C_{20}H_{28}O_3$	316.2038	316.2038	-0.18	20.02	315.1965	285.185 ; 315.196 ; 286.189 ; 316.199	DT	(Sharma et al., 2020)
98	Unknown	$C_{19}H_{26}O_3$	302.1881	302.1883	-0.41	20.02	301.1809	301.180 ; 283.170 ; 302.184 ; 284.173	/	/
99	Rosmanol isomer	$C_{20}H_{26}O_5$	346.1780	346.1780	-0.05	20.02	345.1707	301.180 ; 302.184 ; 258.125 ; 283.169	PT	(Castañeta et al., 2022)
100	Carnosic acid (salvin)	$C_{20}H_{28}O_4$	332.1987	332.1988	-0.30	20.11	331.1915	287.201 ; 288.204 ; 244.146 ; 245.150	DT	(Velamuri et al., 2020)
101	Unknown	$C_{20}H_{26}O_3$	314.1881	314.1884	-0.74	20.22	313.1810	285.185 ; 313.181 ; 286.189 ; 314.184	/	/
102	Methyl carnosate	$C_{21}H_{30}O_4$	346.2144	346.2144	-0.14	20.31	345.2071	286.193 ; 287.197 ; 301.216 ; 302.220	DT	(Hossain et al., 2010; Velamuri et al., 2020)
103	Pisiferol	$C_{20}H_{30}O_2$	302.2245	302.2246	-0.13	20.33	301.2172	286.193 ; 287.197 ; 271.170 ; 285.185	DT	(Rahmani Samani et al., 2021)
104	Steviol	$C_{20}H_{30}O_3$	318.2195	318.2194	0.06	20.40	317.2122	179.106 ; 317.212 ; 318.215 ; 299.201	DT	(Shah et al., 2012)
105	Unknown	$C_{20}H_{30}O_2$	302.2245	302.2248	-0.76	20.33	301.2172	286.193; 287.197; 271.170; 285.185	/	/

Continued on next page

Table 6.11 – Continued from previous page

N°	Tentative Identification	Formulas	Calculated MW	Experimental MW	Δ mass [ppm]	RT [min]	Adduct mass [M-H]-	MS/MS	Class	References
106	Micromeric acid	$C_{30}H_{46}O_3$	454.3446	454.3448	-0.38	21.21	453.3376	453.337; 454.341; 116.927; 180.889	TT	(Velamuri et al., 2020)
107	Betulinic acid	$C_{30}H_{48}O_3$	456.3603	456.3607	-0.84	21.43	455.3534	455.353; 456.356; 454.340; 397.225	TT	(Velamuri et al., 2020)
108	Ursolic acid	$C_{30}H_{48}O_3$	456.3603	456.3607	-0.88	21.59	455.3534	455.353; 456.356; 264.851; 91.507	TT	(Velamuri et al., 2020)
109	Unknown	$C_{35}H_{52}O_5$	552.3814	552.3818	-0.69	22.72	551.3746	551.374 ; 507.384 ; 552.378 ; 287.201	/	/
110	Hydroxyursolic acid	$C_{30}H_{48}O_4$	472.3552	472.3555	-0.50	22.81	471.3481	/	TT	(Avula et al., 2022; Li et al., 2017; Velamuri et al., 2020)

HC : hydroxycoumarins, DT : diterpenes phenols, Fol : flavonol deratives, HBA :hydroxybenzoic acid, PAL : phenolic aldehydes, OA: organic acid, SA: sugar acid, OS: organic sugar, Fon: flavones derivatives, Fva: flavanone derivatives, DRA: derivative of rosmarinic acid, TT: triterpenoids, IsoFon: isoflavones, Ln: lignin, DCA: derivative of carnosic acid, meth-CA: methoxy-cinnamic acid, aryl-flav: 2-arylbenzofuran flavonoids, PG: phenolic glucoside

6.3 Conclusion

This study employed novel statistical methodologies, namely DSD and I-optimal design, to optimize the parameters of UAE and MAE for extracting TPC and antioxidant activity from leaves of *Salvia officinalis* L. Through the utilization of DSD and I-optimal design, the optimization process identified the following optimal conditions: for UAE, a 52% ethanol-water mixture, a solvent to solid ratio of $30\,\mathrm{mL\,g^{-1}}$, a temperature of 60 °C, and an extraction time of 10 min; and for MAE, a 60% ethanol-water concentration, a time of 4.79 min, a microwave power of 600 W, and a solvent-to-solid ratio of $50\,\mathrm{mL\,g^{-1}}$. Furthermore, the MAE optimal extract showed higher TPC (46.12 ± 0.08 $\mathrm{mg_{GAE}/g_{dw}}$) and TEAC (268.39 ± 1.28 $\mu\mathrm{mol_{TE}/g_{dw}}$) than the UAE optimal extract (TPC:31.84 ± 0.24 $\mathrm{mg_{GAE}/g_{dw}}$, TEAC: 237.94 ± 0.77 $\mu\mathrm{mol_{TE}/g_{dw}}$). However, this later exhibited higher TAC (38.92 ± 0.54 $\mathrm{mg_{AAE}/g_{dw}}$) than MAE optimal extract. The qualitative analysis using UHPLC-HRMS confirmed that *Salvia officinalis* L. extract is a potential source of bioactive compounds including phenolic acid and aldehydes, flavonoids, phenolic diterpenes etc. where rosmarinic acid, carnosol, methyl carnosate, carnosic acid were the main phenolic compounds. The relative content analysis of the *Salvia officinalis* L. bioactive compounds revealed that MAE was better than UAE.

General conclusion

The optimization of UAE and MAE of secondary metabolites from *Salvia officinalis* L. and *Carthamus caeruleus* L. of Bouira region through the use of new statistical designs such as DSD and I-optimal design, as well as machine learning including support vectors machine optimized using dragonfly algorithm (SVR-DA) is a promising approach to enhance the efficiency of the extraction process. This not only improves the quality and quantity of the secondary metabolites but also reduces the time and cost of the extraction process.

The optimization of UAE of TPC and TSC using BBD from the rhizome part of *C. caeruleus* L. confirmed that all the independent variables affect the UAE, where the the optimal conditions for extraction were determined as follows: a methanol concentration of 78.66%, a solvent to solid ratio of $23\,\mathrm{mL\,g^{-1}}$, an extraction temperature of 50 °C, and an extraction time of 26 minutes. At these optimal conditions, higher TPC, and TSC were obtained, thus higher antioxidant activity was achieved. In contrast, the SVR-DA model, a supervised learning approach, offers the capability to establish an interface for simultaneous determination of TPC and TSC from *C. caeruleus* L. rhizome. This model allows users to select desired values for various UAE conditions. Consequently, the SVR-DA model provides a direct and convenient means to assess TPC and TSC levels in the rhizome part of *C. caeruleus* L.

Moreover, DSD and I-optimal design presents notable benefits in experimental design. These approaches offer efficient and effective methods for identifying crucial factors related to UAE and MAE that influence TPC and antioxidant capacity from *S. officinalis* L. Importantly, these designs enable accurate results to be obtained while minimizing the number of experimental runs needed. The optimization of UAE revealed that the best optimal conditions were a 52% ethanol-water mixture, a temperature of 60 °C, a solvent to solid ratio of $30\,\mathrm{mL\,g^{-1}}$, and an extraction time of 10 minutes. Conversely, the optimization of MAE confirmed that the optimal conditions for higher TPC, TEAC, and TAC were a 60% ethanol

concentration, 600 W microwave power, a MAE time of 4.79 minutes, and a liquid to solid ratio of $50\,mL\,g^{-1}$. The comparative study of phenolic profile between UAE and MAE extracts using UHPLC-HRMS revealed that the MAE extract yielded high TPC than UAE extracts, thus the MAE as extraction technique is more efficient than UAE.

This study may have a significant impact on the pharmaceutical, food, and cosmetic industries by providing new strategies for the optimization of natural and sustainable source of bioactive compounds from medicinal plants. In addition, this study valorize the medicinal plants of Bouira region that could be a promising avenue for the development of novel and effective therapeutics.

The results obtained open several perspectives to complete our work such as;

- The identification of bioactive compounds present in *C. caeruleus* utilizing the ultra-high-performance liquid chromatography-mass spectrometry (UHPLC-MS) technique.
- The investigation of biological activities of these compounds both *in vitro* and *in vivo*, focusing on their potential anti-inflammatory, anti-cancer, and wound healing properties
- The use artificial intelligence to predict the properties of bioactive compounds, including their efficacy and toxicity, and to design new drugs based on this information.
- The formulation of medicinal plant extracts can play a crucial role in their bio-availability. The use of different techniques such as nanotechnology, solid lipid nanoparticles, liposomes, spray drying and micro-emulsions to optimize the formulation of plant extracts and improve their bio-availability.
- Co-delivery of plant extracts with other compounds such as phospholipids, surfactants, and other bio-enhancers to improve their bio-availability.
- Make preclinical evaluation of plant extracts to provide important insights into their safety and efficacy, where various animal models should be used to evaluate the pharmacokinetics, pharmacodynamics, and toxicity of plant extracts.

Appendix

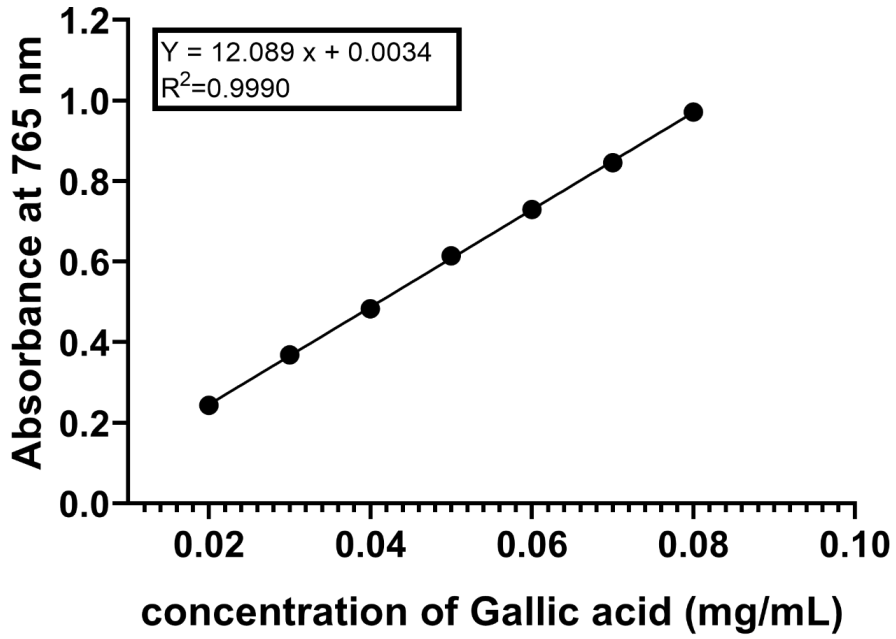

Figure 6.9: The standard curve of Gallic acid used for the estimation of TPC from the rhizome of *C. caeruleus* L.

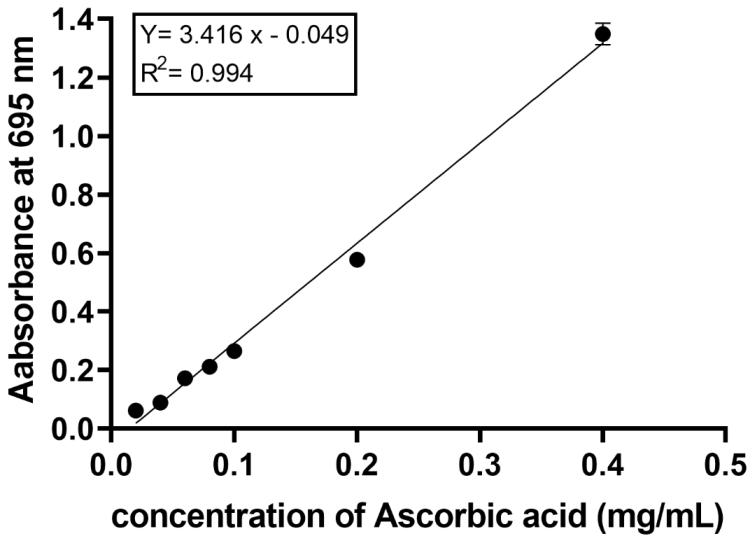

Figure 6.10: The standard curve of Ascorbic acid employed for the evaluation of total antioxidant activity from the rhizome of *C. caeruleus* L.

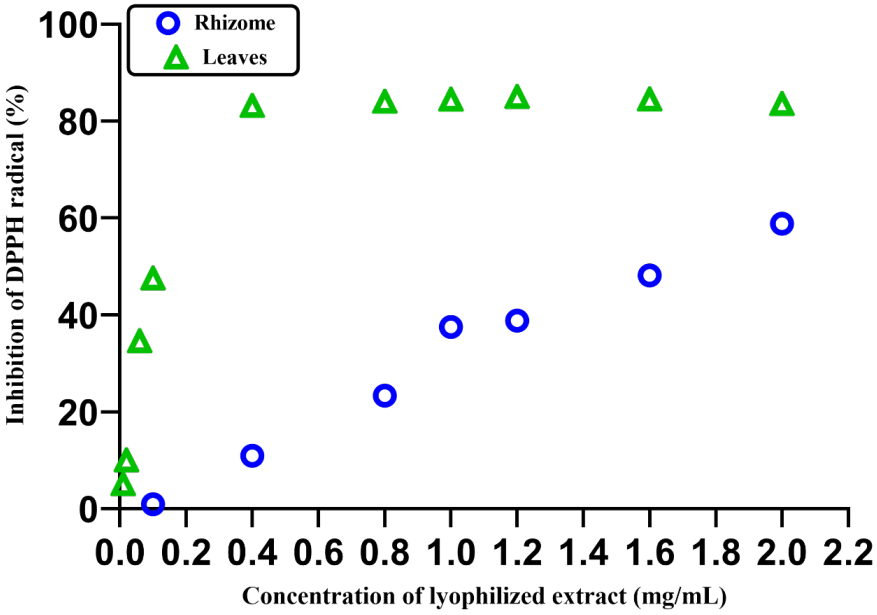

Figure 6.11: Comparative study of scavenging properties of *C. caeruleus* L. leaves and rhizome using DPPH assay

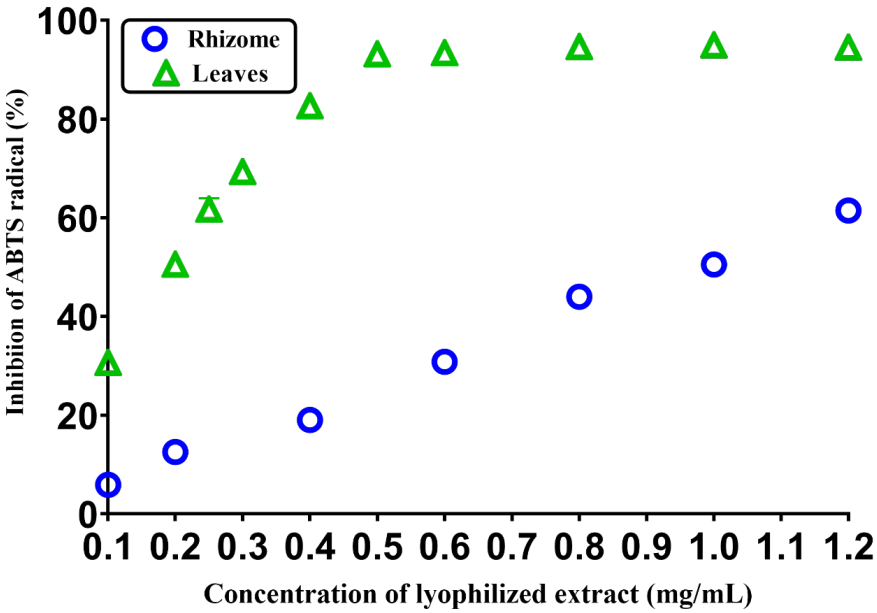

Figure 6.12: Comparative study of scavenging properties of *C. caeruleus* L. leaves and rhizome using decolorization of ABTS* test

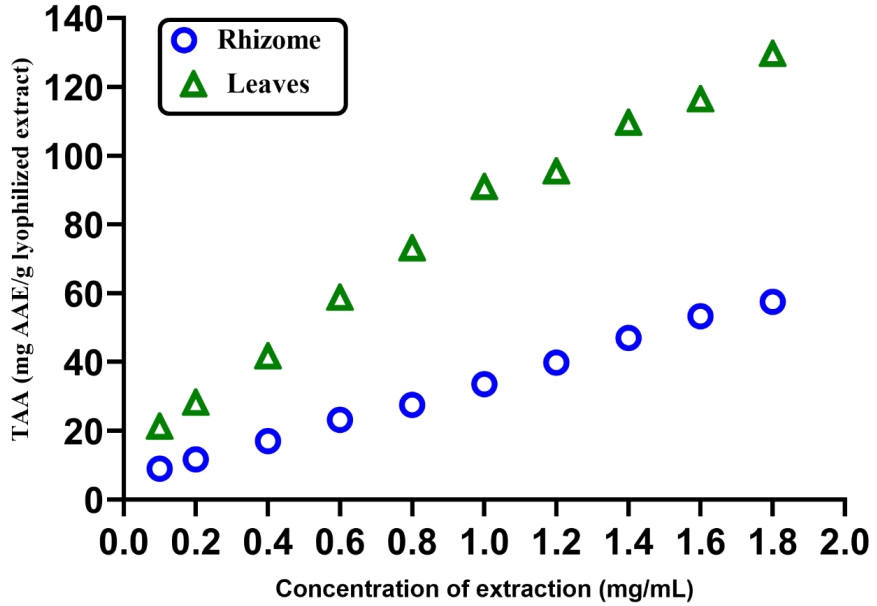

Figure 6.13: Evaluation of total antioxidant of *C. caeruleus* L. leaves and rhizome using phosphomolybdenum assay

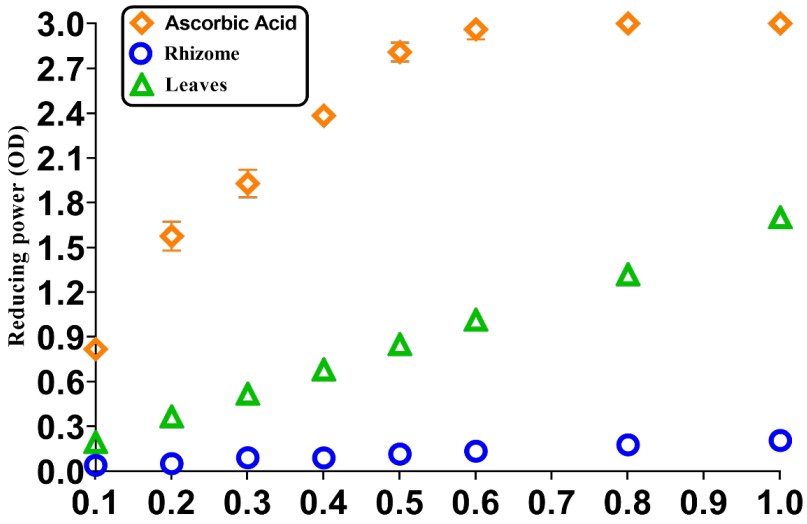

Figure 6.14: Evaluation of antioxidant potential of *C. caeruleus* L. leaves and rhizome using reducing power

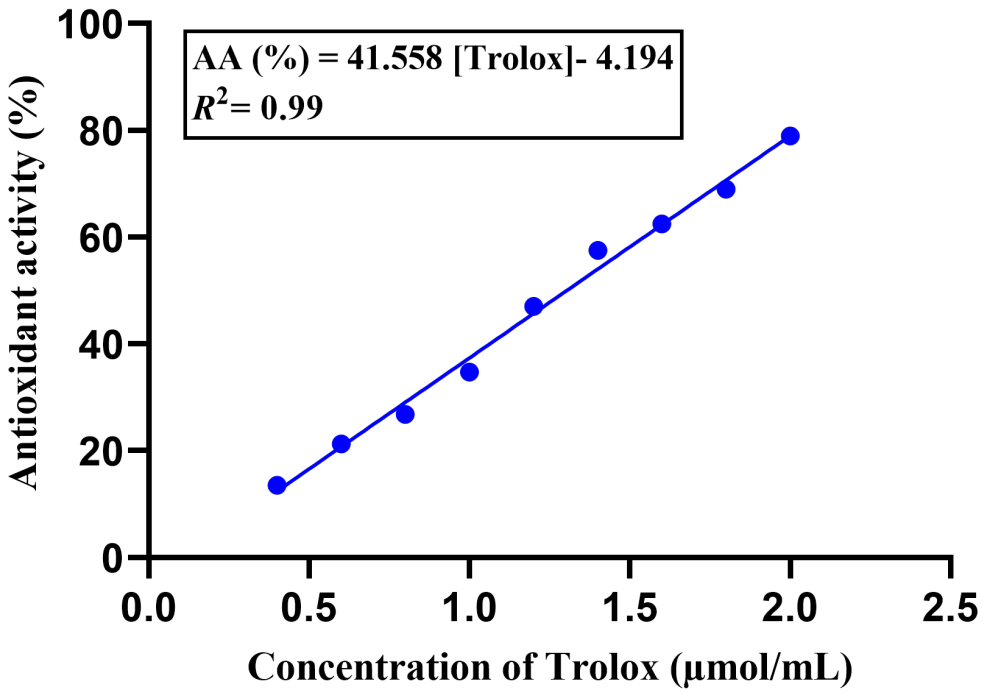

Figure 6.15: Standard curve of Trolox at 734 nm used for Trolox equivalent antioxidant capacity (TEAC)

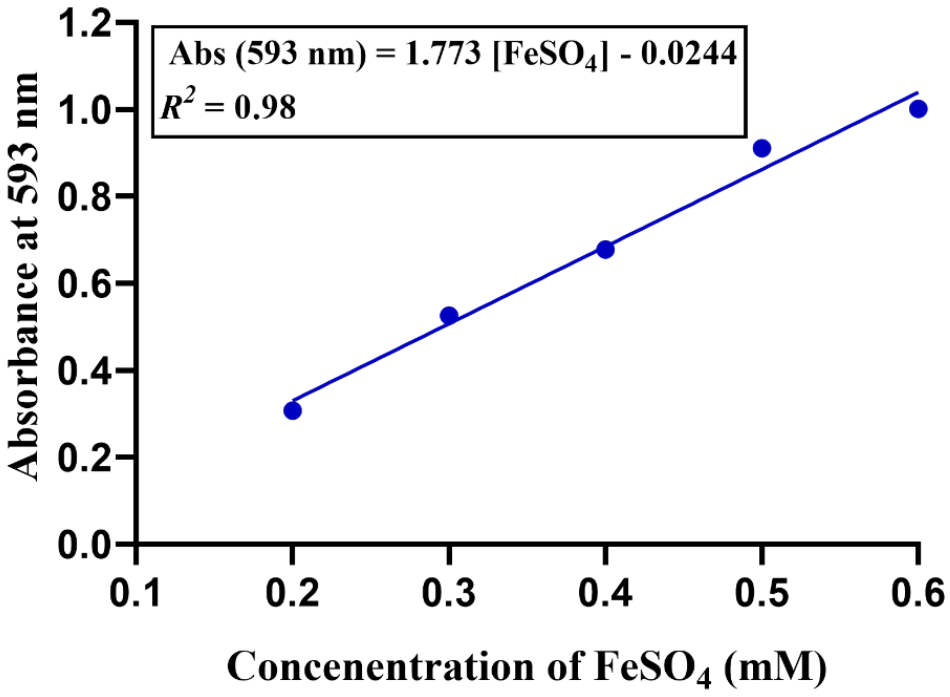

Figure 6.16: Standard curve of FeSO4 at 593 nm used for reducing power

Table 6.12: Chemical reagents employed for the extraction of secondary metabolites from *C. caeruleus* L. rhizome and *S. officinalis* L. leaves and evaluation of their antioxidant activities

Application	Reagents and microbiological mediums	Chemical formulas (linear)	Molar mass (g/mol)	Provider
Extraction	Methanol	CH_3OH	32.04	Merck
	Ethanol	CH_3CH_2OH	46.07	
Determination of total phenolic content	Folin-Ciocalteu	$C_{10}H_5NaO_5S$	260.20	VWR CHEMICALS
	Sodium carbonate	Na_2CO_3	105.98	Merck
	Gallic acid	$C_6H_2(OH)_3COOH$	170.12	
Determination of total saponin content	Vanillin	$C_8H_8O_3$	152.15	Merck
	Sulfuric acid	H_2SO_4	98.07	
Trolox equivalent antioxidant capacity	ABTS	$C_{18}H_{18}N_4O_6S_4$	514.62	Merck
	Potassium persulfate	$K_2S_2O_8$	270.322	
	Trolox	$C_{14}H_{18}O_4$	250.29	
Total antioxidant capacity	Ammonium molybdate tetrahydrate	$(NH_4)_6Mo_7O_{24}\cdot 4\,H_2O$	1235.86	VWR CHEMICALS
	Ascorbic acid	$C_6H_8O_6$	176.12	Merck
Free radicals scavenging activity	DPPH	$C_{18}H_{12}N_5O_6$	394.32	Merck
Reducing Power	Potassium ferricyanide	$K_3Fe(CN)_6$	329.24	Merck
	Trichloroacetic acid	$C_2HCl_3O_2$	163.38	
	Sodium phosphate monobasic	$NaH_2PO_4\cdot H_2O$	137.99	VWR CHEMICALS
	Sodium phosphate dibasic dibasic dodecahydrate	$Na_2HPO_4\cdot 12\,H_2O$	358.14	
	Ferric chloride	$FeCl_3$	162.2	
	Iron(II) sulfate	$FeSO_4$	151.90	

Table 6.13: UAE parameters effect on TPC and TSC from rhizome of *C. caeruleus* L. using single-factor design

Extraction conditions	Level	TPC ($mg_{GAE}/100g_{dw}$)	TSC (Abs)
Temperature (°C)	40	243.692 ± 6.460^{d}	0.125 ± 0.004^{c}
	50	291.879 ± 4.555^{bc}	0.135 ± 0.002^{bc}
	60	274.574 ± 1.263^{c}	0.142 ± 0.001^{b}
	70	310.971 ± 3.343^{a}	0.192 ± 0.002^{a}
Methanol concentration (%)	10	297.184 ± 11.620^{a}	0.348 ± 0.004^{b}
	20	228.527 ± 0.477^{f}	0.355 ± 0.005^{b}
	30	226.597 ± 3.443^{fg}	0.306 ± 0.009^{cd}
	40	219.703 ± 2.188^{g}	0.281 ± 0.010^{e}
	50	236.523 ± 0.955^{e}	0.297 ± 0.008^{d}
	60	286.431 ± 4.703^{ab}	0.311 ± 0.003^{c}
	70	264.372 ± 2.481^{d}	0.312 ± 0.004^{c}
	80	274.574 ± 2.081^{c}	0.317 ± 0.006^{c}
	90	276.229 ± 2.081^{c}	0.372 ± 0.002^{a}
Sonication time (min)	5	244.244 ± 4.244^{b}	0.235 ± 0.005^{bc}
	10	256.652 ± 3.730^{a}	0.205 ± 0.013^{de}
	15	239.280 ± 4.080^{b}	0.279 ± 0.004^{a}
	20	243.416 ± 0.477^{b}	0.218 ± 0.008^{cd}
	30	220.531 ± 7.163^{c}	0.194 ± 0.013^{e}
	40	263.545 ± 10.063^{a}	0.251 ± 0.011^{b}
	50	262.442 ± 4.244^{a}	0.217 ± 0.007^{d}
Solvent to solid ratio (mL.g-1)	10	86.828 ± 1.041^{c}	0.172 ± 0.007^{c}
	15	268.798 ± 5.896^{a}	0.238 ± 0.003^{b}
	20	244.244 ± 7.131^{b}	0.259 ± 0.008^{a}
	25	260.843 ± 4.178^{a}	0.240 ± 0.006^{b}

The levels are not sharing the same superscript letters (a-d) are significantly different at ($p < 0.05$) (student test)

Table 6.14: Metrics and kernel functions employed for SVR-DA to predict TPC and TSC from *C. caeruleus* L. rhizome

	Name of function	Equations
Metrics for evaluation of SVR-DA model	Standard deviation	$SD = \sqrt{\frac{(\sum(y_{exp}-y_{cal})^2)}{n}}$
	Relative Standard deviation	$RSD = \frac{\sqrt{\frac{(\sum(y_{exp}-y_{cal})^2)}{n}}}{mean(y_{exp})} * 100$
	Mean absolute error	$MAE = \frac{\sum\lvert y_{exp}-y_{cal}\rvert}{n}$
	Mean relative percentage error	$MRPE = 100 * \max(\frac{\lvert y_{exp}-y_{ca}\rvert}{y_{exp}})$
	Average absolute relative deviation	$AARD = 100 * \frac{\sum(\frac{\lvert y_{exp}-y_{ca}\rvert}{y_{exp}})}{n}$
	Root mean square error	$RMSE = \sqrt{\frac{\sum_{i=1}^{n}(y_{exp}-y_{cal})^2}{n}}$
	Coefficient of determination	$R^2 = 1 - \frac{SS_{res}}{SS_{tot}} = 1 - \frac{\sum_{i=1}^{n}(y_{exp}-y_{cal})^2}{\sum_{i=1}^{n}(y_{exp}-y_{moy})^2}$
Kernel functions	Linear (dot product)	$G(x_j, x_k) = x_j^{'} x_k$
	Gaussian	$G(x_j, x_k) = exp(-\lVert x_j - x_k\rVert^2)$
	polynomial	$G(x_j, x_k) = (1 + x_j^{'} x_k)^q$, where q is in the set 2,3,..

y_{exp} and y_{cal} are the actual values and predicted values of model respectively; and n represents the total number of experiments, SS_{res} and SS_{tot} are the sums of square of residuals and total of TPC and TSC respectively

Table 6.15: Equations employed to compute the efficiency parameters of DSD and I-optimal design

Efficiency Parameter	Equations	References
D- efficiency	$100\,(\frac{1}{n}\,\lvert\mathbf{X}^{'}\mathbf{X}\rvert^{1/p})$	(Rodríguez et al., 2017)
A-efficiency	$100\,p/(n\,trace\,(\mathbf{X}^{'}\mathbf{X})^{-1})$	(Jones et al., 2020)
G- efficiency	$\max_{\mathbf{x}\epsilon\mathbf{D}}\,\mathbf{f}^{'}(\mathbf{x})(\mathbf{X}^{'}\mathbf{X})^{-1}\mathbf{f}\,(\mathbf{x})$	(Goos, 2012)
Average variance of prediction	$\frac{1}{\int_D d\mathbf{x}} * trace\,[(\mathbf{X}^{'}\mathbf{X})^{-1}\mathbf{M}]$	(Goos and Jones, 2011)

$\mathbf{X}$ is the model matrix, $\mathbf{X}^{'}$ is transpose matrix, $\mathbf{x}$ is a vector of factor levels that corresponds to one of the runs of the design, then $\mathbf{f}^{'}(\mathbf{x})$ is the corresponding row of the matrix $\mathbf{X}$, $\mathbf{f}\,(\mathbf{x})$ is a function that takes a vector of factor settings and expands that vector to its corresponding model terms. $\mathbf{D}$ denotes the experimental region, n is the number of runs in the design, p is the number of terms including the intercept, $\mathbf{M}$ is called the moments matrix

References

Ababsa, Z. E. A., Ali, W. K., Abidli, N., Akkal, S., and Medjroubi, K. (2018). Chemical characterization and biological study of the species senecio cineraria. *World*, 7(3):112–121.

Abdelkader, M., Laidi, M., Hanini, S., Hentabli, M., and Amrane, A. (2021). A grey wolf optimizer-based fractional calculus in studies on solar drying. *Kemija u industriji*, 70(1-2):39–47.

Afonso, A. F., Pereira, O. R., and Cardoso, S. M. (2021). Salvia species as nutraceuticals: Focus on antioxidant, antidiabetic and anti-obesity properties. *Applied Sciences*, 11(20):9365.

Akhondzadeh, S., Noroozian, M., Mohammadi, M., Ohadinia, S., Jamshidi, A., and Khani, M. (2003). Salvia officinalis extract in the treatment of patients with mild to moderate alzheimer's disease: a double blind, randomized and placebo-controlled trial. *Journal of clinical pharmacy and therapeutics*, 28(1):53–59.

Akhtar, I., Javad, S., Yousaf, Z., Iqbal, S., and Jabeen, K. (2019). Microwave assisted extraction of phytochemicals an efficient and modern approach for botanicals and pharmaceuticals. *Pakistan journal of pharmaceutical sciences*, 32(1).

Alara, O. R., Abdurahman, N. H., and Ukaegbu, C. I. (2018). Soxhlet extraction of phenolic compounds from vernonia cinerea leaves and its antioxidant activity. *Journal of Applied Research on Medicinal and Aromatic Plants*, 11:12–17.

Albayrak, S., Aksoy, A., Sagdic, O., and Hamzaoglu, E. (2010). Compositions, antioxidant and antimicrobial activities of helichrysum (asteraceae) species collected from turkey. *Food Chemistry*, 119(1):114–122.

Ali, A., Bashmil, Y. M., Cottrell, J. J., Suleria, H. A. R., and Dunshea, F. R. (2021). Lc-ms/ms-qtof screening and identification of phenolic compounds from australian grown herbs and their antioxidant potential. *Antioxidants (Basel)*, 10(11):1770.

Ali, A., Lim, X. Y., Chong, C. H., Mah, S. H., and Chua, B. L. (2018). Optimization of ultrasound-assisted extraction of natural antioxidants from piper betle using response surface methodology. *LWT*, 89:681–688.

Alrezaki, A., Aldawood, N., Alanazi, S., Arafah, M., Fabova, Z., Badjah, Y., Sirotkin, A. V., Alwasel, S., and Halim Harrath, A. (2021). Consumption of sage (salvia officinalis) promotes ovarian function by stimulating estradiol hormone release and controlling folliculogenesis, steroidogenesis, and autophagy. *Journal of King Saud University - Science*, 33(2):101319.

Altindal, D. and Altindal, N. (2016). *Chapter 81 - Sage (Salvia officinalis) Oils*, pages 715–721. Academic Press, San Diego.

Alvi, T., Asif, Z., and Iqbal Khan, M. K. (2022). Clean label extraction of bioactive compounds from food waste through microwave-assisted extraction technique-a review. *Food Bioscience*, 46:101580.

Amirmohammadi, M., Khajoenia, S., Bahmani, M., Rafieian-Kopaei, M., Eftekhari, Z., and Qorbani, M. (2014). In vivo evaluation of antiparasitic effects of artemisia abrotanum and salvia officinalis extracts on syphacia obvelata, aspiculoris tetrapetra and hymenolepis nana parasites. *Asian Pacific Journal of Tropical Disease*, 4:S250–S254.

Anslyn, E. V. and Dougherty, D. A. (2006). *Modern physical organic chemistry*. University science books.

Arteaga-Crespo, Y., Radice, M., Bravo-Sanchez, L. R., Garcia-Quintana, Y., and Scalvenzi, L. (2020). Optimisation of ultrasound-assisted extraction of phenolic antioxidants from ilex guayusa loes. leaves using response surface methodology. *Heliyon*, 6(1):e03043. Arteaga-Crespo, Yasiel Radice, Matteo Bravo-Sanchez, Luis Ramon Garcia-Quintana, Yudel Scalvenzi, Laura England Heliyon. 2019 Dec 27;6(1):e03043. doi: 10.1016/j.heliyon.2019.e03043. eCollection 2020 Jan.

Asgari, S., Sahari, M. A., and Barzegar, M. (2017). Practical modeling and optimization of ultrasound-assisted bleaching of olive oil using hybrid artificial neural network-genetic algorithm technique. *Computers and Electronics in Agriculture*, 140:422–432.

Ashri, A. and Knowles, P. (1960). Cytogenetics of safflower (carthamus l.) species and their hybrids. *Agronomy Journal*, 52:11–17.

Aslan, N. and Cebeci, Y. (2007). Application of box–behnken design and response surface methodology for modeling of some turkish coals. *Fuel*, 86(1-2):90–97.

Atawodi, S. (2005). Antioxidant potential of african medicinal plants. *African Journal of Biotechnology*, 4(2):128–133.

Avula, B., Bae, J. Y., Chittiboyina, A. G., Wang, Y. H., Wang, M., Srivedavyasasri, R., Ali, Z., Li, J., Wu, C., and Khan, I. A. (2022). Comparative analysis of five salvia species using lc-dad-qtof. *J Pharm Biomed Anal*, 209:114520. Avula, Bharathi Bae, Ji-Yeong Chittiboyina, Amar G Wang, Yan-Hong Wang, Mei Srivedavyasasri, Radhakrishnan Ali, Zulfiqar Li, Jing Wu, Charles Khan, Ikhlas A England J Pharm Biomed Anal. 2022 Feb 5;209:114520. doi: 10.1016/j.jpba.2021.114520. Epub 2021 Dec 5.

Awad, M. and Khanna, R. (2015). *Support vector regression*, pages 67–80. Springer.

Babbar, N., Oberoi, H. S., Uppal, D. S., and Patil, R. T. (2011). Total phenolic content and antioxidant capacity of extracts obtained from six important fruit residues. *Food Research International*, 44(1):391–396.

Bagade, S. B. and Patil, M. (2021). Recent advances in microwave assisted extraction of bioactive compounds from complex herbal samples: A review. *Crit Rev Anal Chem*, 51(2):138–149.

Bagchi, G. D. and Srivastava, G. N. (2003). *SPICES AND FLAVORING (FLAVOURING) CROPS — Leaf and Floral Structures*, pages 5477–5486. Academic Press, Oxford.

Baghiani, A., Boumerfeg, S., Belkhiri, F., Khennouf, S., Charef, N., Harzallah, D., Arrar, L., and Abdel-Wahhab, M. A. (2010). Antioxidant and radical scavenging properties of carthamus caeruleus l extracts grow wild in algeria flora. *Comunicata Scientiae*, 1(2):128.

Battandier, J. A. (1888). *Flore de l'Algérie: Dicotylédones*, volume 1. Adolphe Jourdan.

Benhamou, A. and Fazouane, F. (2013). Ethnobotanical study, phytochemical characterization and healing effect of carthamus coeruleusl. rhizomes.

Benimam, H., Moussa, C. S., Hentabli, M., Hanini, S., and Laidi, M. (2020). Dragonfly-support vector machine for regression modeling of the activity coefficient at infinite dilution of solutes in imidazolium ionic liquids using σ-profile descriptors. *Journal of Chemical & Engineering Data*, 65(6):3161–3172.

Berkani, F., Serralheiro, M. L., Dahmoune, F., Ressaissi, A., Kadri, N., and Remini, H. (2020). Ultrasound assisted extraction of phenolic compounds from a jujube by-product with valuable bioactivities. *Processes*, 8(11):1441.

Bhuyan, D. J., Van Vuong, Q., Chalmers, A. C., van Altena, I. A., Bowyer, M. C., and Scarlett, C. J. (2015). Microwave-assisted extraction of eucalyptus robusta leaf for the optimal yield of total phenolic compounds. *Industrial Crops and Products*, 69:290–299.

Borras Linares, I., Arraez-Roman, D., Herrero, M., Ibanez, E., Segura-Carretero, A., and Fernandez-Gutierrez, A. (2011). Comparison of different extraction procedures for the comprehensive characterization of bioactive phenolic compounds in rosmarinus officinalis by reversed-phase high-performance liquid chromatography with diode array detection coupled to electrospray time-of-flight mass spectrometry. *J Chromatogr A*, 1218(42):7682–90. Borras Linares, I Arraez-Roman, D Herrero, M Ibanez, E Segura-Carretero, A Fernandez-Gutierrez, A Netherlands J Chromatogr A. 2011 Oct 21;1218(42):7682-90. doi: 10.1016/j.chroma.2011.07.021. Epub 2011 Jul 20.

Boufadi, M. Y., Keddari, S., Moulaihacene, F., and Chaa, S. (2020). Chemical composition, antioxidant and anti-inflammatory properties of salvia officinalis extract from algeria. *Pharmacognosy Journal*, 13(2):506–515.

Bouteldja, R., Doucene, R., Aggad, H., Abdi, F. Z., Belkhodja, H., Abdali, M., Zidane, K., and Abaid, S. (2021). Phytochemical characterization, antioxidant and antibacterial activity of salvia officinalis (l.) extracts from the tiaret region. *European Journal of Biological Research*, 11(3):356–366.

Brandão, M., Krettli, A., Soares, L., Nery, C., and Marinuzzi, H. (1997). Antimalarial activity of extracts and fractions from bidens pilosa and other bidens species (asteraceae) correlated with the presence of acetylene and flavonoid compounds. *Journal of ethnopharmacology*, 57(2):131–138.

Capelo-Martínez, J.-L. (2009). *Ultrasound in chemistry: analytical applications*. John Wiley & Sons.

Castañeta, G., Cifuentes, N., Sepulveda, B., Bárcenas-Pérez, D., Cheel, J., and Areche, C. (2022). Untargeted metabolomics by using uhplc–esi–ms/ms of an extract obtained with ethyl lactate green solvent from salvia rosmarinus. *Separations*, 9(11):327.

Celano, R., Piccinelli, A. L., Pagano, I., Roscigno, G., Campone, L., De Falco, E., Russo, M., and Rastrelli, L. (2017). Oil distillation wastewaters from aromatic herbs as new natural source of antioxidant compounds. *Food Research International*, 99:298–307.

Celli, G. B., Tan, C., and Selig, M. J. (2019). *Anthocyanidins and Anthocyanins*, pages 218–223. Academic Press, Oxford.

Chan, C. H., Yusoff, R., Ngoh, G. C., and Kung, F. W. (2011). Microwave-assisted extractions of active ingredients from plants. *J Chromatogr A*, 1218(37):6213–25.

Chaturvedi, A. K. (2018). Extraction of neutraceuticals from plants by microwave assisted extraction. *Systematic Reviews in Pharmacy*, 9(1):31–35.

Cheeseman, K. H. and Slater, T. F. (1993). An introduction to free radical biochemistry. *British medical bulletin*, 49(3):481–493.

Chemat, F. and Cravotto, G. (2012). *Microwave-assisted extraction for bioactive compounds: theory and practice*, volume 4. Springer Science & Business Media.

Chemat, F., Rombaut, N., Sicaire, A. G., Meullemiestre, A., Fabiano-Tixier, A. S., and Abert-Vian, M. (2017). Ultrasound assisted extraction of food and natural products. mechanisms, techniques, combinations, protocols and applications. a review. *Ultrason Sonochem*, 34:540–560. Chemat, Farid Rombaut, Natacha Sicaire, Anne-Gaelle Meullemiestre, Alice Fabiano-Tixier, Anne-Sylvie Abert-Vian, Maryline Netherlands Ultrason Sonochem. 2017 Jan;34:540-560. doi: 10.1016/j.ultsonch.2016.06.035. Epub 2016 Jun 23.

Chen, M., Zhao, Y., and Yu, S. (2015). Optimisation of ultrasonic-assisted extraction of phenolic compounds, antioxidants, and anthocyanins from sugar beet molasses. *Food Chem*, 172:543–50. Chen, Mingshun Zhao, Yi Yu, Shujuan England Food Chem. 2015 Apr 1;172:543-50. doi: 10.1016/j.foodchem.2014.09.110. Epub 2014 Sep 28.

Chen, S., Zeng, Z., Hu, N., Bai, B., Wang, H., and Suo, Y. (2018). Simultaneous optimization of the ultrasound-assisted extraction for phenolic compounds content and antioxidant activity of lycium ruthenicum murr. fruit using response surface methodology. *Food Chem*, 242:1–8. Chen, Shasha Zeng, Zhi Hu, Na Bai, Bo Wang, Honglun Suo, Yourui England Food Chem. 2018 Mar 1;242:1-8. doi: 10.1016/j.foodchem.2017.08.105. Epub 2017 Sep 6.

Chen, Z., Zhong, B., Barrow, C. J., Dunshea, F. R., and Suleria, H. A. R. (2021). Identification of phenolic compounds in australian grown dragon fruits by lc-esi-qtof-ms/ms and determination of their antioxidant potential. *Arabian Journal of Chemistry*, 14(6):103151.

Cheok, C. Y., Chin, N. L., Yusof, Y. A., Talib, R. A., and Law, C. L. (2012). Optimization of total phenolic content extracted from garcinia mangostana linn. hull using response surface methodology versus artificial neural network. *Industrial crops and products*, 40:247–253.

Chew, K., Khoo, M., Ng, S., Thoo, Y. Y., Aida, W. W., and Ho, C. W. (2011). Effect of ethanol concentration, extraction time and extraction temperature on the recovery of phenolic compounds and antioxidant capacity of orthosiphon stamineus extracts. *International Food Research Journal*, 18(4):1427.

Ciric, A., Krajnc, B., Heath, D., and Ogrinc, N. (2020). Response surface methodology and artificial neural network approach for the optimization of ultrasound-assisted extraction of polyphenols from garlic. *Food and Chemical Toxicology*, 135:110976.

Cuppett, S. L. and Hall, C. A. (1998). Antioxidant activity of the labiatae. *Advances in food and nutrition research*, 42:245–272.

Cushnie, T. P. T. and Lamb, A. J. (2005a). Antimicrobial activity of flavonoids. *International Journal of Antimicrobial Agents*, 26(5):343–356.

Cushnie, T. T. and Lamb, A. J. (2005b). Antimicrobial activity of flavonoids. *International journal of antimicrobial agents*, 26(5):343–356.

Dahmani, M. M., Laoufi, R., Selama, O., and Arab, K. (2018). Gas chromatography coupled to mass spectrometry characterization, anti-inflammatory effect, wound-healing potential, and hair growth-promoting activity of algerian carthamus caeruleus l (asteraceae). *Indian Journal of Pharmacology*, 50(3):123.

Dahmoune, F., Remini, H., Dairi, S., Aoun, O., Moussi, K., Bouaoudia-Madi, N., Adjeroud, N., Kadri, N., Lefsih, K., Boughani, L., et al. (2015). Ultrasound assisted extraction of phenolic compounds from p. lentiscus l. leaves: Comparative study of artificial neural network (ann) versus degree of experiment for prediction ability of phenolic compounds recovery. *Industrial Crops and Products*, 77:251–261.

Dahmoune, F., Spigno, G., Moussi, K., Remini, H., Cherbal, A., and Madani, K. (2014). Pistacia lentiscus leaves as a source of phenolic compounds: Microwave-assisted extraction optimized and compared with ultrasound-assisted and conventional solvent extraction. *Industrial Crops and Products*, 61:31–40.

Dai, Y., Witkamp, G.-J., Verpoorte, R., and Choi, Y. H. (2013). Natural deep eutectic solvents as a new extraction media for phenolic metabolites in carthamus tinctorius l. *Analytical chemistry*, 85(13):6272–6278.

Dang, T. T., Van Vuong, Q., Schreider, M. J., Bowyer, M. C., Van Altena, I. A., and Scarlett, C. J. (2017). Optimisation of ultrasound-assisted extraction conditions for phenolic content and antioxidant activities of the alga hormosira banksii

using response surface methodology. *Journal of Applied Phycology*, 29(6):3161–3173.

D'Archivio, M., Filesi, C., Di Benedetto, R., Gargiulo, R., Giovannini, C., and Masella, R. (2007). Polyphenols, dietary sources and bioavailability. *Annali-Istituto Superiore di Sanita*, 43(4):348.

Darvishzadeh, P. and Orsat, V. (2022). Microwave-assisted extraction of antioxidant compounds from russian olive leaves and flowers: Optimization, hplc characterization and comparison with other methods. *Journal of Applied Research on Medicinal and Aromatic Plants*, 27:100368.

De Filippis, B., Ammazzalorso, A., Fantacuzzi, M., Giampietro, L., Maccallini, C., and Amoroso, R. (2017). Anticancer activity of stilbene-based derivatives. *ChemMedChem*, 12(8):558–570. De Filippis, Barbara Ammazzalorso, Alessandra Fantacuzzi, Marialuigia Giampietro, Letizia Maccallini, Cristina Amoroso, Rosa Germany ChemMedChem. 2017 Apr 20;12(8):558-570. doi: 10.1002/cmdc.201700045. Epub 2017 Mar 28.

Deka, P. C. et al. (2014). Support vector machine applications in the field of hydrology: a review. *Applied soft computing*, 19:372–386.

Delazar, A., Nahar, L., Hamedeyazdan, S., and Sarker, S. D. (2012). Microwave-assisted extraction in natural products isolation. *Methods Mol Biol*, 864:89–115.

Dent, M. (2015). Comparison of conventional and ultrasound-assisted extraction techniques on mass fraction of phenolic compounds from sage (salvia officinalis l.). *Chemical and Biochemical Engineering Quarterly*, 29(3):475–484.

Derringer, G. and Suich, R. (1980). Simultaneous optimization of several response variables. *Journal of quality technology*, 12(4):214–219.

Desai, M., Parikh, J., and Parikh, P. A. (2010). Extraction of natural products using microwaves as a heat source. *Separation & Purification Reviews*, 39(1-2):1–32.

Dogan, K., Akman, P. K., and TÖRNÜK, F. (2019). Improvement of bioavailability of sage and mint by ultrasonic extraction. *International Journal of Life Sciences and Biotechnology*, 2(2):122–135.

Dong, J., Liu, Y., Liang, Z., and Wang, W. (2010). Investigation on ultrasound-assisted extraction of salvianolic acid b from salvia miltiorrhiza root. *Ultrasonics Sonochemistry*, 17(1):61–65.

Doymaz, İ. and Karasu, S. (2018). Effect of air temperature on drying kinet-

ics, colour changes and total phenolic content of sage leaves (salvia officinalis). *Quality Assurance and Safety of Crops & Foods*, 10(3):269–276.

Dragovic-Uzelac, V., Garofulic, I. E., Jukic, M., Penic, M., and Dent, M. (2012). The influence of microwave-assisted extraction on the isolation of sage (salvia officinalis l.) polyphenols. *Food Technology and Biotechnology*, 50(3):377.

Durling, N., Catchpole, O., Grey, J., Webby, R., Mitchell, K., Foo, L., and Perry, N. (2007). Extraction of phenolics and essential oil from dried sage (salvia officinalis) using ethanol–water mixtures. *Food Chemistry*, 101(4):1417–1424.

Dzah, C. S., Duan, Y., Zhang, H., Wen, C., Zhang, J., Chen, G., and Ma, H. (2020). The effects of ultrasound assisted extraction on yield, antioxidant, anticancer and antimicrobial activity of polyphenol extracts: A review. *Food Bioscience*, 35:100547.

Eidi, A. and Eidi, M. (2009). Antidiabetic effects of sage (salvia officinalis l.) leaves in normal and streptozotocin-induced diabetic rats. *Diabetes & Metabolic Syndrome: Clinical Research & Reviews*, 3(1):40–44.

El-Feky, A. M. and Aboulthana, W. M. (2016). Phytochemical and biochemical studies of sage (salvia officinalis l.). *Pharmaceutical and Biosciences Journal*, pages 56–62.

Elith, J. and Leathwick, J. (2017). Boosted regression trees for ecological modeling. *R Documentation. Available online: https://cran. r-project. org/web/packages/dismo/vignettes/brt. pdf (accessed on 12 June 2011)*.

EMA (2009). Community herbal monograph on salvia officinalis l., folium.

Esclapez, M. D., García-Pérez, J. V., Mulet, A., and Cárcel, J. A. (2011). Ultrasound-assisted extraction of natural products. *Food Engineering Reviews*, 3(2):108–120.

Et-Touys, A., Fellah, H., Mniouil, M., Bouyahya, A., Dakka, N., Abdennebi, E., Sadak, A., and Bakri, Y. (2016). Screening of antioxidant, antibacterial and antileishmanial activities of salvia officinalis l. extracts from morocco. *Br Microbiol Res J*, 16:1–10.

Favre, H. and Neto, A. C. (2021). An application of definitive screening designs (dsds) to a food product optimization and adaptations to jones & nachtsheim methodology for fitting dsd models. *Food Quality and Preference*, 88:104106.

Ferreira, S. C., Bruns, R., Ferreira, H. S., Matos, G. D., David, J., Brandão, G., da Silva, E. P., Portugal, L., Dos Reis, P., Souza, A., et al. (2007). Box-behnken

design: an alternative for the optimization of analytical methods. *Analytica chimica acta*, 597(2):179–186.

Flórez, N., Conde, E., and Domínguez, H. (2015). Microwave assisted water extraction of plant compounds. *Journal of Chemical Technology & Biotechnology*, 90(4):590–607.

Francik, S., Francik, R., Sadowska, U., Bystrowska, B., Zawislak, A., Knapczyk, A., and Nzeyimana, A. (2020). Identification of phenolic compounds and determination of antioxidant activity in extracts and infusions of salvia leaves. *Materials (Basel)*, 13(24):5811.

Frontuto, D., Carullo, D., Harrison, S., Brunton, N., Ferrari, G., Lyng, J., and Pataro, G. (2019). Optimization of pulsed electric fields-assisted extraction of polyphenols from potato peels using response surface methodology. *Food and Bioprocess Technology*, 12:1708–1720.

Frost, H. M. (1979). *Electromagnetic–ultrasound transducers: Principles, practice, and applications*, volume 14, pages 179–275. Elsevier.

Garcia-Vaquero, M., Ummat, V., Tiwari, B., and Rajauria, G. (2020). Exploring ultrasound, microwave and ultrasound-microwave assisted extraction technologies to increase the extraction of bioactive compounds and antioxidants from brown macroalgae. *Mar Drugs*, 18(3):172.

Georgé, S., Brat, P., Alter, P., and Amiot, M. J. (2005). Rapid determination of polyphenols and vitamin c in plant-derived products. *Journal of Agricultural and food chemistry*, 53(5):1370–1373.

Ghafoor, K., Choi, Y. H., Jeon, J. Y., and Jo, I. H. (2009). Optimization of ultrasound-assisted extraction of phenolic compounds, antioxidants, and anthocyanins from grape (vitis vinifera) seeds. *J Agric Food Chem*, 57(11):4988–94. Ghafoor, Kashif Choi, Yong Hee Jeon, Ju Yeong Jo, In Hee J Agric Food Chem. 2009 Jun 10;57(11):4988-94. doi: 10.1021/jf9001439.

Ghitescu, R.-E., Curteanu, S., Mihailescu, C., Volf, I., Leon, F., Gilca, A. I., and Popa, V. I. (2017). Support vector machine combined with genetic algorithm for optimization of microwave-assisted extraction of polyphenols from spruce wood bark. *Cellulose Chem Technol*, 51(3-4):203–213.

Ghorbani, A. and Esmaeilizadeh, M. (2017). Pharmacological properties of salvia officinalis and its components. *J Tradit Complement Med*, 7(4):433–440. Ghorbani, Ahmad Esmaeilizadeh, Mahdi Netherlands J Tradit Complement Med.

2017 Jan 13;7(4):433-440. doi: 10.1016/j.jtcme.2016.12.014. eCollection 2017 Oct.

Glisic, S. B., Ristic, M., and Skala, D. U. (2011). The combined extraction of sage (salvia officinalis l.): ultrasound followed by supercritical co2 extraction. *Ultrason Sonochem*, 18(1):318–26. Glisic, Sandra B Ristic, Mihajlo Skala, Dejan U Netherlands Ultrason Sonochem. 2011 Jan;18(1):318-26. doi: 10.1016/j.ultsonch.2010.06.011. Epub 2010 Jul 1.

Goos, P. (2012). *The optimal design of blocked and split-plot experiments*, volume 164. Springer Science & Business Media.

Goos, P. and Jones, B. (2011). *Optimal design of experiments: a case study approach*. John Wiley & Sons.

Grdiša, M., Jug-Dujaković, M., Lončarić, M., Carović-Stanko, K., Ninčević, T., Liber, Z., Radosavljević, I., and Šatović, Z. (2015). Dalmatian sage (salvia officinalis l.): A review of biochemical contents, medical properties and genetic diversity. *Agriculturae Conspectus Scientificus*, 80(2):69–78.

Griffin, D. R. and Galambos, R. (1941). The sensory basis of obstacle avoidance by flying bats. *Journal of Experimental Zoology*, 86(3):481–506.

Gurib-Fakim, A. (2006). Medicinal plants: traditions of yesterday and drugs of tomorrow. *Mol Aspects Med*, 27(1):1–93.

Hadidi, M., Ibarz, A., and Pagan, J. (2020). Optimisation and kinetic study of the ultrasonic-assisted extraction of total saponins from alfalfa (medicago sativa) and its bioaccessibility using the response surface methodology. *Food chemistry*, 309:125786.

Hamadi, F., Boudif, K., Gougam, H., Djouab, A., Allane, T., Benmounah, A., and Benamara, S. (2014). Caractérisation d'une préparation semi-solide traditionnelle antibrûlure. *Phytothérapie*, 12(3):149–155.

Hamidpour, M., Hamidpour, R., Hamidpour, S., and Shahlari, M. (2014). Chemistry, pharmacology, and medicinal property of sage (salvia) to prevent and cure illnesses such as obesity, diabetes, depression, dementia, lupus, autism, heart disease, and cancer. *J Tradit Complement Med*, 4(2):82–8. Hamidpour, Mohsen Hamidpour, Rafie Hamidpour, Soheila Shahlari, Mina Netherlands J Tradit Complement Med. 2014 Apr;4(2):82-8. doi: 10.4103/2225-4110.130373.

He, B., Zhang, L. L., Yue, X. Y., Liang, J., Jiang, J., Gao, X. L., and Yue, P. X. (2016). Optimization of ultrasound-assisted extraction of phenolic compounds and anthocyanins from blueberry (vaccinium ashei) wine pomace. *Food Chem*,

204:70–76. He, Bo Zhang, Ling-Li Yue, Xue-Yang Liang, Jin Jiang, Jun Gao, Xue-Ling Yue, Peng-Xiang England Food Chem. 2016 Aug 1;204:70-76. doi: 10.1016/j.foodchem.2016.02.094. Epub 2016 Feb 15.

Heleno, S. A., Martins, A., Queiroz, M. J., and Ferreira, I. C. (2015). Bioactivity of phenolic acids: metabolites versus parent compounds: a review. *Food Chem*, 173:501–13. Heleno, Sandrina A Martins, Anabela Queiroz, Maria Joao R P Ferreira, Isabel C F R England Food Chem. 2015 Apr 15;173:501-13. doi: 10.1016/j.foodchem.2014.10.057. Epub 2014 Oct 19.

Hentabli, M., Belhadj, A.-E., Benimam, H., Dahmoune, F., and Keskes, S. (2021). Vacuum drying of the terbinafine hcl powder: A kinetics study and mathematical modeling. *Powder Technology*, 383:220–232.

herbarium of Gérard de Belair (GdB), T. (2018-08-31). Asteraceae : Carthamus.

Hiai, S., Oura, H., and Nakajima, T. (1976). Color reaction of some sapogenins and saponins with vanillin and sulfur1c acid. *Planta Medica*, 29(02):116–122.

Higuchi, M. (2014). *Chapter 15 - Antioxidant Properties of Wheat Bran against Oxidative Stress*, pages 181–199. Academic Press, San Diego.

Hossain, M. B., Brunton, N. P., Patras, A., Tiwari, B., O'Donnell, C. P., Martin-Diana, A. B., and Barry-Ryan, C. (2012). Optimization of ultrasound assisted extraction of antioxidant compounds from marjoram (origanum majorana l.) using response surface methodology. *Ultrason Sonochem*, 19(3):582–90. Hossain, Mohammad B Brunton, Nigel P Patras, Ankit Tiwari, Brijesh O'Donnell, C P Martin-Diana, Ana B Barry-Ryan, Catherine Netherlands Ultrason Sonochem. 2012 May;19(3):582-90. doi: 10.1016/j.ultsonch.2011.11.001. Epub 2011 Nov 23.

Hossain, M. B., Rai, D. K., Brunton, N. P., Martin-Diana, A. B., and Barry-Ryan, C. (2010). Characterization of phenolic composition in lamiaceae spices by lc-esi-ms/ms. *J Agric Food Chem*, 58(19):10576–81. Hossain, Mohammad B Rai, Dilip K Brunton, Nigel P Martin-Diana, Ana B Barry-Ryan, Catherine J Agric Food Chem. 2010 Oct 13;58(19):10576-81. doi: 10.1021/jf102042g.

Hua, S. and Sun, Z. (2001). Support vector machine approach for protein subcellular localization prediction. *Bioinformatics*, 17(8):721–728.

Ibrahim, R. M., Elmasry, G. F., Refaey, R. H., and El-Shiekh, R. A. (2022). Lepidium meyenii (maca) roots: Uplc-hrms, molecular docking, and molecular dynamics. *ACS Omega*, 7(20):17339–17357. Ibrahim, Rana M Elmasry, Ghada F Refaey, Rana H El-Shiekh, Riham A ACS Omega. 2022 May 11;7(20):17339-17357. doi: 10.1021/acsomega.2c01342. eCollection 2022 May 24.

Institute, S. (2013). *JMP 11 Design of Experiments Guide*. SAS Institute.

Irakli, M., Chatzopoulou, P., and Ekateriniadou, L. (2018). Optimization of ultrasound-assisted extraction of phenolic compounds: Oleuropein, phenolic acids, phenolic alcohols and flavonoids from olive leaves and evaluation of its antioxidant activities. *Industrial Crops and Products*, 124:382–388.

Ismail, B. B., Guo, M., Pu, Y., Wang, W., Ye, X., and Liu, D. (2019). Valorisation of baobab (adansonia digitata) seeds by ultrasound assisted extraction of polyphenolics. optimisation and comparison with conventional methods. *Ultrason Sonochem*, 52:257–267. Ismail, Balarabe B Guo, Mingming Pu, Yunfeng Wang, Wenjun Ye, Xingqian Liu, Donghong Netherlands Ultrason Sonochem. 2019 Apr;52:257-267. doi: 10.1016/j.ultsonch.2018.11.023. Epub 2018 Nov 26.

Iuvone, T., De Filippis, D., Esposito, G., D'Amico, A., and Izzo, A. A. (2006). The spice sage and its active ingredient rosmarinic acid protect pc12 cells from amyloid-beta peptide-induced neurotoxicity. *J Pharmacol Exp Ther*, 317(3):1143–9. Iuvone, Teresa De Filippis, Daniele Esposito, Giuseppe D'Amico, Alessandra Izzo, Angelo A J Pharmacol Exp Ther. 2006 Jun;317(3):1143-9. doi: 10.1124/jpet.105.099317. Epub 2006 Feb 22.

Jafarzadeh, A., Pal, M., Servati, M., FazeliFard, M., and Ghorbani, M. (2016). Comparative analysis of support vector machine and artificial neural network models for soil cation exchange capacity prediction. *International journal of environmental science and technology*, 13(1):87–96.

Jakovljevic, M., Jokic, S., Molnar, M., Jasic, M., Babic, J., Jukic, H., and Banjari, I. (2019). Bioactive profile of various salvia officinalis l. preparations. *Plants (Basel)*, 8(3):55.

Jakovljević, M., Jokić, S., Molnar, M., and Jerković, I. (2021). Application of deep eutectic solvents for the extraction of carnosic acid and carnosol from sage (salvia officinalis l.) with response surface methodology optimization. *Plants*, 10(1):80.

Jang, S., Lee, A. Y., Lee, A. R., Choi, G., and Kim, H. K. (2017). Optimization of ultrasound-assisted extraction of glycyrrhizic acid from licorice using response surface methodology. *Integrative medicine research*, 6(4):388–394.

Jedinák, A., Mučková, M., Košt'álová, D., Maliar, T., and Mašterová, I. (2006). Antiprotease and antimetastatic activity of ursolic acid isolated from salvia officinalis. *Zeitschrift für Naturforschung C*, 61(11-12):777–782.

Jones, B., Allen-Moyer, K., and Goos, P. (2020). A-optimal versus d-optimal design of screening experiments. *Journal of Quality Technology*, 53(4):369–382.

Jones, B. and Nachtsheim, C. J. (2011). A class of three-level designs for definitive screening in the presence of second-order effects. *Journal of Quality Technology*, 43(1):1–15.

Josephen, W. F., Warnars, H. L. H. S., Abdurrachman, E., Assiroj, P., Kistijantoro, A. I., Doucet, A., et al. (2021). Dragonfly algorithm in 2020. *Commun. Math. Biol. Neurosci.*, 2021:Article–ID.

Kaderides, K., Papaoikonomou, L., Serafim, M., and Goula, A. M. (2019). Microwave-assisted extraction of phenolics from pomegranate peels: Optimization, kinetics, and comparison with ultrasounds extraction. *Chemical Engineering and Processing - Process Intensification*, 137:1–11.

Kane, D., Grassi, W., Sturrock, R., and Balint, P. V. (2004). A brief history of musculoskeletal ultrasound: 'from bats and ships to babies and hips'. *Rheumatology (Oxford)*, 43(7):931–3. Kane, D Grassi, W Sturrock, R Balint, P V England Oxford, England Rheumatology (Oxford). 2004 Jul;43(7):931-3. doi: 10.1093/rheumatology/keh004.

Kaproth-Joslin, K. A., Nicola, R., and Dogra, V. S. (2015). The history of us: from bats and boats to the bedside and beyond: Rsna centennial article. *Radiographics*, 35(3):960–970.

Karami, Z., Emam-Djomeh, Z., Mirzaee, H. A., Khomeiri, M., Mahoonak, A. S., and Aydani, E. (2015). Optimization of microwave assisted extraction (mae) and soxhlet extraction of phenolic compound from licorice root. *J Food Sci Technol*, 52(6):3242–53. Karami, Zohreh Emam-Djomeh, Zahra Mirzaee, Habib Allah Khomeiri, Morteza Mahoonak, Alireza Sadeghi Aydani, Emad India J Food Sci Technol. 2015 Jun;52(6):3242-53. doi: 10.1007/s13197-014-1384-9. Epub 2014 Apr 30.

Karima, S., Farida, S., and Mihoub, Z. M. (2013). Antimicrobial activity of an algerian medicinal plant: Carthamus caeruleus l. *Pharmacognosy Communications*, 3(4):71.

Karimzadeh, S. and Farahpour, M. R. (2017). Topical application of salvia officinalis hydroethanolic leaf extract improves wound healing process.

Kerkoub, N., Panda, S. K., Yang, M. R., Lu, J. G., Jiang, Z. H., Nasri, H., and Luyten, W. (2018). Bioassay-guided isolation of anti-candida biofilm compounds from methanol extracts of the aerial parts of salvia officinalis (annaba, algeria).

Front Pharmacol, 9:1418. Kerkoub, Neila Panda, Sujogya Kumar Yang, Ming-Rong Lu, Jing-Guang Jiang, Zhi-Hong Nasri, Hichem Luyten, Walter Switzerland Front Pharmacol. 2018 Dec 10;9:1418. doi: 10.3389/fphar.2018.01418. eCollection 2018.

Keshavarz, M., Mostafaie, A., Mansouri, K., Bidmeshkipour, A., Motlagh, H. R., and Parvaneh, S. (2010). In vitro and ex vivo antiangiogenic activity of salvia officinalis. *Phytother Res*, 24(10):1526–31. Keshavarz, Maryam Mostafaie, Ali Mansouri, Kamran Bidmeshkipour, Ali Motlagh, Hamid Reza Mohammadi Parvaneh, Shahram England Phytother Res. 2010 Oct;24(10):1526-31. doi: 10.1002/ptr.3168.

Khalaf, N. A., Shakya, A. K., Al-Othman, A., El-Agbar, Z., and Farah, H. (2008). Antioxidant activity of some common plants. *Turkish Journal of Biology*, 32(1):51–55.

Khan, M. K., Abert-Vian, M., Fabiano-Tixier, A.-S., Dangles, O., and Chemat, F. (2010). Ultrasound-assisted extraction of polyphenols (flavanone glycosides) from orange (citrus sinensis l.) peel. *Food Chemistry*, 119(2):851–858.

Kiselova-Kaneva, Y., Galunska, B., Nikolova, M., Dincheva, I., and Badjakov, I. (2022). High resolution lc-ms/ms characterization of polyphenolic composition and evaluation of antioxidant activity of sambucus ebulus fruit tea traditionally used in bulgaria as a functional food. *Food Chem*, 367:130759.

Koocheki, A., Taherian, A. R., Razavi, S. M., and Bostan, A. (2009). Response surface methodology for optimization of extraction yield, viscosity, hue and emulsion stability of mucilage extracted from lepidium perfoliatum seeds. *Food Hydrocolloids*, 23(8):2369–2379.

Kubrakova, I. V. and Toropchenova, E. S. (2008). Microwave heating for enhancing efficiency of analytical operations (review). *Inorganic Materials*, 44(14):1509–1519.

Kumar, K., Srivastav, S., and Sharanagat, V. S. (2021). Ultrasound assisted extraction (uae) of bioactive compounds from fruit and vegetable processing by-products: A review. *Ultrason Sonochem*, 70:105325. Kumar, Kshitiz Srivastav, Shivmurti Sharanagat, Vijay Singh Netherlands Ultrason Sonochem. 2021 Jan;70:105325. doi: 10.1016/j.ultsonch.2020.105325. Epub 2020 Sep 1.

Kusznierewicz, B., Mróz, M., Koss-Mikołajczyk, I., and Namieśnik, J. (2021). Comparative evaluation of different methods for determining phytochemicals and antioxidant activity in products containing betalains – verification of beetroot samples. *Food Chem*, 362:130132.

Kwon, J.-H., Bélanger, J. M., and Paré, J. J. (2003). Optimization of microwave-assisted extraction (map) for ginseng components by response surface methodology. *J Agric Food Chem*, 51(7):1807–1810.

Laidi, M., El Hadj, A. A., Si-Moussa, C., Benkortebi, O., Hentabli, M., and Hanini, S. (2021). Cmc of diverse gemini surfactants modeling using a hybrid approach combining svr-da: Original scientific paper. *Chemical Industry & Chemical Engineering Quarterly*, 27(3):299–312.

Lavilla, I. and Bendicho, C. (2017). Fundamentals of ultrasound-assisted extraction. In *Water extraction of bioactive compounds*, pages 291–316. Elsevier.

Li, H., Yao, W., Liu, Q., Xu, J., Bao, B., Shan, M., Cao, Y., Cheng, F., Ding, A., and Zhang, L. (2017). Application of uhplc-esi-q-tof-ms to identify multiple constituents in processed products of the herbal medicine ligustri lucidi fructus. *Molecules*, 22(5):689.

Liu, H., Jiao, Z., Liu, J., Zhang, C., Zheng, X., Lai, S., Chen, F., and Yang, H. (2013). Optimization of supercritical fluid extraction of phenolics from date seeds and characterization of its antioxidant activity. *Food Analytical Methods*, 6:781–788.

Liu, L.-l., Hu, X.-p., Lou, L.-j., Zhang, B., and Nie, J.-q. (2010). Study on microwave-assisted extract and antioxidant activity of ginger flavonoids. In *2010 4th International Conference on Bioinformatics and Biomedical Engineering*, pages 1–4.

Llompart, M., Celeiro, M., and Dagnac, T. (2019). Microwave-assisted extraction of pharmaceuticals, personal care products and industrial contaminants in the environment. *TrAC Trends in Analytical Chemistry*, 116:136–150.

Lopez Gonzalez, G. (1989). Acerca de la clasificación natural del género carthamus l., s.l. *Anales del Jardín Botánico de Madrid (1979)*, (1):11–34.

Lopresti, A. L. (2017). Salvia (sage): A review of its potential cognitive-enhancing and protective effects. *Drugs R D*, 17(1):53–64. Lopresti, Adrian L New Zealand Drugs R D. 2017 Mar;17(1):53-64. doi: 10.1007/s40268-016-0157-5.

Lovrić, V., Putnik, P., Bursać Kovačević, D., Jukić, M., and Dragović-Uzelac, V. (2017). Effect of microwave-assisted extraction on the phenolic compounds and antioxidant capacity of blackthorn flowers. *Food technology and biotechnology*, 55(2):243–250.

Luo, M., Zhou, D. D., Shang, A., Gan, R. Y., and Li, H. B. (2021). Influences of

microwave-assisted extraction parameters on antioxidant activity of the extract from akebia trifoliata peels. *Foods*, 10(6):1432.

Maleš, I., Dragović-Uzelac, V., Jerković, I., Zorić, Z., Pedisić, S., Repajić, M., Garofulić, I. E., and Dobrinčić, A. (2022). Non-volatile and volatile bioactives of salvia officinalis l., thymus serpyllum l. and laurus nobilis l. extracts with potential use in the development of functional beverages. *Antioxidants*, 11(6):1140.

Manbachi, A. and Cobbold, R. S. (2011). Development and application of piezoelectric materials for ultrasound generation and detection. *Ultrasound*, 19(4):187–196.

Mandal, V. and Mandal, S. C. (2010). Design and performance evaluation of a microwave based low carbon yielding extraction technique for naturally occurring bioactive triterpenoid: Oleanolic acid. *Biochemical Engineering Journal*, 50(1-2):63–70.

Mandal, V., Mohan, Y., and Hemalatha, S. (2007). Microwave assisted extraction—an innovative and promising extraction tool for medicinal plant research. *Pharmacognosy reviews*, 1(1):7–18.

Martin, A. and Navarrete, A. (2018). Microwave-assisted process intensification techniques. *Current Opinion in Green and Sustainable Chemistry*, 11:70–75.

Mason, T. J. and Peters, D. (2002). *Practical sonochemistry: Power ultrasound uses and applications*. Woodhead Publishing.

Mayer, B., Baggio, C. H., Freitas, C. S., dos Santos, A. C., Twardowschy, A., Horst, H., Pizzolatti, M. G., Micke, G. A., Heller, M., dos Santos, E. P., Otuki, M. F., and Marques, M. C. (2009). Gastroprotective constituents of salvia officinalis l. *Fitoterapia*, 80(7):421–6. Mayer, Barbara Baggio, Cristiane Hatsuko Freitas, Cristina Setim dos Santos, Ana Cristina Twardowschy, Andre Horst, Heros Pizzolatti, Moacir Geraldo Micke, Gustavo Amadeu Heller, Melina dos Santos, Elide Pereira Otuki, Michel Fleith Marques, Maria Consuelo Andrade Netherlands Fitoterapia. 2009 Oct;80(7):421-6. doi: 10.1016/j.fitote.2009.05.015. Epub 2009 May 28.

McDonald, A. and Edwards, S. (1807). *A Complete Dictionary of Practical Gardening: Comprehending All the Modern Improvements in the Art: Whether in the Raising of the Various Esculent Vegetables Or in the Forcing and Managing of Different Sorts of Fruits and Plants, and that of Laying Out, Ornamenting and Planting Gardens and Pleasure Grounds: with Correct Engravings of the Necessary Apparatus in Buildings and Other Contrivances, as Well as of*

the More Rare and Curious Plants Cultivated for Ornament Or Variety, from Original Drawings by Sydenham Edwards. George Kearsley.

McPherson, M. A., Good, A. G., Keith C. Topinka, A., and Hall, L. M. (2004). Theoretical hybridization potential of transgenic safflower (carthamus tinctorius l.) with weedy relatives in the new world. *Canadian Journal of Plant Science*, 84(3):923–934.

Meddour, R. and Meddour-Sahar, O. (2015). Medicinal plants and their traditional uses in kabylia (tizi ouzou, algeria). *Arabian Journal of Medicinal and Aromatic Plants*, 1(2):137–151.

Medina-Torres, N., Ayora-Talavera, T., Espinosa-Andrews, H., Sánchez-Contreras, A., and Pacheco, N. (2017). Ultrasound assisted extraction for the recovery of phenolic compounds from vegetable sources. *Agronomy*, 7(3):47.

Mena, P., Cirlini, M., Tassotti, M., Herrlinger, K. A., Dall'Asta, C., and Del Rio, D. (2016). Phytochemical profiling of flavonoids, phenolic acids, terpenoids, and volatile fraction of a rosemary (rosmarinus officinalis l.) extract. *Molecules*, 21(11):1576.

Mendes, F. S. F., Garcia, L. M., Moraes, T. D. S., Casemiro, L. A., Alcantara, C. B., Ambrosio, S. R., Veneziani, R. C. S., Miranda, M. L. D., and Martins, C. H. G. (2020). Antibacterial activity of salvia officinalis l. against periodontopathogens: An in vitro study. *Anaerobe*, 63:102194. Mendes, Filipe Santos Ferreira Garcia, Leticia Matanovich Moraes, Thais da Silva Casemiro, Luciana Assirati Alcantara, Clauber Barbosa de Ambrosio, Sergio Ricardo Veneziani, Rodrigo Cassio Sola Miranda, Mayker Lazaro Dantas Martins, Carlos Henrique Gomes England Anaerobe. 2020 Jun;63:102194. doi: 10.1016/j.anaerobe.2020.102194. Epub 2020 Mar 20.

Meraihi, Y., Ramdane-Cherif, A., Acheli, D., and Mahseur, M. (2020). Dragonfly algorithm: a comprehensive review and applications. *Neural Computing and Applications*, 32(21):16625–16646.

Mesellem, Y., Hadj, A. A. E., Laidi, M., Hanini, S., and Hentabli, M. (2021). Computational intelligence techniques for modeling of dynamic adsorption of organic pollutants on activated carbon. *Neural Computing and Applications*, 33:12493–12512.

Mesllem, Y., Hentabli, M., Hanini, S., Laidi, M., and Abdallah, A. E. H. (2021). Artificial neural network modelling of multi-system dynamic adsorption of organic pollutants on activated carbon. *Kemija u industriji*, 70(1-2):1–12.

Meyer, R. K. and Nachtsheim, C. J. (1995). The coordinate-exchange algorithm for constructing exact optimal experimental designs. *Technometrics*, 37(1):60–69.

Mirjalili, S. (2015). Dragonfly algorithm: a new meta-heuristic optimization technique for solving single-objective, discrete, and multi-objective problems. *Neural Computing and Applications*, 27(4):1053–1073.

Mocan, A., Babota, M., Pop, A., Fizesan, I., Diuzheva, A., Locatelli, M., Carradori, S., Campestre, C., Menghini, L., Sisea, C. R., Sokovic, M., Zengin, G., Paltinean, R., Badarau, S., DC, C. V., and Crisan, G. (2020). Chemical constituents and biologic activities of sage species: A comparison between salvia officinalis l., s. glutinosa l. and s. transsylvanica (schur ex griseb. & schenk) schur. *Antioxidants (Basel)*, 9(6):480.

Moreira, M. R., Souza, A. B., Moreira, M. A., Bianchi, T. C., Carneiro, L. J., Estrela, F. T., dos Santos, R. A., Januário, A. H., Martins, C. H. G., Ambrosio, S. R., and Veneziani, R. C. S. (2013). Rp-hplc analysis of manool-rich salvia officinalis extract and its antimicrobial activity against bacteria associated with dental caries. *Revista Brasileira de Farmacognosia*, 23(6):870–876.

Mould, R. F. (2007). Pierre curie, 1859–1906. *Current oncology*, 14(2):74–82.

Muniz-Marquez, D. B., Martinez-Avila, G. C., Wong-Paz, J. E., Belmares-Cerda, R., Rodriguez-Herrera, R., and Aguilar, C. N. (2013). Ultrasound-assisted extraction of phenolic compounds from laurus nobilis l. and their antioxidant activity. *Ultrason Sonochem*, 20(5):1149–54. Muniz-Marquez, Diana B Martinez-Avila, Guillermo C Wong-Paz, Jorge E Belmares-Cerda, Ruth Rodriguez-Herrera, Raul Aguilar, Cristobal N Netherlands Ultrason Sonochem. 2013 Sep;20(5):1149-54. doi: 10.1016/j.ultsonch.2013.02.008. Epub 2013 Mar 7.

Nana, O., Momeni, J., Boyom, F. F., Njintang, N. Y., and Ngassoum, M. B. (2021). Microwave-assisted extraction as an advanced technique for optimisation of limonoid yields and antioxidant potential from trichilia roka (meliaceae). *Current Research in Green and Sustainable Chemistry*, 4:100147.

Nayak, B., Dahmoune, F., Moussi, K., Remini, H., Dairi, S., Aoun, O., and Khodir, M. (2015). Comparison of microwave, ultrasound and accelerated-assisted solvent extraction for recovery of polyphenols from citrus sinensis peels. *Food Chem*, 187:507–516.

Neppiras, E. A. (1980). Acoustic cavitation. *Physics reports*, 61(3):159–251.

Ngamkhae, N., Monthakantirat, O., Chulikhit, Y., Boonyarat, C., Maneenet, J.,

Khamphukdee, C., Kwankhao, P., Pitiporn, S., and Daodee, S. (2022). Optimization of extraction method for kleeb bua daeng formula and comparison between ultrasound-assisted and microwave-assisted extraction. *Journal of Applied Research on Medicinal and Aromatic Plants*, 28:100369.

Nikmehr, B., Ghaznavi, H., Rahbar, A., Sadr, S., and Mehrzadi, S. (2014). In vitro anti-leishmanial activity of methanolic extracts of calendula officinalis flowers, datura stramonium seeds, and salvia officinalis leaves. *Chinese Journal of Natural Medicines*, 12(6):423–427.

Nowacka, M. and Dadan, M. (2022). *Ultrasound-Assisted Drying of Food*, pages 93–112. Springer US, New York, NY.

Obermiller, D. J. (2000). Multiple response optimization using jmp. *The Dow chemical company, Midland, MI*.

Oyaizu, M. (1986). Studies on products of browning reaction antioxidative activities of products of browning reaction prepared from glucosamine. *The Japanese journal of nutrition and dietetics*, 44(6):307–315.

Pachura, N., Zimmer, A., Grzywna, K., Figiel, A., Szumny, A., and Lyczko, J. (2022). Chemical investigation on salvia officinalis l. affected by multiple drying techniques - the comprehensive analytical approach (hs-spme, gc-ms, lc-ms/ms, gc-o and nmr). *Food Chem*, 397:133802. Pachura, Natalia Zimmer, Aleksandra Grzywna, Kacper Figiel, Adam Szumny, Antoni Lyczko, Jacek England Food Chem. 2022 Dec 15;397:133802. doi: 10.1016/j.foodchem.2022.133802. Epub 2022 Jul 26.

Palma, A., Diaz, M. J., Ruiz-Montoya, M., Morales, E., and Giraldez, I. (2021). Ultrasound extraction optimization for bioactive molecules from eucalyptus globulus leaves through antioxidant activity. *Ultrason Sonochem*, 76:105654. Palma, Alberto Diaz, Manuel Jesus Ruiz-Montoya, Mercedes Morales, Emilio Giraldez, Inmaculada Netherlands Ultrason Sonochem. 2021 Aug;76:105654. doi: 10.1016/j.ultsonch.2021.105654. Epub 2021 Jun 25.

Panche, A. N., Diwan, A. D., and Chandra, S. R. (2016). Flavonoids: an overview. *J Nutr Sci*, 5:e47. Panche, A N Diwan, A D Chandra, S R England J Nutr Sci. 2016 Dec 29;5:e47. doi: 10.1017/jns.2016.41. eCollection 2016.

Pandey, A., Belwal, T., Sekar, K. C., Bhatt, I. D., and Rawal, R. S. (2018). Optimization of ultrasonic-assisted extraction (uae) of phenolics and antioxidant compounds from rhizomes of rheum moorcroftianum using response surface methodology (rsm). *Industrial Crops and Products*, 119:218–225.

Paolo, D. and Cravotto, G. (2012). Plant composition comprising the phytocomplex of a plant species and process for preparation. *EP 2520182A1*, 3.

Passero, L. F. D., Bonfim-Melo, A., Corbett, C. E. P., Laurenti, M. D., Toyama, M. H., de Toyama, D. O., Romoff, P., Fávero, O. A., dos Grecco, S. S., and Zalewsky, C. A. (2011). Anti-leishmanial effects of purified compounds from aerial parts of baccharis uncinella c. dc.(asteraceae). *Parasitology research*, 108(3):529–536.

Patil, B. S., Jayaprakasha, G. K., Chidambara Murthy, K. N., and Vikram, A. (2009). Bioactive compounds: historical perspectives, opportunities, and challenges. *J Agric Food Chem*, 57(18):8142–60.

Pavic, V., Jakovljevic, M., Molnar, M., and Jokic, S. (2019). Extraction of carnosic acid and carnosol from sage (salvia officinalis l.) leaves by supercritical fluid extraction and their antioxidant and antibacterial activity. *Plants (Basel)*, 8(1):16.

Pereira, O. R., Catarino, M. D., Afonso, A. F., Silva, A. M. S., and Cardoso, S. M. (2018). Salvia elegans, salvia greggii and salvia officinalis decoctions: Antioxidant activities and inhibition of carbohydrate and lipid metabolic enzymes. *Molecules*, 23(12):3169.

Pérez-Chabela, M. L. and Hernández-Alcántara, A. M. (2018). Agroindustrial coproducts as sources of novel functional ingredients. In *Food processing for increased quality and consumption*, pages 219–250.

Pham, H. N. T., Vuong, Q. V., Bowyer, M. C., and Scarlett, C. J. (2017). Optimization of ultrasound-assisted extraction of helicteres hirsuta lour. for enhanced total phenolic compound and antioxidant yield. *Journal of Applied Research on Medicinal and Aromatic Plants*, 7:113–123.

Pietta, P., Simonetti, P., and Mauri, P. (1998). Antioxidant activity of selected medicinal plants. *Journal of Agricultural and Food Chemistry*, 46(11):4487–4490.

Pisner, D. A. and Schnyer, D. M. (2020). Chapter 6 - support vector machine. In Mechelli, A. and Vieira, S., editors, *Machine Learning*, pages 101–121. Academic Press.

Pomel, A. (1874). *Nouveaux matériaux pour la Flore Atlantique*. Savy.

Prieto, P., Pineda, M., and Aguilar, M. (1999). Spectrophotometric quantitation of antioxidant capacity through the formation of a phosphomolybdenum complex: Specific application to the determination of vitamin e. *Analytical Biochemistry*, 269(2):337–341.

Prothmann, J., Sun, M., Spegel, P., Sandahl, M., and Turner, C. (2017). Ultra-high-performance supercritical fluid chromatography with quadrupole-time-of-flight mass spectrometry (uhpsfc/qtof-ms) for analysis of lignin-derived monomeric compounds in processed lignin samples. *Anal Bioanal Chem*, 409(30):7049–7061. Prothmann, Jens Sun, Mingzhe Spegel, Peter Sandahl, Margareta Turner, Charlotta RBP 14-0052/The Swedish Foundation for Strategic Research (SSF)/ 2013-971/the Swedish Research Council Formas/ 2016-00604/the Swedish Research Council Formas/ Germany Anal Bioanal Chem. 2017 Dec;409(30):7049-7061. doi: 10.1007/s00216-017-0663-5. Epub 2017 Oct 13.

Putnik, P., Kovačević, D. B., Penić, M., Fegeš, M., and Dragović-Uzelac, V. (2016). Microwave-assisted extraction (mae) of dalmatian sage leaves for the optimal yield of polyphenols: Hplc-dad identification and quantification. *Food Analytical Methods*, 9(8):2385–2394.

Quezel, P., Santa, S., and Schotter, O. (1962). Nouvelle flore de l'algerie et des regions desertiques meridionales-v. 1-2.

Radulescu, V., Chiliment, S., and Oprea, E. (2004). Capillary gas chromatography-mass spectrometry of volatile and semi-volatile compounds of salvia officinalis. *J Chromatogr A*, 1027(1-2):121–6. Radulescu, Valeria Chiliment, Silvia Oprea, Eliza Netherlands J Chromatogr A. 2004 Feb 20;1027(1-2):121-6. doi: 10.1016/j.chroma.2003.11.046.

Rahmani Samani, M., D'Urso, G., Montoro, P., Ghasemi Pirbalouti, A., and Piacente, S. (2021). Effects of bio-fertilizers on the production of specialized metabolites in salvia officinalis l. leaves: An analytical approach based on lc-esi/ltq-orbitrap/ms and multivariate data analysis. *J Pharm Biomed Anal*, 197:113951. Rahmani Samani, Marzieh D'Urso, Gilda Montoro, Paola Ghasemi Pirbalouti, Abdollah Piacente, Sonia England J Pharm Biomed Anal. 2021 Apr 15;197:113951. doi: 10.1016/j.jpba.2021.113951. Epub 2021 Feb 3.

Reguigui, A., Ott, P. G., Darcsi, A., Bakonyi, J., Romdhane, M., and Moricz, A. M. (2023). Nine-dimensional bioprofiles of tunisian sages (salvia officinalis, s. aegyptiaca and s. verbenaca) by high-performance thin-layer chromatography - effect-directed analyses. *J Chromatogr A*, 1688:463704. Reguigui, Amira Ott, Peter G Darcsi, Andras Bakonyi, Jozsef Romdhane, Mehrez Moricz, Agnes M Netherlands J Chromatogr A. 2023 Jan 11;1688:463704. doi: 10.1016/j.chroma.2022.463704. Epub 2022 Dec 7.

Rodrigues, S., Pinto, G. A., and Fernandes, F. A. (2008). Optimization of ul-

trasound extraction of phenolic compounds from coconut (cocos nucifera) shell powder by response surface methodology. *Ultrasonics Sonochemistry*, 15(1):95–100.

Rodriguez De Luna, S. L., Ramirez-Garza, R. E., and Serna Saldivar, S. O. (2020). Environmentally friendly methods for flavonoid extraction from plant material: Impact of their operating conditions on yield and antioxidant properties. *ScientificWorldJournal*, 2020:6792069.

Rodríguez, M., Jones, B., Borror, C. M., and Montgomery, D. C. (2017). Generating and assessing exactg-optimal designs. *Journal of Quality Technology*, 42(1):3–20.

Rojas, J. and Buitrago, A. (2019). Antioxidant activity of phenolic compounds biosynthesized by plants and its relationship with prevention of neurodegenerative diseases. In *Bioactive Compounds*, pages 3–31. Elsevier.

Routray, W. and Orsat, V. (2011). Microwave-assisted extraction of flavonoids: A review. *Food and Bioprocess Technology*, 5(2):409–424.

Rutkowska, M., Namieśnik, J., and Konieczka, P. (2017). pages 301–324.

Sahin, S. and Samli, R. (2013). Optimization of olive leaf extract obtained by ultrasound-assisted extraction with response surface methodology. *Ultrason Sonochem*, 20(1):595–602. Sahin, Selin Samli, Ruya Netherlands Ultrason Sonochem. 2013 Jan;20(1):595-602. doi: 10.1016/j.ultsonch.2012.07.029. Epub 2012 Aug 11.

Saparbekova, A. A., Kantureyeva, G. O., Kudasova, D. E., Konarbayeva, Z. K., and Latif, A. S. (2023). Potential of phenolic compounds from pomegranate (punica granatum l.) by-product with significant antioxidant and therapeutic effects: A narrative review. *Saudi J Biol Sci*, 30(2):103553. Saparbekova, A A Kantureyeva, G O Kudasova, D E Konarbayeva, Z K Latif, A S Saudi Arabia Saudi J Biol Sci. 2023 Feb;30(2):103553. doi: 10.1016/j.sjbs.2022.103553. Epub 2022 Dec 28.

Sarvin, B., Stekolshchikova, E., Rodin, I., Stavrianidi, A., and Shpigun, O. (2018). Optimization and comparison of different techniques for complete extraction of saponins from t. terrestris. *Journal of Applied Research on Medicinal and Aromatic Plants*, 8:75–82.

Savic, I. M. and Savic Gajic, I. M. (2020). Optimization of ultrasound-assisted extraction of polyphenols from wheatgrass (triticum aestivum l.). *J Food Sci Technol*, 57(8):2809–2818.

Serakta, M., Djerrou, Z., Mansour-Djaalab, H., Kahlouche-Riachi, F., Hamimed, S., Trifa, W., Belkhiri, A., Edikra, N., and Pacha, Y. H. (2013). Antileishmanial activity of some plants growing in algeria: Juglans regia, lawsonia inermis and salvia officinalis. *African Journal of Traditional, Complementary and Alternative Medicines*, 10(3):427–430.

Shah, R., De Jager, L. S., and Begley, T. H. (2012). Simultaneous determination of steviol and steviol glycosides by liquid chromatography-mass spectrometry. *Food Addit Contam Part A Chem Anal Control Expo Risk Assess*, 29(12):1861–71. Shah, Romina De Jager, Lowri S Begley, Timothy H England Food Addit Contam Part A Chem Anal Control Expo Risk Assess. 2012;29(12):1861-71. doi: 10.1080/19440049.2012.725946. Epub 2012 Oct 10.

Shang, A., Luo, M., Gan, R. Y., Xu, X. Y., Xia, Y., Guo, H., Liu, Y., and Li, H. B. (2020). Effects of microwave-assisted extraction conditions on antioxidant capacity of sweet tea (lithocarpus polystachyus rehd.). *Antioxidants (Basel)*, 9(8):678.

Shao, Z. Y., Fu, J. X., Qi, Y. X., Zhao, Q. C., and Li, Z. B. (2013). Optimization of ultrasonic-assisted extraction of total saponins from ophiopholis mirabilis using response surface methodology. *Advanced Materials Research*, 781-784:687–693.

Sharma, Y., Fagan, J., and Schaefer, J. (2019). Ethnobotany, phytochemistry, cultivation and medicinal properties of garden sage (salvia officinalis l.). *Journal of Pharmacognosy and Phytochemistry*, 8(3):3139–3148.

Sharma, Y., Velamuri, R., Fagan, J., Schaefer, J., Streicher, C., and Stimson, J. (2020). Identification and characterization of polyphenols and volatile terpenoid compounds in different extracts of garden sage (salvia officinalis l.). *Pharmacognosy Research*, 12(2):149.

Shrestha, B. L. and Baik, O. D. (2012). Methanol-water extraction of saponins from seeds ofsaponaria vaccaria l.— calibration equation, extraction condition analysis, and modeling. *Separation Science and Technology*, 47(13):1977–1984.

Silva, C. G., Herdeiro, R. S., Mathias, C. J., Panek, A. D., Silveira, C. S., Rodrigues, V. P., Renno, M. N., Falcao, D. Q., Cerqueira, D. M., Minto, A. B., Nogueira, F. L., Quaresma, C. H., Silva, J. F., Menezes, F. S., and Eleutherio, E. C. (2005). Evaluation of antioxidant activity of brazilian plants. *Pharmacol Res*, 52(3):229–33.

Singla, R. K., Dubey, A. K., Garg, A., Sharma, R. K., Fiorino, M., Ameen, S. M., Haddad, M. A., and Al-Hiary, M. (2019). Natural polyphenols: Chemical classification, definition of classes, subcategories, and structures.

J AOAC Int, 102(5):1397–1400. Singla, Rajeev K Dubey, Ashok K Garg, Arun Sharma, Ramesh K Fiorino, Marco Ameen, Sara M Haddad, Moawiya A Al-Hiary, Masnat England J AOAC Int. 2019 Sep 1;102(5):1397-1400. doi: 10.5740/jaoacint.19-0133. Epub 2019 Jun 14.

Skendi, A., Irakli, M., and Chatzopoulou, P. (2017). Analysis of phenolic compounds in greek plants of lamiaceae family by hplc. *Journal of applied research on medicinal and aromatic plants*, 6:62–69.

Soekarno, I., Hadihardaja, I. K., Cahyono, M., et al. (2014). A study of hold-out and k-fold cross validation for accuracy of groundwater modeling in tidal lowland reclamation using extreme learning machine. In *2014 2nd International Conference on Technology, Informatics, Management, Engineering & Environment*, pages 228–233. IEEE.

Song, J., Li, D., Liu, C., and Zhang, Y. (2011). Optimized microwave-assisted extraction of total phenolics (tp) from ipomoea batatas leaves and its antioxidant activity. *Innovative Food Science & Emerging Technologies*, 12(3):282–287.

Su, C. H., Pham, T. T. T., and Cheng, H. H. (2020). Aqueous enzymatic extraction of rosmarinic acid from salvia officinalis: optimisation using response surface methodology. *Phytochem Anal*, 31(5):575–582. Su, Chia-Hung Pham, Thi Thanh Truc Cheng, Hsien-Hao England Phytochem Anal. 2020 Sep;31(5):575-582. doi: 10.1002/pca.2922. Epub 2020 Jan 29.

Suleiman, A., Tight, M., and Quinn, A. (2016). Hybrid neural networks and boosted regression tree models for predicting roadside particulate matter. *Environmental Modeling & Assessment*, 21:731–750.

Sulniute, V., Pukalskas, A., and Venskutonis, P. R. (2017). Phytochemical composition of fractions isolated from ten salvia species by supercritical carbon dioxide and pressurized liquid extraction methods. *Food Chem*, 224:37–47. Sulniute, Vaida Pukalskas, Audrius Venskutonis, Petras Rimantas England Food Chem. 2017 Jun 1;224:37-47. doi: 10.1016/j.foodchem.2016.12.047. Epub 2016 Dec 18.

Suslick, K. S. (1989). The chemical effects of ultrasound. *Scientific American*, 260(2):80–87.

Sánchez-Camargo, A. d. P., Ballesteros-Vivas, D., Buelvas-Puello, L. M., Martinez-Correa, H. A., Parada-Alfonso, F., Cifuentes, A., Ferreira, S. R. S., and Gutiérrez, L.-F. (2021). Microwave-assisted extraction of phenolic compounds with antioxidant and anti-proliferative activities from supercritical co2 pre-extracted mango peel as valorization strategy. *Lwt*, 137:110414.

Taamalli, A., Arraez-Roman, D., Abaza, L., Iswaldi, I., Fernandez-Gutierrez, A., Zarrouk, M., and Segura-Carretero, A. (2015). Lc-ms-based metabolite profiling of methanolic extracts from the medicinal and aromatic species mentha pulegium and origanum majorana. *Phytochem Anal*, 26(5):320–30. Taamalli, Amani Arraez-Roman, David Abaza, Leila Iswaldi, Ihsan Fernandez-Gutierrez, Alberto Zarrouk, Mokhtar Segura-Carretero, Antonio England Phytochem Anal. 2015 Sep-Oct;26(5):320-30. doi: 10.1002/pca.2566. Epub 2015 May 15.

Tabaraki, R. and Nateghi, A. (2011). Optimization of ultrasonic-assisted extraction of natural antioxidants from rice bran using response surface methodology. *Ultrasonics sonochemistry*, 18(6):1279–1286.

Teh, S. S. and Birch, E. J. (2014). Effect of ultrasonic treatment on the polyphenol content and antioxidant capacity of extract from defatted hemp, flax and canola seed cakes. *Ultrason Sonochem*, 21(1):346–53.

Teka, T., Zhang, L., Ge, X., Li, Y., Han, L., and Yan, X. (2022). Stilbenes: Source plants, chemistry, biosynthesis, pharmacology, application and problems related to their clinical application-a comprehensive review. *Phytochemistry*, 197:113128. Teka, Tekleab Zhang, Lele Ge, Xiaoyan Li, Yanjie Han, Lifeng Yan, Xiaohui England Phytochemistry. 2022 May;197:113128. doi: 10.1016/j.phytochem.2022.113128. Epub 2022 Feb 17.

Tekin, K., Akalın, M. K., and Şeker, M. G. (2015). Ultrasound bath-assisted extraction of essential oils from clove using central composite design. *Industrial Crops and Products*, 77:954–960.

Teng, H. and Choi, Y. H. (2013). Optimization of microwave-assisted extraction of bioactive alkaloid compounds from rhizoma coptidis (coptis chinensis franch.). *Food Science and Biotechnology*, 22(5):1–8.

Teo, C. C., Chong, W. P. K., and Ho, Y. S. (2013). Development and application of microwave-assisted extraction technique in biological sample preparation for small molecule analysis. *Metabolomics*, 9(5):1109–1128.

Tian, Y.-q., Zhao, H.-t., Zhang, X.-l., Zhang, W.-t., Liu, X.-c., and Gao, S.-h. (2020). Comparison of different extraction techniques and optimization of the microwave-assisted extraction of saponins from aralia elata (miq.) seem fruits and rachises. *Chemical Papers*, 74(9):3077–3087.

Tiwari, B. K. (2015). Ultrasound: A clean, green extraction technology. *TrAC Trends in Analytical Chemistry*, 71:100–109.

Toubane, A., Rezzoug, S. A., Besombes, C., and Daoud, K. (2017). Optimization of accelerated solvent extraction of carthamus caeruleus l. evaluation of antioxidant and anti-inflammatory activity of extracts. *Industrial Crops and Products*, 97:620–631.

Tuladhar, P., Sasidharan, S., and Saudagar, P. (2021). *17 - Role of phenols and polyphenols in plant defense response to biotic and abiotic stresses*, pages 419–441. Woodhead Publishing.

Uritu, C. M., Mihai, C. T., Stanciu, G. D., Dodi, G., Alexa-Stratulat, T., Luca, A., Leon-Constantin, M. M., Stefanescu, R., Bild, V., Melnic, S., and Tamba, B. I. (2018). Medicinal plants of the family lamiaceae in pain therapy: A review. *Pain Res Manag*, 2018:7801543. Uritu, Cristina M Mihai, Cosmin T Stanciu, Gabriela-Dumitrita Dodi, Gianina Alexa-Stratulat, Teodora Luca, Andrei Leon-Constantin, Maria-Magdalena Stefanescu, Raluca Bild, Veronica Melnic, Silvia Tamba, Bogdan I Pain Res Manag. 2018 May 8;2018:7801543. doi: 10.1155/2018/7801543. eCollection 2018.

Uy, M. and Telford, J. K. (2009). Optimization by design of experiment techniques. In *2009 IEEE Aerospace conference*, pages 1–10. IEEE.

Valachovic, P., Pechova, A., and Mason, T. (2001). Towards the industrial production of medicinal tincture by ultrasound assisted extraction. *Ultrason Sonochem*, 8(2):111–117.

Velamuri, R., Sharma, Y., Fagan, J., and Schaefer, J. (2020). Application of uhplc-esi-qtof-ms in phytochemical profiling of sage (salvia officinalis) and rosemary (rosmarinus officinalis). *Planta Medica International Open*, 07(04):e133–e144.

Velickovic, D. T., Milenovic, D. M., Ristic, M. S., and Veljkovic, V. B. (2006). Kinetics of ultrasonic extraction of extractive substances from garden (salvia officinalis l.) and glutinous (salvia glutinosa l.) sage. *Ultrason Sonochem*, 13(2):150–6. Velickovic, D T Milenovic, D M Ristic, M S Veljkovic, V B Netherlands Ultrason Sonochem. 2006 Feb;13(2):150-6. doi: 10.1016/j.ultsonch.2005.02.002. Epub 2005 Apr 7.

Vilatersana, R., Susanna, A., Garcia-Jacas, N., and Garnatje, T. (2000). Generic delimitation and phylogeny of thecarduncellus-carthamus complex (asteraceae) based on its sequences. *Plant Systematics and Evolution*, 221(1-2):89–105.

Vinatoru, M. (2001). An overview of the ultrasonically assisted extraction of bioactive principles from herbs. *Ultrason Sonochem*, 8(3):303–313.

Vural, N., Algan Cavuldak, Ö., and Anlı, R. (2018). Multi response optimisation of

polyphenol extraction conditions from grape seeds by using ultrasound assisted extraction (uae). *Separation Science and Technology*, 53(10):1540–1551.

Wang, J., Sun, B., Cao, Y., Tian, Y., and Li, X. (2008). Optimisation of ultrasound-assisted extraction of phenolic compounds from wheat bran. *Food Chemistry*, 106(2):804–810.

Wang, M., Li, J., Rangarajan, M., Shao, Y., LaVoie, E. J., Huang, T.-C., and Ho, C.-T. (1998). Antioxidative phenolic compounds from sage (salvia officinalis). *J Agric Food Chem*, 46(12):4869–4873.

Wang, X., Wu, Y., Chen, G., Yue, W., Liang, Q., and Wu, Q. (2013). Optimisation of ultrasound assisted extraction of phenolic compounds from sparganii rhizoma with response surface methodology. *Ultrason Sonochem*, 20(3):846–54. Wang, Xinsheng Wu, Yanfang Chen, Guangyun Yue, Wei Liang, Qiaoli Wu, Qinan Netherlands Ultrason Sonochem. 2013 May;20(3):846-54. doi: 10.1016/j.ultsonch.2012.11.007. Epub 2012 Nov 29.

Wcislo, G. and Szarlej-Wcislo, K. (2014). *Chapter 8 - Colorectal Cancer Prevention by Wheat Consumption: A Three-Valued Logic – True, False, or Otherwise?*, pages 91–111. Academic Press, San Diego.

Wen, C., Zhang, J., Zhang, H., Dzah, C. S., Zandile, M., Duan, Y., Ma, H., and Luo, X. (2018). Advances in ultrasound assisted extraction of bioactive compounds from cash crops - a review. *Ultrason Sonochem*, 48:538–549. Wen, Chaoting Zhang, Jixian Zhang, Haihui Dzah, Courage Sedem Zandile, Manyakara Duan, Yuqing Ma, Haile Luo, Xiaoping Netherlands Ultrason Sonochem. 2018 Nov;48:538-549. doi: 10.1016/j.ultsonch.2018.07.018. Epub 2018 Jul 18.

Wen, Y., Chen, H., Zhou, X., Deng, Q., Zhao, Y., Zhao, C., and Gong, X. (2015). Optimization of the microwave-assisted extraction and antioxidant activities of anthocyanins from blackberry using a response surface methodology. *RSC Advances*, 5(25):19686–19695.

Wojciechowska, M., Owczarek, A., Kiss, A. K., Grabkowska, R., Olszewska, M. A., and Grzegorczyk-Karolak, I. (2020). Establishment of hairy root cultures of salvia bulleyana diels for production of polyphenolic compounds. *J Biotechnol*, 318:10–19.

Wu, T. Y., Chen, C. P., and Jinn, T. R. (2011). Traditional chinese medicines and alzheimer's disease. *Taiwan J Obstet Gynecol*, 50(2):131–5. Wu, Tzong-Yuan Chen, Chih-Ping Jinn, Tzyy-Rong China (Republic : 1949-) Taiwan J Obstet Gynecol. 2011 Jun;50(2):131-5. doi: 10.1016/j.tjog.2011.04.004.

Wu, Y., Wang, X., and Fan, E. (2012). Optimisation of ultrasound-assisted extraction of puerarin and total isoflavones from puerariae lobatae radix (pueraria lobata (wild.) ohwi) with response surface methodology. *Phytochem Anal*, 23(5):513–9. Wu, Yanfang Wang, Xinsheng Fan, Enguo England Phytochem Anal. 2012 Sep-Oct;23(5):513-9. doi: 10.1002/pca.2349. Epub 2012 Jan 18.

Xiao, L., Lin, D. K., and Bai, F. (2012). Constructing definitive screening designs using conference matrices. *Journal of Quality Technology*, 44(1):2–8.

Xie, T., Yao, J., and Zhou, Z. (2019). Da-based parameter optimization of combined kernel support vector machine for cancer diagnosis. *Processes*, 7(5):263.

Xu, B., Tao, R., Huang, Z., Zhu, D., and Liu, J. (2020). Process optimization of microwave-assisted extraction of flavonoids from salvia plebeian using response surface methodology. *Journal of Physics: Conference Series*, 1578(1):012222.

Xueling, Z., Benguo, L., Limin, L., and Xiaoai, Z. (2011). Microwave-assisted extraction and antioxidant activity of total phenolic compounds from pomegranate peel. *Journal of medicinal plants research*, 5(6):1004–1011.

Yetilmezsoy, K., Demirel, S., and Vanderbei, R. J. (2009). Response surface modeling of pb(ii) removal from aqueous solution by pistacia vera l.: Box-behnken experimental design. *J Hazard Mater*, 171(1-3):551–62.

Yu, P.-S., Chen, S.-T., and Chang, I. F. (2006). Support vector regression for real-time flood stage forecasting. *Journal of Hydrology*, 328(3-4):704–716.

Yu, S. Y., Lee, Y. J., Kim, J. D., Kang, S. N., Lee, S. K., Jang, J. Y., Lee, H. K., Lim, J. H., and Lee, O. H. (2013). Phenolic composition, antioxidant activity and anti-adipogenic effect of hot water extract from safflower (carthamus tinctorius l.) seed. *Nutrients*, 5(12):4894–907.

Yusoff, I. M., Mat Taher, Z., Rahmat, Z., and Chua, L. S. (2022). A review of ultrasound-assisted extraction for plant bioactive compounds: Phenolics, flavonoids, thymols, saponins and proteins. *Food Res Int*, 157:111268. Yusoff, Ida Madiha Mat Taher, Zarani Rahmat, Zaidah Chua, Lee Suan Canada Ottawa, Ont. Food Res Int. 2022 Jul;157:111268. doi: 10.1016/j.foodres.2022.111268. Epub 2022 Apr 22.

Zeković, Z., Pintać, D., Majkić, T., Vidović, S., Mimica-Dukić, N., Teslić, N., Versari, A., and Pavlić, B. (2017a). Utilization of sage by-products as raw material for antioxidants recovery—ultrasound versus microwave-assisted extraction. *Industrial Crops and Products*, 99:49–59.

Zeković, Z., Pintać, D., Majkić, T., Vidović, S., Mimica-Dukić, N., Teslić, N., Ver-

sari, A., and Pavlić, B. (2017b). Utilization of sage by-products as raw material for antioxidants recovery—ultrasound versus microwave-assisted extraction. *Industrial Crops and Products*, 99:49–59.

Zhang, H., Birch, J., Xie, C., Yang, H., and El-Din Bekhit, A. (2019). Optimization of ultrasound assisted extraction method for phytochemical compounds and in-vitro antioxidant activity of new zealand and china asparagus cultivars (officinalis l.) roots extracts. *Food Chem*, 294:276–284.

Zhang, Q.-Q., Xin, D., Xin-Guang, L., Wen, G., Ping, L., and Hua, Y. (2016). Rapid separation and identification of multiple constituents in danhong injection by ultra-high performance liquid chromatography coupled to electrospray ionization quadrupole time-of-flight tandem mass spectrometry. *Chinese journal of natural medicines*, 14(2):147–160.

Zhang, Y., Smuts, J. P., Dodbiba, E., Rangarajan, R., Lang, J. C., and Armstrong, D. W. (2012). Degradation study of carnosic acid, carnosol, rosmarinic acid, and rosemary extract (rosmarinus officinalis l.) assessed using hplc. *J Agric Food Chem*, 60(36):9305–14.

Zhu, L., Ma, S., Li, K., Xiong, P., Qin, S., and Cai, W. (2022). Systematic screening of chemical constituents in the traditional chinese medicine arnebiae radix by uhplc-q-exactive orbitrap mass spectrometry. *Molecules*, 27(9):2631.

Ziaková, A. and Brandšteterová, E. (2003). Validation of hplc determination of phenolic acids present in some lamiaceae family plants. *Journal of Liquid Chromatography & Related Technologies*, 26(3):443–453.

Ziani, B. E. C., Heleno, S. A., Bachari, K., Dias, M. I., Alves, M. J., Barros, L., and Ferreira, I. (2019). Phenolic compounds characterization by lc-dad- esi/msn and bioactive properties of thymus algeriensis boiss. & reut. and ephedra alata decne. *Food Res Int*, 116:312–319.

Zimmerman, D. (2002). Paul langevin and the discovery of active sonar or asdic. *The Northern Mariner/Le Marin du Nord*, 12(1):39–52.

Čulina, P., Cvitković, D., Pfeifer, D., Zorić, Z., Repajić, M., Elez Garofulić, I., Balbino, S., and Pedisić, S. (2021). Phenolic profile and antioxidant capacity of selected medicinal and aromatic plants: Diversity upon plant species and extraction technique. *Processes*, 9(12):2207.

ŞÜMnÜ, S. G., ŞAhİN, S., and İNce, A. E. (2013). Extraction of phenolic compounds from melissa using microwave and ultrasound. *Turkish Journal of Agriculture and Forestry*, 37(1):69–75.

Chemometrics and Intelligent Laboratory Systems 222 (2022) 104493

Contents lists available at ScienceDirect

Chemometrics and Intelligent Laboratory Systems

journal homepage: www.elsevier.com/locate/chemometrics

Optimization of ultrasound-assisted extraction of phenolic-saponin content from *Carthamus caeruleus* L. rhizome and predictive model based on support vector regression optimized by dragonfly algorithm

Hamza Moussa [a,b,*], Farid Dahmoune [b,c], Mohamed Hentabli [d], Hocine Remini [b,c], Lotfi Mouni [a,b]

[a] Laboratoire de Gestion et Valorisation des Ressources Naturelles et Assurance Qualité (LGVRNAQ), Faculté des Sciences de la Nature et de la Vie et des Sciences de la Terre, Université de Bouira, 10000, Bouira, Algeria
[b] Département des Sciences Biologiques, Faculté des Sciences de la Nature et de la Vie et des Sciences de la Terre, Université de Bouira, 10000, Bouira, Algeria
[c] Laboratoire de Biomathématiques, Biophysique Biochimie et de Scientométrie (LBBBS), Université Abderrahmane Mira de Béjaïa, Béjaïa, 06000, Algeria
[d] Laboratoire de Biomatériaux et Phénomènes de Transport (LBMPT), Université Yahia Fares de Médéa, Médéa, 26000, Algeria

ARTICLE INFO

Keywords:
Carthamus caeruleus L.
Ultrasound-assisted extraction
Box-Behnken design
Support vector regression
Dragonfly algorithm

ABSTRACT

Box-Behnken design and support vector regression optimized using dragonfly algorithm as chemometrics techniques were employed to optimize and predict total phenolic (TPC) and saponin content (TSC) from *Carthamus caeruleus* L. rhizome using ultrasound-assisted extraction. Moreover, the comparative study of the antioxidant activity of rhizomes and leaves parts was also performed using different assays including scavenging free radical ($ABTS^{\bullet}$, $DPPH^{\bullet}$) activity, FRAP, and phosphomolybdenum assays. The results confirmed that the Box-Behnken design was achieved and the optimal conditions for the recovery of maximum TPC and TSC were obtained with 87.66 % methanol concentration, a solvent to solid ratio of 23 $mL.g^{-1}$, a temperature of 50 °C, and 26 min sonication time. The established SVR-DA model has been successfully predicted the extraction of TPC and TSC from *C. caeruleus* L. rhizome with a higher $R^2 = 0.99$ and low error. Matlab graphical user interface of optimized SVR-DA model was developed to predict TPC and TSC that could be used in pharmaceutical purposes. Furthermore, the optimal extract of rhizome and leaves extract showed high capacity of antioxidants, thus the *C. caeruleus* L. can be a promising candidate for the cosmetic and pharmaceutical industry.

1. Introduction

In recent years, chemometrics tools have been frequently employed to the optimization of analytical methods [1], and optimization of the extraction conditions of bioactive compounds [2–4], considering their advantages for the reduction of time, economical costs, and environmental impacts. Design of experiment (DoE) and machine learning technique (ML) become more attractive as chemometrics techniques. The DoE as full factorial design, Box-Behnken, and central composite design, etc., are multivariate optimization designs, in which the levels of all the variables are changed simultaneously [5]. Furthermore, the DoE offers the global optimal conditions while, the univariate approaches take many experiments and give local optimal conditions, which may fail when the effect of one variable is dependent on the level of the other variables involved in the optimization process [5,6]. The DoE experiment such as a Box-Behnken design is a statistical tool highly used for solving optimization problems by studying the effects of several input variables that affect the output variables by performing a low number of experiments [7]. The BBD has an advantage, in which all factors are simultaneously at their highest or lowest levels, thus the BBD is useful in avoiding experiments performed under extreme conditions [8]. As well as the efficiency of BBD was also reported by Ferreira, Bruns, Ferreira, Matos, David, Brandao, da Silva, Portugal, dos Reis, Souza and dos Santos [5], where the efficiency of the design is defined as the number of coefficients in the estimated model divided by the number of experiments. The BBD in the last decade taken a significant place as a tool for the optimization process where it has already been used to optimize microwave-assisted extraction of phenolic compounds from *Pistacia lentiscus* leaves [8], as well as the design was used as statistical modeling for ultrasound-assisted extraction of corn silk polysaccharide [9]. The BBD was also employed to optimize Pb (II) removal from aqueous solution by *Pistacia vera* L [7].

* Corresponding author. GVRNAQ Laboratory, Bouira University, Rue Drissi Yahia, Bouira, 10000, Algeria.
E-mail address: h.moussa@univ-bouira.dz (H. Moussa).

https://doi.org/10.1016/j.chemolab.2022.104493
Received 4 October 2021; Received in revised form 5 January 2022; Accepted 6 January 2022
Available online 13 January 2022

The Support vector machine is a kernel-based machine learning model that solves big data classification problems or performing function estimation in regression problems [10–12]. Recently, SVMs have been attracted the chemometrics community, which they have been adopted widely for the analysis of chemical data. Many scientific papers have been focused on the comparison of SVMs with more traditional chemometrics approaches [13,14]. In addition, SVMs have been used in several applications in forecasting soil water, soil moisture prediction, estimation of soil hydraulic parameters, modeling soil diffuse reflectance spectra, and soil type classification [15–17]. More than that, the SVM is employed to predict the correct diagnosis for cancer [18], as well as the prediction of the critical micelle concentration (CMC) of diverse Gemini surfactants from their structure characteristics [19]. Moreover, the SVM was used for the optimization of microwave-assisted extraction of polyphenols from spruce wood bark [20].

Carthamus caeruleus L., its rhizomes are used traditionally in the North African region (Algeria) for the treatment of burns and wounds [21]. The rhizomes parts are a good source for many bioactive compounds such as tannins, flavonoids, anthocyanins, leucoanthocyanins, sennosides, free quinones, saponins, glycosides, mucilage, and coumarins, these bioactive molecules possess several biological activities which include antimicrobial, anti-inflammatory, antioxidant activity, and wound-healing and hair-growth promoting capacity [21–23].

To understand the biological activities displayed by the rhizome part of *C. caeruleus* L., the phenolic and saponin compounds were investigated. Total saponin content, their name is derived from their ability to form stable foams in aqueous solutions because of asymmetric distribution of their hydrophobic (aglycone) and hydrophilic (sugar) moieties, they are a chemically complex group of compounds which distributed naturally in plants [24,25]. According to Furuya [26], saponin compounds generally were classified according to aglycone part for three main types; triterpene glycosides, steroidal glycosides, and steroidal alkaloid glycosides. The saponin compounds are showed several biological activities including; burn-wound healing capacity of red Ginseng roots by increasing angiogenesis phenomena during skin wound repair *via* the stimulation of the growth factor's production as explained by Kimura, Sumiyoshi, Kawahira and Sakanaka [27]. Moreover, the antioxidant and anticancer capacity of papaya leaves' saponin extracts were suggested by Vuong, Hirun, Chuen, Goldsmith, Murchie, Bowyer, Phillips and Scarlett [28], In addition to the biological capacity of saponin, the phenolic compounds are secondary metabolites with one or more aromatic rings, at least one hydroxyl group, and could contain a distinctive additional functional group [29]. These compounds have received the most attention in several fields in the last decades; in food applications, they are used as an ingredient for the development of functional foods, as well as they can provide physiological benefits such as health-promoting properties or disease prevention [30]. In human health, the phenolic compounds play a beneficial role in the prevention of cardiovascular diseases, cancer, and osteoporosis, and support their contribution to the prevention of neurodegenerative diseases such as Parkinson's and Alzheimer's disease [31].

The extraction of natural products is the crucial step for the recovery, and identification, and utilization of their bioactive molecules. The conventional extraction methods such as hydrodistillation, soxhlet, maceration, etc. were performed traditionally where a large amount of solvent had been used with longer extraction time, which they are not enough efficiently for recovering acceptable yields of specific compounds from natural sources [32,33]. Recent trends in extraction technologies have focused on intensification of the extraction process, which could provide higher extraction yield and higher purity and quality of the product by decreasing extraction time, energy consumption, and quantity of solvents and decreasing in many unit operations [33]. Among the advanced green extraction, ultrasound-assisted extraction is the most widely used in the extraction of bioactive compounds due to its fitting to these requirements.

Unfortunately, there is a paucity of investigations regarding the optimization and prediction of phenolic and saponin content from *Carthamus caeruleus* L. rhizome using ultrasound-assisted extraction based on chemometrics strategies such as Box-Behnken design (response surface methodology) and support vector machine optimized by dragonfly algorithm.

The present investigation attempts firstly to optimize the ultrasound-assisted extraction of saponin and phenolic compounds from the rhizome part of *C. caeruleus* L. using the Box-Behnken design. Secondly, the input and output variables employed in the optimization process were used to establish a predictive model based on support vector regression optimized by the dragonfly algorithm. Moreover, the antioxidant capacity of the optimal extract of rhizome and leaves extract were also evaluated using different methods *in vitro*.

Table 1
Coded and real levels of symbolized input variables defined for Box-Behnken design.

	Coded levels		
Independent variables	−1	0	+1
x_1: **Concentration of solvent (%)**	60	75	90
x_2: **Temperature (°C)**	50	60	70
x_3 : **Time (min)**	15	27.5	40
x_4: **Sample to solvent ratio (mL g^{-1})**	10	17.5	25

2. Materials and methods

2.1. Materials and reagents

Methanol, ethanol, chloroform, and sulfuric acid were purchased from SIGMA-ALDRICH, sodium carbonate (Na_2CO_3), Vanillin, and DPPH (2, 2-Diphenyl-1-picrylhydrazyl), Gallic acid, Ascorbic acid, ABTS (2, 2′-azino-bis(3-ethylbenzothiazoline-6-sulfonic acid)), potassium persulfate ($K_2S_2O_8$), potassium ferricyanide ($K_3Fe(CN)_6$), trichloroacetic acid ($C_2HCl_3O_2$), ferric chloride ($FeCl_3$) were purchased from SIGMA-ALDRICH. Folin-Ciocalteu's reagent, ammonium molybdate tetrahydrate ($(NH_4)_6Mo_7O_{24} \cdot 4H_2O$), sodium phosphate monobasic ($NaH_2PO_4 \cdot H_2O$), and sodium phosphate dibasic ($Na_2HPO_4 \cdot 12H_2O$) were purchased from VWR CHEMICALS. All the reagents were analytical grade.

2.2. Ultrasound-assisted extraction of phenolic-saponin content

The rhizome part and leaves of *C. caeruleus* L. were collected from *Bouir*a region (latitude 36.381707; longitude 3.711553, altitude 798 m) in February 2019. The rhizome and leaves parts were cleaned by distilled water the large impurities and cut into small parts with 1 mm of thickness and dehumidified at 40 °C in a ventilated oven (Venticell) until constant weight. The dried rhizome and leaves were milled using an electric grinder (High star AR-1045) to obtain a fine powder with a diameter of 200 μm. The powders were stored in airtight containers until use, where the rhizome powder was only used for the optimization and prediction of TPC and TSC, while the leaves powder was used for a comparative study of antioxidant capacity between the parts of plants.

The phenolic-saponin extract of rhizome was extracted using a sonication water bath (J.P. SELECTA, s. a, Spain, 40 kHz, Power generator 120 W, Power heater 75 W, SN. 3000865, and internal dimensions: 15 × 24 × 14 cm) under the designed conditions. The working ultrasound's frequency and power were fixed at 40 kHz and 120 W respectively. The extractions were performed when the temperature changed (50–70 °C) and methanol concentration (60–90%), solvent to solid ratio (10–25 mL.g^{-1}), and sonication time varied (15–40 min) as mentioned in Table 1, A.1. At the end of an extraction cycle, the obtained methanolic extracts with different volumes were filtrated from the residual plant material, and then the liquid extracts were equilibrated to the final volume and stored at 4 °C until use for optimization and prediction purposes (Table 1, A.1).

Table 2
Dataset for Box-Behnken design: matrix with 27 runs, and measured values of output variables (TPC, TSC) are given in table.

Runs	Extraction conditions				Experimental results	
	x_1	x_2	x_3	x_4	TPC (mg GAE/100 g_{dw})	TSC (Abs)
1	-1	-1	0	0	267.737 ± 2.602	0.263 ± 0.006
2	-1	0	-1	0	223.274 ± 2.152	0.200 ± 0.004
3	-1	0	0	-1	187.085 ± 5.204	0.155 ± 0.004
4	-1	0	0	+1	301.169 ± 4.179	0.255 ± 0.003
5	-1	0	+1	0	310.130 ± 4.775	0.250 ± 0.003
6	-1	+1	0	0	321.849 ± 4.662	0.286 ± 0.004
7	0	-1	-1	0	302.892 ± 4.775	0.284 ± 0.005
8	0	-1	0	-1	192.255 ± 2.984	0.203 ± 0.006
9	0	-1	0	+1	323.572 ± 2.152	0.328 ± 0.002
10	0	-1	+1	0	294.276 ± 7.237	0.309 ± 0.004
11	0	0	-1	-1	170.196 ± 1.034	0.145 ± 0.0006
12	0	0	-1	+1	326.330 ± 1.790	0.275 ± 0.004
13	0	0	+1	-1	188.808 ± 2.067	0.19 ± 0.005
14	0	0	+1	+1	348.733 ± 0.600	0.273 ± 0.002
15	0	+1	-1	0	266.703 ± 6.728	0.272 ± 0.003
16	0	+1	0	-1	227.411 ± 2.602	0.208 ± 0.009
17	0	+1	0	+1	393.540 ± 5.757	0.271± 0.003
18	0	+1	+1	0	371.481 ± 1.580	0.255 ± 0.009
19	+1	-1	0	0	272.217 ± 0.598	0.275 ± 0.002
20	+1	0	-1	0	242.231 ± 4.304	0.248 ± 0.002
21	+1	0	0	-1	136.419 ± 6.059	0.159 ± 0.004
22	+1	0	0	+1	286.693 ± 1.579	0.279 ± 0.003
23	+1	0	+1	0	198.114 ± 4.738	0.190 ± 0.002
24	+1	+1	0	0	1780.813 ± 1.579	0.207 ± 0.001
25	0	0	0	0	342.874 ± 5.167	0.280 ± 0.005
26	0	0	0	0	348.388 ± 9.827	0.288 ± 0.01
27	0	0	0	0	357.694 ± 9.325	0.271 ± 0.003

The values are expressed as means + standard deviations (n=3), **mg GAE/100:** mg Gallic acid equivalent per 100 g dry weight of rhizome powder, **Abs;** Absorbance.

To study the antioxidant capacity of rhizome and leaves of *C. caeruleus* L., the two parts of the plant were extracted under the optimal conditions obtained from the Box-Behnken design, using the same procedure mentioned above where the extracts were lyophilized and stored until use.

2.3. Optimization and prediction procedures

2.3.1. Box-Behnken design

To investigate the critical influence of the UAE factors on the extraction of TPC and TSC from *C. caeruleus* L. rhizome by UAE, a single-factor experiment as a preliminary study was used to determine approximate ranges of independent variables including the concentration of methanol (x_1), temperature (x_2), time (x_3), and solvent to solid ratio (x_4) (Table 1, A.1). As a result, all the independent variables were selected for subsequent modeling (Table 1, A.1). Based on these results, the BBD was then adopted to determine the best combinations of extraction variables for the extraction of TPC and TSC (Tables 1 and 2). Three levels (−1, 0, and +1) of four variables including methanol concentration (60–90%), temperature (50–70 °C), time (15–40 min), and solvent to solid ratio (10–25 $mL.g^{-1}$) were selected as depicted in Table 1. The BBD matrix consists of 27 experiments and three replicates at the central point as depicted in Table 2.

The total phenolic, total saponin compounds were correlated with the four independent variables under the following second-order polynomial equation (Eq. (1)):

$$Y = B_0 + \sum_{i=1}^{K} B_i x_i + \sum_{i=1}^{K} B_{ii} x_i^2 + \sum_{i=1}^{K-1} \sum_{j=2}^{K} B_{ij} x_i x_j + e \quad (1)$$

where; Y is the output variables (TPC, and TSC), and B_0, B_i, $B_{ii}(i = 1, 2, \ldots, k)$, $B_{ij}(i = 1, 2, \ldots, k; j = 1, 2, \ldots, k)$ are the regression coefficients for the mean, linear, quadratic, and interaction terms respectively, x_i and x_j are the coded variables as described in Table 2, e is the error. The independent variables were labeled as x_i, based on the following equation (Eq. (2)):

$$x_i = \frac{X_i - X_0}{\Delta X_i} \quad (2)$$

where x_i is the (dimensionless) coded value of the variable X_i; X_i is the actual value of variable; X_0 is the actual value of x_j at the center point and ΔX_i is the step change [8].

2.3.2. Support vector regression optimized using dragonfly algorithm (DA) for predicting the TPC and TSC from C. caeruleus L. Rhizome

As a supervised-learning approach, SVM is a powerful tool for nonlinear classification, time series prediction, and regression, based on the structural risk minimization principle from computational learning theory [16,20]. The support vector machine (SVM) is an effective tool in real-value function estimation with excellent generalization capability and high prediction accuracy by using the sparse solution, kernels, Vapnik-Chervonenkis (VC) control of the margin, and the number of support vectors [34]. In recent years, the SVM's parameters have been optimized using different meta-heuristic algorithms, such as particle swarm optimization (PSO), the dragonfly algorithm (DA), genetic algorithm (GA), and bat algorithm (BA) [18]. Dragonfly algorithm (DA) is meta-heuristic algorithms proposed by Mirjalili [35] that is inspired by the natural behavior of static and dynamic swarming of dragonfly, these static and dynamic swarming are served as exploration and exploitation behavior of the dragonfly algorithm [36]. DA is used to solve a large variety of optimization problems, which several variants of standard DA including Binary dragonfly algorithm, Fuzzy-based dragonfly algorithm, chaotic and adaptive dragonfly algorithm, and dragonfly algorithm with support vector machine have been suggested to provide a good balance between exploration and exploitation by increasing the diversity of the solutions [37]. DA has been used to solve different optimization problems of SVM, the values of kernel and penalty parameters were sent by the DA for training the SVM using the training data [19,38]. Many previous studies reported that the performance of SVR was achieved when the hyper-parameters are optimized using the Dragonfly algorithm [19]. The support vector machine (SVM), theoretically minimizes the expected error of a learning machine and so reduces the problem of overfitting [39]. Furthermore, the kernel method in SVM not only can improve the computational efficiency of SVM training but also can be a convenient way to help prevent overfitting classification problems [40].

Due to the power of support vector regression and Dragonfly algorithm for solving regression problems were chosen to predict and optimize the total phenolic and saponin content from *C. caeruleus* L. rhizome using ultrasound-assisted extraction. The SVR-DA model was developed based on input and output variables used in the Box-Behnken design, which had the goal of predicting and optimizing the TPC and TSC. The function used to predict TPC and TSC is expressed using the equation (Eq. (3)):

$$f(x) = \sum_{n=1}^{N} \left(a_n - a_n^*\right) G\left(x_n, x\right) + b \quad (3)$$

where $G\left(x_n, x\right)$ a kernel function as is mentioned in Table A2, which three kernel functions including Gaussian RBF, Linear, and Polynomial were tested, and the Gaussian RBF kernel that gave the best results was employed for the construction of the model. Alpha is the dual problem coefficient specified as a vector of numeric values. *Alpha* contains m elements, where m is the number of support vectors in the trained SVM regression model. The dual problem introduces two Lagrange multipliers

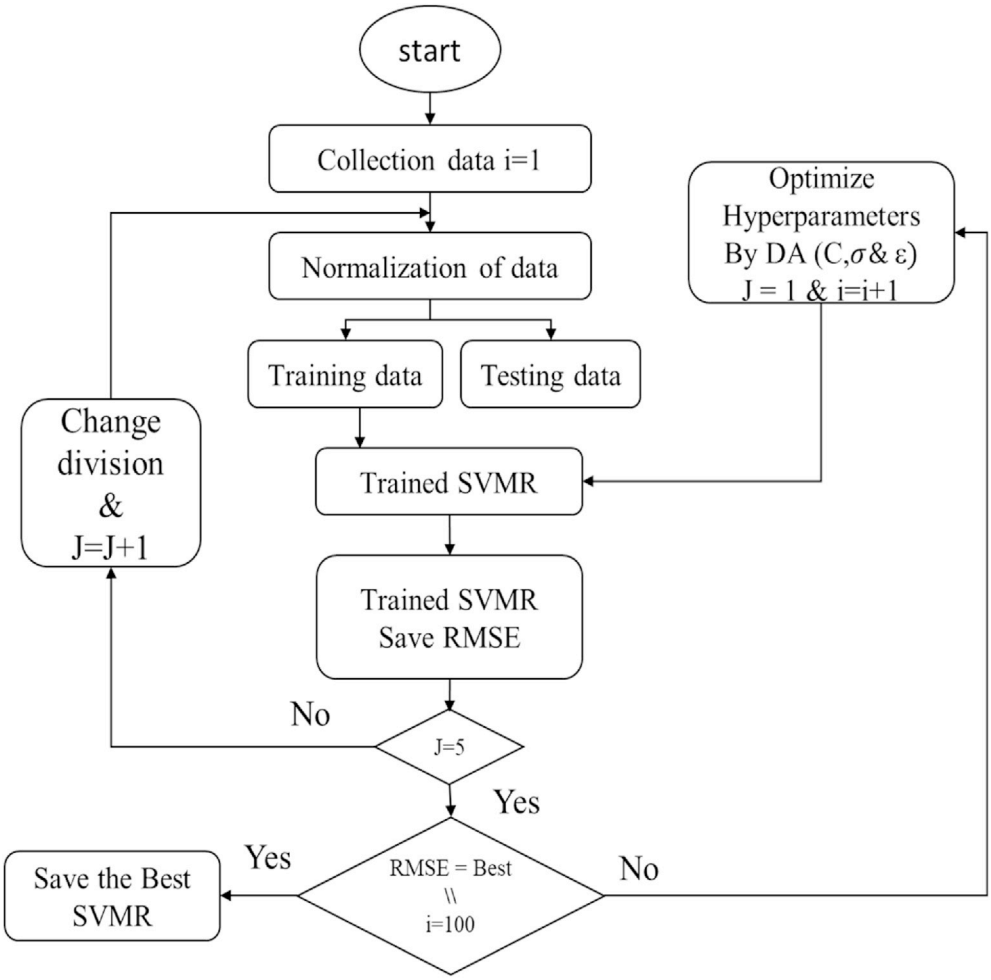

Fig. 1. SVR-DA technique used for predicting TPC and TSC from *C. caeruleus* L. rhizome **(Laidi, Abdallah et al. 2020)**.

for each support vector. The values of *Alpha* are the differences between the two estimated Lagrange multipliers for the support vectors $(a_n - a_n^*)$, and b is bias term.

The applied methodology and optimization of hyper-parameters can be drawn following the flowchart in Fig. 1 [38,41–43]. Firstly, The numeric values of the input data matrix (x_1, x_2, x_3, and x_4) have been normalized to improve the optimization and speed convergence. The normalization function is expressed by the equation (Eq. (4)):

$$x_n = x^{0.1} \tag{4}$$

where x_n is normalized input dataset and x is input data.

Secondly, the total datasets of TPC and TSC from *C. caeruleus* L. rhizome were divided randomly to avoid the overfitting into 80%, 20% for training, and validation data sets respectively, using the Holdout function included in the statistical and machine learning toolbox of Matlab. Furthermore, the validation data set was an independent data set used to test the SVM-DA model [19,44]. DA initially feeds the SVM with a random combination of hyper-parameters in their pre-defined ranges including the penalty parameter (C), size of the insensitive zone (ε), and sigma (σ). In five iterations, the steps established with the data division and up to the development of the SVR model are repeated and the lower RMSE obtained is saving the best value. In addition, the DA make a new population of hyper-parameters for the SVR algorithm, and the same set of steps is repeated to obtain the new best RMSE, and this step is implemented for 100 trials, in which the lower and best RMSE corresponds to the resulting optimal DA-SVM model [19,42]. The RMSE and R^2 were calculated according to equations illustrated in Table A2 to assess the predictive power of the SVR-DA model.

The relative standard deviation (RSD) or the coefficient of variance, the mean absolute error (MAE), the mean relative percentage error (MRPE), the Average absolute relative deviation (AARD), the root mean square error (RMSE), the determination coefficient (R^2) were used in this study to evaluate the goodness of adjustment of the models as well as the prediction precision of the optimized model.

2.4. Determination of total phenolic compounds

The total phenolic compounds of the UAE extracts of *C. caeruleus* L. dried rhizome were determined using a spectrophotometric method as described by Georgé, Brat, Alter and Amiot [45]. A 625 μL diluted Folin-Ciolcateu reagent (1/10 *V/V*) was added to the different methanol extracts (125 μL). The mixture was left for 2 min at room temperature, and then 500 μL of Na_2CO_3 solution (7.5% *w/V*) was added. The mixture was incubated for 15 min at 50 °C in an unstirred water bath (NÜVE Bath, NB20), the reactional mixture was finally cooled in a water-ice bath. The specific absorbance was measured at 760 nm using a UV–vis Spectrophotometer (Optizen pop, Korea).

The concentrations were calculated using the Gallic acid standard curve, where different concentrations of Gallic acid ranged from 0.02 to 0.08 mg/mL were used to plot the standard curve using GraphPad software (Fig. A1). The linear equation was obtained ($y = 12.089X + 0.0034$, $R^2 = 0.999$) and the TPC from the rhizome were expressed as mg Gallic acid equivalent per 100 g of dry weight of the fine powder of *C. caeruleus*

Table 3
Standards regression and significance of input variables on TPC, TSC of *C. caeruleus* L. rhizome.

		TPC (mg GAE/100 g_{dw})		TSC (Abs)	
	Parameters	Estimated coefficient	ρ-value	Estimated coefficient	ρ-value
Estimated parameters	Intercept	349.652	<0.0001[a]	0.279	<0.0001[a]
	Linear effects				
	x_1	−24.730	0.0009[a]	−0.004	0.3101[b]
	x_2	8.904	0.1402[b]	−0.014	0.0041_a
	x_3	14.993	0.0208[a]	0.003	0.3858[b]
	x_4	73.155	<0.0001[a]	0.051	<0.0001[a]
	Quadratic effects				
	x_1^2	−72.940	<0.0001[a]	−0.035	<0.0001[a]
	x_2^2	−12.063	0.1792[b]	0.014	0.0257[a]
	x_3^2	−33.260	0,0020[a]	−0.019	0.0061[a]
	x_4^2	−53.380	<0.0001[a]	−0.038	<0.0001[a]
	Interaction effects				
	$x_1 * x_2$	−36.879	0.0026[a]	−0.023	0.0051[a]
	$x_1 * x_3$	−32.743	0.0057[a]	−0.027	0.0016[a]
	$x_1 * x_4$	9.047	0.3723[b]	0.005	0.4580[b]
	$x_2 * x_3$	28.349	0.0132[a]	−0.010	0.1420[b]
	$x_2 * x_4$	8.703	0.3902[b]	−0.015	0.0384[a]
	$x_3 * x_4$	0.948	0.9243[b]	−0.011	0.0995[b]
Regression results	R^2	0.96		0.97	
	R^2_{Adj}	0.92		0.93	
	RMSE	19.53[a]		0.013[b]	
	C.V (%)	7.14		5.3	
	ANOVA (Model)	<0.0001[a]		<0.0001[a]	
	Lack of fit	0.116[b]		0,288[b]	

TPC; Total phenolic compounds, **TSC;** Total saponin content, **EC;** Estimated coefficient, **RMSE;** Root Mean Square Error, **C.V;** Coefficient of variance, **ρ-value [a];** statistically significant, **ρ-value [b];** statistically not significant; **RMSE[a]** of TPC is expressed in mg GAE/100 g_{dw}; **RMSE[b]** of TSC is expressed in (Abs).

L. (mg GAE/100 g_{dw}) according to the equation (Eq. (5)). The analyses were carried out in triplicate and the mean ± SD was calculated.

$$TPC(\text{mg GAE}/100\ g_{dw}) = \frac{c \times V \times \text{DF}}{g_{dw\ \text{rhizome powder}}} \times 100 \quad (5)$$

where $c(\text{mg/mL})$ is the concentration of TPC from the standard curve of Gallic acid, V (mL) is the volume of solvent used in the extraction, DF is the factor of dilution, and g_{dw} is the dry weight of rhizome powder.

2.5. Quantitative determination of total saponin content

The Vanillin-acid sulfuric method of Hiai, Oura and Nakajima [46] was used for optimization purposes, the colorimetric assay was applied for the determination of steroidal sapogenins, triterpenoid sapogenins, sterols, and bile acids, which have an OH group at their C-3 position, gave chromogens with the reagents. Consistently, 125 μL of diluted extracts (1/5 V/V) of dry weight of rhizome powder were added to 125 μL of 8% (w/V) vanillin solution (dissolved in ethanol) and then sulfuric acid 72% (V/V) was added (1.25 mL), the final mixture was shaken and incubated in a water bath (NÜVE Bath, NB20) at 60 °C for 10 min. The absorbance of the cold mixture was recorded against methanol blank with the other reagents (strong yellow color). The wavelength was scanned by using a UV/Vis spectrophotometer (Optizen pop, Korea), and the results showed that the maximum adsorption was at 515 nm. The analyses were carried out in triplicate and the mean ± SD was calculated.

2.6. Evaluation of free radical scavenging activity of phenolic-saponin extract from C. caeruleus L

The antioxidant potential of lyophilized optimal extract of rhizome and leaves extract from *C. caeruleus* L. was evaluated using scavenging free radicals (DPPH•, ABTS•) activity, reducing power and phosphomolybdenum assays were selected in this study.

The DPPH free radical scavenging capacity of the rhizome and leaves parts of *C. caeruleus* L. extracts were analyzed using the method described by Dahmoune, Remini, Dairi, Aoun, Moussi, Bouaoudia-Madi, Adjeroud, Kadri, Lefsih, Boughani, Mouni, Nayak and Madani [47] with slight modification. Concisely, 1 mL of DPPH solution in methanol (60 μM) was mixed with 100 μL of different concentrations of lyophilized extract and the mixture was incubated for 30 min in the dark at room temperature, the absorbance of the mixture was determined at 517 nm against methanol as blanc using a UV–vis Spectrophotometer.

The ABTS assay was performed according to Dahmoune, Spigno, Moussi, Remini, Cherbal and Madani [8], the assay was based on the decolorization of ABTS free radical in the presence of antioxidants. Briefly, a stock solution of ABTS was prepared using 7 mM ABTS and 2.45 mM potassium persulfate. After 16 h of incubation in the dark, the stock solution was diluted by ethanol to final absorbance of 0.700 ± 0.02 at 734 nm, then 75 μL of different centration of lyophilized extracts of leaves and rhizome were added to 1425 μL of diluted ABTS solution. The antioxidant capacity (%) was measured after 6 min of incubation in the dark at 734 nm.

The antioxidant capacity was expressed as a percentage of scavenging of free radical (DPPH• and ABTS•) and was calculated according to equation (Eq. (6)):

$$\text{Free radical inhibition } (\%) = \frac{A_{blanc} - A_{Sample}}{A_{Control}} * 100 \quad (6)$$

A_{Sample} is the absorbance of free radical solution (ABTS• or DPPH•) + sample extract at the required time, A_{blanc} is the absorbance of free radical solution (ABTS• or DPPH•) + extraction solvent, $A_{Control}$ is the absorbance of the working free radical solution. The concentration required for inhibition of 50% of free radical (DPPH• and ABTS•) was also calculated from the inhibition curve.

The total antioxidant assay was also performed using a phosphomolybdenum reagent. According to Prieto, Pineda and Aguilar [48], 200 μL of different concentrations of the lyophilized extract of rhizome, and leaves were mixed with 2 mL of test solution consisting of 0.6 M sulfuric acid, 4 mM ammonium molybdate tetrahydrate, and 28 mM sodium phosphate. The mixture was incubated for 90 min at 95 °C. After cooling at room temperature, the absorbance was measured at 695 nm. Different

concentrations of Ascorbic were used (0.02–0.4 mg/mL) to plot the standard curve ($y = 3.4169\,x - 0.0498$, $R^2 = 0.994$) by evaluating its total antioxidant activity under the same conditions mentioned above (Fig. A2). The results of TAA were expressed as mg AAE/g of lyophilized extract based on Eq. (7):

$$\mathrm{TAA}\ \left(\mathrm{mg\ \ AAE}\,/\,\mathrm{g_{dry\ \ extract}}\right) = \frac{c(\mathrm{mg\ \ AAE/mL})}{c(\mathrm{g/mL})} \tag{7}$$

where $c\,(\mathrm{mg\ \ AAE}\,/\mathrm{mL})$ is the TAA of rhizome and leaves parts calculated from the standard curve, $c(\mathrm{g}\,/\mathrm{mL})$ is the concentration of lyophilized extract.

The reducing power of *C. caeruleus* L. was evaluated using previously published methods of Oyaizu [49], 0.2 mL of various concentrations of the leaves and rhizome extracts were added separately to 0.5 mL of phosphate buffer (0.2 M, pH 6.6) and 0.5 mL of 1% potassium ferricyanide. The reaction was incubated in a water bath at 50 °C for 20 min. After cooling at room temperature, 0.5 mL of 10% TCA was added to the reactional mixture, and then centrifuged at 3000 rpm for 10 min. The supernatant (0.5 mL) was collected and mixed with 0.5 mL of distilled water and 0.1 mL of Ferric chloride (0.1%) and the absorbance was measured directly at 700 nm.

2.7. Hardware and software

The JMP® Pro 13.0.0 (64-bit) software under Microsoft Windows 10 Professionnel (10.0.15063.0) operating system was used to construct the BBD and to analyze all the results. All procedures and the metrics (Table A2) used for construction and analyze SVR-DA were carried out by means of MATLAB R2019 (b) software (Mathworks, Natick, MA, USA) under Microsoft Windows 10 operating system using a high-performance (Random Access Memory 6 G, Hard Drive 500 G). The statistical and machine-learning toolbox was used to build the SVM model and the dragonfly algorithm toolbox added by Mirjalili [35] was used for the optimization method. The GraphPad prism 8.0.2 (263) software was used to plot all the standard curves and graphs of antioxidant activity.

3. Results and discussion

3.1. Fitting the response surface model

Fitting the Box-Behnken model (Table 2) for TPC and TSC was assessed, using analysis of variance (ANOVA) and lack of fit (LOF), R-square (R^2), adjusted R-square (R^2_{Adj}), and the coefficient of variation (CV).

In the RSM, a good adjustment was obtained with R-squared values of 0.96, 0.97, for TPC, TSC respectively, this high R^2 values of TPC and TSC revealed that 96% and 97% of the data fit the regression model, with a coefficient of variance (CV) less than 10% for all responses (Table 3). Also, a higher adjusted R-square (R^2_{Adj}) indicated that 92%, 93% of the variation is explained by only those independent variables that affected the TPC, TSC extraction (Table 3). Concerning the ANOVA (Table 3), the significant model (higher F-value, p-value < 0.0001) with lack of fit not significant (smaller F-value, p-value > 0.05) of each response (TPC, TSC) indicated that there was a relationship between the observed values of the responses and any predictors. Therefore, the BBD model was suitable and will explain at least some of the variations in the responses.

It is important to note that the second-order polynomial equations found were used to predict the responses for several levels of each factor considered. A polynomial equation is useful for identifying the influence of the independent variables by comparing the estimated coefficients. The regression model for total phenolic content, total saponin content were shown in Eqs. (8) and (9):

$$\begin{aligned}\mathrm{TPC\ \ (mg\ \ GAE/100\ \ g_{dw})} = {} & 349.652 - 24.730x_1 + 8.904x_2 + 14.993x_3 \\ & + 73.155x_4 - 72.940x_1^2 - 12.063x_2^2 - 33.260x_3^2 \\ & - 53.380x_4^2 - 36.879x_1x_2 - 32.743x_1x_3 \\ & + 9.047x_1x_4 + 28.349\ \ x_2x_3 + 8.703x_2x_4 \\ & + 0.948x_3x_4\end{aligned} \tag{8}$$

$$\begin{aligned}\mathrm{TSC\ \ (Abs)} = {} & 0.279 - 0.004x_1 - 0.0014x_2 + 0.003x_3 + 0.051x_4 - 0.035x_1^2 \\ & + 0.014x_2^2 - 0.019x_3^2 - 0.038x_4^2 - 0.023x_1x_2 - 0.027x_1x_3 + 0.005x_1x_4 \\ & - 0.010x_2x_3 - 0.015x_2x_4 - 0.011x_3x_4\end{aligned} \tag{9}$$

3.2. Influence of temperature on dependent variables

From Table 3 and Eq. (8), the linear effect of temperature (50–70 °C) was statistically not significant on TPC extraction using ultrasound, even though the interaction between the methanol concentration and temperature (x_1x_2) was significantly negative on the extraction of TPC with an important estimated coefficient. In addition to the interaction terms (x_1x_2), the interaction between temperature and sonication time (x_2x_3) also showed a significantly positive effect on TPC extraction, which indicates that the temperature effect depends on the effects of methanol concentration (x_1) and sonication time (x_2).

As regards the effect of UAE temperature on saponin extraction, Table 3, and Eq. (9), show that the effect of temperature on TSC was significantly negative in linear and interaction terms (x_1x_2, x_2x_4).

Fig. 2a and 2d shows the response plots of total phenolic compounds, total saponin content of rhizome of *C. caeruleus* L. by varying two variables at the same time, while the third and fourth variable constant at zero levels, these plots illustrate the temperature effect on TPC, TSC in interaction with the methanol concentration. The temperature effect was studied in two parts, which was noticed that there was an inverse correlation, when the methanol concentration was below 75%, the yield of TPC and TSC reached their higher values when the temperature increased from 50 °C to 70 °C. This similar trend of total phenolic and saponin content is explained by the fact that, increasing in extraction temperature, enhance the solubility of solute and diffusion coefficient of TPC and TSC [50,51], Moreover, Teh and Birch [52] confirmed that heating temperature increase cavitation phenomena of ultrasound by helping in cell wall breaking for TPC and TSC extraction.

In the second part, when the methanol concentration was above 75%, the TPC and TSC decreased significantly at higher temperature degrees. It can be considered that a higher amount of methanol in the extraction solvent leads to a decrease of a boiling point in the mixture solvent, so at higher extraction temperature, it can be easily vaporized during extraction thereby decreasing in TPC and TSC.

In brief, the higher values of TPC yield were obtained at higher temperatures with a lower methanol concentration although, TSC yield was obtained at a higher concentration of solvent with lower temperature. To understand more the interactive effect of extraction temperature with the other parameters, Fig. 2c confirms that when sonication time was above 25 min, the TPC yield raised significantly with the increase in the temperature of extraction. Inversely the TPC yield decreased when temperature increased when sonication time was below 25 min, and this allows us to conclude that a higher yield of total phenolic compounds yield was found at a higher temperature and higher sonication time. Furthermore, the total saponin content was found a higher value of yield at lower temperatures around 50 °C when the solvent to solid ratio was upper than 17.5 mL. g^{-1} and then decreased significantly when the temperature enhanced to 70 °C (Fig. 5f). Ali, Lim, Chong, Mah and Chua [53] suggested that, even though extraction temperature enhances the

solubility of the solvent into the plant cell by reducing the viscosity of the medium, the thermal degradation of the phenolic compounds was the reason behind the decrease of TPC at high temperatures upper than 52 °C.

In conclusion, the effect of the extraction temperature on recovery of TPC, and saponin content from the rhizome of *C. caeruleus* L. was associated with the type and different bounds forms of the phenolic compounds and saponin that are presented in the plant, also the extraction temperature of UAE was strongly correlated to the other independent parameters.

3.3. Influence of methanol concentration on TPC and TSC

The influence of methanol concentration was significantly negative ($p < 0.05$) in linear terms for total phenolic content but not significant ($p > 0.05$) for total saponin content, despite the influence of methanol concentration was significantly negative for all responses (TPC, TSC) in interaction terms (x_1x_2, and x_1x_3) (Table 3, Eq. (8) and (9)).

Fig. 2a and 2b, illustrates the effect of the interaction of methanol concentration and temperature (x_1x_2), methanol concentration and time (x_1x_3) on total phenolic compounds yield from the rhizome of *C. caeruleus* L. respectively. Temperature and time were fixed at zero levels, the yield of TPC raised to their maximum values when the methanol concentration was approximately 65% then TPC decreased significantly with an increase in the methanol concentration upper than 65%. These similar findings were observed by Cheok, Chin, Yusof, Talib and Law [54], which found that the TPC yield was decreased as methanol concentration increased from 70% to 80%, and higher TPC was obtained at 69.77% of methanol concentration. Moreover, the results of this study were in agreement with the "like dissolve like" approach [55], where, the adding of water into the methanol increase the polarity of the mixture, hence increasing the yield of polyphenolic compounds. From the results outlined above based on the polarity of optimal extraction solvent, *C. caeruleus*' rhizome possesses hydrophilic phenolic compounds.

On the other hand, increasing methanol concentration from 60 to 90%, the total saponin content was increased significantly, where the highest of TSC was obtained at a higher concentration of methanol in aqueous methanol (75–90%) (Fig. 2d and 2e), this result was supported by Pham, Vuong, Bowyer and Scarlett [51], which confirmed that the highest saponin yield was observed in either absolute methanol or 75% methanol extracts. Furthermore, Sarvin, Stekolshchikova, Rodin, Stavrianidi and Shpigun [56] also confirmed that Steroidal saponin compounds from *T. terrestris* L. are easily dissolved by low-polar organic solvent solutions such as ethanol and methanol, with different levels of water. Methanol-water mixture exhibited extended structures in solution, this characteristic might have an impact on the solubility and diffusivity of large hydrocarbon molecules of Saponin [57]. According to the similarity and intermiscibility theory, when the polarity of solute and solvent is similar, the solutes dissolve from the cells [58].

3.4. Influence of sonication time on TPC and TSC

According to Table 3 and Eq. (8), and Eq. (9), sonication time range from 15 to 40 min was found as a significant factor only for TPC in linear terms, but in interaction terms, the sonication time was a significant factor for TPC (x_1x_3, x_2x_3), TSC (x_1x_3). These results were supported by Zhang, Birch, Xie, Yang and El-Din Bekhit [59], which confirmed that a high concentration of phenolic compounds was noticed at extended sonication time and a higher amount of solvent to solid ratio simultaneously. However, the sonication time factor showed a significantly negative influence in interaction with methanol concentration (x_1x_3), where higher TPC and TSC were observed at longer sonication time when the concentration of methanol was lower between 60 and 75%, and lower yield of all responses was obtained at longer sonication time and a higher concentration of methanol (Fig. 2b and 2e). From the findings mentioned above, the sonication time was found as an important parameter in ultrasound-assisted extraction of phenolic and saponin compounds from the rhizome of *C. caeruleus* L. and was directly correlated with the other independent parameters. Many findings were found a sonication time range from 20 to 35 min is the suitable range for effective extraction of phenolic and saponin compounds [51,52,57,60]. Increasing in sonication time continuously, the cell wall of the plant will be more exposed to ultrasound acoustic cavitation thereby increasing the yields of bioactive compounds. Although Dong, Liu, Liang and Wang [61] reported that the extended time after the maximum extraction yields lead to the lower permeability of the solvent into the cell plant and decreasing bioactive compounds yield by suspending the impurities including insoluble molecules, cytosol, and lipids in the liquid extraction, also the re-absorbing of released molecules on the large smashed plant particles.

3.5. Influence of solvent to solid ratio on TPC and TSC

According to the results of this study, solvent to solid ratio was considered as the most significant factor, which affected positively TPC and TSC extraction from the rhizome of *C. caeruleus* L. The effect of solvent to solid ratio was highly significant on TPC and TSC in linear terms, as well as the following interaction terms: x_2x_4 for TSC and, x_3x_4 for antioxidant activity was significant (Table 3, Eqs. (8) and (9)).

Firstly, the influence of solvent to solid ratio was highly significant for the extraction of total phenolic compounds, in which the content of TPC increased with an increase in the solvent to solid ratio (Table 3). The higher total phenolic compounds can be explained by the fact that the solubility of phenolic compounds improved with increase in the solvent to solid ratio until reached the saturation of solvent. In contrast, many trends confirmed that higher sample-to-solvent ratios increase the suspension density of the solution, which negatively affected the solvation of released bioactive compounds [51].

On the other hand, Fig. 2f illustrates the effect of the combination of temperature and solvent to solid ratio on the variation of TSC from the rhizome of *C. caeruleus* L. Increasing in the solvent to solid ratio from 10 to 25 ($mL.g^{-1}$), the TSC increased and reached a maximum yield at a higher solvent to solid ratio and lower temperature. The presence more of methanol-water mixture create a gradient of concentration in the medium, which improved the mass transfer phenomena of the system thereby enhancing the recovery of saponin content, Tian, Zhao, Zhang, Zhang, Liu and Gao [62] were working on optimization of the microwave-assisted extraction of saponin from *Aralia elata* (Miq.) Seem fruits and rachises and were found that 20 and 30 ($mL.g^{-1}$) of solvent to solid ratio were the best ratios for the extraction of saponin. Besides Ali, Lim, Chong, Mah and Chua [53] mentioned that increasing solvent to solid ratio continuously, more protein and polysaccharides were dissolved in solution, interfering with the dissolution of saponin. Furthermore, an excessive ratio of solvent is not cost-effective and did not always lead to a higher yield of bioactive compounds, which may be due to the larger amount of solvent that causing excessive swelling of raw materials and increasing the absorption of target compounds [56,62].

3.6. Box-Behnken optimization and model validation

A maximum desirability function was carried out to identify the best possible combination that can achieve maximum extraction yield of TPC and TSC from *C. caeruleus* L. rhizome. The optimized condition was determined at 78.66% Methanol concentration with a ratio of 23 ($mL.\ g^{-1}$) at a temperature of 50 °C and 26 min of extraction time. The predicted value of TPC was 349.209 mg GAE/100 g_{dw} with Confidence interval [321.826–377.494], and TSC was 0.339 (Abs) with Confidence interval [0.320–0.358]. The experimental results produced an extraction yield of TPC of 363.209 ± 11.284 mg GAE/100 g_{dw}, and 0.325 ± 0.005 (Abs) respectively, which indicates the high accuracy of the response surface model. The results were fitted the prediction values in the range of 95% prediction intervals that were obtained from second-

Table 5
Optimum parameter values of SVR model optimized by dragonfly algorithm.

Penalty parameter *C*	Sigma σ	Size of the insensitive zone (ε)	Kernel function	Amount of support vectors	Output	RMSE Training 80%	RMSE Validation 20%	RMSE ALL
900	2.47	2.46 *10^{-4}	Gaussian	40	TPC TSC	0.2039[a] 0.000162[b]	11.0150[a] 0.0068[b]	6.1900[a] 0.0027[b]

RMSE[a] of TPC is expressed in mg GAE/100 g_{dw}; RMSE[b] of TSC is expressed in (Abs).

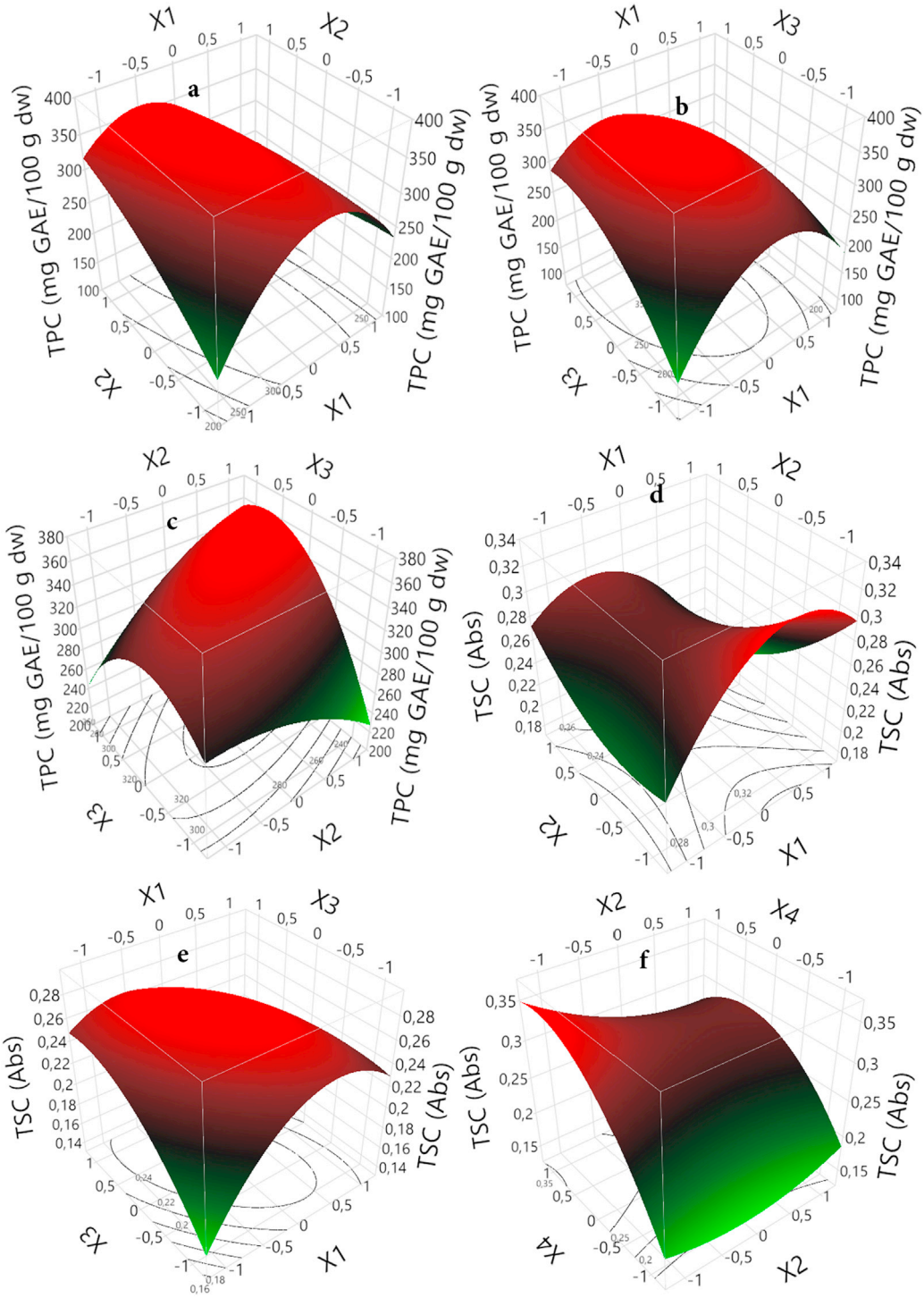

Fig. 2. Three-dimensional plots of *C. caeruleus* L. rhizome showing the influence UAE factors on recovery of TPC (a, b, c), Total saponin content (d, e, f).

order models. In addition, the overall desirability for all responses is defined as the geometric mean of the desirability functions for the individual responses [63,64]. In this study, the overall desirability was 0.88, which indicates that all the responses were achieved. A good

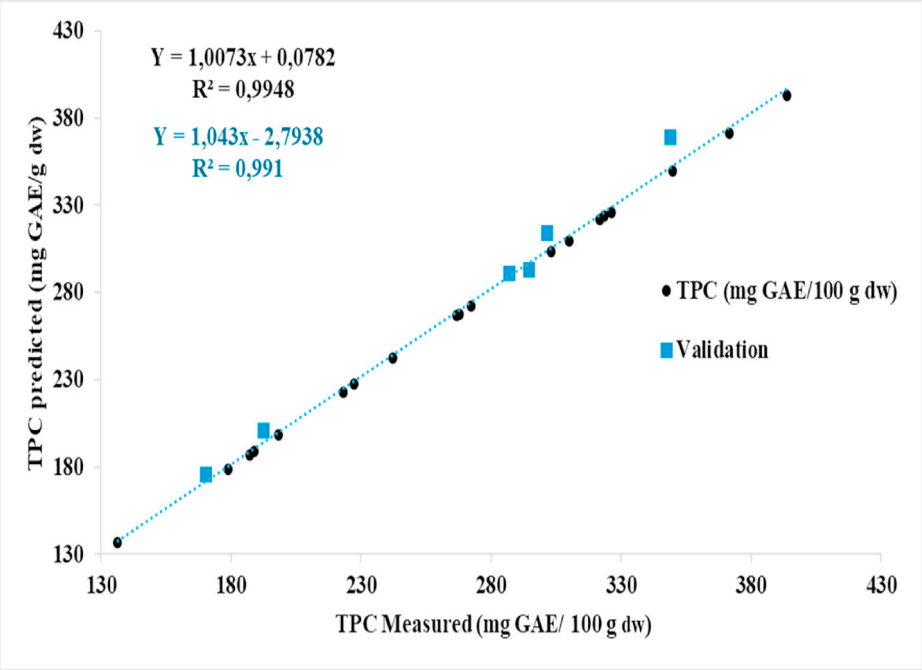

Fig. 3. Scatter plot of measured and predicted total phenolic compounds obtained by SVR-DA model.

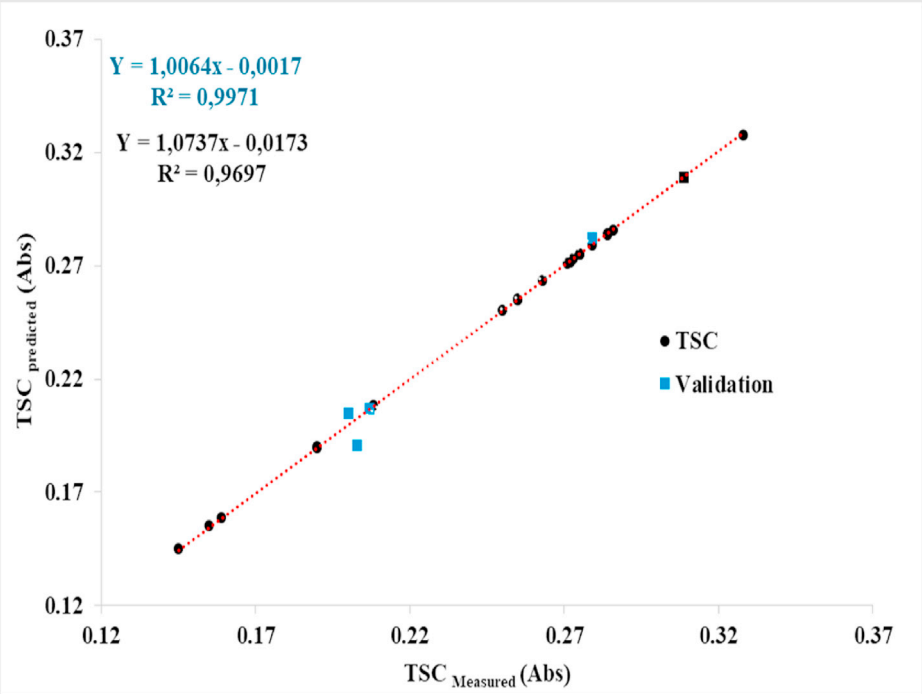

Fig. 4. Scatter plot of measured and predicted total saponin content obtained by SVR-DA model.

correlation between the predicted and observed responses confirmed that the models obtained could perfectly predict the ultrasound-assisted extraction of phenolic, saponin compounds from *C. caeruleus* L. rhizome.

3.7. SVR-DA for predicting the TPC and TSC from C. caeruleus L. Rhizome

In this work, the prediction of TPC and TSC from *C. caeruleus* L. rhizome using UAE was established by the support vector regression model optimized by the dragonfly algorithm. After optimizing process, the values of the penalty parameter (C), size of the insensitive zone (ε), sigma (σ), and 40 support vectors were obtained as mentioned in Table 5, some of the kernel functions were tested as depicted in Table A2, Gaussian RBF kernel gave very satisfactory results as shown in Table 5. The dataset was randomly divided into two groups: training, and validation set, composed of 80%, 20% respectively by the HOLDOUT method [19,44,65]. Based on the optimized hyper-parameters (C = 900, σ = 2.47, $\varepsilon = 2.46 * 10^{-4}$), Fig. 3 shows the correlation between the measured and predicted TPC, the R^2 of training and validation set are 0.99, where the RMSE of TPC is 6.190 mg GAE/100 g_{dw} (Table 5). Regarding the total saponin content, the R^2 of the training and validation set are 0.99

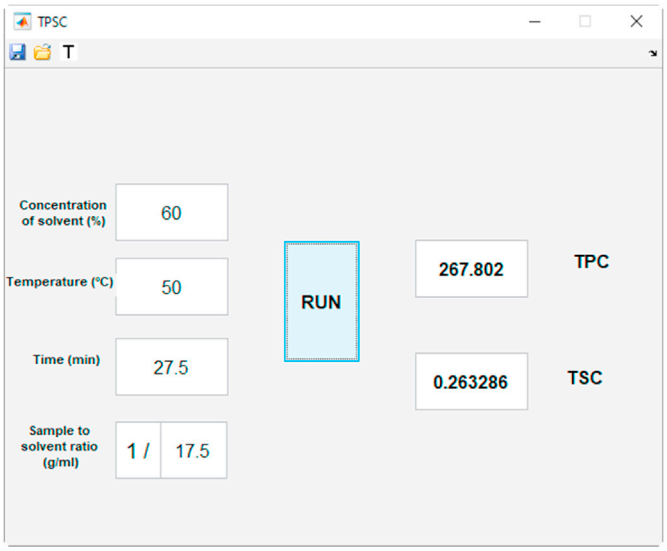

Fig. 5. Matlab interface for predicting TPC and TSC from *C. caeruleus* L. rhizome.

and 0.96 respectively (Fig. 4), where the RMSE of TSC is 0.0027 (Abs) (Table 5).

To evaluate the prediction accuracy of the SVR-DA model, different metrics including the RMSE, R^2, AARD, MRPE, MAE, RSD are calculated and their values are shown in Table 6, where the optimized SVR-DA model presents the predictive R^2 = 0.9951, RMSE = 4.2702, and AARD, MRPE, RSD, MAE were 0.6460%, 5.9748%, 1.6881%, 1.6165 respectively. These results confirmed that the optimized model is more suitable for modeling using limited experimental data and exhibited higher prediction accuracy. In addition, the marginal loss between the R^2 for training and validation of an optimal SVR-DA model is insignificant which indicated its high generalization performance in terms of R^2. These findings were in agreement with the results of Benimam, Moussa, Hentabli, Hanini and Laidi [38] and Mesellem, Hadj, Laidi, Hanini and Hentabli [44]. Moreover, to provide an easy way to predict the total phenolic and saponin content, from *C. caeruleus* L. rhizome a Matlab graphical user interface was designed for executing the optimized SVR-DA model (Fig. 5). It is a powerful tool with direct utilization to calculate the output variables (TPC, TSC) at the same time by selecting the desired values of the extraction conditions including concentration of solvent (%), temperature (°C), time (min), solvent to solid ratio (mL.g^{-1}).

3.8. Antioxidant activity of C. caeruleus L

C. caeruleus L. was used for therapeutic benefit for many years, in this study, The optimal rhizome's extract under the optimal extraction parameters including a methanol concentration of 78.66%, a solvent to solid ratio of 23 mL.g^{-1}, a temperature of 50 °C and 26 min sonication time obtained by BBD design was used to evaluate its antioxidant activity using different antioxidant assays including DPPH$^{\bullet}$, ABTS$^{\bullet}$, reducing power, and phosphomolybdenum assays, which are based on different mechanisms. Furthermore, the antioxidant activity of *C. caeruleus* L. leaves extract under the same optimal conditions was also studied. The results obtained are illustrated in figures A.3 - A.6. From DPPH$^{\bullet}$ scavenging activity's results, the leaves part exhibited higher scavenging free radical activity with an IC_{50} of 0.157 ± 0.003 mg/mL of lyophilized powder, which the IC_{50} of rhizome was 1.606 ± 0.05 mg/mL of lyophilized powder (Fig. A3). The same tendency was observed in the decolorization of ABTS$^{\bullet}$ radical with the antioxidant of different parts of the plant, where the IC_{50} of leaves was 0.191 ± 0.003 mg/mL and the IC_{50} of rhizome was 0.950 ± 0.022 mg/mL (Fig. A4). These results confirmed that the leaves part of *C. caeruleus* L. showed the highest antioxidant capacity than the rhizome part, although, the rhizome and leaves the part of *C. caeruleus* L. exhibited the higher capacity of scavenging free radical than the rhizome extract of the same medicinal plant extracted using accelerated solvent extraction [66]. On other hand, *C. caeruleus* L. also showed higher capacity than *Carthamus tinctorius* L. seed [67].

The total antioxidant activity of different parts of *C. caeruleus* L. was also measured using phosphomolybdenum assay, the leaves part showed higher TAC than rhizome, at 1 mg/mL of lyophilized extract the TAC were 90.917 ± 1.628 mg EAA/g, and 33,551 ± 0,735 mg EAA/g for leaves and rhizome respectively (Fig. A5). In addition, in the reducing power test, the two parts of the plant showed a great capacity of reduction of ferric (Fe^{3+}) iron to the ferrous (Fe^{2+}) molecules, where the highest value was observed for the leaves part with 1698 ± 0.007 of absorbance. While, the absorbance of the rhizome part was 0,206 ± 0,013 at a concentration of 1 mg/mL of lyophilized extract, but in this case, the ascorbic acid was more effective for reducing power than *C. caeruleus* L. (Fig. A6). The higher and lower antioxidant activity of leaves and rhizome of *C. caeruleus* L. may be explained by the fact that the leaves produce bioactive molecules that display a higher donating capacity of hydrogen ions than the molecules produced by the rhizome part. Silva, Herdeiro, Mathias, Panek, Silveira, Rodrigues, Renno, Falcao, Cerqueira, Minto, Nogueira, Quaresma, Silva, Menezes and Eleutherio [68] reported that the structure of bioactive molecules of both planar and spatial it is important for the antioxidant activity, and the molecules derived from the shikimate pathway displayed more antioxidant potential than derived from the acetate pathway, which can avoid oxidative damage of cell membranes.

4. Conclusion

To summarize, the optimization of ultrasonic-assisted extraction of phenolic-saponin fraction from the rhizome of *Carthamus caeruleus* L. using Box-Behnken design based on response surface methodology is successfully achieved. The independent factors including time, temperature, solvent to solid ratio, the concentration of solvent are the most important parameter that affected the UAE method, which the optimum extraction conditions were 78.66% methanol concentration with a solvent to solid ratio of 23 mL g^{-1} at a temperature of 50 °C and 26 min of extraction time.

The support vector regression optimized with the dragonfly algorithm shows high accuracy to predict the TPC and TSC from *C. caeruleus* L. rhizome with good correlative (R^2 = 0.99, and low RMSE). In addition, Matlab graphical user interface was designed for predicting the TPC and TSC from *C. caeruleus* L. rhizome.

The optimal extract of rhizome and leaves extract exhibit a high potential of scavenging free radicals with IC_{50} 0.951 ± 0.022 and 0.196 ± 0.0029 mg/mL and IC_{50} of 0.106 ± 0.001 and 1.637 ± 0.025 mg/mL of lyophilized powder for ABTS and DPPH assay respectively. As well as the leaves and rhizome show higher antioxidant capacity for reducing power and phosphomolybdenum assay. In folk medicine, the rhizome of

Table 6
Prediction performance of SVR-DA to predict TPC and TSC from rhizome of *C. caeruleus* L.

	RMSE	R^2	R	b	slop	AARD (%)	MRPE (%)	MAE	RSD (%)
Training	0.1829	1.0000	1.0000	0.2245	0.9991	0.0593	0.1087	0.1570	0.0720
Validation	9.5415	0.9722	0,9933	-12.9697	1.0716	2.9927	5.9748	7.4548	4.0517
All	4.2702	0.9951	0,9978	-1.6218	1.0101	0.6460	5.9748	1.6165	1.6881

C. caeruleus L. was used for healing burns and wounds, where, saponin and phenolic compounds are considered as major bioactive compounds that are involved in the healing process, therefore, our study provides a powerful tool using the Matlab interface to predict TPC and TSC that can be employed in the pharmaceutical industry.

Authorship contributions

Category 1.

Conception and design of study: H. Moussa, F. Dahmoune.

Software: H. Moussa, F. Dahmoune, M. Hentabli.

Acquisition of data: H. Moussa.

Analysis and/or interpretation of data: H. Moussa, F. Dahmoune, M. Hentabli.

Category 2.

Supervision: F. Dahmoune, H. Remini.

Drafting the manuscript: H. Moussa, F. Dahmoune.

Revising the manuscript critically for important intellectual content: H. Moussa, F. Dahmoune, H. Remini, L. Mouni.

Category 3.

Approval of the version of the manuscript to be published: H. Moussa, F. Dahmoune, M. Hentabli, H. Remini, L. Mouni.

Funding

This research did not receive any specific grant from funding agencies in the public, commercial, or not-for-profit sectors.

Declaration of competing interest

The authors declare that they have no known competing financial interests or personal relationships that could have appeared to influence the work reported in this paper.

Acknowledgements

Hamza Moussa designed and carried out the experiments and wrote the manuscript, as well as optimization process, Mohamed Hentabli designed the SVR-DA for this study, Farid Dahmoune and Hocine Remini, Mouni Loutfi supervised and reviewed the final manuscript. All authors read and approved the final manuscript.

Appendix A. Supplementary data

Supplementary data related to this article can be found at https://doi.org/10.1016/j.chemolab.2022.104493.

References

[1] M.J. Adams, Chemometrics in Analytical Spectroscopy, Royal Society of Chemistry, 2004.
[2] C. Apel, J.G. Lyng, K. Papoutsis, S.M. Harrison, N.P. Brunton, Screening the effect of different extraction methods (ultrasound-assisted extraction and solid–liquid extraction) on the recovery of glycoalkaloids from potato peels: optimisation of the extraction conditions using chemometric tools, Food Bioprod. Process. 119 (2020) 277–286.
[3] E.E. Santos, R.C. Amaro, C.C.C. Bustamante, M.H.A. Guerra, L.C. Soares, R.E.S. Froes, Extraction of pectin from agroindustrial residue with an ecofriendly solvent: use of FTIR and chemometrics to differentiate pectins according to degree of methyl esterification, Food Hydrocolloids 107 (2020) 105921.
[4] N. Kumar, A. Bansal, G.S. Sarma, R.K. Rawal, Chemometrics tools used in analytical chemistry: an overview, Talanta 123 (2014) 186–199.
[5] S.L. Ferreira, R.E. Bruns, H.S. Ferreira, G.D. Matos, J.M. David, G.C. Brandao, E.G. da Silva, L.A. Portugal, P.S. dos Reis, A.S. Souza, W.N. dos Santos, Box-Behnken design: an alternative for the optimization of analytical methods, Anal. Chim. Acta 597 (2007) 179–186.
[6] I.M. Savic, I.M. Savic Gajic, Optimization of ultrasound-assisted extraction of polyphenols from wheatgrass (*Triticum aestivum* L.), J. Food Sci. Technol. 57 (2020) 2809–2818.
[7] K. Yetilmezsoy, S. Demirel, R.J. Vanderbei, Response surface modeling of Pb(II) removal from aqueous solution by *Pistacia vera* L.: Box-Behnken experimental design, J. Hazard Mater. 171 (2009) 551–562.
[8] F. Dahmoune, G. Spigno, K. Moussi, H. Remini, A. Cherbal, K. Madani, *Pistacia lentiscus* leaves as a source of phenolic compounds: microwave-assisted extraction optimized and compared with ultrasound-assisted and conventional solvent extraction, Ind. Crop. Prod. 61 (2014) 31–40.
[9] J. Prakash Maran, S. Manikandan, K. Thirugnanasambandham, C. Vigna Nivetha, R. Dinesh, Box-Behnken design based statistical modeling for ultrasound-assisted extraction of corn silk polysaccharide, Carbohydr. Polym. 92 (2013) 604–611.
[10] Y. Ma, G. Guo, Support Vector Machines Applications, 2014. Springer.
[11] J. Cervantes, F. Garcia-Lamont, L. Rodríguez-Mazahua, A. Lopez, A comprehensive survey on support vector machine classification: applications, challenges and trends, Neurocomputing 408 (2020) 189–215.
[12] Y. Xu, S. Zomer, R.G. Brereton, Support vector machines: a recent method for classification in chemometrics, Crit. Rev. Anal. Chem. 36 (2006) 177–188.
[13] S.R. Amendolia, G. Cossu, M. Ganadu, B. Golosio, G.L. Masala, G.M. Mura, A comparative study of k-nearest neighbour, support vector machine and multi-layer perceptron for thalassemia screening, Chemometr. Intell. Lab. Syst. 69 (2003) 13–20.
[14] U. Thissen, M. Pepers, B. Üstün, W.J. Melssen, L.M.C. Buydens, Comparing support vector machines to PLS for spectral regression applications, Chemometr. Intell. Lab. Syst. 73 (2004) 169–179.
[15] W. Wu, X. Wang, D. Xie, H. Liu, Soil water content forecasting by support vector machine in purple hilly region, in: International Conference on Computer and Computing Technologies in Agriculture, Springer, 2007, pp. 223–230.
[16] A.A. Jafarzadeh, M. Pal, M. Servati, M.H. FazeliFard, M.A. Ghorbani, Comparative analysis of support vector machine and artificial neural network models for soil cation exchange capacity prediction, Int. J. Environ. Sci. Technol. 13 (2015) 87–96.
[17] N.K.C. Twarakavi, J. Šimůnek, M.G. Schaap, Development of pedotransfer functions for estimation of soil hydraulic parameters using support vector machines, Soil Sci. Soc. Am. J. 73 (2009) 1443–1452.
[18] T. Xie, J. Yao, Z. Zhou, DA-based parameter optimization of combined kernel support vector machine for cancer diagnosis, Processes 7 (2019) 263.
[19] M. Laidi, e.H.A. Abdallah, C. Si-Moussa, O. Benkortebi, M. Hentabli, S. Hanini, CMC of diverse Gemini surfactants modelling using a hybrid approach combining SVR-DA, Chem. Ind. Chem. Eng. Q. (2020), 48-48.
[20] R.-E. Ghitescu, S. Curteanu, C. Mihailescu, I. Volf, F. Leon, A.I. Gilca, V.I. Popa, Support vector machine combined with genetic algorithm for optimization of microwave-assisted extraction of polyphenols from spruce wood bark, Cellul. Chem. Technol. 51 (2017) 203–213.
[21] A. Benhamou, F. Fazouane, Ethnobotanical Study, Phytochemical Characterization and Healing Effect of *Carthamus Caeruleus* L. Rhizomes, 2013.
[22] M.M. Dahmani, R. Laoufi, O. Selama, K. Arab, Gas chromatography coupled to mass spectrometry characterization, anti-inflammatory effect, wound-healing potential, and hair growth-promoting activity of Algerian *Carthamus caeruleus* L (Asteraceae), Indian J. Pharmacol. 50 (2018) 123–129.
[23] S. Karima, S. Farida, Z.M. Mihoub, Antimicrobial activity of an Algerian medicinal plant: *Carthamus caeruleus* L, Pharmacogn. Commun. 3 (2013).
[24] J.F. D'Mello, C.M. Duffus, J.H. Duffus, Toxic Substances in Crop Plants, Woodhead Publishing, 1991.
[25] J.B. Press, R.C. Reynolds, R.D. May, D.J. Marciani, Structure/function relationships of immunostimulating saponins, in: Studies in Natural Products Chemistry, 2000, pp. 131–174. Elsevier.
[26] T. Furuya, Saponins (Ginseng Saponins), Phytochemicals in Plant Cell Cultures, Elsevier, 1988, pp. 213–234.
[27] Y. Kimura, M. Sumiyoshi, K. Kawahira, M. Sakanaka, Effects of ginseng saponins isolated from Red Ginseng roots on burn wound healing in mice, Br. J. Pharmacol. 148 (2006) 860–870.
[28] Q.V. Vuong, S. Hirun, T.L.K. Chuen, C.D. Goldsmith, S. Murchie, M.C. Bowyer, P.A. Phillips, C.J. Scarlett, Antioxidant and anticancer capacity of saponin-enriched *Carica papaya* leaf extracts, Int. J. Food Sci. Technol. 50 (2015) 169–177.
[29] M.L. Luna-Guevara, J.J. Luna-Guevara, P. Hernández-Carranza, H. Ruíz-Espinosa, C.E. Ochoa-Velasco, Phenolic compounds: a good choice against chronic degenerative diseases 59 (2018) 79–108.
[30] B.J. Arroyo, A.P. Santos, E. de Almeida de Melo, A. Campos, L. Lins, L.C. Boyano-Orozco, Bioactive Compounds and Their Potential Use as Ingredients for Food and its Application in Food Packaging, 2019, pp. 143–156.
[31] T. Garde-Cerdán, A. Gonzalo-Diago, E.P. Pérez-Álvarez, Phenolic Compounds: Types, Effects and Research, Nova Science Publishers, 2017.
[32] P. Panja, Green extraction methods of food polyphenols from vegetable materials, Curr. Opin. Food Sci. 23 (2018) 173–182.
[33] F. Chemat, M. Abert-Vian, A.S. Fabiano-Tixier, J. Strube, L. Uhlenbrock, V. Gunjevic, G. Cravotto, Green extraction of natural products. Origins, current status, and future challenges, Trac. Trends Anal. Chem. 118 (2019) 248–263.
[34] M. Awad, R. Khanna, Support Vector Regression, Efficient Learning Machines, Springer, 2015, pp. 67–80.
[35] S. Mirjalili, Dragonfly algorithm: a new meta-heuristic optimization technique for solving single-objective, discrete, and multi-objective problems, Neural Comput. Appl. 27 (2015) 1053–1073.
[36] Dragonfly algorithm in 2020: review, Commun. Mathemat Biology Neurosci. (2021).
[37] Y. Meraihi, A. Ramdane-Cherif, D. Acheli, M. Mahseur, Dragonfly algorithm: a comprehensive review and applications, Neural Comput. Appl. 32 (2020) 16625–16646.

[38] H. Benimam, C.S. Moussa, M. Hentabli, S. Hanini, M. Laidi, Dragonfly-support vector machine for regression modeling of the activity coefficient at infinite dilution of solutes in imidazolium ionic liquids using σ-profile descriptors, J. Chem. Eng. Data 65 (2020) 3161–3172.
[39] P.-S. Yu, S.-T. Chen, I.F. Chang, Support vector regression for real-time flood stage forecasting, J. Hydrol. 328 (2006) 704–716.
[40] D.A. Pisner, D.M. Schnyer, Support Vector Machine, 2020, pp. 101–121.
[41] M. Abdelkader, A. Amrane, M. Hentabli, S. Hanini, M. Laidi, A grey Wolf optimizer-based fractional calculus in studies on solar drying, Kemija u Industriji 70 (2021) 39–47.
[42] M. Hentabli, A.-E. Belhadj, H. Benimam, F. Dahmoune, S. Keskes, Vacuum drying of the Terbinafine HCl powder: a kinetics study and mathematical modeling, Powder Technol. 383 (2021) 220–232.
[43] Y. Mesllem, M. Hentabli, S. Hanini, M. Laidi, A.E.H. Abdallah, Artificial neural network modelling of multi-system dynamic adsorption of organic pollutants on activated carbon, Kemija u Industriji 70 (2021) 1–12.
[44] Y. Mesellem, A.A.E. Hadj, M. Laidi, S. Hanini, M. Hentabli, Computational Intelligence Techniques for Modeling of Dynamic Adsorption of Organic Pollutants on Activated Carbon, Neural Computing and Applications, 2021.
[45] S. Georgé, P. Brat, P. Alter, M.J. Amiot, Rapid determination of polyphenols and vitamin C in plant-derived products, J. Agric. Food Chem. 53 (2005) 1370–1373.
[46] S. Hiai, H. Oura, T. Nakajima, Color reaction of some sapogenins and saponins with vanillin and sulfur1c acid, Planta Med. 29 (1976) 116–122.
[47] F. Dahmoune, H. Remini, S. Dairi, O. Aoun, K. Moussi, N. Bouaoudia-Madi, N. Adjeroud, N. Kadri, K. Lefsih, L. Boughani, L. Mouni, B. Nayak, K. Madani, Ultrasound assisted extraction of phenolic compounds from P. lentiscus L. leaves: comparative study of artificial neural network (ANN) versus degree of experiment for prediction ability of phenolic compounds recovery, Ind. Crop. Prod. 77 (2015) 251–261.
[48] P. Prieto, M. Pineda, M. Aguilar, Spectrophotometric quantitation of antioxidant capacity through the formation of a phosphomolybdenum complex: specific application to the determination of vitamin E, Anal. Biochem. 269 (1999) 337–341.
[49] M. Oyaizu, Studies on products of browning reaction antioxidative activities of products of browning reaction prepared from glucosamine, Japanese J. Nutrition Dietetics 44 (1986) 307–315.
[50] S. Jang, A.Y. Lee, A.R. Lee, G. Choi, H.K. Kim, Optimization of ultrasound-assisted extraction of glycyrrhizic acid from licorice using response surface methodology, Integrat. Med. Res. 6 (2017) 388–394.
[51] H.N.T. Pham, Q.V. Vuong, M.C. Bowyer, C.J. Scarlett, Optimization of ultrasound-assisted extraction of *Helicteres hirsuta* Lour. for enhanced total phenolic compound and antioxidant yield, J. Appl. Res. Med. Aromatic Plants 7 (2017) 113–123.
[52] S.S. Teh, E.J. Birch, Effect of ultrasonic treatment on the polyphenol content and antioxidant capacity of extract from defatted hemp, flax and canola seed cakes, Ultrason. Sonochem. 21 (2014) 346–353.
[53] A. Ali, X.Y. Lim, C.H. Chong, S.H. Mah, B.L. Chua, Optimization of ultrasound-assisted extraction of natural antioxidants from *Piper betle* using response surface methodology, LWT (Lebensm.-Wiss. & Technol.) 89 (2018) 681–688.
[54] C.Y. Cheok, N.L. Chin, Y.A. Yusof, R.A. Talib, C.L. Law, Optimization of total phenolic content extracted from *Garcinia mangostana* Linn. hull using response surface methodology versus artificial neural network, Ind. Crop. Prod. 40 (2012) 247–253.
[55] E.V. Anslyn, D.A. Dougherty, Modern Physical Organic Chemistry, University science books, 2006.
[56] B. Sarvin, E. Stekolshchikova, I. Rodin, A. Stavrianidi, O. Shpigun, Optimization and comparison of different techniques for complete extraction of saponins from *T. terrestris*, J. Appl. Res. Med. Aromatic Plants 8 (2018) 75–82.
[57] B.L. Shrestha, O.D. Baik, Methanol-water extraction of saponins from seeds of Saponaria vaccaria L.— calibration equation, extraction condition analysis, and modeling, Separ. Sci. Technol. 47 (2012) 1977–1984.
[58] M. Hadidi, A. Ibarz, J. Pagan, Optimisation and kinetic study of the ultrasonic-assisted extraction of total saponins from alfalfa (*Medicago sativa*) and its bioaccessibility using the response surface methodology, Food Chem. 309 (2020) 125786.
[59] H. Zhang, J. Birch, C. Xie, H. Yang, A. El-Din Bekhit, Optimization of ultrasound assisted extraction method for phytochemical compounds and in-vitro antioxidant activity of New Zealand and China Asparagus cultivars (*officinalis* L.) roots extracts, Food Chem. 294 (2019) 276–284.
[60] Z.Y. Shao, J.X. Fu, Y.X. Qi, Q.C. Zhao, Z.B. Li, Optimization of ultrasonic-assisted extraction of total saponins from *Ophiopholis mirabilis* using response surface methodology, Adv. Mater. Res. 781–784 (2013) 687–693.
[61] J. Dong, Y. Liu, Z. Liang, W. Wang, Investigation on ultrasound-assisted extraction of salvianolic acid B from *Salvia miltiorrhiza* root, Ultrason. Sonochem. 17 (2010) 61–65.
[62] Y.-q. Tian, H.-t. Zhao, X.-l. Zhang, W.-t. Zhang, X.-c. Liu, S.-h. Gao, Comparison of different extraction techniques and optimization of the microwave-assisted extraction of saponins from Aralia elata (Miq.) Seem fruits and rachises, Chem. Pap. 74 (2020) 3077–3087.
[63] D.J. Obermiller, Multiple Response Optimization Using JMP, The Dow chemical company, Midland, MI, 2000.
[64] G. Derringer, R. Suich, Simultaneous optimization of several response variables, J. Qual. Technol. 12 (1980) 214–219.
[65] I. Soekarno, I.K. Hadihardaja, M. Cahyono, A study of hold-out and k-fold cross validation for accuracy of groundwater modeling in tidal lowland reclamation using extreme learning machine, in: 2nd International Conference on Technology, Informatics, Management, Engineering & Environment, 2014.
[66] A. Toubane, S.A. Rezzoug, C. Besombes, K. Daoud, Optimization of accelerated solvent extraction of *Carthamus caeruleus* L. Evaluation of antioxidant and anti-inflammatory activity of extracts, Ind. Crop. Prod. 97 (2017) 620–631.
[67] S.Y. Yu, Y.J. Lee, J.D. Kim, S.N. Kang, S.K. Lee, J.Y. Jang, H.K. Lee, J.H. Lim, O.H. Lee, Phenolic composition, antioxidant activity and anti-adipogenic effect of hot water extract from safflower (*Carthamus tinctorius* L.) seed, Nutrients 5 (2013) 4894–4907.
[68] C.G. Silva, R.S. Herdeiro, C.J. Mathias, A.D. Panek, C.S. Silveira, V.P. Rodrigues, M.N. Renno, D.Q. Falcao, D.M. Cerqueira, A.B. Minto, F.L. Nogueira, C.H. Quaresma, J.F. Silva, F.S. Menezes, E.C. Eleutherio, Evaluation of antioxidant activity of Brazilian plants, Pharmacol. Res. 52 (2005) 229–233.

Farid Dahmoune - Département des Sciences Biologiques, Faculté des Sciences de la Nature et de la Vie et des Sciences de la Terre, Université de Bouira, 10000 Bouira, Algérie; Laboratoire de Biomathématiques, Biophysique Biochimie et de Scientométrie (LBBBS), Université Abderrahmane Mira de Béjaïa, Béjaïa 06000, Algérie.

Mohamed Hentabli - Laboratoire de Biomatériaux et Phénomènes de Transport (LBMPT), Université Yahia Fares de Médéa, Médéa, 26000, Algérie

Hocine Remini - Département des Sciences Biologiques, Faculté des Sciences de la Nature et de la Vie et des Sciences de la Terre, Université de Bouira, 10000 Bouira, Algérie; Laboratoire de Biomathématiques, Biophysique Biochimie et de Scientométrie (LBBBS), Université Abderrahmane Mira de Béjaïa, Béjaïa 06000, Algérie.

Lotfi Mouni - Laboratoire de Gestion et Valorisation des Ressources Naturelles et Assurance Qualité (LGVRNAQ), Faculté des Sciences de la Nature et de la Vie et des Sciences de la Terre, Université de Bouira, 10000 Bouira, Algérie

Sustainable Chemistry and Pharmacy 29 (2022) 100820

Contents lists available at ScienceDirect

Sustainable Chemistry and Pharmacy

journal homepage: www.elsevier.com/locate/scp

Definitive screening design and *I*-optimal design for optimization of ultrasound-assisted extraction of phenolic content and antioxidant capacity from *Salvia officinalis* L. leaves

Hamza Moussa [a,b,*], Farid Dahmoune [b,c], Mohamed malik Mahdjoub [b], Nabil Kadri [b,c], Hocine Remini [b,c]

[a] *Laboratoire de Gestion et Valorisation des Ressources Naturelles et Assurance Qualité (LGVRNAQ), Faculté des Sciences de la Nature et de la Vie et des Sciences de la Terre, Université de Bouira, 10000, Bouira, Algeria*

[b] *Département des Sciences Biologiques, Faculté des Sciences de la Nature et de la Vie et des Sciences de la Terre, Université de Bouira, 10000, Bouira, Algeria*

[c] *Laboratoire de Biomathématiques, Biophysique Biochimie et de Scientométrie (LBBBS), Université Abderrahmane Mira de Béjaïa, Béjaïa, 06000, Algeria*

ARTICLE INFO

Keywords:
Multivariate optimization
D-optimal design
Custom design
Ultrasound-assisted extraction
Biological activities

ABSTRACT

A definitive screening design and an *I*-optimal design were carried out for the screening and optimization of ultrasound's extraction conditions of total phenolic compounds (TPC) and antioxidant capacities (TEAC and TAC) from *S. officinalis* L. leaves. The optimal conditions for maximum TPC, TEAC, and TAC were 52% ethanol-water, 60 °C temperature, 30 mL g^{-1} solvent to solid ratio, and 10 min of extraction time. The optimal extract showed higher TPC, TEAC, and TAC with 31.84 ± 0.248 mg_{GAE}/g_{dw}, 237.95 ± 0.771 $\mu mol_{TE}/g_{dw}$, and 38.928 ± 0.548 mg_{AAE}/g_{dw} respectively. Furthermore, the optimal extract obtained exhibited a higher scavenging activity against $DPPH^{\bullet}$, $NO^{\bullet}$ free radicals, and β-carotene/linoleic acid bleaching activity with IC_{50} of 0.276 ± 0.001 mg/mL, and 0.069 ± 0.0005 mg/mL, and 0.159 ± 0.008 mg/mL respectively. The reducing power of the optimal extract at 0.3 mg/mL of lyophilized powder was approximately 2 mmol Fe+2 equivalent/g. Thus, *S. officinalis* L. leaves are expected to be an excellent source for pharmaceutical and cosmetic industries for developing potential drugs.

1. Introduction

The common sage (*Salvia officinalis* L.) belongs to the *Lamiaceae* family, which is a perennial plant with woody stems and grayish leaves (Mitić and Tošić, 2019). The sage is native to the Mediterranean region and is cultivated worldwide (Dent 2015), which is a valuable medicinal plant used traditionally as an herbal tea, spice, and food flavoring agent (Zekovic and Pintac, 2017). Sage has been used industrially in the production of several pharmaceutic formulations or food preservation owing to its wide range of biological activities, including antimicrobial, preservative, immunomodulatory, antioxidant, and anticancer proprieties (Glisic and Ristic, 2011; Zekovic and Pintac, 2017). These biological activities have been attributed to the phenolic compounds present in *S. officinalis* L. including carnosolic acid, carnosol, rosmarinic acid, rosmanol, epirosmanol, and isorosmanol (Dent 2015; Pavlić and Vidović, 2016). However, sage also contains several volatile compounds such as thujone, which possesses a certain toxicity, and the allowed

* Corresponding author.GVRNAQ Laboratory, Bouira University, Rue Drissi Yahia Bouira, 10000, Algeria.
E-mail address: h.moussa@univ-bouira.dz (H. Moussa).

https://doi.org/10.1016/j.scp.2022.100820
Received 3 April 2022; Received in revised form 13 July 2022; Accepted 15 August 2022

concentration in food products is 0.5 mg/kg (Mocan and Babota, 2020). Furthermore, it has been reported that the chemical composition and relative variability of *S. officinalis* L. are correlated to several factors such as environmental, physiological factors including genotypes, environmental stress, agronomic procedures, climatic change, and culture site (Mocan and Babota, 2020).

For better extractability of bioactive compounds from medicinal plants, various novel extraction techniques have been developed, where ultrasound-assisted extraction (UAE) has been the most popular method in recent years due to its advantage of minimizing time, extraction solvent, and energy consumption (Ghafoor and Choi, 2009; Hossain and Brunton, 2012; Shivamathi and Moorthy, 2019; Liu and Liu, 2021). In this context, the extraction parameters used in ultrasound, such as concentration of the solvent, time, temperature, and solid to solvent ratio, are important and should be optimized using experimental designs and predictive models to enhance the quality and quantity of bioactive compounds. Box-Behnken and central composite design as experimental design were the most used in the optimization process (Shivamathi and Moorthy, 2019; Liu and Liu, 2021; Moussa and Dahmoune, 2022).

Definitive screening design (DSD) is a new class of three-level design for definitive screening of quantitative and qualitative variables. The DSD was proposed by Jones and Nachtsheim (2011). DSD has several desirable advantages, including that the number of runs required for DSD construction is one more than twice the number of factors (Jones and Nachtsheim 2011). Contrary to fractional factorial design, the main effects are completely independent of two-factor interactions, and two-factor interactions are not completely aliased with other two-factor interactions (Jones and Nachtsheim 2011). Furthermore, a DSD could estimate all quadratic effects by adding center points where the quadratic effects are orthogonal to the main effect and not completely aliased (Jones and Nachtsheim 2011). The DSD with six through twelve independent variables shows the capability of estimating full quadratic models including two or three factors (Jones and Nachtsheim 2011). DSD was employed as a chemometric method to optimize mass spectrometry (UPLC-MS/MS) parameters using standard glycans (Hecht and McCord, 2015). In addition, the DSD was applied to investigate the electrochemical decolorization of the reactive violet azo dye Reactive Violet 5 (RV5) that is used in textile dyeing, where its poor fixation to the fiber leads to a negative impact on the environment and human health, due to the toxicity and potential carcinogenicity (Fidaleo and Lavecchia, 2016). DSD was also used to investigate the effects of temperature, time and solvent concentration on direct biodiesel production from wet microalgae (Felix and Ubando, 2019).

Moreover, the optimal design (custom design) is a flexible special design that was employed for both screening and optimization processes using the *I*-optimality and *D*-optimality criteria. The optimal design creates the optimal set of experiments based on the coordinate-exchange algorithm proposed by Meyer and Nachtsheim (1995), The optimal design provides maximum accuracy in estimating regression coefficients because it was the best combination of experimental runs that were selected. (Haji and Qavamnia, 2018). In addition, it has been reported that the optimal design is generally applied for cost analysis and product formulation in the food and pharmaceutical industries (Cigeroglu and Aras, 2018). The optimal design produces a very flat fraction of the design space curves for most of the design space (Oladipo and Betiku 2019), which makes the optimal design more suitable for predicting the maximum of oleuropein from olive leaves using an ultrasonic probe (Vural et al., 2021). The optimal design was also employed for the optimization of both quantitative and qualitative variables used for the ultrasound-assisted extraction of bioactive compounds from medicinal plants (Cigeroglu and Aras, 2018; Turker and Isleroglu 2021).

The effect of UAE conditions on the extraction of phenolic compounds from medicinal plants using classical experimental designs such as full factorial design, Box-Behnken, central composite design, etc., have been extensively investigated (Pavlić and Vidović, 2016; Su and Pham, 2020; Brahmi and Blando, 2022; Carrasco-Sandoval and Falcó, 2022). To the best of our knowledge, there is a paucity of studies regarding the effects of UAE conditions on the extraction of phenolic compounds and antioxidant capacity of *S. officinalis* L. leaves using new classes of experimental designs such as DSD and *I*-optimal design.

The current study aimed to screen the UAE extraction conditions of phenolic compounds (TPC) and antioxidant capacity, including Trolox equivalent antioxidant capacity (TEAC) and total antioxidant capacity (TAC) from *S. officinalis* L. using a new class of experimental design, including DSD. After the screening process, the *I*-optimal design was carried out to optimize the effect of UAE extraction parameters for enhancing the TPC, TEAC, and TAC from *S. officinalis* L. Furthermore, the optimal extract was evaluated using several assays, including $DPPH^{\bullet}$, $NO^{\bullet}$ scavenging activity, β-carotene/linoleic acid bleaching activity, and reducing power.

2. Materials and methods

2.1. Materials

Methanol, ethanol, and chloroform were purchased from SIGMA-ALDRICH, sodium carbonate (Na_2CO_3), and DPPH ($2,2-$ Diphenyl $-1-$ picrylhydrazyl), ABTS ($2,2^{'}-$ azino $-$ bis $(3-$ ethylbenzothiazoline $-6-$ sulfonic acid$)$), potassium persulfate ($K_2S_2O_8$), TPTZ (2,4,6-tripyridyl-*s*-triazine), β-carotene, linoleic acid, trichloroacetic acid ($C_2HCl_3O_2$), ferric chloride ($FeCl_3$), Gallic acid, Trolox, ascorbic acid, Phosphoric acid, Dimethyl sulfoxide ($(CH_3)_2SO$), Folin-Ciocalteu's reagent, ammonium molybdate tetrahydrate ($(NH_4)_6Mo_7O_{24}\cdot 4H_2O$), sodium phosphate monobasic ($NaH_2PO_4\cdot H_2O$), and sodium phosphate dibasic ($Na_2HPO_4\cdot 12H_2O$) were purchased from VWR CHEMICALS. Sodium nitroprusside ($Na_2[Fe(CN)_5NO]2H_2O$), Sulfanilamide ($C_6H_8N_2O_2S$), naphthyl-ethylenediamine dichloride ($C_{12}H_{14}N_2.2HCl$) were provided from Alfa Aesar.

2.2. Ultrasound-assisted extraction (UAE)

Fresh leaves of *S. Officinalis* L. were harvested from Ain Bessem (latitude 36.325295; longitude 3.674675, altitude 690 m) province of Bouira (Algeria) in April 2021. S. *officinalis* L. leaves were washed using distilled water to remove the impurities, and then they were oven-dried in a ventilated oven (MEMMERT, B319.0656, Germany) at 40 °C until the moisture level was constant. After the drying process, the leaves were milled using an electrical grinder (Moulinex, AR110510 French) and passed through a sieve with a diameter of

0.2 mm.

The phenolic compounds of *Salvia officinalis* L. leaves were extracted using an ultrasound-cleaning bath at 40 kHz (J.P. SELECTA, s. a, Spain, SN. 3000865, Power generator 120 W, Power heater 75 W) with cavity dimensions of 15 × 24 × 14 cm (H/W/D). This system includes two piezo-electric steel-aluminum transducers located at the bottom of the ultrasound bath. The UAE of phenolic compounds was carried out according to DSD and *I*-optimal design, where 1 g of powder of *S. officinalis* L. leaves was immersed in different volumes (10, 20, and 30 mL) of ethanol-water mixture (30%, 55%, and 80%). The samples were exposed to the sonication effect at different times (10, 35, and 60 min). The ultrasonic temperature were controlled by thermostat water bath and was adjusted using the ultrasound panel to 30, 45, and 60 °C. During the sonication process, the samples were poured into a 250-mL flat-bottom flask coupled with condenser placed in front of flask contain ice cubes to ensure that the temperature was always maintained constant. The ethanolic-water extracts were recovered by filtration using centrifugation (Sigma 3–16 L, 172577, Germany) at 5000 rpm for 10 min to eliminate insoluble matters and equilibrated to the final volume. *S. officinalis* L. extracts were stored at 4 °C for further analysis.

2.3. Optimization and prediction procedures

2.3.1. Definitive screening design

A DSD was used for screening the continuous factors to avoid confounding between the linear factors and interaction factors as well as to identify factors that have a nonlinear effect on the response. In this study, the DSD was used to identify the continuous factors that have the most substantial effects on the extraction of phenolic compounds and their bioactivities from *S. officinalis* L. leaves extracts. All the factors including x_1: ethanol-water mixture, x_2: sonication time, x_3: extraction temperature, x_4: solvent to solid ratio were studied at three levels, low, medium, and high level as shown in Table 1. The DSD's matrix of selected factors was constructed by JMP software 13.0.0 Pro, with high D-efficiency (85.61), G-efficiency (82.32), and A-efficiency (85.36). The average variance prediction of this design was 0.154, as depicted in Tables 4 and 5. To screen the effect of UAE factors on TPC, TEAC, and TAC, a matrix of 17 experiments including four extra runs was designed (Table 2). Moreover, the upper left corner of the color map of correlation from Fig. 1 confirms that the continuous main effects are uncorrelated with two-factor interaction effects; this means that any two-factor interactions will not bias several main effects.

2.3.2. I-Optimal design

The *I*-Optimality was established to optimize the phenolic compounds extracted from *S. officinalis* L. powder and their bioactivities against the TEAC and TAC assays. The *I*-optimal designs minimize the average variance of prediction over the design space (Rodríguez and Jones, 2017), Thus, the *I*-optimality criterion is more appropriate than *D*-optimality to predict a response, determine optimum operating conditions, and determine regions in the design space where the response falls within an acceptable range (Rodríguez and Jones, 2017). The prediction variance relative to the unknown error variance at a point x in the design space can be calculated using the following Eq. (1) (Goos 2012):

$$var\left(\widehat{Y}/\mathbf{x}\right) = f\left(\mathbf{x}\right)^{'}\left(\mathbf{X}^{'}\mathbf{X}\right)^{-1}f(\mathbf{x}) \tag{1}$$

where **X** is the model matrix.

I-optimal designs minimize the integral *I* of the prediction variance over the entire design space, where *I* is given as follows(Eq. (2)) (Goos 2012):

$$I = \int_R f(\mathbf{x})^{'}\left(\mathbf{X}^{'}\mathbf{X}\right)^{-1}f(\mathbf{x})dx = trace\left[\left(\mathbf{X}^{'}\mathbf{X}\right)^{-1}\mathbf{M}\right] \tag{2}$$

where **M** is the moments' matrix (Eq. (3)),

$$\mathbf{M} = \int_R f(\mathbf{x})f(\mathbf{x})^{'}dx \tag{3}$$

To optimize *I*-optimality criteria, the coordinate-exchange algorithm of Meyer and Nachtsheim (1995) was used. The coordinate-exchange algorithm is repeated a large number of times with more than 40000 random starts until the maximum of the optimality criterion is achieved, as mentioned in Tables 4 and 5 The *D*, *G*, and *A*-efficiency obtained in this study were 42, 77, and 29, respectively. The average variance of prediction for this design was 0.351.

For three continuous factors and three responses, including TPC, TEAC, and TAC, the *I*-optimal matrix designed has 16 runs,

Tables 1
The input variables and their levels employed for the screening and optimization process.

	Levels		
Independent variables	−1	0	+1
x_1: Ethanol-water mixture (%)	30	55	80
x_2: Time (min)	10	35	60
x_3 : Temperature (°C)	30	45	60
x_4: solvent to solid ratio (mL.g^{-1})	10	20	30

Table 2
Definitive screening design Matrix with the four input and three output variables; TPC, TEAC and TAC.

Runs	x_1	x_2	x_3	x_4	TPC [a] experimental	TPC [a] Predict	TEAC [b] experimental	TEAC [b] Predict	TAC [C] experimental	TAC [C] predict
1	−1	−1	−1	+1	21.15 ± 0.46	20.99	186.32 ± 2.72	185.98	25.40 ± 0.26	26.12
2	−1	−1	+1	−1	8.99 ± 0.20	10.58	109.32 ± 1.48	111.79	13.67 ± 0.53	16.63
3	−1	−1	+1	+1	27.82 ± 0.19	25.99	223.31 ± 1.84	221.95	34.90 ± 0.22	33.21
4	−1	0	−1	−1	7.64 ± 0.33	5.788	71.27 ± 1.45	73.79	11.46 ± 0.13	9.04
5	−1	+1	−1	+1	19.48 ± 0.17	21.40	181.16 ± 2.55	181.93	23.47 ± 0.24	25.10
6	−1	+1	0	−1	7.20 ± 0.02	8.49	85.73 ± 0.29	89.75	11.20 ± 0.16	12.07
7	−1	+1	+1	0	22.72 ± 0.55	21.78	216.47 ± 2.63	208.39	28.63 ± 0.26	26.56
8	0	−1	−1	−1	16.77 ± 0.20	15.73	138.37 ± 1.48	128.27	24.55 ± 0.21	23.64
9	0	0	0	0	28.81 ± 0.45	28.69	234.25 ± 0.29	234.60	34.95 ± 0.11	35.30
10	0	+1	+1	+1	34.34 ± 0.24	35.49	240.06 ± 2.96	249.80	41.09 ± 0.15	41.64
11	+1	−1	−1	0	22.23 ± 0.42	23.29	195.12 ± 4.39	202.84	29.45 ± 0.12	31.16
12	+1	−1	0	+1	27.22 ± 0.13	29.35	207.72 ± 3.06	209.79	37.48 ± 0.22	35.69
13	+1	−1	+1	−1	16.02 ± 0.15	15.55	141.79 ± 2.66	141.45	25.01 ± 0.24	24.69
14	+1	0	+1	+1	31.64 ± 1.24	31.05	223.14 ± 3.63	220.00	35.60 ± 0.11	36.31
15	+1	+1	−1	−1	11.94 ± 0.44	12.97	108.98 ± 0.88	112.93	21.73 ± 0.05	21.41
16	+1	+1	−1	+1	30.88 ± 0.29	28.26	201.26 ± 1.84	193.51	33.67 ± 0.11	33.54
17	+1	+1	+1	−1	16.50 ± 0.24	15.96	139.91 ± 0.59	137.39	23.53 ± 0.13	23.67

TPC [a]: mg_{GAE}/g_{dw} (mg Gallic acid equivalent per g of dry weight), **TEAC [b]: $\mu mol_{TE}/g_{dw}$** (μmole Trolox equivalent per g of dry weight), **TAC [C]: mg_{AAE}/g_{dw}** (mg Ascorbic acid equivalent per g of dry weight), **TPC:** Total phenolic compounds, **TEAC:** Trolox equivalent antioxidant capacity, **TAC:** Total antioxidant capacity.

Table 3
I-Optimal design matrix with the three input variables and three output variables (TPC, TEAC, and TAC).

Runs	x_1	x_3	x_4	TPC [a] experimental	TPC [a] Predict	TEAC [b] experimental	TEAC [b] Predict	TAC [C] experimental	TAC [C] predict
1	−1	+1	+1	29.42 ± 0.25	29.31	228.35 ± 1.27	221.22	35.34 ± 0.15	34.26
2	−1	0	−1	9.79 ± 0.15	11.17	89.69 ± 2.78	84.50	14.70 ± 0.48	14.17
3	0	0	0	24.61 ± 0.40	24.99	216.88 ± 3.49	214.92	34.95 ± 0.11	34.17
4	0	0	+1	31.94 ± 0.13	31.05	240.35 ± 10.98	243.78	39.63 ± 0.62	39.80
5	+1	−1	+1	30.17 ± 0.11	30.48	218.93 ± 6.87	209.27	36.70 ± 0.64	35.50
6	+1	+1	+1	28.88 ± 0.22	28.84	191.60 ± 6.72	192.88	36.79 ± 0.07	37.30
7	0	0	0	25.39 ± 0.24	24.99	216.55 ± 3.22	214.92	34.54 ± 0.11	34.17
8	0	0	0	25.20 ± 0.07	24.99	227.05 ± 7.45	214.92	33.95 ± 0.13	34.17
9	0	+1	0	27.60 ± 0.07	29.05	210.48 ± 1.50	217.87	34.57 ± 0.06	35.34
10	+1	+1	−1	14.62 ± 0.60	14.35	152.70 ± 5.42	142.05	25.01 ± 0.69	23.65
11	−1	−1	+1	28.08 ± 0.10	28.81	182.08 ± 4.04	194.16	28.51 ± 0.59	30.11
12	+1	−1	−1	10.38 ± 0.25	10.64	126.38 ± 5.10	128.16	22.31 ± 0.38	23.08
13	+1	0	0	20.31 ± 0.46	20.03	178.14 ± 9.22	195.63	30.75 ± 0.43	32.03
14	−0.11	−1	−1	15.96 ± 0.30	15.61	110.73 ± 1.16	115.69	22.77 ± 0.63	22.74
15	−1	+1	−1	18.12 ± 15.96	17.10	96.76 ± 4.04	105.87	14.48 ± 0.46	15.62
16	−1	−1	0	22.92 ± 0.24	21.98	150.78 ± 6.58	141.61	24.67 ± 0.26	23.54

TPC [a]: mg_{GAE}/g_{dw} (mg Gallic acid equivalent per g of dry weight), **TEAC [b]: $\mu mol_{TE}/g_{dw}$** (μmole Trolox equivalent per g of dry weight), **TAC [C]: mg_{AAE}/g_{dw}** (mg Ascorbic acid equivalent per g of dry weight), **TPC:** Total phenolic compounds, **TEAC:** Trolox equivalent antioxidant capacity, **TAC:** Total antioxidant capacity.

Table 4
Equations used for the calculation of the efficiency parameters of DSD and optimal design.

Efficiency Parameter	Equations	References
D- efficiency	$100\left(\frac{1}{n}\lvert\mathbf{X}'\mathbf{X}\rvert^{1/p}\right)$	(Rodríguez and Jones, 2017)
A-efficiency	$100\,p/(n\mathrm{Trace}(\mathbf{X}'\mathbf{X})^{-1})$	(Jones and Allen-Moyer, 2020)
G- efficiency	$\max_{\mathbf{x}\in\mathbf{D}}\mathbf{f}'(\mathbf{x})(\mathbf{X}'\mathbf{X})^{-1}\mathbf{f}(\mathbf{x})$	Goos (2012)
Average variance of prediction	$\frac{1}{\int_D d\,\mathbf{x}} * trace\,[(\mathbf{X}'\mathbf{X})^{-1}\mathbf{M}]$	Goos and Jones (2011)

X is the model matrix, $\mathbf{X}'$ is transpose matrix, **x** is a vector of factor levels that corresponds to one of the runs of the design, then $\mathbf{f}'(\mathbf{x})$ is the corresponding row of the matrix **X,** $\mathbf{f}(\mathbf{x})$ is a function that takes a vector of factor settings and expands that vector to its corresponding model terms. *D* denotes the experimental region, *n* is the number of runs in the design, ***p*** is the number of terms including the intercept, **M** is called the moments matrix.

Table 5
Efficiency measures of definitive screening design and *I*-optimal design.

	DSD	Optimal Design
Optimality Criteria	/	*I*-Optimality
D-Efficiency	85.61	42.01
G-Efficiency	82.32	77.05
A-Efficiency	85.36	29.20
Average variance of prediction	0.154	0.3518

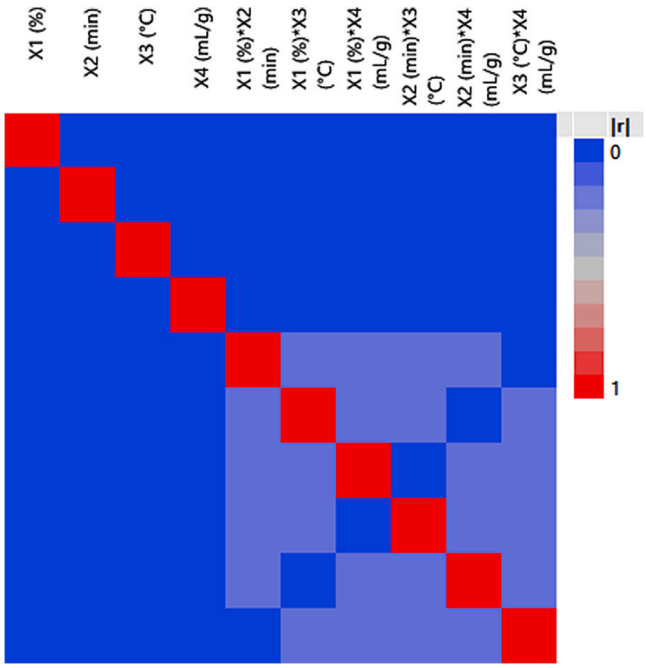

Fig. 1. Color maps of the definitive screening design for absolute correlations between UAE extraction parameters using an intensity scale. (For interpretation of the references to color in this figure legend, the reader is referred to the Web version of this article.)

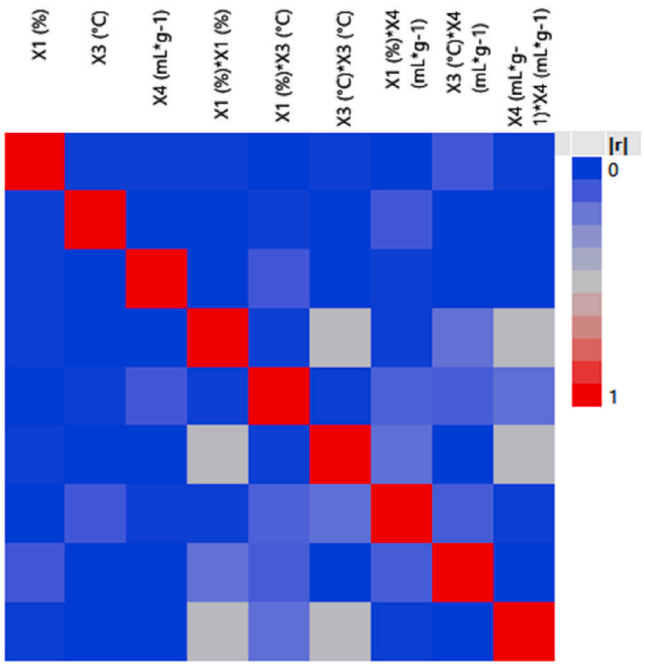

Fig. 2. Correlations maps of UAE extraction parameters using an intensity scale for *I*-optimal design.

including the center points (Table 3). The color map on correlations shows the correlation between the effects of the UAE extraction parameters (Fig. 2). The main effects are represented by the 4 terms in the upper left corner of the map. The deep blue color corresponds to the uncorrelated effects between the main effects and other main effects. This means that all main effects are orthogonal and can be estimated independently. The red line in Fig. 1b is on the main diagonal, reflecting that each extraction parameter is perfectly correlated with itself. It follows that no main effect is completely confounded by any two-way interaction.

The mathematical equations of DSD and *I*-optimal design (Eq. (4)) show the relation and the effect of each UAE factor on TPC, TEAC, or TAC (Goos and Jones 2011; Jones and Nachtsheim 2017).

$$y_i = B_0 + \sum_{j=1}^{k} B_j x_{i,j} + \sum_{j=1}^{k-1} \sum_{k=j+1}^{k} B_{ijk} x_{i,j} x_{i,k} + \sum_{j=1}^{k} B_{jj} x_{i,j}^2 + \varepsilon_i \quad (4)$$

where k is the number of continuous factors, and B_0, B_{ijk}, B_{jj} are the estimated coefficients for linear, interaction, and quadratic effects respectively, $x_{i,j}$, $x_{i,k}$, $x_{i,j}^2$ are the coded factors, y_i is the output variable (TPC, TEAC, or TAC), and ε_i is the error.

2.4. Total phenolic compounds

The TPC of ethanol-water extracts of *S. officinalis* L. was determined by Folin's assay as reported in previous work (Moussa and Dahmoune, 2022). A Gallic acid standard was used for the calibration curve to calculate the total phenolic compounds of *S. officinalis* L. as mg_{GAE}/g_{dw}, where all results were expressed as means (N = 3) ± standard deviations (SD).

2.5. Total antioxidant capacity

The total antioxidant capacity of UAE extracts was evaluated using the phosphomolybdenum assay used in previous work (Moussa and Dahmoune, 2022). Total antioxidant activity was expressed as mg of ascorbic acid equivalent (AAE)/g_{dw} using the calibration curve (Moussa and Dahmoune, 2022). All the assays were performed in triplicate and the results were expressed as mean ± SD.

2.6. Trolox equivalent antioxidant capacity

The method is based on the ability of antioxidant molecules of *S. officinalis* L. to reduce ABTS radical, compared with Trolox, which is a water-soluble vitamin E analog as described by Babbar and Oberoi (2011). A blue-green chromophore stock solution of ABTS was prepared by the reaction of a 7 mmol/L aqueous solution of ABTS with 2.45 mmol/L potassium persulfate and allowing the mixture to stand in the dark at room temperature for 16 h before use. The ABTS working solution was obtained by the dilution of the stock solution in ethanol to an absorbance of 0.70 ± 0.02 AU at 734 nm. 2 ml diluted ABTS solution was added to 20 μL of diluted *S. officinalis*' ethanol-water extract. The contents were mixed well, and absorbance was read after 6 min using a UV–visible spectrophotometer (Optima, SP-3000nano, 5T5701-143132-00, Japan). The antioxidant capacity was calculated against the Trolox standard curve as depicted in fig. A1 (Appendix A. supplementary data), and the results were expressed as μmol Trolox equivalent (TE)/g_{dw} of *S. officinalis* powder. All the assays were performed in triplicate and the results were expressed as mean ± SD.

2.7. Biological activity of the optimal extract from S. officinalis L

2.7.1. Scavenging DPPH• free radical activity

The antioxidant activity of the optimal extracts of *S. officinalis* L. leaves using scavenging of DPPH• free radical activity was studied as reported in our previous work (Moussa and Dahmoune, 2022). The antioxidant activity was expressed as an inhibition percentage, where all analyses were performed in triplicates.

2.7.2. Ferric reducing power

The Ferric reducing capacity of the optimal extract of *S. officinalis* L. was determined based on the reduction of Fe^{3+}-TPTZ to a blue-colored Fe^{2+}-TPTZ as described by Abeysiri and Dharmadasa (2013). A volume of 200 μL of the optimal extract was mixed with 1.8 mL of freshly prepared FRAP reagent at pH 3.6 containing 2.5 mL of 10 mmol/L of 2,4,6-Tripyridyl-*s*-Triazine (TPTZ) solution in 40 mmol/L of HCl, 2.5 ml of 20 mmol/L of FeCl3, and 25 mL of 0.3 mol/L of acetate buffer. The absorbance of the reaction was measured at 593 nm using the spectrophotometer (Optima, SP-3000nano, 5T5701-143132-00, Japan) after incubating for 4 min. For the calibration curve, different concentrations of $FeSO_4$ from 0.2 to 0.6 mM of $FeSO_4$ were prepared as shown in fig. A2 (Appendix A. supplementary data). The results were expressed as mmol Fe^{2+} equivalents per gram of lyophilized extract from *S. officinalis* leaves, where all the results were expressed as mean ± SD.

2.7.3. Beta-carotene/linoleic acid bleaching activity

The antioxidant evaluation of *S. officinalis* L. extract using the β-carotene/linoleic acid system according to Moreira and de Carvalho (2019). A solution of β-carotene in chloroform (2 mg/mL) was mixed with 40 mg of linoleic acid and 400 mg of Tween 80. The solvent was evaporated from the mixture, which was then diluted with oxygenated distilled water to 0.8–0.7 of absorbance. A 2.5 mL aliquot of the emulsion was added to different concentrations of lyophilized extracts of *S. officinalis* (0.07–0.7 mg/mL) and the absorbance was measured at 470 nm with an immediate reading and 240 min. All of the reaction mixtures were incubated in a 50 °C water bath. The control was prepared with 2.5 mL of the oxidizing medium and 100 μL of 55% ethanol. All analyses were carried out in triplicates. The antioxidant activity was expressed as an inhibition percentage relative to the control using Eq. (5):

$$\text{Antioxidant activity } (\%) = \left(\frac{DR_c - DR_s}{DR_C}\right) * 100 \quad (5)$$

where DR_c is the degradation rate of β-carotene in the control sample, which was calculated by the following equation, $\{[\ln(a_c/b_c)]/t\}$, DR_s is the degradation rate of β-carotene in the presence of sample extract $= \{[\ln(a_s/b_s)]/t\}$, where, a is the absorbance at time = 0 (min), b = absorbance at 240 min, t = time (min). The IC_{50} of the extract needed to reduce the percent of the oxidation of linoleic acid by 50% was calculated using an inhibition curve. All the assays were performed in triplicate and the results were expressed as mean ± SD.

2.7.3.1. Nitric oxide scavenging activity. Nitric oxide ($NO^{\bullet}$) is generated in biological tissues by nitric oxide synthases, which is a key signaling molecule in various physiological processes; On the other hand, excessive and unregulated NO synthesis has been implicated in many pathophysiological conditions, including cancer (Korde Choudhari, Chaudhary, 2013). Under aerobic conditions, 2 mL of 10 mM sodium nitroprusside dissolved in 0.5 mL of phosphate buffer saline (pH 7.4) were mixed with 0.5 mL of sample at various concentrations (0.05–1 mg/mL). The mixture is then incubated at 25 °C. After 150 min of incubation in front of the polychromatic light source (25 W tungsten lamp), 0.5 mL of the incubated solution was mixed with 0.5 mL of Griess reagent (1% sulfanilic acid reagent, 0.1% naphthyl-ethylenediamine dichloride, 2% phosphoric acid) (Alam and Bristi, 2013). The mixture's color was measured at 546 nm using a UV–visible spectrophotometer (Optima, SP-3000nano, 5T5701-143132-00, Japan) after 30 min of incubation at room temperature. The antioxidant capacity against the $NO^{\bullet}$ free radical was calculated using Eq. (6).

$$AA\ (\%) = \frac{A_B - A_S}{A_C} * 100 \quad (6)$$

where A_S is the absorbance of the free radical solution + sample extract at the required time, A_B is the absorbance of the free radical solution + extraction solvent at the required time, A_C is the absorbance of the working free radical solution at (t = 0 min). The concentration required for inhibition of 50% of free radicals was also calculated from the inhibition curve. All the results were expressed as mean (N = 3) ± SD.

2.8. Statistical analysis

All experimental results were reported as mean values (n = 3) with their corresponding standard deviations. JMP® Pro 13.0.0 software (SAS Institute Inc.) was used for the screening and optimization process. Three-dimensional response surfaces were plotted according to the fitted model using JMP® Pro 13.0.0 software, by keeping one of the three independent variables constant at level-coded zero. The adequacy and accuracy of DSD and *I*-optimal models were evaluated using analysis of variance (ANOVA), lack of fit (LOF), and determination coefficient of R^2 obtained. Statistical significance of both DSD and *I*-optimal models and estimated coefficients of UAE parameters were established at $p < 0.05$. The desirability function and the optimal extraction conditions for multiple responses (TPC, TEAC, TAC) were investigated by using JMP® Pro 13.0.0 software.

In order to evaluate the goodness of fitting and prediction accuracy of DSD and I-optimal designs, statistical parameters such as mean absolute error (MAE), mean square error (MSE), root mean square error (RMSE), absolute average deviation (AAD), standard error of prediction (SEP), and relative percent deviation (RPD) were carried out between experimental and predicted data. In addition to the statistical parameters including adequate precision (AP), correlation coefficients (R^2), and adjusted determination coefficient

Table 6
Regression results of the definitive screening design and the estimated parameters of the TPC, TEAC, and TAC.

		TPC (mg_{GAE}/g_{dw})		TEAC ($\mu mol_{TE}/g_{dw}$)		TAC (mg_{AAE}/g_{dw})	
	Parameters	EC	ρ-value	EC	ρ-value	EC	ρ-value
Estimated parameters	**Intercept**	28.698	<0.0001[a]	234.609	<0.0001[a]	35.308	<0.0001[a]
	Linear effects						
	x_1	2.959	0.0006[a]	10.309	0.0009[a]	4.123	<0.0001[a]
	x_3	1.997	0.0059[a]	15.107	<0.0001[a]	2.335	0.0028[a]
	x_4	7.676	<0.0001[a]	47.685	<0.0001[a]	7.176	<0.0001[a]
	x_2	0.204	0.7317[b]	−2.0267	0.3414[b]	−0.509	0.3811[b]
	Quadratic effects						
	x_1x_1	−6.662	0.0001[a]	−31.866	0.0002[a]	−7.649	0.0004[a]
	x_4x_4	−3.082	0.0602[b]	−45.571	<0.0001[a]	−2.662	0.1019[b]
Regression results	**Interaction effects**						
	x_1x_4	−0.028	0.9625[b]	−7.397	0.0099[a]	−1.112	0.1026[b]
	x_1x_3	−0.502	0.4524[b]	−2.877	0.2599[b]	−1.207	0.1007[b]
	R^2	0.97		0.99		0.97	
	R^2_{Adj}	0.94		0.98		0.94	
	RMSE	2.0120		7.497		2.057	
	C.V (%)	9.7		4.3		7.6	
	ANOVA (Model)	<0.0001[a]		<0.0001[a]		<0.0001[a]	
	Lack of fit	/		/		/	

TPC; Total phenolic compounds, **TEAC;** Trolox equivalent antioxidant capacity, **TAC**; Total antioxidant capacity **EC;** Estimated coefficient, **RMSE;** Root Mean Square Error, **C.V;** Coefficient of variance, **ρ-value [a];** statistically significant, **ρ-value [b];** statistically not significant.

(R^2_{Adj}) were also employed in this study. The formulas used are shown in Table 9 (Rafigh and Yazdi, 2014; Dahmoune and Remini, 2015; Sarve and Sonawane, 2015).

3. Results and discussion

3.1. Optimization process

3.1.1. Definitive screening design

The DSD was conducted to screen the effects of the ethanol-water mixture, extraction temperature, sonication time, and solvent to solid ratio on the extraction of TPC, TEAC, and TAC. Table 2 presents the DSD and corresponding response data. The analysis of variance (ANOVA) and lack of fit results of the model are illustrated in Table 6. The model was highly significant (p-value < 0.0001) with an insignificant lack of fit. The results reflect a good model performance for predicting the relevant responses as well as high correlation coefficients $R^2 \geq 0.97$, and $R^2_{Adj} \geq 0.94$ for all responses (TPC, TEA, and TAC) that indicate a good fitness of the selected model. All these results point to the higher accuracy of the DSD model, confirmed by a good correlation between experimental and predicted responses. Furthermore, the variation coefficient (CV) describes the degree to which the data were dispersed; a CV of less than 10% is generally desired (Koocheki and Taherian, 2009). Our results confirmed that the CVs were 9.7, 4.3, and 7.6% for TPC, TEAC, and TAC, respectively; therefore, the suggested model was reproducible with high precision.

The mathematical equations (Eqs. (7)–(9)) of DSD represent the relationship between TPC, TEAC, TAC, and the extraction factors as follows:

$$TPC\ (\mathrm{mg_{GAE}}/\mathrm{g_{dw}}) = 28.698 + 2.959x_1 + 1.997x_3 + 7.676x_4 - 6.662x_1^2 \quad (7)$$

$$TEAC\ (\mu\mathrm{mol_{TE}}/\mathrm{g_{dw}}) = 234.609 + 10.309\,x_1 + 15.107\,x_3 + 47.685\,x_4 - 31.866\,x_1^2 - 45.571\,x_4^2 - 7.397\,x_1x_4 \quad (8)$$

$$TAC\ \ (\mathrm{mg_{AAE}}/\mathrm{g_{dw}}) = 35.308 + 4.123\,x_1 + 2.335\,x_3 + 7.176\,x_4 - 7.649\,x_1^2 \quad (9)$$

According to the results obtained from DSD, the continuous factors, including ethanol-water mixture, temperature, and solvent to solid solvent ratio, exhibited a high effect on TPC, TEAC, and TAC ($p < 0.05$). While the extraction time showed no effect on phenolic extraction compounds and antioxidant activities with a *p*-value of 0.05 (Table 6). Regarding the quadratic effects of UAE factors on TPC, TEAC, and TAC, they were also considered, where only the ethanol-water mixture was the highly significant factor on the TPC and TCA ($p < 0.01$). Concerning the quadratic effects the ethanol-water mixture, and solvent to solid ratio showed a high impact on the TEAC (Table 6). Furthermore, the significant synergic effect of the ethanol-water mixture and solvent to solid ratio on TEAC was observed with a small *p*-value ($p < 0.01$) as depicted in Table 6.

3.1.2. I-optimal design

According to the results of the DSD, three factors, including the ethanol-water mixture, temperature, and solvent to solid ratio, were identified as significant factors in TPC extraction, TEAC, and TAC from *S. officinalis* L. leaves (Tables 2 and 6), hence, these factors were selected for the optimization process as mentioned in Table 3. Table 7 showed the analysis of variance and the estimated parameters of the optimal design. The experiment data were analyzed by ANOVA and multiple regression analysis. The factors x_1, x_3, and x_4 were

Table 7
Regression results of *I*-optimal design and the estimated parameters of the TPC, TEAC, and TAC.

		TPC ($\mathbf{mg_{GAE}/g_{dw}}$)		TEAC ($\mu\mathbf{mole_{TE}/g_{dw}}$)		TAC ($\mathbf{mg_{AAE}/g_{dw}}$)	
	Parameters	EC	ρ-value	EC	ρ-value	EC	ρ-value
Estimated parameters	**Intercept**	24.998	<0.0001[a]	214.925	<0.0001[a]	34.174	<0.0001[a]
	Linear effects						
	x_1	−0.268	0.4933[b]	12.820	0.0270[a]	3.355	0.0004[a]
	x_3	1.054	0.0059[a]	10.236	0.0593[b]	1.182	0.0493[a]
	x_4	8.013	<0.0001[a]	49.113	<0.0001[a]	7.766	<0.0001[a]
	Quadratic effects						
	x_1x_1	−4.697	0.0007[a]	−32.106	0.0107[a]	−5.495	0.0012[a]
	x_4x_4	−1.952	0.0371[a]	−20.258	0.0602[b]	0.956	0.0669[b]
Regression results	x_3x_3	3.001	0.0064[a]	−7.287	0.4376[b]	−0.011	0.9912[b]
	Interaction effects						
	x_1x_3	−0.537	0.2540[b]	−10.859	0.0773[b]	−0.587	0.3320[b]
	x_1x_4	0.569	0.2294[b]	−16.127	0.0195[a]	−1.247	0.0663[b]
	x_3x_4	−1.340	0.0201[a]	−7.569	0.1893[b]	0.308	0.6005[b]
	R^2	0.99		0.97		0.99	
	R^2_{Adj}	0.97		0.92		0.96	
	RMSE	1.15		13.86		1.51	
	C.V (%)	5.09		7.82		5.15	
	ANOVA (Model)	<0.0001[a]		0.0007[a]		<0.0001[a]	
	Lack of fit	0.0806		0.1199		0.0713	

TPC; Total phenolic compounds, **TEAC;** Trolox equivalent antioxidant capacity, **TAC**; Total antioxidant capacity **EC;** Estimated coefficient, **RMSE;** Root Mean Square Error, **C.V;** Coefficient of variance, **ρ-value [a];** statistically significant, **ρ-value [b];** statistically not significant.

taken into consideration, and the *I*-optimal model for TPC, TEAC, and TAC were obtained as shown in Eq. (10), Eq. (11), and Eq. (12) respectively.

$$\text{TPC}\ \ (\text{mg}_{\text{GAE}}/\text{g}_{\text{dw}}) = 24.998 + 1.054\,x_3 + 8.013\,x_4 - 4.697\,x_1^2 + 3.001\,x_3^2 - 1.952\,x_4^2 - 1.340\,x_3x_4 \quad (10)$$

$$\text{TEAC}\ \ (\mu\text{mol}_{\text{TE}}/\text{g}_{\text{dw}})214.925 + 12.820\,x_1 + 49.113\,x_4 - 32.106\,x_1^2 - 16.127\,x_1x_4 \quad (11)$$

$$\text{TAC}\ \ (\text{mg}_{\text{AAE}}/\text{g}_{\text{dw}}) = 34.174 + 3.355\,x_1 + 1.182\,x_3 + 7.766\,x_4 - 5.495\,x_1^2 \quad (12)$$

A summary ANOVA for the UAE optimization parameters using the optimal design is given in Table 7. ANOVA showed that the model showed a lower *P*-value (<0.01) for TPC, TAC, and TEAC. Based on these results, the models for all tested responses were significant, with an insignificant lack of fit for all responses, which indicates good model performance for predicting the relevant response (Table 7). Moreover, the calculated adjusted coefficients (R^2_{Adj}) (TPC, TEAC, and TAC) were close to the determination coefficients (R^2) (Table 7). Regarding linear interaction, and quadratic effects, they were identified as significant ($P < 0.05$). It could be observed that all the linear effects (x_1, x_3, x_4), quadratic effects (x_1^2, x_3^2, x_4^2), and interaction effects (x_1x_4, x_3x_4) exhibited a significant effect on the extraction of TPC, TEAC, and TAC (Table 7).

3.1.2.1. The effects of UAE factors on TPC, TEAC, and TAC. The *I*-optimal design was carried out to optimize the extraction of TPC and the antioxidant activities of *S. officinalis* L. leaves using TEAC and TAC assays. The experimental design and the results of TPC, TEAC, and TAC are illustrated in Table 3. The analysis of variance of the model and the estimated coefficient of each extraction parameter on TPC, TAEC, and TAC are depicted in Table 7.

Fig. 3a showed the interaction effect of ethanol-water and temperature while the third variable was kept at a constant level. The two variables affected positively the TPC yield from 16 to 31 $\text{mg}_{\text{GAE}}/\text{g}_{\text{dw}}$, where the maximum of phenolic content was reached at 50% of the ethanol-water mixture and 60 °C, of UAE temperature with TPC value of 31 $\text{mg}_{\text{GAE}}/\text{g}_{\text{dw}}$ (Fig. 3a). TPC of *S. officinalis* leaf extract obtained in this study was closer to the TPC (27.05 $\text{mg}_{\text{GAE}}/\text{g}_{\text{dw}}$) reported by Maleš and Dragović-Uzelac (2022), and high than TPC

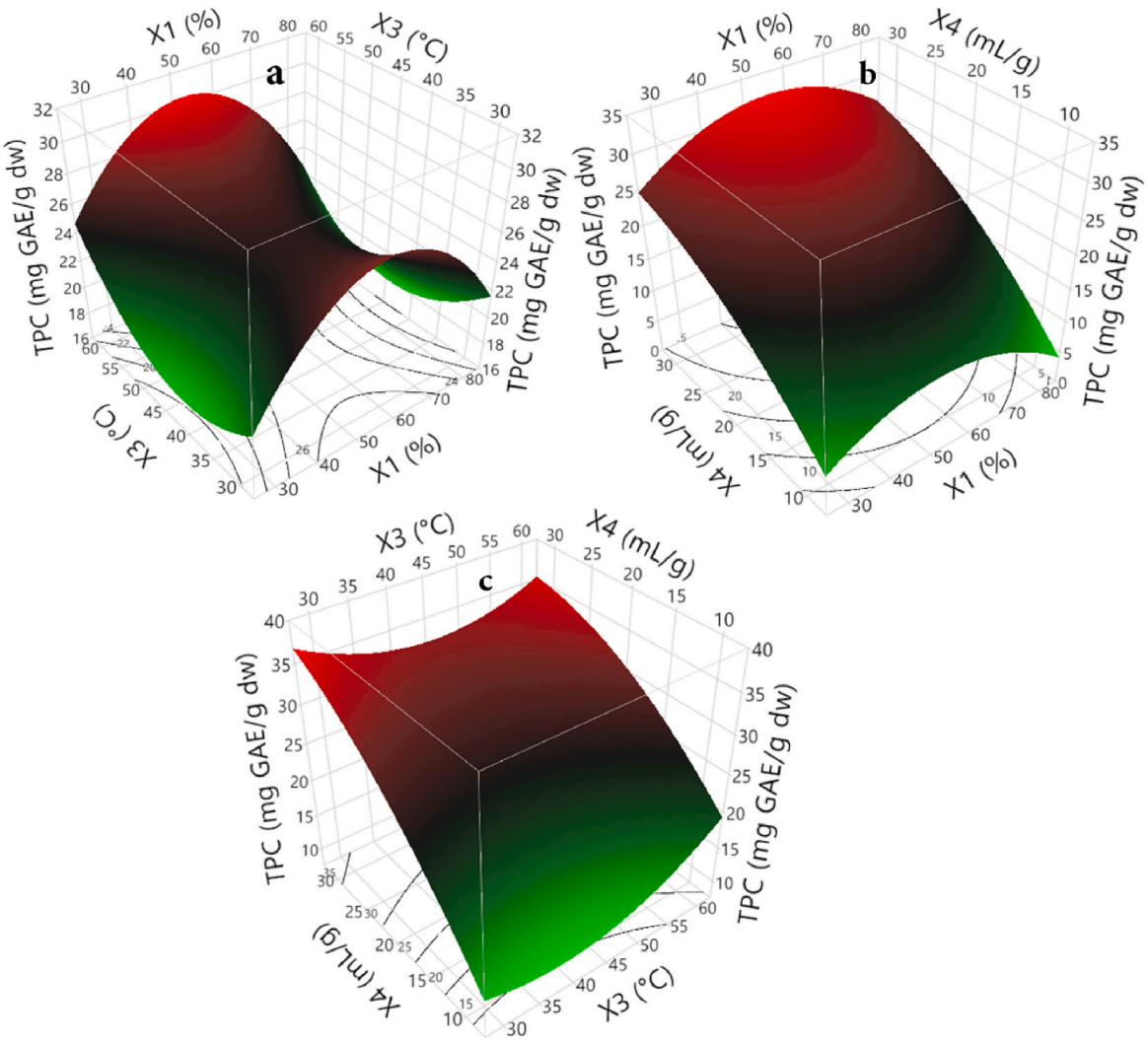

Fig. 3. Three-dimensional plots of *S. officinalis* L. leaves showing the influence of UAE factors on the recovery of TPC.

(25.58 mg_{GAE}/g_{dw}) of hydro-methanolic extract reported by Doymaz and Karasu (2018). In addition, the TPC of optimal *S. officinalis* extract was higher than the 9.15 mg_{GAE}/g_{dw} in supercritical fluid sage leaf extract, and higher than 17.1 mg mg_{GAE}/g_{dw} in sage methanol-acetone extract reported by Pavic and Jakovljevic (2019) and Francik and Francik (2020) respectively.

The same effect of ethanol-water and temperature on TEAC and TAC was also noticed as depicted in Fig. 4a and d, where the antioxidant activities for both assays increased with an increase in ethanol concentration and temperature, where the highest TEAC (220 $\mu mol_{TE}/g_{dw}$) and TAC (36 mg $_{AAE}/g_{dw}$) were observed at 60 °C and a 50% ethanol-water mixture. However, a downward trend in phenolic compounds and antioxidant activities was observed when the ethanol concentration was increased from 50% to 90% (Fig. 4a and d). Savic and Savic Gajic (2020) reported that the optimal conditions for UAE of total phenolic compounds *Triticum aestivum* L were 56% (v/v) ethanol, temperature of 59 °C, where the TPC varied from 105 to 155 mg $_{GAE}/g_{dw}$. Furthermore, the optimal UAE parameters obtained in this study was in accordance with the results obtained by Berkani and Serralheiro (2020), which found that the ethanol concentration with 50.16% exhibited high total phenolic content of 23.83 ± 0.87 mg $_{GAE}/g_{dw}$ from *Zizyphus lotus* fruits. Regarding the antioxidant activity, Chew and Khoo (2011) showed that 60 °C of extraction temperature exhibited higher antioxidant capacity (7.65 $\mu mol_{TE}/g$) from *Orthosiphon stamineus* extract.

The effect of ethanol concentration could be explained based on the similarity and intermiscibility principle. When the ethanol-water mixture reached 50%, its polarity was closer to the polarity of antioxidant compounds, thus the antioxidant activity of

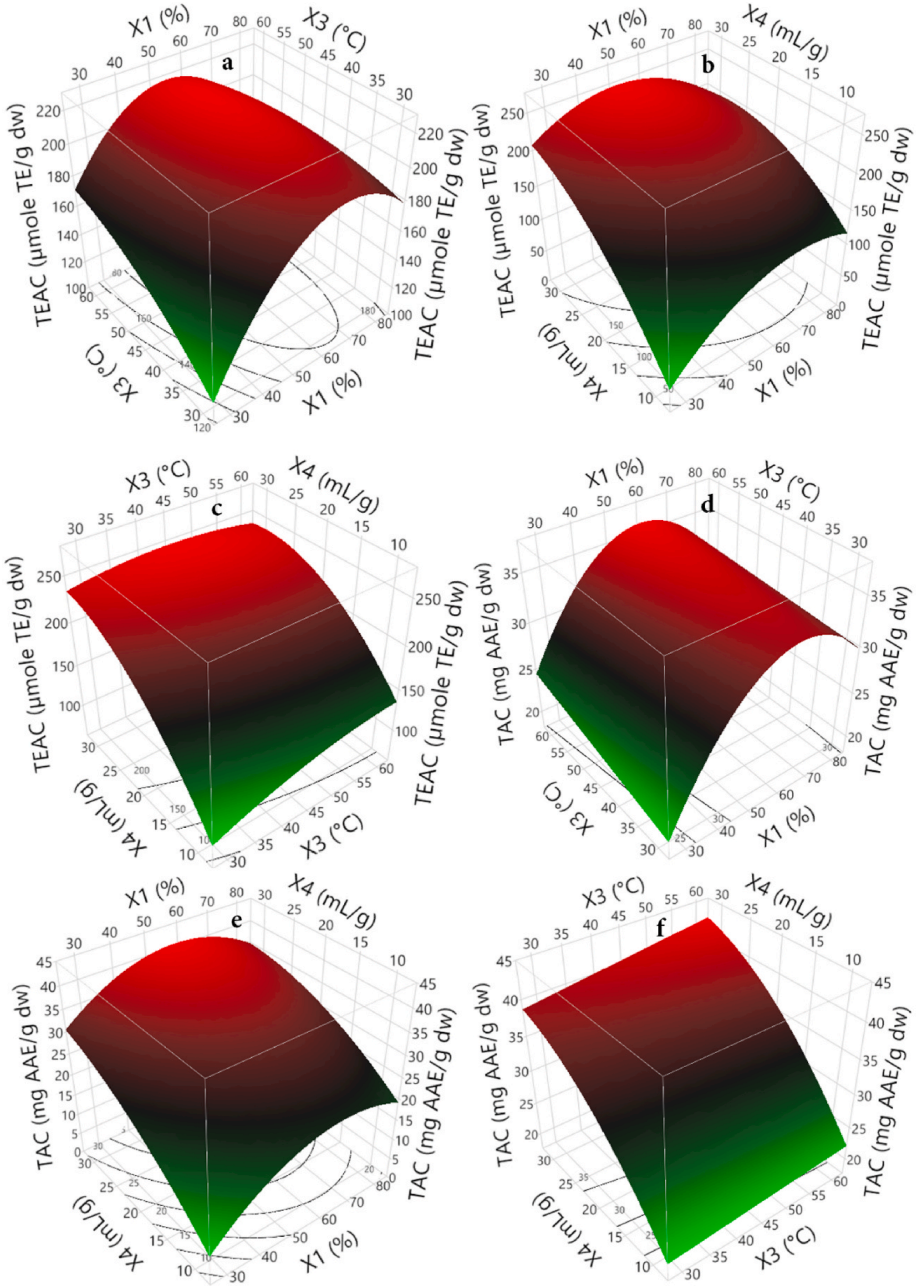

Fig. 4. Three-dimensional plots of *S. officinalis* L. leaves showing the influence of UAE factors on TEAC (a, b, c) and TAC (d, e, f) respectively.

S. officinalis L. leaves enhanced significantly. Several studies have reported that TPC and TFC are highly soluble in hydroalcoholic solutions, whereas compounds with antioxidant capacity are more hydrophilic (Arteaga-Crespo and Radice, 2020; Palma and Diaz, 2021). Moreover, the increase in ethanol concentration could enhance the solubility of antioxidant compounds by enhancing the area between the extraction solvent and solutes (Ali and Lim, 2018).

To understand more about the effect of temperature, the Figs. 3c, 4c and 4e showed the interaction effect of temperature with solvent to solid ratio on TPC, TEAC, and TAC, respectively, where the temperature effect was studied at two different levels (high and low amount of solvent to solid ratios). According to Figs. 3c, 4c and 4e, the TPC, TEAC, and TAC were increased gradually with an increase in extraction temperature when the solvent to solid ratio was at low values. On the other hand, the extraction of TPC was slightly decreased when the temperature was increased from 30 °C to 45 °C, and then the TPC increased gradually again with an increase in temperature from 45 °C to 60 °C when the solvent to solid ratio was at high values (Fig. 3c). Furthermore, the insignificant effect of temperature on TEAC was obtained at a high solvent to solid ratio, while TAC was increased gradually with an increase in temperature from 30 °C to 60 °C. As a result, the highest levels of TPC (35 mg $_{GAE}/g_{dw}$), TEAC (250 μmol $_{TE}/g_{dw}$), and TAC (42 mg $_{AAE}/g_{dw}$) were obtained near the upper limits of both temperature (60 °C) and solvent to solid ratio (30 mL.g-1).

The same tendency was obtained by Ismail and Guo (2019) and Pandey and Belwal (2018) which found that 30 mL/g solvent to solid ratio as optimal UAE parameter for maximum of phenolic and antioxidant compounds from plant extracts. The higher temperature could improve the extraction of TPC and antioxidant activity of medicinal plants by increasing vapor pressure and decreasing the surface tension of the medium. Consequently, more solvent vapors could fill the bubble cavity and numerous cavitation bubbles could be produced (Chemat and Rombaut, 2017). Moreover, the elevation in temperature enhances the mass transfer phenomena by providing energy to the analyte molecules to overcome the energy barriers that bind them to the matrix (Capelo-Martínez 2009).

Furthermore, the solvent to solid ratio factor showed a positive effect on TPC, TEAC, and TAC, where all tested responses were increased exponentially with an increase in the solvent to solid ratio up to 30 mL g^{-1} (Fig. 3b, c, 4b, 4c, 4e, and 4f). Vural et al. (2018) mentioned that a solvent to solid ratio of 30 mL/g as optimal extraction parameters exhibited high TPC, and antioxidant activity of 25.87 ± 0.92 mg GAE/g and 92.33% ± 0.47 respectively from grape seeds extract. As stated in previous work, increasing the amount of solvent provides more surface area for the acoustic wave to form cavitation bubbles, which increases mass transfer between the solvent and sample (Ngamkhae and Monthakantirat, 2022). In addition, a high solvent to solid ratio increases the suspension density of the solution, which adversely impacts the solvation of liberated cellular compounds (Pham and Vuong, 2017). On the other hand, the high viscosity of the solution at a low solvent to solid ratio poses more difficulty in the cavitation effect, where the negative pressure in the rarefaction cycle has to overcome a stronger cohesive force in the high viscous solution (Kumar and Srivastav, 2021).

3.1.3. Optimization of extraction parameters

The optimization of UAE parameters was performed with the aim of maximizing the three responses simultaneously (TPC, TEAC, and TAC) due to the relationship between the phenolic compounds and their antioxidant activities. The validation of the DSD and the *I*-optimal design was performed at their optimal conditions. The optimal conditions obtained by both models were 60 °C of temperature and 30 mL.g^{-1} of solvent to solid ratio, where 57% and 52% of the ethanol-water mixture were obtained by the DSD and *I*-optimal models, respectively. The predicted TPC, TEAC, and TAC have fitted the predicted values in the range of 95% of prediction intervals generated from the DSD model as depicted in Table 8. These results confirmed the accuracy and adequacy of the DSD and *I*-optimal models for screening and optimization of the ultrasound-assisted extraction of TPC and antioxidant activity from S. officinalis L. leaves.

A comparative evaluation of DSD and *I*-optimal design for predicting TPC, TEAC, and TAC was also carried out, and the results are shown in Table 9. However, the overall predictive capability of the model is usually determined by the coefficient of determination (R^2). The efficiency of a model may not be explained by R^2 alone (Rafigh and Yazdi, 2014), which could be explained by other statistical parameters such as R^2_{Adj}, MAE, MSE, RMSE, AAD, SEP, RPD, and AP. In terms of R^2 and R^2_{Adj}, the *I*-optimal design showed higher values for both TPC ($R^2 = 0.99$, $R^2_{Adj} = 0.97$) and TAC ($R^2 = 0.99$, $R^2_{Adj} = 0.96$), while DSD model exhibited higher prediction accuracy for TEAC ($R^2 = 0.99$, $R^2_{Adj} = 0.98$). In addition, for a good model, the prediction error values must be as small as possible. In this context, the *I*-optimal design showed a smaller prediction error for TPC (RMSE = 1.16, AAD = 2.99, SEP = 5.10, MAE = 0.56, RPD = 2.98) and TAC (RMSE = 1.51, AAD = 3.07, SEP = 5.15, MAE = 0.80, RPD = 3.06) than the DSD model for the prediction of TPC and TAC as depicted in Table 9. For the TEAC, the DSD model exhibited lower prediction error than the *I*-optimal design with RMSE = 7.49, AAD = 2.50, SEP = 4.38, MAE = 3.95, and RPD = 2.52 (Table 9). Furthermore, AP compares the range of the predicted values at the design points with the average prediction error, indicating adequate model discrimination when values are greater than 4.0 (Gonzalez-Centeno and Knoerzer, 2014). In this study, all the values of AP presented in Table 9 were more than 4.0, which indicates the

Table 8
Predicted, obtained values and confidence intervals of optimal extract from *S. officinalis* L. leaves, generated by definitive screening design and *I*-optimal design.

	Response	Predicted response	95% PI low	Observed response [a]	95% PI high
DSD	**TPC (mg_{GAE}/g_{dw})**	35.27	31.70	32.77 ± 0.35	38.83
	TEAC ($\mu mol_{TE}/g_{dw}$)	253.48	240.20	241.33 ± 1.26	266.76
	TAC (mg AAE/g_{dw})	42.77	32.12	38.76 ± 0.23	46.41
***I*-Optimal design**	**TPC (mg_{GAE}/g_{dw})**	33.64	31.38	31.84 ± 0.24	35.90
	TEAC ($\mu mol_{TE}/g_{dw}$)	240.60	213.51	237.94 ± 0.77	267.70
	TAC (mg_{AAE}/g_{dw})	40.96	38.01	38.92 ± 0.54	43.92

PI: Predicted interval, superscript [a] Values are expressed as mean ± standard deviation (n = 3).

Table 9
Comparison of the performance of the definitive screening design and the *I*-optimal design.

Performance equations	Definitive screening design			*I*-optimal design		
	TPC	TEAC	TAC	TPC	TEAC	TAC
$R^2 = \frac{\sum_{i=1}^{n}(X_i - Y_i)^2}{\sum_{i=1}^{n}(\overline{Y}_i - Y_i)^2}$	0.97	0.99	0.97	0.99	0.97	0.99
$R^2_{Adj} = 1 - \left[(1 - R^2) * \frac{N-1}{N-K-1}\right]$	0.94	0.98	0.94	0.97	0.92	0.96
$SEP = \frac{RMSE}{Y_e} * 100$	9.73	4.38	7.67	5.10	7.81	5.15
$MAE = \frac{1}{n}\sum_{i=1}^{n}(\lvert Yi_{exp} - Yi_{pred}\rvert)$	1.19	3.95	1.13	0.56	7.19	0.80
$AAD = \left(\frac{1}{n}\sum_{i=1}^{n}\left(\frac{\lvert Yi_{exp} - Yi_{pred}\rvert}{Yi_{exp}}\right)\right) * 100$	7.60	2.50	5.60	2.99	4.40	3.07
$AP = \frac{Yi_{pred}^{Max} - Yi_{pred}^{min}}{\sqrt{\frac{P^* \sigma^2}{n}}} > 4$	20.99	36.59	29.22	26.67	20.55	30.29
$RPD = \frac{100}{n}\sum_{i=1}^{n}\frac{\lvert(Yi_{pred} - Yi_{exp})\rvert}{Yi_{exp}}$	7.58	2.52	5.57	2.98	4.42	3.06
$MSE = \frac{\sum_{i=1}^{n}(Yi_{exp} - Yi_{pred})^2}{n-p-1}$	4.05	56.20	4.23	1.34	192.22	2.29
$RMSE = \sqrt{\frac{\sum_{i=1}^{n}(Yi_{exp} - Yi_{pred})^2}{n-p-1}}$	2.01	7.49	2.05	1.16	13.86	1.51

n is the numbers of experiment, ***p*** is the number of terms other than the intercept in the model, Y_e is the mean value of experimental data. ***P*** is the is the number of significant terms of the mathematical model including the model constant, and σ^2 is the MS residual value from the ANOVA analysis, N is the total number of observations, ***K*** is the number of input variables.

adequacy and accuracy of both models. However, *I*-optimal design showed high AP values for both TPC and TAC, and a higher AP value was obtained using the DSD model for predicting TEAC (Table 9). From all the results obtained, the *I*-optimal design has shown a significantly higher predictive capacity of TPC and TAC than the DSD model, while the DSD model exhibited a higher predictive capacity of TEAC.

3.2. Antioxidant activity

The oxidative stress plays a key role in the development of several pathophysiological conditions, such as neurodegenerative and cardiovascular diseases, cancer, and diabetes (Almada-Taylor and Diaz-Rubio, 2018). The mechanisms of action of antioxidant compounds derived from herbal medicines have been extensively studied, and as a result, many in vitro methods for evaluating antioxidant capacity were used to gain a better understanding of how different phenolic compounds or complexes can act as modulators of oxidative processes. (Babota and Frumuzachi, 2022). In this context, the antioxidant activity of the *S. officinalis* L. optimal extract was carried out using the DPPH$^{\bullet}$ scavenging assay, ferric reducing power, β-carotene/linoleic acid bleaching activity, and NO$^{\bullet}$ scavenging activity. As shown in Fig. 4, the antioxidant activities using different assays increased proportionally with an increase in the extract concentration, where at 0.6 mg/mL, the antioxidant activity using DPPH$^{\bullet}$ radical scavenging, and β-carotene/linoleic acid bleaching, and NO$^{\bullet}$ scavenging radical were 90%, 90%, and 70%, respectively (Fig. 5). According to the half-maximal inhibitory concentrations (IC_{50}) obtained from each assay, *S. officinalis* L. extract showed a substantially higher antioxidant with an IC_{50} of 0.069 ± 0.0005 mg/mL against the NO$^{\bullet}$ free radicals (Fig. 5). The IC_{50} value of NO$^{\bullet}$ scavenging capacity obtained in this work was higher than the value reported by Pereira and Catarino (2018) for *S. officinalis* L. extract (IC_{50} = 0.118 ± 0.16 mg/mL). Furthermore, Mervic, Bival Stefan, (2022) reported that at concentration of 100 μg/mL, the extract of all the extracts of investigated *salvia* species exhibited higher NO$^{\bullet}$ scavenging activity than 50%.

In the β-carotene/linoleic acid model system, a rapid discoloration of β-carotene could occur in the absence of an antioxidant compounds (Hamrouni-Sellami and Rahali, 2012). Based on the obtained results, the optimal extract reduced the extent of β-carotene bleaching by scavenging the linoleate acid free radical with an IC_{50} of 0.159 ± 0.008 mg/mL (Fig. 5). The IC_{50} of optimal extract was low than the IC_{50} of *S. Nemorosa*, *S. Pratenis*, *S. Sclarea*, and *S. Verticillata* with values ranged from 116.83 μg/mL to 327.23 μg/mL obtained by Mervic, Bival Stefan, (2022), therefore the optimal extract showed higher potential scavenging than the salvia species.

Furthermore, as a stable free radical, DPPH$^{\bullet}$ is probably the most widely used free radical for in *vitro* evaluation of antioxidant capacity. The optimal *S. officinalis* L. extract scavenged strongly DPPH-free radicals in a dose-dependent manner, yielding a good antioxidant activity with an IC_{50} of 0.276 ± 0.001 mg/mL (Fig. 5), where this result obtained was in agreement with the IC_{50} of methanolic extract of *S. officinalis* L (0.233 mg/mL) obtained by Aghaei Jeshvaghani, Rahimmalek, (2015). In addition, the optimal extract from *S. officinalis* L. leaves also exhibited high reducing power to reduce TPTZ–Fe (III) complex to TPTZ–Fe (II) complex, where at 0.3 mg/mL of lyophilized powder, the reducing power was approximately 2 mmol Fe^{+2} equivalent/g as depicted in Fig. 6. Pereira and Catarino (2018) and Lu and Foo (2001) reported that the superior antioxidant activities in salvia species were strongly correlated to caffeic acid, rosmarinic acid, salvianolic acid K, salvianolic acid I, sagecoumarin, and sagerinic acid.

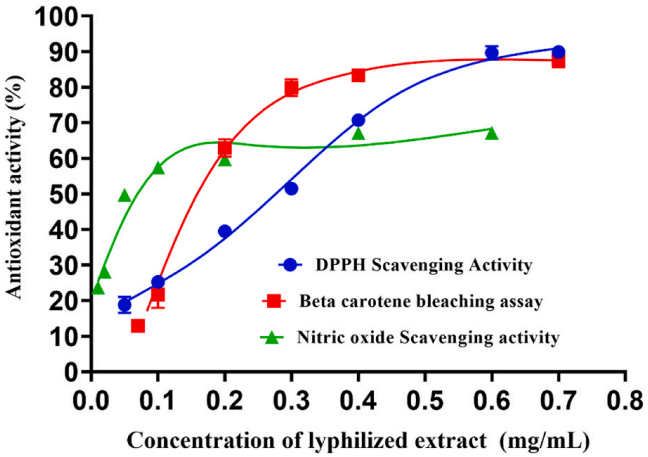

Fig. 5. Evaluation of antioxidant activity of the optimal extract from *S. officinilis* L. using DPPH$^{\bullet}$ scavenging activity, Beta carotene bleaching assay, and nitric oxide scavenging activity.

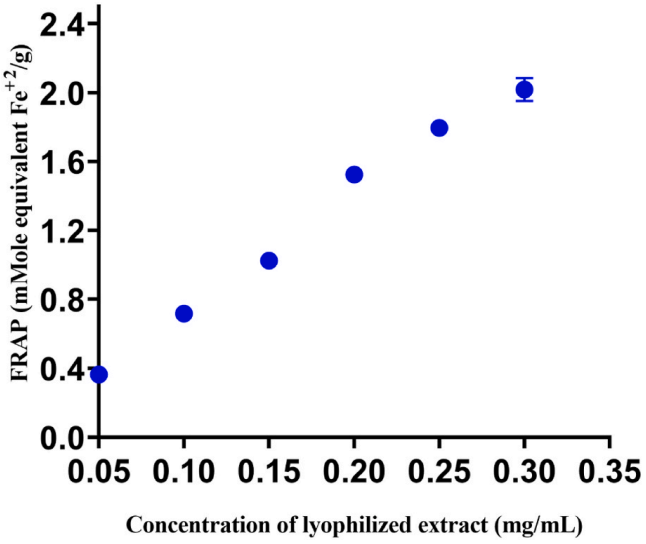

Fig. 6. Evaluation of antioxidant activity of the optimal extract from *S. officinilis* L. using ferric reducing power.

4. Conclusion

In this study, two modeling approaches, DSD and optimal design, were used to optimize UAE parameters for the extraction of total phenolic compounds and for the antioxidant activity of *S. officinalis* L. leaves. After the optimization process, the DSD and optimal design demonstrated higher R^2 and lower RMSE values, which indicate the performance of both models with fewer experimental runs. Based on the results obtained by DSD, only three extraction parameters showed a significant effect on TPC extraction, TEAC, and TAC. Optimization of the UAE process by the *I*-optimal design indicated that maximum values of TPC, TEAC, and TAC were 31.843 ± 0.248 mg_{GAE}/g_{dw}, 237.946 ± 0.771 $\mu mol_{TE}/g_{dw}$, and 38.928 ± 0.548 mg_{AAE}/g_{dw} under the optimum conditions of 52% of the ethanol-water mixture, 60% of the temperature, 30 mL.g-1 of solvent to solid ratio, and 10 min of extraction time. Based on the statistical parameters employed to evaluate the predictive efficiency of both models, the *I*-optimal design showed more predictive capability for TPC and TAC, while the DSD model exhibited more efficiency in predicting the TEAC.

Furthermore, the current research findings for UAE optimization could be used as an efficient and eco-friendly alternative to conventional extraction in extracting the phenolic compounds from plant matrices. The optimal extract from *S. officinalis* L. leaves exhibited higher antioxidant activity using DPPH$^{\bullet}$ and NO$^{\bullet}$ scavenging activity, β-carotene/linoleic acid bleaching activity, and reducing power. The IC_{50} values for DPPH$^{\bullet}$ and NO$^{\bullet}$ scavenging, as well as -carotene/linoleic acid bleaching, were 0.276 ± 0.001 mg/mL, 0.069 ± 0.0005 mg/mL, and 0.159 ± 0.008 mg/mL, respectively. The reducing power of the optimal extract was 0.3 mg/mL of lyophilized powder. The reducing power was approximately 2 mmol Fe^{+2} equivalent/g, which could be an effective medicinal plant used for treating and healing many diseases.

Funding

This research did not receive any specific grants from funding agencies in the public, commercial, or not-for-profit sectors.

Authorship statement

Category 1: **Conception and design of study:** H. Moussa, F. Dahmoune: **Software:** H. Moussa, F. Dahmoune: **Acquisition of data**: H. Moussa. **Analysis and/or interpretation of data:** H. Moussa, F. Dahmoune,

Category 2: **Supervision:** F. Dahmoune, H. Remini. **Drafting the manuscript:** H. Moussa, F. Dahmoune. **Revising the manuscript critically for important intellectual content:** H. Moussa, F. Dahmoune, H. Remini, M. M. Mahdjoub, N.Kadri.

Category 3: All authors were approved the version of the manuscript to be published

Declaration of competing interest

The authors declare that they have no known competing financial interests or personal relationships that could have appeared to influence the work reported in this paper.

Data availability

Data will be made available on request.

Appendix A. Supplementary data

Supplementary data to this article can be found online at https://doi.org/10.1016/j.scp.2022.100820.

References

Abeysiri, G.R.P.I., Dharmadasa, R.M., et al., 2013. Screening of phytochemical, physico-chemical and bioactivity of different parts of Acmella oleraceae Murr. (Asteraceae), a natural remedy for toothache. Ind. Crop. Prod. 50, 852–856.

Aghaei Jeshvaghani, Z., Rahimmalek, M., et al., 2015. Comparison of total phenolic content and antioxidant activity in different Salvia species using three model systems. Ind. Crop. Prod. 77, 409–414.

Alam, M.N., Bristi, N.J., et al., 2013. Review on in vivo and in vitro methods evaluation of antioxidant activity. Saudi Pharmaceut. J. 21 (2), 143–152.

Ali, A., Lim, X.Y., et al., 2018. Optimization of ultrasound-assisted extraction of natural antioxidants from Piper betle using response surface methodology. LWT (Lebensm.-Wiss. & Technol.) 89, 681–688.

Almada-Taylor, G., Diaz-Rubio, L., et al., 2018. Biological activities of extracts from aerial parts of *Salvia pachyphylla* epling ex munz. Plants (Basel) 7 (4).

Arteaga-Crespo, Y., Radice, M., et al., 2020. Optimisation of ultrasound-assisted extraction of phenolic antioxidants from *Ilex guayusa* Loes. leaves using response surface methodology. Heliyon 6 (1), e03043.

Babbar, N., Oberoi, H.S., et al., 2011. Total phenolic content and antioxidant capacity of extracts obtained from six important fruit residues. Food Res. Int. 44 (1), 391–396.

Babota, M., Frumuzachi, O., et al., 2022. Optimized ultrasound-assisted extraction of phenolic compounds from *Thymus comosus* Heuff. ex Griseb. et Schenk (wild thyme) and their bioactive potential. Ultrason. Sonochem., 105954

Berkani, F., Serralheiro, M.L., et al., 2020. Ultrasound assisted extraction of phenolic compounds from a jujube by-product with valuable bioactivities. Processes 8 (11), 1441.

Brahmi, F., Blando, F., et al., 2022. Optimization of the conditions for ultrasound-assisted extraction of phenolic compounds from *Opuntia ficus-indica* [L.] Mill. flowers and comparison with conventional procedures. Ind. Crop. Prod. 184, 114977.

Capelo-Martínez, J.-L., 2009. Ultrasound in Chemistry: Analytical Applications. John Wiley & Sons.

Carrasco-Sandoval, J., Falcó, I., et al., 2022. Multivariable optimization of ultrasound-assisted extraction for the determination of phenolic and antioxidants compounds from arrayan (*Luma apiculata* (DC.) Burret) leaves by microplate-based methods and mass spectrometry. J. Appl. Res. Med. Aromatic Plants 28, 100356.

Chemat, F., Rombaut, N., et al., 2017. Ultrasound assisted extraction of food and natural products. Mechanisms, techniques, combinations, protocols and applications. A review. Ultrason. Sonochem. 34, 540–560.

Chew, K., Khoo, M., et al., 2011. Effect of ethanol concentration, extraction time and extraction temperature on the recovery of phenolic compounds and antioxidant capacity of *Orthosiphon stamineus* extracts. Int. Food Res. J. 18 (4), 1427.

Cigeroglu, Z., Aras, O., et al., 2018. Optimization of ultrasound-assisted extraction of phenolic compounds from grapefruit (*Citrus paradisi* Macf.) leaves via D-optimal design and artificial neural network design with categorical and quantitative variables. J. Sci. Food Agric. 98 (12), 4584–4596.

Dahmoune, F., Remini, H., et al., 2015. Ultrasound assisted extraction of phenolic compounds from *P. lentiscus* L. leaves: comparative study of artificial neural network (ANN) versus degree of experiment for prediction ability of phenolic compounds recovery. Ind. Crop. Prod. 77, 251–261.

Dent, M., 2015. Comparison of conventional and ultrasound-assisted extraction techniques on mass fraction of phenolic compounds from sage (*Salvia officinalis* L.). Chem. Biochem. Eng. Q. 29 (3), 475–484.

Doymaz, İ., Karasu, S., 2018. Effect of air temperature on drying kinetics, colour changes and total phenolic content of sage leaves (*Salvia officinalis*). Qual. Assur. Saf. Crop Foods 10 (3), 269–276.

Felix, C., Ubando, A., et al., 2019. Investigation of direct biodiesel production from wet microalgae using definitive screening design. Energy Proc. 158, 1149–1154.

Fidaleo, M., Lavecchia, R., et al., 2016. Application of a novel definitive screening design to decolorization of an azo dye on boron-doped diamond electrodes. Int. J. Environ. Sci. Technol. 13 (3), 835–842.

Francik, S., Francik, R., et al., 2020. Identification of phenolic compounds and determination of antioxidant activity in extracts and infusions of salvia leaves. Materials (Basel) 13 (24).

Ghafoor, K., Choi, Y.H., et al., 2009. Optimization of ultrasound-assisted extraction of phenolic compounds, antioxidants, and anthocyanins from grape (*Vitis vinifera*) seeds. J. Agric. Food Chem. 57 (11), 4988–4994.

Glisic, S.B., Ristic, M., et al., 2011. The combined extraction of sage (*Salvia officinalis* L.): ultrasound followed by supercritical CO2 extraction. Ultrason. Sonochem. 18 (1), 318–326.

Gonzalez-Centeno, M.R., Knoerzer, K., et al., 2014. Effect of acoustic frequency and power density on the aqueous ultrasonic-assisted extraction of grape pomace (*Vitis vinifera* L.) - a response surface approach. Ultrason. Sonochem. 21 (6), 2176–2184.

Goos, P., 2012. The Optimal Design of Blocked and Split-Plot Experiments. Springer Science & Business Media.

Goos, P., Jones, B., 2011. Optimal Design of Experiments: a Case Study Approach. John Wiley & Sons.

Haji, A., Qavamnia, S.S., et al., 2018. The use of D-optimal design in optimization of wool dyeing with Juglans regia bark. Industria Textila 69 (2), 104–110.

Hamrouni-Sellami, I., Rahali, F.Z., et al., 2012. Total phenolics, flavonoids, and antioxidant activity of sage (salvia officinalis L.) plants as affected by different drying methods. Food Bioprocess Technol. 6 (3), 806–817.
Hecht, E.S., McCord, J.P., et al., 2015. Definitive screening design optimization of mass spectrometry parameters for sensitive comparison of filter and solid phase extraction purified, INLIGHT plasma N-glycans. Anal. Chem. 87 (14), 7305–7312.
Hossain, M.B., Brunton, N.P., et al., 2012. Optimization of ultrasound assisted extraction of antioxidant compounds from marjoram (*Origanum majorana* L.) using response surface methodology. Ultrason. Sonochem. 19 (3), 582–590.
Ismail, B.B., Guo, M., et al., 2019. Valorisation of baobab (*Adansonia digitata*) seeds by ultrasound assisted extraction of polyphenolics. Optimisation and comparison with conventional methods. Ultrason. Sonochem. 52, 257–267.
Jones, B., Allen-Moyer, K., et al., 2020. A-optimal versus D-optimal design of screening experiments. J. Qual. Technol. **53** (4), 369–382.
Jones, B., Nachtsheim, C.J., 2011. A class of three-level designs for definitive screening in the presence of second-order effects. J. Qual. Technol. 43 (1), 1–15.
Jones, B., Nachtsheim, C.J., 2017. A class of three-level designs for definitive screening in the presence of second-order effects. J. Qual. Technol. 43 (1), 1–15.
Koocheki, A., Taherian, A.R., et al., 2009. Response surface methodology for optimization of extraction yield, viscosity, hue and emulsion stability of mucilage extracted from *Lepidium perfoliatum* seeds. Food Hydrocolloids 23 (8), 2369–2379.
Korde Choudhari, S., Chaudhary, M., et al., 2013. Nitric oxide and cancer: a review. World J. Surg. Oncol. 11 (1), 118.
Kumar, K., Srivastav, S., et al., 2021. Ultrasound assisted extraction (UAE) of bioactive compounds from fruit and vegetable processing by-products: a review. Ultrason. Sonochem. 70, 105325.
Liu, Y., Liu, H.-Y., et al., 2021. Screening and process optimization of ultrasound-assisted extraction of main antioxidants from sweet tea (*Lithocarpus litseifolius* [Hance] Chun). Food Biosci. 43, 101277.
Lu, Y., Foo, L.Y., 2001. Antioxidant activities of polyphenols from sage (*Salvia officinalis*). Food Chem. 75 (2), 197–202.
Maleš, I., Dragović-Uzelac, V., et al., 2022. Non-volatile and volatile bioactives of *Salvia officinalis* L., *Thymus serpyllum* L. And *Laurus nobilis* L. Extracts with potential use in the development of functional beverages. Antioxidants 11 (6), 1140.
Mervic, M., Bival Stefan, M., et al., 2022. Comparative antioxidant, anti-acetylcholinesterase and anti-alpha-glucosidase activities of mediterranean salvia species. Plants (Basel) 11 (5).
Meyer, R.K., Nachtsheim, C.J., 1995. The coordinate-exchange algorithm for constructing exact optimal experimental designs. Technometrics 37 (1), 60–69.
Mitić, M., Tošić, S., et al., 2019. Optimization of the extraction process of minerals from *Salvia officinalis* L. using factorial design methodology. Microchem. J. 145, 1224–1230.
Mocan, A., Babota, M., et al., 2020. Chemical constituents and biologic activities of sage species: a comparison between salvia officinalis L., *S. glutinosa* L. and *S. transsylvanica* (schur ex griseb. & schenk) schur. Antioxidants (Basel) 9 (6).
Moreira, B.O., de Carvalho, A.L., et al., 2019. Evaluation of anti-inflammatory, antinociceptive and biological activities of *Cenostigma macrophyllum* standardized extracts and determination and quantification of the main metabolites. RSC Adv. 9 (70), 41256–41268.
Moussa, H., Dahmoune, F., et al., 2022. Optimization of ultrasound-assisted extraction of phenolic-saponin content from *Carthamus caeruleus* L. rhizome and predictive model based on support vector regression optimized by dragonfly algorithm. Chemometr. Intell. Lab. Syst. 222, 104493.
Ngamkhae, N., Monthakantirat, O., et al., 2022. Optimization of extraction method for Kleeb Bua Daeng formula and comparison between ultrasound-assisted and microwave-assisted extraction. J. Appl. Res. Med. Aromatic Plants 28, 100369.
Oladipo, B., Betiku, E., 2019. Process optimization of solvent extraction of seed oil from *Moringa oleifera*: an appraisal of quantitative and qualitative process variables on oil quality using D-optimal design. Biocatal. Agric. Biotechnol. 20, 101187.
Palma, A., Diaz, M.J., et al., 2021. Ultrasound extraction optimization for bioactive molecules from *Eucalyptus globulus* leaves through antioxidant activity. Ultrason. Sonochem. 76, 105654.
Pandey, A., Belwal, T., et al., 2018. Optimization of ultrasonic-assisted extraction (UAE) of phenolics and antioxidant compounds from rhizomes of *Rheum moorcroftianum* using response surface methodology (RSM). Ind. Crop. Prod. 119, 218–225.
Pavic, V., Jakovljevic, M., et al., 2019. Extraction of carnosic acid and carnosol from sage (*Salvia officinalis* L.) leaves by supercritical fluid extraction and their antioxidant and antibacterial activity. Plants (Basel) 8 (1).
Pavlić, B., Vidović, S., et al., 2016. Subcritical water extraction of sage (*Salvia officinalis* L.) by-products—process optimization by response surface methodology. J. Supercrit. Fluids 116, 36–45.
Pereira, O.R., Catarino, M.D., et al., 2018. *Salvia elegans, Salvia greggii* and *Salvia officinalis* decoctions: antioxidant activities and inhibition of carbohydrate and lipid metabolic enzymes. Molecules 23 (12).
Pham, H.N.T., Vuong, Q.V., et al., 2017. Optimization of ultrasound-assisted extraction of *Helicteres hirsuta* Lour. for enhanced total phenolic compound and antioxidant yield. J. Appl. Res. Med. Aromatic Plants 7, 113–123.
Rafigh, S.M., Yazdi, A.V., et al., 2014. Optimization of culture medium and modeling of curdlan production from *Paenibacillus polymyxa* by RSM and ANN. Int. J. Biol. Macromol. 70, 463–473.
Rodríguez, M., Jones, B., et al., 2017. Generating and assessing exact G-optimal designs. J. Qual. Technol. 42 (1), 3–20.
Sarve, A., Sonawane, S.S., et al., 2015. Ultrasound assisted biodiesel production from sesame (*Sesamum indicum* L.) oil using barium hydroxide as a heterogeneous catalyst: comparative assessment of prediction abilities between response surface methodology (RSM) and artificial neural network (ANN). Ultrason. Sonochem. 26, 218–228.
Savic, I.M., Savic Gajic, I.M., 2020. Optimization of ultrasound-assisted extraction of polyphenols from wheatgrass (*Triticum aestivum* L.). J. Food Sci. Technol. 57 (8), 2809–2818.
Shivamathi, C.S., Moorthy, I.G., et al., 2019. Optimization of ultrasound assisted extraction of pectin from custard apple peel: potential and new source. Carbohydr. Polym. 225, 115240.
Su, C.H., Pham, T.T.T., et al., 2020. Aqueous enzymatic extraction of rosmarinic acid from *Salvia officinalis*: optimisation using response surface methodology. Phytochem. Anal. 31 (5), 575–582.
Turker, I., Isleroglu, H., 2021. Optimization of extraction conditions of bioactive compounds by ultrasonic-assisted extraction from artichoke wastes. Acta Chim. Slov. 68 (3), 658–666.
Vural, N., Algan Cavuldak, Ö., et al., 2018. Multi response optimisation of polyphenol extraction conditions from grape seeds by using ultrasound assisted extraction (UAE). Separ. Sci. Technol. 53 (10), 1540–1551.
Vural, N., Algan Cavuldak, Ö., et al., 2021. D-Optimal design and multi-objective optimization for green extraction conditions developed with ultrasonic probe for oleuropein. J. Appl. Res. Med. Aromatic Plants 20, 100279.
Zeković, Z., Pintać, D., et al., 2017. Utilization of sage by-products as raw material for antioxidants recovery—ultrasound versus microwave-assisted extraction. Ind. Crop. Prod. 99, 49–59.

Sustainable Chemistry and Pharmacy 35 (2023) 101194

Contents lists available at ScienceDirect

Sustainable Chemistry and Pharmacy

journal homepage: www.elsevier.com/locate/scp

Efficient optimization approaches for microwave assisted extraction of high-quality antioxidant compounds from *Salvia officinalis* L.: UHPLC-HRMS differential analysis of phenolic profiles obtained by ultrasound and microwave extraction

Hamza Moussa [a,b,*], Farid Dahmoune [b,c], Marika Mróz [d], Hocine Remini [b,c], Nabil Kadri [c], Sarah Hamid [e], Barbara Kusznierewicz [d,f]

[a] *Laboratoire de Gestion et Valorisation des Ressources Naturelles et Assurance Qualité (LGVRNAQ), Faculté des Sciences de la Nature et de la Vie et des Sciences de la Terre, Université de Bouira, 10000, Bouira, Algeria*
[b] *Département des Sciences Biologiques, Faculté des Sciences de la Nature et de la Vie et des Sciences de la Terre, Université de Bouira, 10000, Bouira, Algeria*
[c] *Laboratoire de Biomathématiques, Biophysique Biochimie et de Scientométrie (LBBBS), Université Abderrahmane Mira de Béjaïa, Béjaïa, 06000, Algeria*
[d] *Department of Food Chemistry, Technology and Biotechnology, Faculty of Chemistry, Gdańsk University of Technology, Narutowicza 11/12 St., 80-233, Gdańsk, Poland*
[e] *Laboratory of Plant Biotechnology and Ethnobotany, Faculty of Natural Sciences and Life, University Abderrahman Mira, 06000, Bejaia, Algeria*
[f] *BioTechMed Center, Gdańsk University of Technology, Narutowicza 11/12 St., 80-233, Gdańsk, Poland*

A R T I C L E I N F O

Handling Editor: Vania Zuin

Keywords:
D-optimal
I-optimal
Q-orbitrap-HRMS
Phenolic profile

A B S T R A C T

The study aims to optimize MAE of total phenolic compounds (TPC) and antioxidant capacity from *Salvia officinalis* L. leaves using a definitive screening design (DSD) and *I*-optimal design. UHPLC-HRMS analysis was used to identify and compare the composition of MAE and UAE optimal extracts. The results showed that DSD and *I*-optimal design were successfully applied for the optimization of MAE targeting phenolics and other antioxidants from *S. officinalis* L. with the following optimum conditions: 60% ethanolic solvent, time of 4.75 min, power of 600 W, and L/S ratio of 50 mL g^{-1}. The UHPLC-MS analysis results allowed the identification of more than 80 compounds, and the differential analysis indicated that the MAE yielded a higher level of 181 substance peaks, while the UAE yielded a higher level of 87 substance peaks. This study provides valuable information for selecting the appropriate extraction technique when targeting specific compounds.

1. Introduction

Salvia officinalis L. (Lamiaceae), known as common sage is a culinary herb and medicinal plant widely spread around the world, which has been used in food as a spice, appetizer, or garnish (Pachura et al., 2022). Moreover, common sage has been used to treat dementia, ameliorate memory, speed up sensory responses, thinking, and behavior as well as treat depression, digestive and circulatory disorders and reduce sweating (Sulniute et al., 2017). Many bioactive compounds have been identified in *S. officinals* L. such as

* Corresponding author. GVRNAQ Laboratory, Bouira University, Rue Drissi Yahia, Bouira, 10000, Algeria.
E-mail address: h.moussa@univ-bouira.dz (H. Moussa).

https://doi.org/10.1016/j.scp.2023.101194
Received 9 April 2023; Received in revised form 19 June 2023; Accepted 13 July 2023
Available online 25 July 2023

flavonoids (luteolin 7-glucoside, apigenin, hispidulin, kaempferol, and quercetin), phenolic acids (rosmarinic, caffeic, and salvianolic acids), diterpenes (tanshinones, carnosic acid, and carnosol), triterpenes (ursolic acid and oleanolic acid) (Reguigui et al., 2023; Sabry et al., 2022). The quality and quantity of these bioactive compounds are dependent on the plant chemotype, drying, and extraction techniques, thus, the interest in a more systematic and comprehensive characterization using LC-MS, GC-MS, and HPTLC have been employed (Nayak et al., 2015; Pachura et al., 2022; Reguigui et al., 2023).

The extraction technique is an essential step used to obtain bioactive compounds that have therapeutic potential. These bioactive compounds can be used to formulate drugs, dietary supplements, cosmetics, and other health products. The ultrasound-assisted extraction (UAE), microwave-assisted extraction (MAE), ultrasound-microwave-assisted extraction (UMAE) and supercritical fluid extraction (SFE) are more advanced and effective technologies used for the extraction of bioactive compounds from plant matrices (Berkani et al., 2020; Dahmoune et al., 2015b; Darvishzadeh and Orsat, 2022; Moussa et al., 2022). The heat and pressure generated by using these technologies are significantly accelerate the extraction process (Eskilsson and Björklund, 2000). MAE has various advantages compared to traditional procedures, including less solvent usage, less waste released into the environment, rapid extraction, and energy savings because microwaves effectively heat the sample (Tomasi et al., 2023). Different extraction parameters such as the nature of extraction solvent, microwave power, time, solvent-to-solid ratio, temperature, pressure, and on the characteristics of plant matrices could affect significantly the efficiency of MAE (Tomasi et al., 2022), thus several reports were established to optimize these extraction parameters (Khajeh and Ghanbari, 2011; Pan et al., 2001).

Many statistical designs were applied to enhance the MAE of bioactive compounds from plant materials. In recent years, Box-Behnken (Xu et al., 2020), central composite (Kwon et al., 2003), and Plackett-Burman design (Chen et al., 2023) have been used extensively for the optimization process. However, one notable drawback of the Plackett-Burman design is the occurrence of aliasing among factors interactions (Beres and Hawkins, 2001). This limitation becomes critical as interactions between factors often play a crucial role in various processes, and the absence of interaction information can significantly compromise the accuracy of the resulting model (Beres and Hawkins, 2001). On the other hand, both the Box-Behnken and central composite designs require a relatively large number of experimental runs compared to newer statistical designs like the definitive screening design (DSD) and *I*-optimal design. The need for a higher number of experimental runs can pose resource challenges, particularly when the studied process is time-consuming or expensive (Ferreira et al., 2007; Rakić et al., 2014).

DSD and *I*-optimal design are new statistical designs have been created by Jones and Nachtsheim (2011), and Goos and Jones (2011). The DSD with a few of experimental runs is an excellent screening design that could be attributed to its proprieties namely the main effects are not aliased with two-factor interactions, as well as the DSD could estimate all quadratic effects, where quadratic terms in the model are orthogonal to the main effect and not completely aliased (Jones and Nachtsheim, 2011). On the other hand, the *I*-optimal design is a custom design that was used for the optimization process. The experimental matrix of *I*-optimal is generated using the coordinate-exchange algorithm of Meyer and Nachtsheim (1995), which provides high accuracy for the prediction of output variables (Moussa et al., 2022).

According to the authors' best knowledge, no optimization studies were conducted on MAE of total phenolic compounds and antioxidant capacity from *S. officinalis* L. leaves using DSD and *I*-optimal design. Also, there is a paucity of investigation about the influence of MAE and UAE on the bioactive compounds of *S. officinalis* L. Therefore, the present work aims to optimize MAE of total phenolic content, and antioxidant capacities including Trolox equivalent antioxidant capacity (TEAC), and total antioxidant capacity (TAC) from *S. officinalis* L. using *I*-optimal design as response surface methodology. As a first step to optimizing the MAE, an initial screening of extraction parameters was carried out using DSD. Furthermore, a differential analysis using UHPLC-HRMS between phenolics profile of MAE optimal extract and UAE optimal extract obtained in our previous work (Moussa et al., 2022) were carried out to evaluate the effect of MAE and UAE on TPC, TEAC, and TAC.

2. Materials and methods

2.1. Reagents

Methanol and ethanol were purchased from SIGMA-ALDRICH (Co.,3050 Spruce, St. Louis, MO 63103 USA 314-771-5765, Product of Denmark), sodium carbonate (Na_2CO_3), ABTS ($2,2^{'}-$ azino $-$ bis $(3-$ ethylbenzothiazoline $-6-$ sulfonic acid), potassium persulfate ($K_2S_2O_8$), gallic acid, Trolox, and ascorbic acid were purchased from SIGMA-ALDRICH (Co.,3050 Spruce, St. Louis, MO 63103 USA 314-771-5765, Product of Denmark). Folin-Ciocalteu's reagent, ammonium molybdate tetrahydrate ($(NH_4)_6Mo_7O_{24} \bullet 4H_2O$), sodium phosphate monobasic ($NaH_2PO_4 \bullet H_2O$), and sodium phosphate dibasic ($Na_2HPO_4 \bullet 12H_2O$) were purchased from VWR CHEMICALS (VWR International S.A.S. 201 Rue Carnot - F-94126 Fontenay-sous-Bois France, Product of France).

Table 1
The input variables and their levels employed for the screening and optimization of MAE.

Independent variables	Levels		
	-1	0	+1
x_1: Ethanol-water mixture (%)	30	55	80
x_2: Time (s)	60	180	300
x_3: Microwave power (W)	200	400	600
x_4: Solvent to solid ratio ($mL.g^{-1}$)	20	35	50

2.2. Microwave-assisted extraction

The microwave-assisted extraction of phenolic and antioxidant compounds from *S. officinalis* L. leaves was carried out using a microwave equipped with a time controller and a circulating water-cooling system (NN S674MF, Samsung, Malaysia); with a cavity size of 22.5 cm × 37.5 cm × 38.6 cm, and frequency of 2450 kHz. A total of 1 g of dried *S. officinalis* L. leaves, which were finely ground into a powder, were placed in a 250 mL vessel. Samples were mixed into different concentrations of aqueous ethanol (30 to 80%), at the various solvent-to-solid ratios (20 to 50 mL g^{-1}). The vessel was placed into the microwave cavity for extraction. Furthermore, the other MAE parameters studied were microwave power (200-600 W), and extraction time (60 to 300 s), and the experiments were performed as presented in Table 1, Table A.1, and Table A.2. After each MAE, the extract was centrifugated (Sigma 3-16L, 172577, Germany) at 5000 rpm for 10 min followed by filtration through a Whatman No. 4 filter paper, and the supernatant was stored at 4 °C for further analysis.

2.3. Optimization and prediction procedure

To screen and optimize MAE parameters for maximizing the TPC and antioxidant compounds from *S. officinalis* L. leaves, an ethanol-water mixture (x_1), time (x_2), microwave power (x_3) and solvent to solid ratio (x_4) were evaluated using DSD and *I*-optimal design, respectively.

2.3.1. Definitive screening design

DSD was employed to screen and investigate the simultaneous effect of MAE parameters on TPC and antioxidant activity of *S. officinalis* L. leaves extract. The experimental design, regression analysis, and model building have been studied using JMP® Pro 13.0.0 software Pro (SAS Institute Inc, Cary, North of Carolina, US). A DSD design was carried out with three levels (maximum, minimum, and central) of each variable to determine the response pattern and establish a model. The MAE parameters with their units and notation are given in Table 1. The matrix of DSD with 17 experimental combinations (Table A.1) for MAE parameters (x_1, x_2, x_3 and x_4) showed high D-efficiency (85.61), G-efficiency (92.32), A-efficiency (85.36), and the average variance prediction of this design was 0.154. Moreover, according to Fig. A.1, the main effects of MAE parameters are uncorrelated with two-factor interaction effects.

2.3.2. I-optimal design

The results of DSD revealed the significant effect of MAE parameters, namely ethanol-water mixture (x_1), time (x_2), microwave power (x_3) and solvent to solid ratio (x_4) on TPC, TEAC, and TAC. Hence, the optimization of these MAE parameters to maximize the TPC, TEAC, and TAC was carried out using an *I*-optimal design. The actual and coded levels of the studied parameters are depicted in Table 1. A three-level (1, 0, and +1) factor design comprising 21 experimental runs including 3 replicates at the center point was employed (Table A.2). The *I*-optimal design was constructed using JMP® Pro 13.0.0 software, where D, G, and A-efficiency were 42.41, 65.61, and 30.63, respectively. As well as the average variance prediction was 0.358. According to Fig. A.2, all the linear effects are orthogonal and can be estimated independently.

For each response (TPC, TEAC, or TAC) the empiric polynomial model of DSD and *I*-optimal design is shown in Eq. (1):

Table 2
DSD's regression results and the estimated MAE parameters of the TPC, TEAC, and TAC.

Parameters		TPC (mg_{GAE}/g_{dw})		TEAC ($\mu mol_{TE}/g_{dw}$)		TAC (mg_{AAE}/g_{dw})	
		EC	ρ-value	EC	ρ-value	EC	ρ-value
Estimated parameters	**Intercept**	32.503	< 0.0001[a]	245.065	< 0.0001[a]	33.147	< 0.0001[a]
	Linear effects						
	x_1	0.206	0.604[b]	3.016	0.215[b]	2.007	0.0005[a]
	x_3	$7.143 \times E^{-10}$	1.000[b]	-0.011	0.995[b]	-1.436	0.0032[a]
	x_4	6.290	<0.0001[a]	25.601	<0.0001[a]	2.626	< 0.0001[a]
	x_2	-0.214	0.7317[b]	12.337	0.0008[b]	2.601	< 0.0001[a]
	Quadratic effects						
	x_1x_1	-0.978	0.365[b]	-20.508	0.0102[a]	-6.270	0.0002[a]
	x_2x_2	-0.282	0.798[b]	-14.630	0.0503[b]	0.309	0.745[b]
	x_4x_4	1.399	0.230[b]	-15.150	0.0445[a]	-2.169	0.0499[a]
	Interaction effects						
	x_1x_3	-0.199	0.365[b]	5.212	0.188[b]	1.107	0.0380[a]
	x_2x_4	-0.240	0.594[b]	11.247	0.0034[a]	-0.186	0.6420[b]
Regression results	R^2	0.97		0.99		0.97	
	R^2_{Adj}	0.94		0.93		0.94	
	RMSE	1.42		8.29		1.22	
	C.V (%)	4.35		4.07		4.60	
	ANOVA (Model)	< 0.0001[a]		0.0001[a]		< 0.0001[a]	
	Lack of fit	/		/		/	

TPC; Total phenolic compounds, **TEAC**; Trolox equivalent antioxidant capacity, **TAC**; Total antioxidant capacity **EC**; Estimated coefficient, **RMSE**; Root Mean Square Error, **C.V**; Coefficient of variance, **ρ-value [a]**; statistically significant, **ρ-value [b]**; statistically not significant.

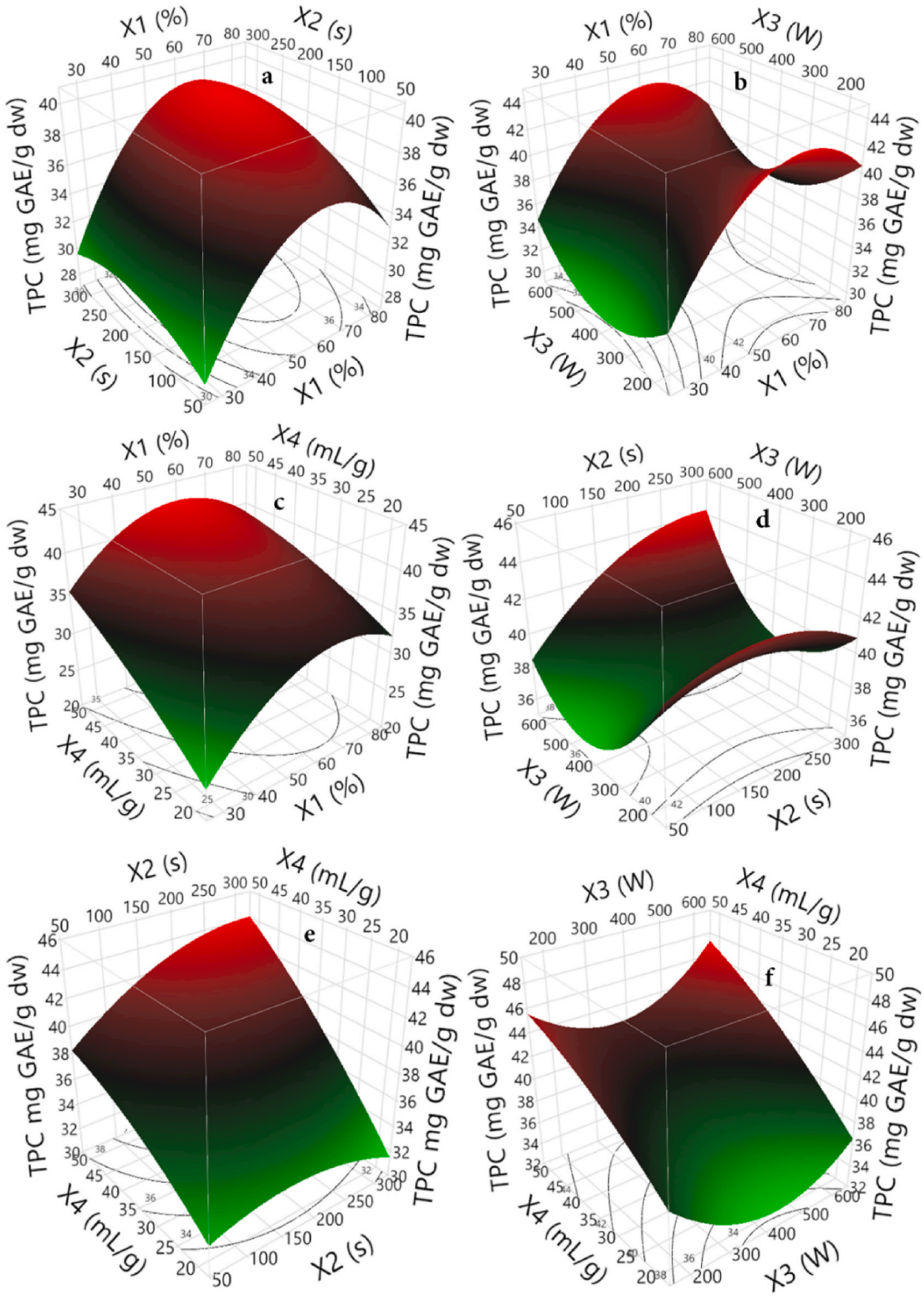

Fig. 1. Three dimensional response surface plot showing the effects of MAE parameters on TPC from *S. officinalis* L. **a**: effect of ethanol-water mixture and time, **b**: effect of ethanol-water mixture and microwave power, **c**: effect of ethanol-water mixture and solvent to solid ratio, **d**: effect of time and microwave power, **e**: effect of time and solvent to solid ratio, **f**: effect of microwave power and solvent to solid ratio.

$$y_i = B_0 + \sum_{j=1}^{k} B_j x_{i,j} + \sum_{j=1}^{k-1} \sum_{k=j+1}^{k} B_{ijk} x_{i,j} x_{i,k} + \sum_{j=1}^{k} B_{jj} x_{i,j}^2 + \varepsilon_i \quad (1)$$

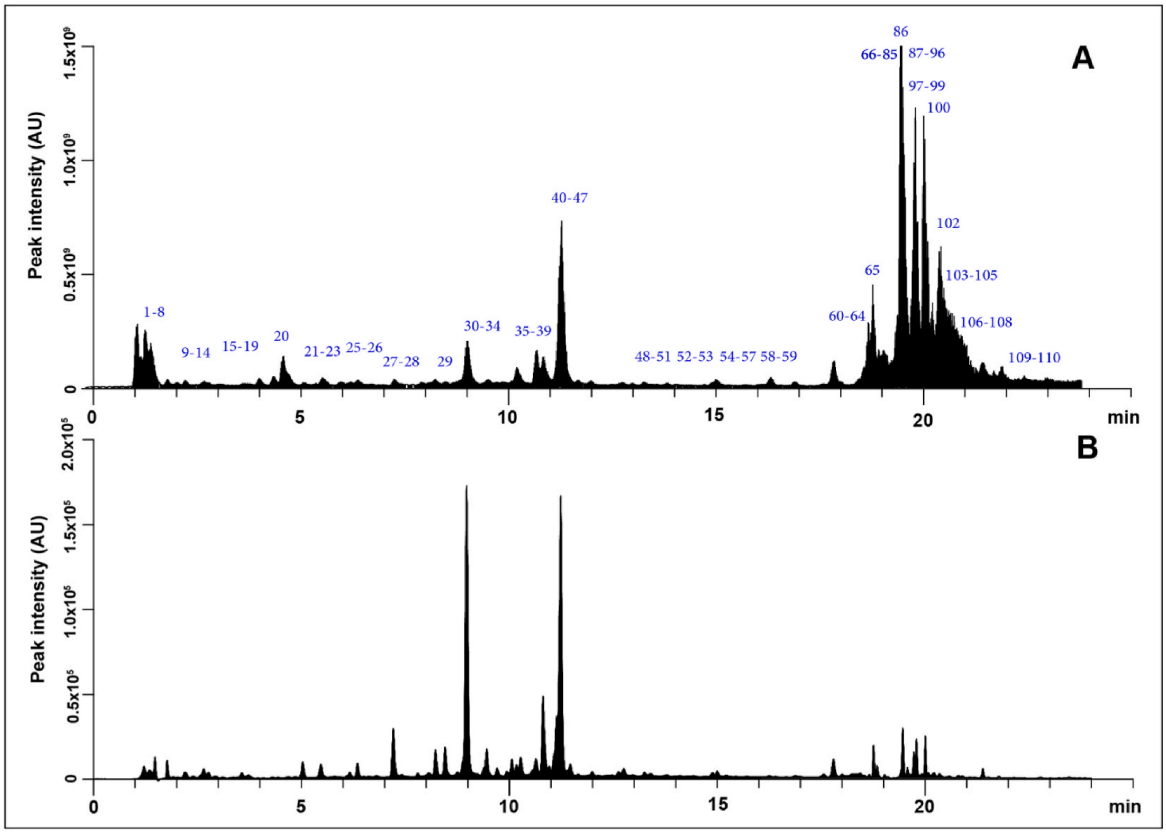

Fig. 2. Total ion chromatogram of *S. officinalis* MAE extract detected by LC-Q-Orbitrap in negative mode (A) set with chromatogram registered by UV-Vis detector at 270 nm (B).

where k is the number of MAE parameters, and B_0, B_{ijk}, B_{jj} are the estimated regression coefficients for linear, interaction, and quadratic effects, respectively, $x_{i,j}$, $x_{i,k}$, $x^2_{i,j}$ are the coded MAE factors, y_i is the responses (TPC, TEAC, or TAC), and ε_i is the error.

2.4. Determination of TPC and antioxidant capacity of S. officinalis L

The TPC of MAE extracts of S. *officinalis* L. was determined by Folin's assay as mentioned in previous work (Moussa et al., 2022). A standard curve of Gallic acid was used to calculate the TPC from *S. officinalis* L. as mg_{GAE}/g_{dw}, where all results were expressed as means ± standard deviations (SD).

The TAC of MAE extracts obtained according to DSD and *I*-optimal design was estimated according to the assays described in our previous work (Moussa et al., 2022). TAC was expressed as mg of ascorbic acid equivalent (AAE)/g_{dw} using the calibration curve's equation (Moussa et al., 2022). All the assays were performed in triplicate and the results were expressed as mean ± SD. The Trolox equivalent antioxidant capacity of MAE extracts were estimated using the protocol used for the evaluation of UAE extracts of *S. officinalis* L. leaves (Moussa et al., 2022). The TEAC was determined using the Trolox standard curve's equation and given as µmol Trolox equivalent (TE)/g_{dw} of *S. officinalis* L. powder. All experiments were carried out in triplicate, and the findings were presented as mean standard deviation.

2.5. UHPLC-MS Characterization of bioactive compounds from common sage leaves extracts

To evaluate the bioactive compounds profiles of *S. officinalis* L. obtained by MAE, and ultrasound-assisted extraction (UAE), the high-resolution tandem liquid chromatography-mass spectrometry (UHPLC-HRMS, Dionex Ultimate 3000, RS Autosampler) was employed as reported in the previous work of Kusznierewicz et al. (2021). Chromatographic separation was carried out with a C_{18} column (LUNA OMEGA 1.6 µm Polar C18, 100 A°, 150 × 2.1 mm). In this case, the mobile phase consisting of 0.1% (v/v) formic acid in water (A) and 0.1% (v/v) formic acid in acetonitrile (B) was pumped at a flow rate of 0.3 mL min^{-1} with gradient elution: 0 min, 15% B; 15 min, 40% B; 16 min, 100% B; 24 min, 100% B and finally, the initial conditions were held for 7 min as a re-equilibration step. The injection volume was 1 µL for both UAE and MAE extracts.

The UHPLC was coupled to a Dionex Ultimate 3000 RS-DAD and Q-Exactive™ Focus quadrupole-Orbitrap mass spectrometer (Thermo Fisher Scientific, Bremen, Germany) with a heated electrospray ionization source (HESI II). The HESI parameters in negative polarity included: sheath gas flow rate, 35 arb; auxiliary gas flow rate, 15 arb; sweep gas flow rate, 3 arb; spray voltage, 2.5 kV; capillary temperature, 350 °C; S-lens RF level, 50; heater temperature, 300 °C. Full scan data in the negative mode was acquired at a resolving power of 70.000 FWHM; AGC target, 1e6; max IT, auto. A scan range of 100 –1200 *m/z* was selected for the compounds of

interest. The parameters of data-dependent MS^2 were as follows: resolution, 17,500; isolation window, 3.0 *m/z*; normalized collision energy, 30; AGC target, 1e6; max IT, auto. Mass calibration was carried out using a combination of *n*-butylamine, caffeine, Met-Arg-Phe-Ala (MRFA), and Ultramark 1621 in both positive and negative modes.

Compound Discoverer (CD) software (v. 2.1, Thermo, Waltham, USA) was used to interpret the information contained in the raw UPLC-HRMS data. Accurate mass and fragmentation patterns were used to identify the components of the extracts. These compounds were identified based on the customized database of various classes of phytochemicals that was built from available literature data on the *Salvia* species and implemented in the CD software. Raw data of six experimental replicates from MAE, UAE *Salvia*'s extracts, and extraction solvent (blank) were processed using a workflow based on the template for Food Research w Statistics Unknown ID w Online and Local Database Searches.

2.6. Statistical analysis

JMP® Pro 13.0.0 software was used to create the experimental data. The analysis of variance (ANOVA) was used to investigate the fitness of the DSD and *I*-optimal models, as well as the significance of MAE parameters. The 3D response surface plots were used to assess the influence of each MAE parameter and its interactions on the responses (TPC, TEAC, and TAC). The differential analysis of MS data was performed with Compound Discoverer 2.1 software.

3. Results and discussion

3.1. Definitive screening design

3.1.1. Model fitting

A 17-run DSD with four MAE parameters and three levels was employed to assess the effects of MAE parameters and their interaction on TPC, TEAC, and TAC from *S. officinalis* L. leaves, where, the DSD results were presented in Table A.1. The second-order polynomial regression analysis and statistical analysis of variance (ANOVA) were presented in Table 2. The relationship between the TPC, TEAC, and TAC and MAE parameters was described in Eq. (2), Eq. (3), and Eq. (4), respectively:

$$\boldsymbol{TPC}\ \left(\boldsymbol{mg_{GAE}}/\mathbf{g_{dw}}\right) = 32.50 + 0.20\,x_1 - 0.21\,x_2 + 7.14 * E^{-10}x_3 + 6.29\,x_4 - 0.97\,x_1^2 - 0.28\,x_2^2 + 1.39\,x_4^2 - 0.19\,x_1x_3 - 0.24\,x_2x_4 \quad (2)$$

$$\boldsymbol{TEAC}\ \left(\boldsymbol{\mu mol_{TE}}/\mathbf{g_{dw}}\right) = 245.06 + 3.01\,x_1 - 12.33\,x_2 - 0.01\,x_3 + 25.60\,x_4 - 20.50\,x_1^2 - 14.63\,x_2^2 - 15.15\,x_4^2 - 5.21\,x_1x_3 - 11.24\,x_2x_4 \quad (3)$$

$$\boldsymbol{TAC}\ \left(\boldsymbol{mg_{AAE}}/\mathbf{g_{dw}}\right) = 33.14 + 2.01\,x_1 - 2.60\,x_2 - 1.43\,x_3 + 2.62\,x_4 - 6.27\,x_1^2 - 0.30\,x_2^2 - 2.16\,x_4^2 + 1.10\,x_1x_3 - 0.18\,x_2x_4 \quad (4)$$

Table 2 summarizes the analysis of variance and goodness-of-fit of the DSD model. TPC, TEAC, and TAC's high model significance were

Table 3
Regression results of *I*-optimal design and the estimated parameters of the TPC, TEAC, and TAC.

Parameters		TPC ($\mathbf{mg_{GAE}/g_{dw}}$)		TEAC ($\boldsymbol{\mu}\mathbf{mol_{TE}/g_{dw}}$)		TAC ($\mathbf{mg_{AAE}/g_{dw}}$)	
		EC	ρ-value	EC	ρ-value	EC	ρ-value
Estimated parameters	**Intercept**	38.858	< 0.0001[a]	247.748	< 0.0001[a]	34.278	< 0.0001[a]
	Linear effects						
	x_1	2.428	< 0.0001[a]	13.093	0.0005[a]	1.121	0.0564[b]
	x_2	1.240	0.0014 [a]	1.158	0.569[b]	0.103	0.833[b]
	x_3	-0.013	0.953[b]	4.974	0.0415[a]	-0.113	0.817[b]
	x_4	3.867	<0.0001[a]	21.885	<0.0001[a]	2.690	< 0.0013[a]
	Quadratic effects						
	x_1x_1	-3.784	< 0.0001[a]	-22.214	0.0006[a]	-5.391	0.0006[a]
	x_2x_2	-1.175	0.033[a]	2.109	0.588[b]	-0.682	0.479[b]
	x_3x_3	2.491	0.0011[a]	1.929	0.619[b]	-0.304	0.747[b]
	x_4x_4	-0.623	0.193[b]	-6.755	0.117[b]	-1.532	0.141[b]
	Interaction effects						
	x_1x_2	0.506	0.109[b]	-0.571	0.814[b]	-0.012	0.983[b]
	x_1x_3	-0.189	0.508[b]	5.466	0.0578[b]	0.120	0.839[b]
	x_1x_4	-0.792	0.026[a]	-0.231	0.924[b]	-0.560	0.364[b]
	x_2x_3	1.143	0.0039[a]	-0.722	0.751[b]	-0.482	0.405[b]
	x_2x_4	1.278	0.0023[a]	-0.701	0.758[b]	0.192	0.731[b]
	x_3x_4	0.623	0.0478[a]	5.918	0.0349[a]	0.277	0.622[b]
	R^2	0.99		0.97		0.94	
	R^2_{Adj}	0.97		0.92		0.83	
	RMSE	0.79		6.90		1.69	
Regression results	**C.V (%)**	2.15		3.02		5.88	
	ANOVA (Model)	< 0.0001[a]		0.0008[a]		< 0.0088[a]	
	Lack of fit	0.732[b]		0.859[b]		0.602[b]	

TPC; Total phenolic compounds, **TEAC ;** Trolox equivalent antioxidant capacity, **TAC**; Total antioxidant capacity **EC;** Estimated coefficient, **RMSE;** Root Mean Square Error, **C.V;** Coefficient of variance, **ρ-value [a];** statistically significant, **ρ-value [b];** statistically not significant.

validated by their lower *p*-value (<0.0001). The determination coefficient (R^2), adjusted determination coefficient (R^2_{adj}) and coefficient of variance (C.V.) are all used to determine the goodness-of-fit of the DSD model. For TPC, TEAC, and TAC, the R^2 values were more than 0.97, and R^2_{adj} higher than 0.93. The C.V. for all responses was lower than 5% (Table 2). The high values of R^2, and R^2_{adj} and low value of C.V. confirmed that the DSD model could explain the most variation with high precision and reliability. According to the level of *p*-value, it can be concluded that only the linear coefficients (x_4), was significant for TPC, whereas the linear coefficients (x_4), quadratic coefficients (x_1^2, and x_4^2), and interaction term coefficients (x_2x_4) were all significant ($p < 0.05$) for TEAC. Furthermore, TAC was affected by all the linear coefficients ($x_1, x_2, x_3,$ and x_4), quadratic coefficients (x_1^2, and x_4^2), and interaction term coefficients (x_1x_4).

3.2. *I*-optimal design

3.2.1. Model fitting

Based on the DSD model (Table A.1, and Table 2), the MAE parameters including ethanol-water mixture (x_1), time (x_2), microwave power (x_3) and solvent to solid ratio (x_4) exhibited a higher influence on TPC, TEAC, and TAC, hence all the MAE parameters were selected for the optimization using *I*-optimal design.

To study deeply the combined effect of MAE parameters on TPC, TEAC, and TAC, an *I*-optimal design was performed with different combinations of MAE parameters and the results are shown in Table A.2, which includes the experimental and predicted values. The *I*-optimal design's accuracy was estimated based on the experimental data using different tests including the analysis of variance, lack of fit, and model summary statistics as mentioned in Table 3. The quadratic model for all responses was found to have maximum R^2, and R^2_{adj} and showed a low C.V. (<6%). The *I*-optimal design with lower *p*-values (<0.0001) and non-significant lack of fit was found to be the most suitable model for the extraction of TPC, TEAC, and TAC from *S. officinalis* L. The second-order polynomial equation was generated to describe the empirical relationship between the response (TPC, TEAC, and TAC) and MAE parameters in terms of coded values, following the predictive Eq. (5), Eq. (6), and Eq. (7):

$$\begin{aligned} \boldsymbol{TPC}\ \left(\mathbf{mg_{GAE}}\,/\,\mathbf{g}_{dw}\right) = {} & 38.85 + 2.42\,x_1 - 1.24\,x_2 - 0.01\,x_3 + 3.86\,x_4 - 3.78\,x_1^2 - 1.17\,x_2^2 + 2.49\,x_3^2 - 0.62\,x_4^2 + 0.50\,x_1x_2 - 0.18\,x_1x_3 \\ & - 0.79\,x_1x_4 + 1.14\,x_2x_3 + 1.27\,x_2x_4 + 0.62\,x_3x_4 \end{aligned} \tag{5}$$

$$\begin{aligned} \boldsymbol{TEAC}\ \left(\boldsymbol{\mu}\mathbf{mol_{TE}}\,/\,\mathbf{g}_{dw}\right) = {} & 247.74 + 13.09\,x_1 + 1.15\,x_2 + 4.97\,x_3 + 21.88\,x_4 - 22.21\,x_1^2 + 2.10\,x_2^2 + 1.92\,x_3^2 - 6.755\,x_4^2 - 0.57\,x_1x_2 \\ & + 5.46\,x_1x_3 - 0.23\,x_1x_4 - 0.72\,x_2x_3 - 0.70\,x_2x_4 + 5.91\,x_3x_4 \end{aligned} \tag{6}$$

$$\begin{aligned} \boldsymbol{TAC}\ \left(\mathbf{mg_{AAE}}\,/\,\mathbf{g}_{dw}\right) = {} & 34.27 + 1.12\,x_1 + 0.10\,x_2 - 0.11\,x_3 + 2.69\,x_4 - 5.39\,x_1^2 - 0.68\,x_2^2 - 0.30\,x_3^2 - 0.14\,x_4^2 - 0.01\,x_1x_2 + 0.12\,x_1x_3 \\ & - 0.56\,x_1x_4 - 0.48\,x_2x_3 + 0.19\,x_2x_4 + 0.27\,x_3x_4 \end{aligned} \tag{7}$$

3.2.2. Effect of MAE parameters on TPC

Three levels of *I*-optimal design were carried out to investigate the effect of MAE parameters such as ethanol-water mixture (x_1), time (x_2), microwave power (x_3) and solvent to solid ratio (x_4) on the MAE of TPC from *S. officinalis* L. From the *I*-optimal design, the three-dimensional response surface was constructed to demonstrate the interactive effects of MAE parameters on a TPC, by varying two extraction parameters while keeping the other extraction parameter constant.

High TPC extraction yield (varying from 20 to 48 mg_{GAE}/g_{dw}) was obtained under the conditions studied. Based on estimated coefficients (Table 3), the ethanol-water mixture exhibited a positive and negative effect on TPC for linear and quadratic effects, respectively. As shown in Fig. 1a-b, TPC was mainly influenced by the effect of the ethanol-water mixture. When this extraction parameter increased from 30 to 58%, the TPC increased significantly, this rise can be attributed to the enhanced extraction efficiency facilitated by the ethanol-water mixture within this range. The dissipation factor plays a crucial role in assessing the effectiveness of a solvent in MAE (Ašperger et al., 2022). A higher dissipation factor signifies a superior capacity to convert microwave energy into heat. Among various solvents, ethanol and its aqueous solutions exhibit notably higher dissipation factors, thereby enabling more efficient translation of microwave energy into heat. This, in turn, leads to a local temperature increase that positively impacts the denaturation and degradation of cell walls (Ašperger et al., 2022). Consequently, the extraction of bioactive compounds from plant matrices using aqueous ethanol becomes easier due to these effects (Ašperger et al., 2022). Moreover, the presence of water in solvent system would increase the penetration of solvent into sample matrix, improving the heating efficiency (Chan et al., 2011). However, beyond the 58% threshold of the ethanol-water mixture, we observed a remarkable decline in TPC. This decline indicates that there is an upper limit to the optimal composition of the ethanol-water mixture for TPC extraction. It is important to note that this observed trend was consistent across all MAE parameters tested, as depicted in Fig. 1a-b. This suggests that the interaction between the ethanol-water mixture and the MAE parameters is significant and must be taken into account when optimizing the extraction process. These results could be explained by the fact that a high concentration of ethanol can cause protein denaturation, preventing the dissolution of polyphenols and then influencing the extraction rate (Dahmoune et al., 2015a). Furthermore, the findings reported by Darvishzadeh and Orsat (2022) provide additional support for our results. They reported that ethanol-water mixtures of 59% and 66% showed higher extraction of TPC from Russian olive leaves and flowers.

Regarding the MAE time, the linear and quadratic terms had a significant effect on TPC. Which linear term showed a positive effect, while the quadratic term exhibited a negative effect (Table 3). According to Fig. 1a, the MAE time showed a slight positive effect on TPC in interaction with the ethanol-water mixture, the TPC increased from 20 to 30 mg_{GAE}/g_{dw} when the MAE time extended from 50 to 300 s. This trend was observed when the time was in interaction with microwave power and solvent to solid ratio as depicted in

Fig. 1d and Fig. 1e, respectively. The shorter duration of exposure to microwave radiation resulted in a higher yield of TPC, and this it could be due to the efficient breakdown of cell structures and release of TPC from the solid matrix within a short time period. Additionally, irradiation time can enhance the mass transfer between the solid matrix and the solvent, leading to the increase in the extraction efficiency of TPC and antioxidant capacity. Similar reports were carried out and showed that 5 to 6 min in microwave exhibited high TPC extraction (Karami et al., 2015; Teng and Choi, 2013).

Another important parameter examined in the MAE of TPC is the solvent-to-solid ratio. The estimated coefficient confirmed that the solvent-to-solid ratio showed a positive and highly significant effect on TPC (Table 3). The TPC values of the extract increased with the increase in the solvent-to-solid ratio, and high TPC was obtained at 50 mL/g of solvent to solid ratio, which the results obtained from 3D surface plots (Fig. 1c, 1e, and Fig. 1f) are compatible with the mass transfer principles. These results were in agreement with the results obtained by Sánchez-Camargo et al. (2021).

Furthermore, the linear effect of microwave power displayed a non-significant effect on TPC, while the quadratic effect exhibited a highly significant effect on TPC as shown in the estimated coefficient results reported in Table 3. According to three-dimensional response surface plots (Fig. 1b, 1d, and Fig. 1f), the TPC was decreased slightly from 200 to 300 W then TPC raised significantly at high microwave power (600 W). This microwave power effect on TPC was also noticed in interaction with other MAE parameters including ethanol-water mixture, irradiation time, and solvent to solid ratio. Notably, the maximum TPC was achieved when using a high power level of 600 W, an ethanol-water mixture of 58%, an irradiation time of 300 s, and a solvent to solid ratio of 50 mL g^{-1}. These findings can be attributed to the impact of microwave power on the heating rate and temperature distribution during the extraction process. Higher power levels result in increased energy input, leading to a more rapid and uniform heating of the sample. This accelerated heating facilitates the release of phenolic compounds from the matrix and enhances their solubility in the extraction solvent (Dahmoune et al., 2015a). Nana et al. (2021) mentioned that 600 W of microwave power was the optimal MAE condition for extraction of total limonoid and antioxidant capacity from *Trichilia roka*. Furthermore, Berkani et al. (2020) reported that high microwave power (600 W) and extended MAE time were the best operational parameters for the extraction of polysaccharides from Algerian jujube. Moreover, the optimal level of microwave power (600 W) obtained explained by the high solvent to solid ratio (50 mL g^{-1}), which a large amount of solvent needs more absorption of microwave energy to heat the medium (Mandal and Mandal, 2010).

3.2.3. *Effect of MAE parameters on TEAC and TAC*

The TEAC and TAC of *S. officinalis* L. extracts varied from 160 to 279 $\mu mol_{TE}/g_{dw}$, 20 to 35 mg_{AAE}/g_{dw}, respectively as depicted in Fig. A.3 and Fig. A.4. According to the *p*-values of regression coefficients (Table 3), the linear effects (x_1, x_3, and x_4) showed significant effects on TEAC, however only the linear effect (x_4) exhibited a significant effect on TAC. Furthermore, only the quadratic effect (x_1^2) showed a negative effect on both TEAC and TAC. Regarding the interaction effect terms, the x_3x_4 had a positive effect on TEAC, whereas all the other interactions showed a non-significant effect on TEAC and TAC.

According to response surface methodology (Fig. A.3 and Fig. A.4), the lowest TEAC, and TAC were obtained at a lower level of ethanol concentration (30%) and extraction time (60 s), and lower level of microwave power (200 W), and solvent to solid ratio (20 mL g^{-1}). Furthermore, the TEAC was found to be highest at a middle level of ethanol concentration (58%) and extraction time (300 s), higher level of microwave power (600 W), and higher solvent-to-solid ratio (50 mL g^{-1}). The TAC was higher at 58% of ethanol concentration and extraction time (267 s), microwave power (600 W), and solvent to solid ratio (50 mL g^{-1}). The same effect of the ethanol-water mixture was observed for TEAC and TAC, where the increase of ethanol-water mixture from 30% to 58% increased the TEAC and TAC, then the two responses declined significantly with increasing the ethanol-water mixture from 58% to 80%. Similar

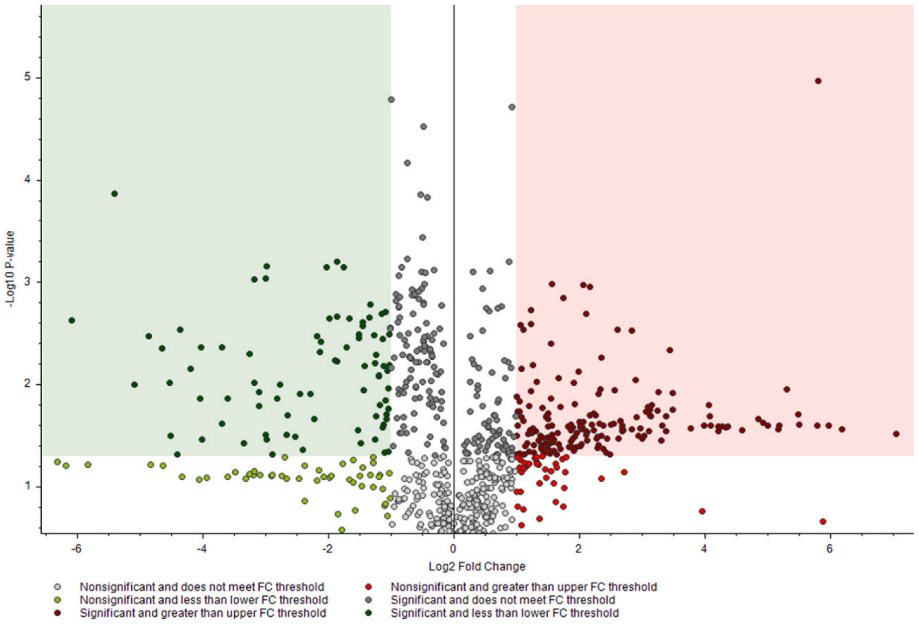

Fig. 3. Differential content visualization of identified and unidentified MAE and UAE bioactive compounds with Volcano plot (Log 2 Fold change = 1).

results were found in the literature, mentioned that high antioxidant activity of medicinal plants was obtained at 49% - 58% of ethanol-water mixture (Luo et al., 2021; Shang et al., 2020; Song et al., 2011; Wen et al., 2015). The differences of antioxidant activity of *S. officinalis* L. leaves may be attributed to the difference in dielectric properties of the solvent, the loss tangent (tan δ) of methanol and water at 2.450 MHz and room temperature is 0.94, and 9.88, respectively, which the higher value of loss tangent, the better the material will heat under MW irradiation (Chemat and Cravotto, 2013).

Another MAE parameter studied for the extraction of antioxidants from *S. officinalis* L. is the extraction time. The effect of time on TEAC and TAC in interaction with the ethanol-water mixture, and the solvent-to-solid ratio was found to be a less important parameter (Fig. A.3a, A.3e, A.4a, and Fig. A.4e). As the extraction time increased, the extraction efficiency of antioxidants increased slightly. In addition, the effect of extraction time in interaction with microwave power was more significant on TEAC and TAC (Fig. A.3d, and Fig. A.4d), which at low levels of microwave power the TEAC and TAC raised significantly with an increase in extraction time. However, at high levels of microwave power, the TEAC decreased significantly, when the time was prolonged from 60 to 150 s, then the TEAC increased when the time was more than 150 s (Fig. A.3d). Furthermore, at high levels of microwave power, the TAC increased slightly when the time prolonged from 60 to 150 s, and then the TEAC declined significantly when the time extended from 150 to 300 s (Fig. A.4d). Wen et al. (2015) and Lovrić et al. (2017) reported that 4 and 5 min of extraction time is sufficient for the recovery of phenolic and antioxidant compounds from blackberry and blackthorn flowers, respectively.

In addition, the microwave power showed to be a significant factor affecting the antioxidant capacity of *S. officinalis* L. leaves, which exhibited a positive effect on TEAC (x_3, and x_3x_4), and a non-significant effect on TAC (Table 3). The increase in microwave power from 200 to 600 W significantly enhanced antioxidant capacity (Fig. A.3b, A.3d, and A.4d). The influencing of microwave on antioxidant activity of *S. officinalis* L. leaves extracts were also similar to those reported in the previous papers (Liu et al., 2010; Xueling et al., 2011).

On the other hand, according to the results obtained from Table 3, Fig. A.3, and Fig. A.4, the solvent-to-solid ratio is considered the most MAE parameter that enhances the TEAC and TAC from *S. officinalis* L. leaves. The solvent-to-solid ratio showed a highly positive effect (p-value > 0.001). All the response surface plots (Fig. A.3c, A.3e, A.3f, A.4c, A.4e, and A.4f) show similar trends on the antioxidant capacity, where the increase in the solvent-to-solid ratio increased the TEAC and TAC which creates a better contact surface for the extraction of antioxidant compounds from *S. officinalis* L. leaves. Therefore, the optimal solvent-to-solid ratio for high antioxidant capacity was 50 mL g^{-1}. These results are in line with the results of Zeković et al. (2017), Bhuyan et al. (2015) and Kaderides et al. (2019), which found that a large amount of solvent between 40 and 60 mL g^{-1} showed high recovery of polyphenols from *Salvia officinalis* L. by-products.

3.3. Optimization of MAE of TPC and antioxidant capacity

The DSD and *I*-optimal design were used for screening and optimization the MAE parameters, respectively. Based on desirability function, the optimal MAE conditions for the maximum of TPC, and TEAC, and TAC given by DSD were: ethanol concentration of 55%, microwave power of 200 W, MAE time of 4.35 min, solid–liquid ratio of 50 mL g^{-1}. Under these optimal MAE conditions, the desirability value was 0.90. While the optimal MAE conditions for the maximum of TPC, and TEAC, and TAC given by *I*-optimal design were: ethanol concentration of 60%, microwave power of 600 W, MAE time of 4.79 min, solid–liquid ratio of 50 mL g^{-1}. Under these optimal MAE conditions, the desirability value was 0.92.

For the validation of the optimum MAE conditions for both DSD and *I*-optimal design, the average of TPC, TEAC, and TAC were compared to the predicted values given by the employed models. The experimental values of TPC, TEAC, and TAC of DSD were 39.97 ± 1.58 mg_{GAE}/g_{dw}, 266.05 ± 1.54 $\mu mol_{TE}/g_{dw}$, 35.85 ± 0.72 mg_{AAE}/g_{dw}, while the predicted values of TPC, TEAC, and TAC were 39.68 mg_{GAE}/g_{dw} with predicted interval of [39.68 to 42.28], 264.99 $\mu mol_{TE}/g_{dw}$ with predicted interval of [249.84.99 to 280.15], and 37.03 mg_{AAE}/g_{dw} with predicted interval of [34.79 to 39.27]. Moreover, the experimental values of TPC, TEAC, and TAC of *I*-optimal design were 46.12 ± 0.08 mg_{GAE}/g_{dw}, 268.39 ± 1.28 $\mu mol_{TE}/g_{dw}$, 36.79 ± 0.20 mg_{AAE}/g_{dw}, while the predicted values of TPC, TEAC, and TAC were 47.60 mg_{GAE}/g_{dw} with predicted interval of [45.96 to 49.24], 278.79 $\mu mol_{TE}/g_{dw}$ with predicted interval of [264.59 to 292.99], and 34.67 mg_{AAE}/g_{dw} with predicted interval of [31.19 to 38.15]. The results were closely related to the data obtained from the optimization process, indicating that DSD and *I*-optimal design could be effectively used to screen and optimize the MAE for a maximum phenolic and antioxidant capacity.

3.4. Differential analysis of MAE and UAE

To evaluate the efficiency of extraction techniques, the optimal MAE extract obtained in this study was compared to the optimal UAE extract obtained by Moussa et al. (2022). The optimal MAE extract of common sage exhibited higher TPC (46.12 ± 0.08 mg_{GAE}/g_{dw}) and TEAC (268.39 ± 1.28 $\mu mol_{TE}/g_{dw}$) than optimal extract obtained by UAE, where TPC and TEAC were 31.84 ± 0.248 mg_{GAE}/g_{dw}, 237.95 ± 0.771 $\mu mol_{TE}/g_{dw}$, respectively. However, the UAE extract showed higher TAC (38.928 ± 0.548 mg_{AAE}/g_{dw}) than the MAE extract with a TAC of 36.79 ± 0.20 mg_{AAE}/g_{dw}. These results could be explained by the ability of microwave energy to enter the cell matrix, interact with polar molecules, and heat the biomaterial evenly as microwaves are absorbed by the whole sample equally, which in turn raises the pressure inside the plant cells. As the pressure increases, cell walls break down and phenolic compounds are released (Nayak et al., 2015).

In order to characterize the quality and quantity of phenolic compounds of common sage leaves present in MAE and UAE optimal extracts, UHPLC-HRMS was applied to identify the major phenolic compounds present in both extracts. As most phenolic compounds contain one or more hydroxyl, carboxylic acid groups, or both, MS data were obtained in the negative ionization mode (Irakli et al., 2021). Total ion chromatograms of MAE and UAE extracts of common sage are shown in Fig. 2, and Fig. A.5, while the major peaks

identified by UHPLC-HRMS analysis are presented in Table A.3 (Supplementary data). Each identification was confirmed by comparing the observed compounds' MS^2 spectra to those described in the literature. UHPLC-HRMS analysis of common sage leaves extracts allowed us to identify more than 80 different phenolic compounds present in both MAE and UAE optimal extracts. As mentioned in Table A.3 (Supplementary data), different types of bioactive compounds were assigned including hydroxycoumarins, phenolic diterpenes, flavonols and derivatives, flavones and derivatives, flavanones and derivatives, isoflavones, 2-arylbenzofuran flavones, phenolic acids and aldehydes, triterpenoids, lignin, sesquiterpenes, beta-hydroxyacids, tricarboxylic acids, organic acid, organic sugar, and sugar acid.

The volcano plot of UHPLC-HRMS analysis generated by Compound Discoverer software (Fig. 3) provides an effective tool for visualizing the direction, magnitude, and significance of changes in the concentration of bioactive compounds present in both MAE and UAE extracts. Each point on the Volcano plot represents one detected compound. The log 2-fold values are plotted on the x-axis and the -log10 *p*-values are plotted on the y-axis for each compound detected by CD Software. The horizontal dashed line represents the significance threshold (p-value <0.05). A total of 268 points lying above a horizontal threshold were recognized as statistically different between MAE and UAE extracts. When the value of log 2-fold change is closer to 1 it indicates less difference, while moving away from 1 in either direction indicates more difference in terms of contents of particular compound. According to this 181 compounds were found to be more abundant in MAE extract (on the right of 0 on the x-axis) including caffeic acid galactoside, caffeic acid glucoside, caffeoyl-hexosyl-hexose, 6-hydroxyluteolin-7-O-glucoside, 6-hydroxyluteolin 7-O-rhamnoside, luteolin, hydroxyursolic acid, quercetin-3-O-malonylglucoside, luteolin-7-O-glucoside, micromeric acid, ursolic acid, genistin, luteolin O-malonyl hexoside, isorhamnetin-O-hexose, nepitrin, homoplantaginin, trihexoside, dihexoside (Fig. 3, Table A.3). On the other hand, 87 compounds were found to be better extracted in UAE (on the left of 0 on the x-axis) including 3,5-dimethoxycinnamic acid, *p*-coumaric acid/*m*-coumaric acid, rosmadial, epirosmanol, salvianolic acid B, epiisorosmanol, apigenin (Fig. 3, Table A.3). To conclude, the results show that phenolic acids, triterpenoids, and organic sugars were more abundant in MAE extract, which could be explained by the microwave heating provided by microwave power that acts as a driving force for MAE to destroy the cell wall of plant matrix (Chan et al., 2011). Similar results were obtained by Dahmoune et al. (2014), Nayak et al. (2015), İnce et al. (2013). However, MAE causes poor extraction of phenolic diterpenes due to their sensitivity to microwave heating which confirm that ultrasound assistance is more suitable for fragile bioactive compounds that require gentle extraction, while microwave is more suitable for more resistant compounds that require rapid extraction.

4. Conclusion

The present study was an attempt to optimize the MAE of phenolic compounds and antioxidant capacity from *S. officinalis* L. using two new statistical design including DSD and *I*-optimal design. Statistical and RSM analysis showed that ethanol concentration of 60%, microwave power of 600 W MAE time of 4.79 min, solid–liquid ratio of 50 mL g^{-1} were the optimal conditions for maximum of TPC, TEAC, and TAC. The MAE optimized based on the new statistical design is as an efficient and eco-friendly alternative method for the recovery of the bioactive compounds from plant matrices. The qualitative analysis using UHPLC-HRMS revealed that *S. officinalis* L. extract is an excellent source of bioactive compounds including phenolic acid and aldehydes, flavonoids, phenolic diterpenes, etc., where rosmarinic acid, carnosol, carnosic acid, and methyl carnosate were the main phenolic compounds. The relative content analysis of the *Salvia officinalis* L. bioactive compounds proved that MAE was better than UAE in term of quantity and extraction time. The differential analysis made it possible to indicate compounds that are particularly affected by the extraction method used. For this reason, when they are specifically targeted for extraction, an appropriate method would have to be considered.

Declaration of competing interest

The authors declare that they have no known competing financial interests or personal relationships that could have appeared to influence the work reported in this paper.

Data availability

No data was used for the research described in the article.

Acknowledgments

This work was supported financially by the Ministry of Higher Education and Scientific Research of Algeria.

Appendix A. Supplementary data

Supplementary data to this article can be found online at https://doi.org/10.1016/j.scp.2023.101194.

References

Ašperger, D., Gavranić, M., Prišlin, B., Rendulić, N., Šikuten, I., Marković, Z., Tomaz, I., 2022. Optimization of microwave-assisted extraction and matrix solid-phase dispersion for the extraction of polyphenolic compounds from grape Skin. Separations 9 (9).

Beres, D.L., Hawkins, D.M., 2001. Plackett–Burman technique for sensitivity analysis of many-parametered models. Ecol. Model. 141 (1–3), 171–183.
Berkani, F., Dahmoune, F., Achat, S., Dairi, S., Kadri, N., Zeghichi-Hamri, S., Madani, K., 2020. Response surface methodology optimization of microwave-assisted polysaccharide extraction from Algerian jujube (*Zizyphus lotus* L.) pulp and peel. J. Pharmaceut.Innovat. 16 (4), 630–642.
Bhuyan, D.J., Van Vuong, Q., Chalmers, A.C., van Altena, I.A., Bowyer, M.C., Scarlett, C.J., 2015. Microwave-assisted extraction of *Eucalyptus robusta* leaf for the optimal yield of total phenolic compounds. Ind. Crop. Prod. 69, 290–299.
Chan, C.-H., Yusoff, R., Ngoh, G.-C., Kung, F.W.-L., 2011. Microwave-assisted extractions of active ingredients from plants. J. Chromatogr. A 1218 (37), 6213–6225.
Chemat, F., Cravotto, G. (Eds.), 2013. Microwave-assisted Extraction for Bioactive Compounds, first ed., Vol. 4. Springer, New York, NY (Springer).
Chen, X., Yang, S., Yang, H., Zhang, J., Huang, Y., Zhang, Y., 2023. Extraction of Flavonoids and Phenolics from *Berberis kongboensis* Fruit. Biomass Conversion and Biorefinery.
Dahmoune, F., Nayak, B., Moussi, K., Remini, H., Madani, K.J. F.c., 2015a. Optimization of microwave-assisted extraction of polyphenols from *Myrtus communis* L. leaves. Food Chem. 166, 585–595.
Dahmoune, F., Remini, H., Dairi, S., Aoun, O., Moussi, K., Bouaoudia-Madi, N., Madani, K., 2015b. Ultrasound assisted extraction of phenolic compounds from *P. lentiscus* L. leaves: comparative study of artificial neural network (ANN) versus degree of experiment for prediction ability of phenolic compounds recovery. Ind. Crop. Prod. 77, 251–261.
Dahmoune, F., Spigno, G., Moussi, K., Remini, H., Cherbal, A., Madani, K., 2014. *Pistacia lentiscus* leaves as a source of phenolic compounds: microwave-assisted extraction optimized and compared with ultrasound-assisted and conventional solvent extraction. Ind. Crop. Prod. 61, 31–40.
Darvishzadeh, P., Orsat, V., 2022. Microwave-assisted extraction of antioxidant compounds from Russian olive leaves and flowers: optimization, HPLC characterization and comparison with other methods. J.Appl. Res.Med. Aromatic Plants 27, 100368.
Eskilsson, C.S., Björklund, E., 2000. Analytical-scale microwave-assisted extraction. J. Chromatogr. A 902 (1), 227–250.
Ferreira, S.L.C., Bruns, R.E., Ferreira, H.S., Matos, G.D., David, J.M., Brandão, G.C., et al., 2007. Box-behnken design: an alternative for the optimization of analytical methods. Anal. Chim. Acta 597 (2), 179–186.
Goos, P., Jones, B., 2011. Optimal Design of Experiments: a Case Study Approach. John Wiley & Sons.
Irakli, M., Skendi, A., Bouloumpasi, E., Chatzopoulou, P., Biliaderis, C.G., 2021. LC-MS identification and quantification of phenolic compounds in solid residues from the essential oil industry. Antioxidants 10 (12), 2016.
İnce, A.E., Şahin, S., Şumnu, S.G., 2013. Extraction of phenolic compounds from Melissa using microwave and ultrasound. Turkish Journal of Agriculture and Forestry 37 (1), 69–75.
Jones, B., Nachtsheim, C.J., 2011. A class of three-level designs for definitive screening in the presence of second-order effects. J. Qual. Technol. 43 (1), 1–15.
Kaderides, K., Papaoikonomou, L., Serafim, M., Goula, A.M., 2019. Microwave-assisted extraction of phenolics from pomegranate peels: optimization, kinetics, and comparison with ultrasounds extraction. Chem. Eng. Process.Process Intensif. 137, 1–11.
Karami, Z., Emam-Djomeh, Z., Mirzaee, H.A., Khomeiri, M., Mahoonak, A.S., Aydani, E., 2015. Optimization of microwave assisted extraction (MAE) and soxhlet extraction of phenolic compound from licorice root. J. Food Sci. Technol. 52 (6), 3242–3253.
Khajeh, M., Ghanbari, A., 2011. Application of factorial design and Box-Behnken matrix in the optimisation of a microwave-assisted extraction of essential oils from *Salvia mirzayanii*. Nat. Prod. Res. 25 (18), 1766–1770.
Kusznierewicz, B., Mróz, M., Koss-Mikołajczyk, I., Namieśnik, J., 2021. Comparative evaluation of different methods for determining phytochemicals and antioxidant activity in products containing betalains – verification of beetroot samples. Food Chem. 362, 130132.
Kwon, J.-H., Bélanger, J.M., Paré, J.R., 2003. Optimization of microwave-assisted extraction (MAP) for ginseng components by response surface methodology. J. Agric. Food Chem. 51 (7), 1807–1810.
Liu, L., Hu, X., Lou, L., Zhang, B., Nie, J., 2010. Study on microwave-assisted extract and antioxidant activity of ginger flavonoids. In: 4th International Conference on Bioinformatics and Biomedical Engineering, 2010.
Lovrić, V., Putnik, P., Bursać Kovačević, D., Jukić, M., Dragović-Uzelac, V., 2017. Effect of microwave-assisted extraction on the phenolic compounds and antioxidant capacity of blackthorn flowers. Food Technol. Biotechnol. 55 (2), 243–250.
Luo, M., Zhou, D.D., Shang, A., Gan, R.Y., Li, H.B., 2021. Influences of microwave-assisted extraction parameters on antioxidant activity of the extract from *Akebia trifoliata* peels. Foods 10 (6).
Mandal, V., Mandal, S.C., 2010. Design and performance evaluation of a microwave based low carbon yielding extraction technique for naturally occurring bioactive triterpenoid: oleanolic acid. Biochem. Eng. J. 50 (1-2), 63–70.
Meyer, R.K., Nachtsheim, C.J., 1995. The coordinate-exchange algorithm for constructing exact optimal experimental designs. Technometrics 37 (1), 60–69.
Moussa, H., Dahmoune, F., Mahdjoub, M.m., Kadri, N., Remini, H., 2022. Definitive screening design and I-optimal design for optimization of ultrasound-assisted extraction of phenolic content and antioxidant capacity from *Salvia officinalis* L. leaves. Sustain. Chem.Pharm 29, 100820.
Nana, O., Momeni, J., Boyom, F.F., Njintang, N.Y., Ngassoum, M.B., 2021. Microwave-assisted extraction as an advanced technique for optimization of limonoid yields and antioxidant potential from *Trichilia roka* (Meliaceae). Curr. Res.Green. Sustain. Chem 4, 100147.
Nayak, B., Dahmoune, F., Moussi, K., Remini, H., Dairi, S., Aoun, O., Khodir, M., 2015. Comparison of microwave, ultrasound and accelerated-assisted solvent extraction for recovery of polyphenols from *Citrus sinensis* peels. Food Chem. 187, 507–516.
Pachura, N., Zimmer, A., Grzywna, K., Figiel, A., Szumny, A., Lyczko, J., 2022. Chemical investigation on *Salvia officinalis* L. Affected by multiple drying techniques - the comprehensive analytical approach (HS-SPME, GC-MS, LC-MS/MS, GC-O and NMR). Food Chem. 397, 133802.
Pan, X., Niu, G., Liu, H., 2001. Microwave-assisted extraction of tanshinones from *Salvia miltiorrhiza* bunge with analysis by high-performance liquid chromatography. J. Chromatogr. A 922 (1-2), 371–375.
Rakić, T., Kasagić-Vujanović, I., Jovanović, M., Jančić-Stojanović, B., Ivanović, D., 2014. Comparison of full factorial design, central composite design, and Box-Behnken design in chromatographic method development for the determination of fluconazole and its impurities. Anal. Lett. 47 (8), 1334–1347.
Reguigui, A., Ott, P.G., Darcsi, A., Bakonyi, J., Romdhane, M., Moricz, A.M., 2023. Nine-dimensional bioprofiles of Tunisian sages (*Salvia officinalis, S. aegyptiaca* and *S. verbenaca*) by high-performance thin-layer chromatography - effect-directed analyses. J. Chromatogr. A 1688, 463704.
Sabry, M.M., Abdel-Rahman, R.F., El-Shenawy, S.M., Hassan, A.M., El-Gayed, S.H., 2022. Estrogenic activity of sage (*Salvia officinalis* L.) aerial parts and its isolated ferulic acid in immature ovariectomized female rats. J. Ethnopharmacol. 282, 114579.
Sánchez-Camargo, A.d.P., Ballesteros-Vivas, D., Buelvas-Puello, L.M., Martinez-Correa, H.A., Parada-Alfonso, F., Cifuentes, A., Gutiérrez, L.-F., 2021. Microwave-assisted extraction of phenolic compounds with antioxidant and anti-proliferative activities from supercritical CO_2 pre-extracted mango peel as valorization strategy. Lwt 137, 110414.
Shang, A., Luo, M., Gan, R.Y., Xu, X.Y., Xia, Y., Guo, H., Li, H.B., 2020. Effects of microwave-assisted extraction conditions on antioxidant capacity of sweet tea (*Lithocarpus polystachyus* Rehd.). Antioxidants 9 (8), 678.
Song, J., Li, D., Liu, C., Zhang, Y., 2011. Optimized microwave-assisted extraction of total phenolics (TP) from *Ipomoea batatas* leaves and its antioxidant activity. Innovat. Food Sci. Emerg. Technol. 12 (3), 282–287.
Sulniute, V., Pukalskas, A., Venskutonis, P.R., 2017. Phytochemical composition of fractions isolated from ten Salvia species by supercritical carbon dioxide and pressurized liquid extraction methods. Food Chem. 224, 37–47.
Teng, H., Choi, Y.H., 2013. Optimization of microwave-assisted extraction of bioactive alkaloid compounds from Rhizoma Coptidis (*Coptis chinensis* Franch.). Food Sci. Biotechnol. 22 (5), 1–8.
Tomasi, I.T., Machado, C.A., Boaventura, R.A.R., Botelho, C.M.S., Santos, S.C.R., 2022. Tannin-based coagulants: current development and prospects on synthesis and uses. Sci. Total Environ. 822, 153454.
Tomasi, I.T., Santos, S.C.R., Boaventura, R.A.R., Botelho, C.M.S., 2023. Optimization of microwave-assisted extraction of phenolic compounds from chestnut processing waste using response surface methodology. J. Clean. Prod. 395, 136452.
Wen, Y., Chen, H., Zhou, X., Deng, Q., Zhao, Y., Zhao, C., Gong, X., 2015. Optimization of the microwave-assisted extraction and antioxidant activities of anthocyanins from blackberry using a response surface methodology. RSC Adv. 5 (25), 19686–19695.

Xu, B., Tao, R., Huang, Z., Zhu, D., Liu, J., 2020. Process optimization of microwave-assisted extraction of flavonoids from *Salvia plebeian* using response surface methodology. J. Phys. Conf. 1578 (1), 012222.
Xueling, Z., Benguo, L., Limin, L., Xiaoai, Z., 2011. Microwave-assisted extraction and antioxidant activity of total phenolic compounds from pomegranate peel. J. Med. Plants Res. 5 (6), 1004–1011.
Zeković, Z., Pintać, D., Majkić, T., Vidović, S., Mimica-Dukić, N., Teslić, N., Pavlić, B., 2017. Utilization of sage by-products as raw material for antioxidants recovery—ultrasound versus microwave-assisted extraction. Ind. Crop. Prod. 99, 49–59.

Abstract

The valorization of medicinal plants has gained significant attention due to their therapeutic properties. In this study, the optimization of the extraction of secondary metabolites and antioxidant activity from medicinal plants of Bouira region including *C. caeruleus* L. and *S. officinalis* L. using ultrasound and microwave-assisted techniques were carried out. New statistical design (Definitive screening design and *I*-optimal design) and supervised learning model (Support vector regression optimized using dragonfly algorithm) were used in this study. Furthermore, identifying secondary metabolites from medicinal plants is crucial for their potential use in pharmaceuticals. UHPLC-HRMS was employed to identify the *S. officinalis* L. compounds due to its high sensitivity and accuracy in detecting complex mixtures of compounds. These approaches demonstrated promising results in extracting and identifying bioactive compounds from medicinal plants. The use of a new statistical design and supervised learning model enhances the efficiency of the extraction process, while UHPLC-HRMS allows for the identification of bioactive compounds with high precision and sensitivity. Overall, these approaches provide a sustainable and efficient means of producing pharmaceuticals while preserving natural resources.

Résumé

La valorisation des plantes médicinales a suscité une attention considérable en raison de leurs propriétés thérapeutiques. Dans cette étude, l'optimisation de l'extraction des métabolites secondaires à partir de *C. caeruleus* L. et *S. officinalis* L. de la région de Bouira a été réalisée à l'aide des techniques assistées par ultrasons et micro-ondes. De nouveaux modèles statistiques y compris le plan de criblage définitif le plan *I*-optimal et le modèle Machine à vecteurs de support optimisée à l'aide de l'algorithme dragonfly ont été utilisés. De plus, l'identification des métabolites secondaires des plantes médicinales est cruciale pour leur utilisation potentielle en pharmacie, la chromatographie en phase liquide a ultra-haute couplée à la spectroscopie de masse haute résolution (CLUHP-SMHR) a été utilisée afin d'identifier les composés bioactifs de *S. officinalis* L. Ces approches et techniques ont démontré des résultats prometteurs dans l'extraction et l'identification de composés bioactifs des plantes médicinales. L'utilisation de nouveaux modèles statistiques et modèle à vecteurs supports améliore l'efficacité du processus d'extraction, tandis que CLUHP-SMHR permet l'identification de composés bioactifs avec une grande précision et sensibilité. Dans l'ensemble, ces approches fournissent un moyen durable et efficace pour la production des molécules et produits pharmaceutiques tout en préservant les ressources naturelles.

ملخص

النباتات الطبية ومستخلصاتها تلقى اهتمامًا كبيرًا بسبب خصائصها العلاجية الطبيعية. في هذه الدراسة تم تطوير و تحسين طرق استخلاص المركبات الثانوية الغنية بمضادات الأكسدة من نبات *C. caeruleus* L و *S. officinalis* L المتواجدة في منطقة البويرة باستخدام تقنيات الأمواج فوق الصوتية (Ultrasound) والميكروويف (Microwave) باستخدام تصاميم و نماذج إحصائية جديدة بما في ذلك Definitive screening design and I-optimal design و Support vector regression optimized using dragonfly algorithm. علاوة على ذلك، فإن تحديد المركبات الثانوية من النباتات الطبية أمر بالغ الأهمية لاستخدامها المحتمل في المستحضرات الصيدلانية. نظرا لدقة تقنية UHPLC-HRMS وحساسيتها الفعالة في كشف وتحديد المركبات الطبيعة، تم استخدامها لتحديد المركبات و المكونات المستخلصة من نبتة *S. officinalis* L حيث أظهرت هذه الأساليب نتائج واعدة في استخلاص وتحديد المركبات النشطة بيولوجيا من النباتات الطبية. حيث تعزز النماذج الاحصائية المستعملة كفاءة عملية في استخلاص هذه المركبات، بينما تسمح تقنية UHPLC-HRMS بتحديد المركبات النشطة بيولوجيًا بدقة وحساسية عاليتين. بشكل عام، توفر هذه الأساليب وسيلة مستدامة وفعالة لإنتاج الأدوية مع الحفاظ على الموارد الطبيعية.